Diss. ETH No. 16090

# Soft Ionization Mass Spectrometry of Biomolecules

## A Dissertation on ESI and AP-MALDI Mass Spectrometry

submitted to the

**SWISS FEDERAL INSTITUTE OF TECHNOLOGY ZURICH**

for the degree of

**Doctor of Natural Sciences**

presented by

**Jürg M. Daniel**

Dipl. Chem. ETH

Born September 28, 1975

Rheinfelden (Aargau)

Accepted on the recommendation of

Prof. Dr. Renato Zenobi, ETH Zurich, examiner

Dr. Vladimir Doroshenko, MassTech Inc., co-examiner

Prof. Ernö Pretsch, ETH Zürich, co-examiner

2005

## Acknowledgement

I sincerely thank Prof. Renato Zenobi for the opportunity to work on interesting projects and for the freedom to direct these by my own ideas. I also thank Prof. Ernö Pretsch and Dr. Vladimir Doroshenko for being my co-examinators.

Many thanks for their collaboration in different stages of my thesis go to Dr. Sebastian Friess, Dr. Suda Rajagopalan, Dr. Silke Wendt, Sille Ehala, Gregor McCombie, and the group of Prof. Hilvert.

I owe special thanks to Mass Tech Inc., especially to Dr. Valdimir Doroshenko, Dr. Victor Laiko, and Dr. Gavin Black, for the opportunity to work on the project of AP-IRIS in their laboratory. I also want to thank Science and Engineering Services, Inc. (SESI) and its team for providing and maintaining the infrared laser for these experiments.

Many thanks go to our electronics engineer Heinz Benz, to Kurt Baumgartner, René Dreier, and Beat Huber from the workshop producing everything I ever wanted, to Guido Krucker who has taken care of all the wastes produced, and to the "Schalter"-team providing chemicals, materials, and always a smile. Furthermore I want to thank the Bistro-Team, especially Nives and Chorche, for providing a good atmosphere for recreation, and our sports trainer for having compensated the mental exposure by physical workout.

I wish to acknowledge my current and former office mates, they contributed to prosperous discussions and to a good time beyond work. I also wish to thank all current and former members of the Zenobi-Group for creating a good atmosphere, both scientific and non-scientific.

Special thanks go to Dr. Sebastian Friess especially for his friendship, but also for his discussions, for the holidays we shared together, and for carefully proofreading this manuscript. I also owe special thanks to Patrick Setz for his patience to endure me in the office, for helping organizing my marriage, for cooking together, and for going

together to numerous sport lessons. Furthermore I want to thank Fiona Ford for helping with all kind of administrative challenges, for having good times at the labor-bar, and for sharing the latest soccer results.

I sincerely thank my wife Daniela Daniel-Ebneter for her love, her patience and her support during my thesis. I am the luckiest and happiest man ever. I also want to gratefully thank my parents and stepparents for their financial and mental support during my time as a student. I thank them for giving me the opportunity to study.

## Parts of this Thesis have been published

**Daniel JM**, Friess SD, Rajagopalan S, Wendt S, Zenobi R
"Quantitative Determination of Noncovalent Binding Interactions using Soft Ionization Mass Spectrometry (review)"
*J. Am. Soc. Mass Spectrom.*, 2002, **216**, 1-27.

**Daniel JM**, McCombie G, Wendt S, Zenobi R
"Mass Spectrometric Determination of Association Constants of Adenylate Kinase with Two Noncovalent Inhibitors"
*J. Am. Soc. Mass Spectrom.*, 2003, **14**, 442-448.

Wendt S, McCombie G, **Daniel JM**, Kienhöfer A, Hilvert D, Zenobi R
"Quantitative Evaluation of Noncovalent Chorismate Mutase-Inhibitor Binding by ESI-MS"
*J. Am. Soc. Mass Spectrom.*, 2003, **14**, 1470-1476.

**Daniel JM**, Ehala S, Friess SD, Zenobi R
"On-line Atmospheric Pressure Matrix-Assisted Laser Desorption / Ionization Mass Spectrometry"
*Analyst*, 2004, **129**, 574-578.

**Daniel JM**, Laiko V, Doroshenko V, Zenobi R
"Flow-injection Liquid Atmospheric Pressure Matrix Assisted Laser Desorption / Ionization"
in preparation.

## Parts of this thesis have been presented as a poster

**Daniel JM**, Zenobi R
"Noncovalent Complexes in ESI Mass Spectrometry: Protein-Ligand Interactions"
4. Igler MS-Tage, Igls (AT), February 8-9th, 2001.

**Daniel JM**, Zenobi R

"Determination of Solution Phase Binding Constants of Adenylate Kinase with Non-covalent Inhibitors by ESI MS"

American Society of Mass Spectrometry meeting, Orlando (USA), June 2-6th, 2002.

**Daniel JM**, Zenobi R

"Determination of the Association Constants of Adenylate Kinase with two Noncovalent Inhibitors by ESI-MS"

5. Igler MS-Tage, Igls (AT), February 20-21th, 2003

**Daniel JM**, Ehala S, Zenobi R

"A new Strategy for On-line Coupling of Liquid Chromatography with MALDI Mass Spectrometry by using Atmospheric Pressure Ionization"

International Mass Spectrometry Conference, Edinburgh (GB), September 1-5th, 2003

## Patents

Ørsnes H, Zenobi R, **Daniel JM**, Atmospheric-pressure ionization device and method for analysis of a sample, 2002, Europ. Patent EP1193730.

# Table of Contents

## Summary

The present thesis is divided into three main topics: instrumentation development, application of electrospray ionization (ESI) mass spectrometery (MS) to measure noncovalent interactions, and design of coupling approaches for atmospheric pressure matrix-assisted laser desorption / ionization (AP-MALDI) and atmospheric pressure ionization from solution (AP-IRIS).

At the starting point of the present thesis, our in-house time-of-flight mass spectrometer exhibited rather low sensitivity and showed several artifacts. The source for the artifacts was identified and could be eliminated using different approaches. The sensitivity of the instrument was improved enormously. In order to compare different variants of electrospray, a nano electrospray source was built and successfully applied to measure proteins.

Noncovalent interactions play an important role in biochemistry; many processes in biology are controlled by noncovalent complexes, *e.g.* protein structure, drug - receptor interactions, and DNA base pairing. Different approaches and possibilities, already employed by different research groups, are introduced. The interaction strength of adenylate kinase with the two inhibitors $P^1$,$P^4$-di(adenosine-5')tetraphosphate and $P^1$,$P^5$-di(adenosine-5') pentaphosphate was determined. Because the addition of the inhibitors reduces the total ionization efficiency, the analysis method is based on the relative intensities of the bare protein and the corresponding complex. It is thus independent from the total ionization efficiency. Going from smaller proteins to bigger ones, the width of the mass signals for the protein and its complexes gets broader preventing the mass resolution of the bare protein and its complex. We have thus developed a method where the bare protein signal and the signal of its complexes do not need to be fully resolved. As a proof-of-principle, the interaction strength of chorismate mutase with a transition state analogue inhibitor was determined.

Coupling continuous flow separation techniques to MALDI MS has been a challenge for a long time and a lot of approaches have emerged. Using the benefit of AP-

MALDI, *i.e.* the sample must not be vacuum stable, a novel coupling approach is presented based on liquid samples containing co-dissolved matrices. The applicability of the proposed method is shown for different classes of compounds, *i.e.* peptides, proteins, and polymers. The upper mass limit of 13'000 Da was defined by instrumental limitations rather than by the desorption / ionization method. Since the effluent of most of the separation methods used for biological samples consists of high fractions of water, the use of water as the matrix for desorption / ionization is beneficial. The characteristics of water employed as a matrix in AP-IRIS MS was investigated. A novel coupling approach, based on single droplet AP-IRIS, is introduced and the principle is proven. The limit of detection for this method is yet not sufficient and will need further improvement.

In conclusion, the present thesis shows that new experimental methods can largely depend on instrumentation modification. Building new devices and/or setup designs for mass spectrometric analysis may not be trivial, however, crucial for successfully applying the personal research ideas.

## Zusammenfassung

Die vorliegende Doktorarbeit ist in drei Schwerpunkte aufgegliedert: instrumentelle Entwicklungen, Anwendung von Elektrospray Ionisierung Massenspektrometrie (MS) zur Bestimmung von nichtkovalenten Wechselwirkungen, und Planung und Entwicklung von Methoden zur Kopplung von Flüssigchromatographie mit Matrix-unterstützter Laser Desoption / Ionisation (MALDI) bei Atmosphärendruck (AP-MALDI) und mit Infrarot Laser Desorption aus Lösung bei Atmosphärendruck (AP-IRIS).

Zu Beginn der vorliegenden Doktorarbeit besass das Flugzeitmassenspektrometer eine limitierte Empfindlichkeit und für jedes Massensignal wurden kleine Artefaktsignale beobachtet. Die Quellen dieser Artefaktsignale konnten lokalisiert werden und wurden durch verschiedene Ansätze letztlich unterbunden, gleichzeitig konnte die Empfindlichkeit enorm gesteigert werden. Um eine Auswahl an verschiedenen Elektrospray-Varianten zur Verfügung zu haben, wurde eine Nanoelektrosprayquelle gebaut, mit welcher erfolgreich Proteine gemessen werden konnten.

Nichtkovalente Wechselwirkungen gehören in der Biologie zu den wichtigsten Wechselwirkungen. Viele biochemische Prozesse werden durch nichtkovalente Komplexe gesteuert: Proteinstrukturen, Medikament-Rezeptor Wechselwirkungen, oder beispielsweise DNA Basenpaarung. Es wurden bereits verschiedene Möglichkeiten erforscht, nichtkovalente Wechselwirkungen mit Hilfe von Massenspektrometrie zu bestimmen; diese werden vorgestellt. Neu werden die Komplexbildungskonstante der nichtkovalenten Komplexe von Adenylate Kinase mit den Inhibitoren $P^1$,$P^4$-di(adenosine-5')tetraphosphat und $P^1$,$P^5$-di(adenosine-5') pentaphosphat mit Hilfe der Massenspektrometrie bestimmt. Da das Hinzufügen der Inhibitoren die Gesamtintensität der erhaltenen Spektren negativ beeinflusste, wurde eine Methode erarbeitet, die nur auf dem Verhältnis der Integrale des reinen Proteins und des entsprechenden Komplexes aufbaut und damit von der totalen Signalintensität unabhängig wird. Bei der Messung grösserer Proteine beobachtet man eine starke Verbreiterung der Signale durch unspezifische Anlagerung von Lösungsmittel- und Puffermolekülen. Dadurch kann das reine Protein und sein Komplex mit einem klei-

neren Molekül nicht mehr massen-aufgelöst werden. Die Stärke der nichtkovalenten Wechselwirkung von Chorismate Mutase mit einem Übergangszustandsanalogon wurde mit einer Methode bestimmt, die die Auflösung der Signale des reinen Proteins und des Komplexes nicht mehr voraussetzt.

Die Kopplung zwischen Flüssigkeitschromatographie und Matrix-unterstützter Desorption / Ionisierung stellt seit längerer Zeit eine Herausforderung dar und verschiedene Lösungsansätze wurden bereits präsentiert. Ein neuer Lösungsansatz wird hier vorgestellt, welcher den Vorteil der Matrix-unterstützten Desorption / Ionisierung unter Atmosphärendruck ausnützt, dass die Proben nicht vakuumstabil sein müssen. Der Analyt wird zu einer Lösung von Matrix zugegeben und direkt aus der Lösung desorbiert. Das Funktionieren dieses Lösungsansatzes konnte für verschiedene Klassen von Analyten, z. B. Peptiden, Proteinen und Polymeren, gezeigt werden. Die experimentell bestimmte obere Massengrenze von 13'000 Da wurde durch instrumentelle Parameter begrenzt und nicht durch die Methode. Da die Elutionsmittel für Flüssigchromatographie bei biologischen Proben meist einen hohen Wasseranteil besitzen, ist es von Vorteil, Wasser als Matrix zu verwenden. Die Eigenschaften von Wasser als Matrix in AP-IRIS wurden untersucht. Eine neue Kopplungsmethode, basierend auf der Desorption von einzelnen Tropfen, wurde entwickelt und dessen Funktionieren wurde bewiesen; allerdings ist die Empfindlichkeit noch ungenügend und muss künftig noch verbessert werden.

Zusammenfassend zeigt die vorliegende Arbeit, wie wichtig Geräte-spezifische Modifikationen für massenspektrometrische Messungen sein können. Das Überarbeiten von bestehenden Bauteilen oder gar ein Neu-Design mögen zwar ein manchmal schwerlicher Weg sein, dies ist aber letztlich der einzige erfolgsversprechende Ansatz für neue Forschungsergebnisse.

## List of Abbreviations

| | |
|---|---|
| AC | alternating current |
| A/D | analog / digital |
| AK | adenylate kinase |
| AP | atmospheric pressure |
| AP-MALDI | atmospheric pressure matrix-assisted laser desorption / ionization |
| BCA | bovine carbonic anhydrase |
| BIRD | blackbody infrared radiative dissociation |
| BSA | bovine serum albumin |
| BsCM | chorismate mutase from bacillus subtilis |
| CD | circular dichroism |
| CE | capillary electrophoresis |
| CI | chemical ionization |
| CID | collision induced dissociation |
| CM | chorismate mutase |
| CS | citrate synthase |
| CSD | charge state distribution |
| Da | Dalton, unit of mass, 1 Da = $1.657 \times 10^{-24}$ g |
| DC | direct current |
| DIOS | desorption / ionization on silicon |
| EDTA | ethylenediamine tetraacetic acid |
| EHMS | electrohydrodynamic mass spectrometry |
| EI | electron impact ionization |
| EM | electron multiplier |
| ESI | electrospray ionization |

| | |
|---|---|
| FAB | fast atom bombardment |
| FT | Fourier-transform |
| FWHM | full width at half maximum |
| HCCA | α-cyano-4-hydroxycinnamic acid |
| HCD | heated capillary dissociation |
| ICR | ion cyclotron resonance |
| i.d. | inner diameter |
| IRIS | infrared ionization from solution |
| $K_a$ | association constant, $K_a=K_d^{-1}$ |
| $K_d$ | dissociation constant, $K_d = K_a^{-1}$ |
| kV | kilovolt |
| LASER | light amplification by stimulated emission of radiation |
| LC | liquid chromatography |
| M | molar, M = mol· $l^{-1}$ |
| MALDI | matrix assisted laser desorption / ionization |
| MCP | multi channel plate |
| MS | mass spectrometry |
| m/z | mass-to-charge ratio |
| nanoESI | nanoelectrospray ionization |
| NMR | nuclear magnetic resonance |
| o.d. | outer diameter |
| ROBIN | rotating ball inlet |
| S/N | signal-to-noise ratio |
| slm | $l \cdot min^{-1}$ at 25 °C and 1 bar |
| TOF | time of flight |

| | |
|---|---|
| UV | ultraviolet |
| V | Volt |
| VC | cone voltage |
| $VC_{50}$ | cone voltage driven dissociation |
| vdW | van der Waals |
| YAG | Yttrium-Aluminium-Garnet |

# CHAPTER 1

# INTRODUCTION

Seite Leer /
Blank leaf

Mass spectrometry determines the mass-to-charge (m/z) ratio of atoms, molecules or assemblies of molecules. A prerequisite for a successful measurement of the mass of a species is the ionization of the latter, and their successful transfer into gas phase. Once the conditions are fulfilled, the different masses are separated by magnetic and electric fields in vacuum and detected by different kind of detectors.

Nowadays, mass spectrometry is employed in a wide range of applications and research in industry as well as in academia. The applications covers elemental analysis, analysis of small organic and inorganic compounds, detection in gas chromatography (GC) as well as in liquid chromatography (LC), and thanks to the soft ionization methods, the detection of high mass biomolecules and of non-covalent assemblies.

The present chapter introduces some of the most important developments, concepts, and principles. Its is by far not complete, but covers all necessary basics for a comprehensive reading of the following chapters.

## 1.1 Motivation

With the development of pulsed ionization techniques and fast electronic devices, time-of-flight mass spectrometry gained more and more attention. The challenge to fully understand the technique and the ability to optimize mass spectrometric instruments deeply appealed to me. The work with mass spectrometers did not only provoke a profound technical understanding but also resulted in enforced practical skills. The real driving force was entering new research fields, such as the analysis of non-covalent complexes by mass spectrometry. It is intriguing to obtain results by means of own methods that are comparable with results obtained by well established methods. Also the possibility to design new ionization sources and to practically implement these did motivate me enormously. To see the own ideas and concepts growing and ending up in yielding results, acquired by own developments, is definitively the best motivation in science.

## 1.2 Historical Development and Trends in Mass Spectrometry

This year, mass spectrometry (MS) is celebrating its 100 year anniversary, a surprisingly old technology. The improvements started very slowly but after World War II the interest in mass spectrometric methods increased and thus the research was intensified leading to new spectrometers and ionization methods. Soon, MS became a key method for the investigation of inorganic and organic compounds, and later on also in biological applications.

### The First Mass Spectrometer

The experiments leading to the discovery of the first ionization source and to the invention of the mass spectrometer were performed by the German physicist Eugen Goldstein. In 1886, he discovered the *Kanalstrahlen* (*"canal rays"*). By passing an electric discharge through a gas at low pressure in a glas tube equipped with a perforated cathode, canal rays are produced. It has been shown that canal rays consist of positively charged particles. In 1898, Wilhelm Wien showed that these particles can be deflected by strong electric and magnetic fields [1]. He observed that particles with different charge-to-mass (e/m) ratio followed different parabolic curves. Fascinated by Wien's experimental results, J. J. Thomson began his own studies of Goldstein's canal rays in 1905. By reducing the pressure in the glas tube, he could achieve sharp parabolic curves for different ions. By replacing the photographic plate (used so far for detection) with electric plates, the first mass spectrometer was born. In the following years, mass spectrometry was mainly used to study isotopes.

The equations of ion motion for the parabolic mass spectrometer are expressed in terms of charge-to-mass ratio. Accordingly, data from early instruments were reported in the scientific literature. Only later did physicists and chemists adopt the more physically meaningful unit mass-to-charge (m/z). In recognition of J. J. Thomson's scientific contribution, mass-to-charge ratios are now measured by the unit *Thomson* (Th).

**Instrument Development**

In the early 1940$^{ties}$, most researchers used magnetic deflection instruments of the type introduced by Arthur Dempster [2, 3]. These devices used massive electromagnets and therefore were bulky and expensive. This motivated Alfred Nier in 1940 to develop a new sector mass spectrometer which used smaller magnets based on 60 or 90 degree sectors. Both instrument types were employed in the first commercial mass spectrometers available on the market.

In 1946, a new mass spectrometric technique was introduced [4]. The advances in electronics made it possible to deal with electronic pulses in the time frame of microseconds. Stephens proposed that ions are pulsed every millisecond into a vacuum tube (flight tube). The velocity of ions with different m/z ratios but with the same acceleration energy vary. Their resulting different arrival times can be recorded on an oscillograph and easily photographed. Note that this is the first description of a time-of-flight (TOF) mass spectrometer! In the following years this method was improved by improved design of the ion source and by introducing electrostatic mirrors (reflectron).

Just three years after the first proposal of a TOF mass spectrometer, Hipple, Sommer and Thomas presented mass spectra recorded with a new technique called ion cyclotron resonance (ICR) mass spectrometery [5]. The ions are trapped in a magnetic field and perform a cyclotron trajectory with a frequency depending on their m/z ratio. A uniform rf-electric field of variable frequency accelerates ions of a selected m/z at resonance until they strike the collector and the resulting current is measured. A big disadvantage of this frequency sweep ICR mass spectrometer is the need for scanning over the interesting mass range. In 1974 Comisarow and Marshall employed a fixed-frequency electric field pulse to excite all ions in the ICR cell and a broad-band detection, digitalization of the transient response. The absorption spectrum was produced by Fourier transforming the time response [6]. The Fourier transform ion cyclotron resonance mass spectrometer (FT-ICR) was born.

But this was still not satisfying the current needs. A TOF analyzer needs very fast electronics which was (and still is) very expensive; an ICR mass spectrometer needs a

huge magnet, which is neither cheap nor convenient. In 1953 Paul and Steinwedel proposed a new mass spectrometric method: the quadrupole mass filter (QMS) [7]. The mass filtering is based on the m/z dependence of a stable ion trajectory in a quadrupole field. Today, this is probably the most widely used mass spectrometer type; it is simple, small, does not need very low pressure, and is not very expensive.

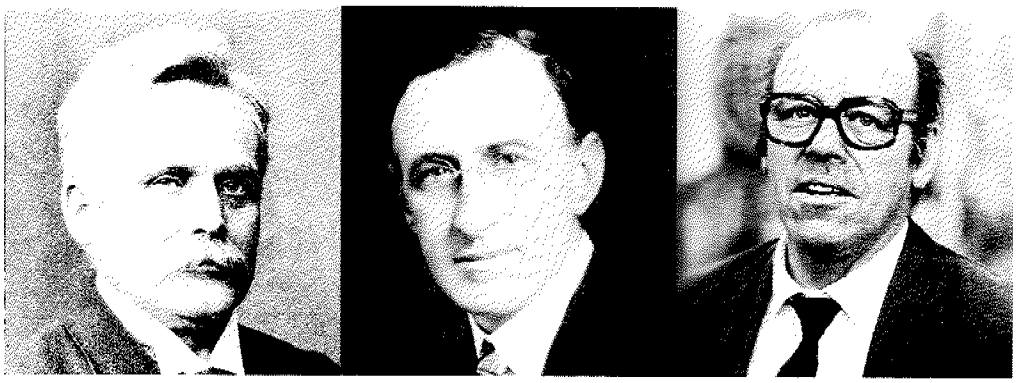

**Figure 1.1: From left to the right: Wilhelm Wien, Arthur Dempster, and Nobel laureate Wolfgang Paul. Reprinted with permission from [8]. Copyright 2002 American Society for Mass Spectrometry.**

### Ionization of Molecules

In all mass spectrometric techniques the m/z ratios are determined which implies that only ions can be measured. Therefore the first step to investigate molecules with mass spectrometry is the ionization of the neutral molecules. Nowadays there are many different ionization methods available depending on the actual molecules to ionize, on degree of fragmentation desired and on selectivity.

The first ionization method, apart from *canal rays*, was presented in 1918 by Dempster [2]. Electrons produced by a heated cathode (filament) were accelerated within an electric field up to an energy of 60-80 eV. The neutral molecules in the gas phase were bombarded by this high energy electrons with the effects that the molecules got a positive charge. This is called electron impact (EI) ionization (figure 1.2). The high impact energy of the electrons and the produced radical cations lead to a high degree of fragmentation of the molecule, eventually leading to structural information and to defined fingerprints for different molecules. Today, the EI ionization is widely used in GC-MS in order to identify and quantify substances.

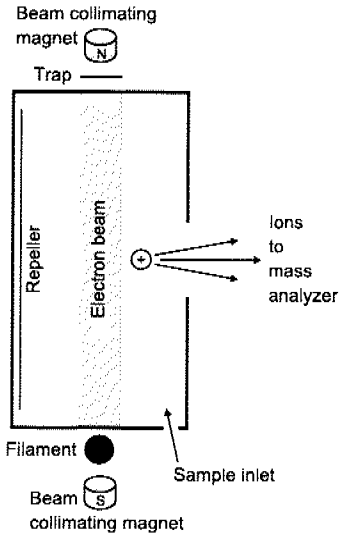


**Figure 1.2: Electron impact ionization source. The typical pressure within the ion source is between $10^{-7}$ and $10^{-5}$ mbar.**

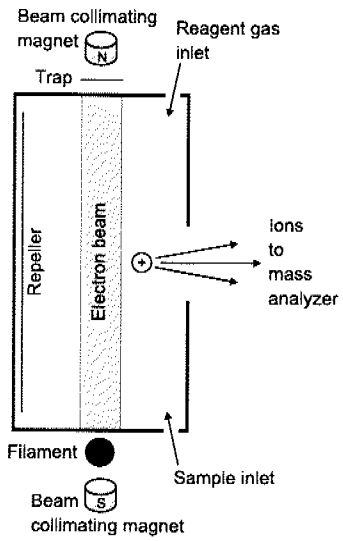


**Figure 1.3: Chemical ionization source. The typical pressure within the ion source is higher than in EI ionization, it is between $10^{-3}$ and 1 mbar.**

The industry, in particular the petroleum industry, requested rather instruments with shorter duty cycles and better sensitivities than the development of alternative ionization methods. Not until 1966, Munson and Field presented the chemical ionization (CI) method [9, 10] (figure 1.3). The source of the mass spectrometer is filled with an auxiliary or "ionization" gas, *e.g.* methane, and with the analyte gas whereas the concentration of the analyte gas is usually 1000 smaller than the concentration of the ionization gas. Under these conditions practically all electrons, generated by an EI source and passing through the gas within the source, will ionize the ionization gas and direct ionization of the analyte gas by electron impact will be negligible. The analyte is mostly soft-ionized by proton transfer reactions of the ionization gas with the analyte gas. The generated mass spectra are very different from those which are produced by conventional EI MS. The parent or quasi-parent ion has a much higher abundance and the degree of fragmentation is much less pronounced. Thus CI is better suited than electron impact ionization for higher molecular weight compounds.

In 1968, Malcom Dole presented the first electrospray ionization (ESI) experiments: he used ESI to generate a beam of polymeric macroions [11, 12]. The resulting ions from

the ESI process were not yet measured by mass spectrometry but rather the ion current was recorded with help of a Faraday plate. The great benefit of spraying and ionizing an analyte by spraying the analyte solution with high electric fields was found much later. In 1984 John Fenn and Masamichi Yamashita began to investigate the technique with mass spectrometry in more detail [13, 14]. They showed that ESI is capable of spraying and ionizing large biomolecules [15]. In 1991, Matthias Wilm and Matthias Mann introduced the nano-electrospray (nanoESI) and showed improvements in detection limits and salt tolerance [16]. In the same year, Bruce Ganem and co-workers published the first mass spectrum of a noncovalent receptor-ligand complex by ESI MS [17]. In the following years, ESI developed to one of the key ionization methods in organic, polymeric and especially bioorganic mass spectrometry.

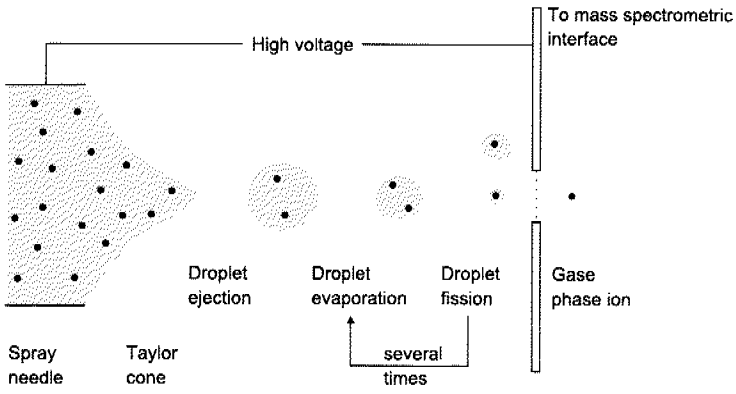


**Figure 1.4: The electrospray process.**

An electrospray is induced by applying a high potential difference between a spray needle and a counter electrode (figure 1.4). This results in a charge polarization and in the formation of a Taylor cone from which small droplets are ejected. The emitted droplets shrink due to solvent evaporation. When the charge repulsion overcomes the surface tension (Rayleigh limit), the droplets undergo a fission process where smaller droplets are generated. This process is repeated several times leading at the end to gas-phase ions.

As the first method to desorb thermolabile and involatile compounds, Barber et al. presented in 1981 the fast atom bombardment (FAB) ionization source for mass spectrometry [18, 19]. Argon gas was ionized by a cold cathode discharge source. The produced argon ions were accelerated onto a surface containing the analyte molecules. The impact of the argon atoms induced the desorption and the ionization of the ana-

lyte. They showed the possibility of investigating peptides, glycoside antibiotics and organometallic compounds [20] by this method.

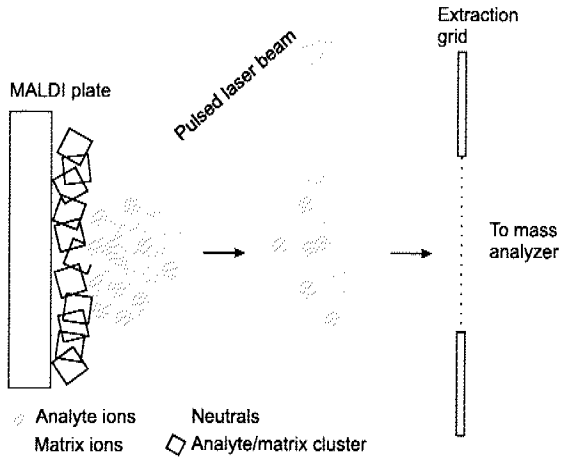


**Figure 1.5: The MALDI process. Please be aware that the neutrals-to-ion ratio is about $10^4$, *i.e.* there are 10'000 times more neutrals than ions.**

Just a few years after the presentation of FAB and ESI for biomolecules, a third ionization method was developed. In 1987, Koichi Tanaka presented the first particle-assisted laser desorption / ionization measurements of proteins up to masses of 34'000 Da [21]. In the following year, Hillenkamp and Karas introduced matrix-assisted laser desorption / ionization (MALDI) (figure 1.5), where an organic matrix instead of particles was employed [22, 23]. In conventional MALDI the analyte and a matrix are co-crystallized on a sample target. The co-crystallized sample is introduced into the high vacuum of a mass spectrometer. By focusing a pulsed UV laser onto the sample, analyte molecules are desorbed and ionized. Unfortunately, the ratio of neutrals-to-ions ejected was found to be in the order of $10^4$ [24], limiting the sensitivity of MALDI. MALDI is a soft ionization method, although not as soft as ESI, showing very little fragmentation and high intensity of mainly singly charged the molecular ion. In the year 2000, Victor Laiko discovered that a MALDI source may be effectively operated at atmospheric pressure (AP-MALDI) [25, 26]. The ions produced at atmospheric pressure are guided by a differentially pumped interface into the mass spectrometer. AP-MALDI simplifies the sample handling and is known to be softer [27] in comparison to conventional MALDI. Since the results obtained for non-volatile compounds are better for MALDI and ESI, nowadays, FAB is rarely employed anymore.

Koichi Tanaka and John Fenn were awarded the Nobel-Prize 2002 in chemistry for their contribution to the development and investigation of the two ionization meth-

ods soft laser desorption / ionization and ESI and their application in the field of biochemistry.

Some ionization methods such as field desorption (FD), plasma desorption (PD), inductively coupled plasma (ICP) and others are not mentioned here. The description of all ionization methods would go far beyond the scope of this introduction.

**Trends in Mass Spectrometry**

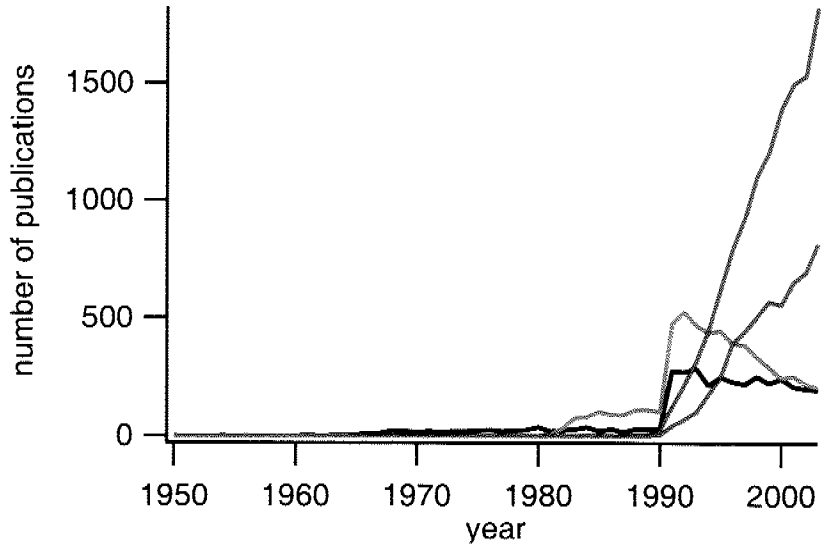


**Figure 1.6: Number of publications per year using ESI (blue), MALDI (green), FAB (red) and EI (black) as ionization methods in the experiments.**

With help of a literature search, the trends of mass spectrometry mainly concerning the used ionization methods are elucidated. To obtain the number of publications for a specific method, the *ISI Web of Science Database* has been searched with specific keywords for the corresponding ionization method as summarized in table 1.1. The enquiry is not complete and there are several papers that do not state the ionization method used for the MS experiments, especially in GC-MS work. But nevertheless the data obtained allow to show some trends in MS ionization methods and MS in general (figure 1.6).

| | Search String |
|---|---|
| **ESI** | electrospray AND (Mass OR Ion* OR spectrometry) |
| **MALDI** | MALDI OR (matrix AND Laser AND desorption AND (ion* OR mass spectrometry)) |
| **FAB** | ((fast AND atom AND bombardment) OR FAB) AND (mass OR ion* OR spectrometry) |
| **EI** | ((electron impact) OR EI) AND (mass spectrometry OR (ion* AND mass)) |

**Table 1.1: Used search strings to obtain the number of publication using a specific ionization method.**

As already mentioned in the historical paragraph the interest in different ionization methods evolved rather late (around the mid sixties) in the development of mass spectrometry. New ionization methods stimulated the use of mass spectrometers for novel scientific and industrial applications. The development of FAB in the beginning of the eighties caused an increase in total publications. The real boost for mass spectrometry, however, came with the invention of the two major soft ionization methods ESI and MALDI. This opened an absolutely new field: the use of MS in biochemistry. Since then, there is a real boom in MS indicated by the fact that nowadays almost every better laboratory has its own mass spectrometers. The influence of the first soft ionization method, FAB, is decreasing rapidly whereas publications with ESI and MALDI are still increasing. Publications using electron impact ionization are remaining more or less constant indicating that this ionization technique still is and will be further employed.

## 1.3 References


1. W. Wien, *Ann. Physik*, 1898, **65**, 440.
2. A. J. Dempster, *Phys. Rev.*, 1918, **11** (4), 316-325.
3. H. W. Washburn, H. F. Wiley and S. M. Rock, *Ind. Eng. Chem. Anal. Ed.*, 1943, **15** (9), 541-547.
4. W. E. Stephens, *Phys. Rev.*, 1946, **69** (11-12), 691-691.
5. J. A. Hipple, H. Sommer and H. A. Thomas, *Phys. Rev.*, 1949, **76**, 1877-1878.
6. M. B. Comisarow and A. G. Marshall, *Chem. Phys. Lett.*, 1974, **25** (2), 282-283.
7. W. Paul and H. Steinwedel, *Z. Naturforsch. Sect. A*, 1953, **8** (7), 448-450.
8. M. A. Grayson, *Measuring Mass: From Positive Rays to Proteins*, 2002, Santa Fe, American Society of Mass Spectrometry.
9. M. S. B. Munson and F. H. Field, *J. Am. Chem. Soc.*, 1966, **88** (19), 4337-4345.
10. M. S. B. Munson and F. H. Field, *J. Am. Chem. Soc.*, 1966, **88** (12), 2621-2630.
11. L. L. Mack, P. Kralik, A. Rheude and M. Dole, *J. Chem. Phys.*, 1970, **52** (10), 4977-4986.
12. M. Dole, L. L. Mack and R. L. Hines, *J. Chem. Phys.*, 1968, **49** (5), 2240-2249.
13. M. Yamashita and J. B. Fenn, *J. Phys. Chem.*, 1984, **88** (20), 4451-4459.
14. M. Yamashita and J. B. Fenn, *J. Phys. Chem.*, 1984, **88** (20), 4671-4675.
15. J. B. Fenn, M. Mann, C. K. Meng, S. F. Wong and C. M. Whitehouse, *Science*, 1989, **246** (4926), 64-71.
16. M. S. Wilm and M. Mann, *Int. J. Mass Spectrom. Ion Proc.*, 1994, **136**, 167-180.
17. B. Ganem, Y. T. Li and J. D. Henion, *J. Am. Chem. Soc.*, 1991, **113**, 6294-6296.
18. M. Barber, R. S. Bordoli, R. D. Sedgwick, A. N. Tyler and B. W. Bycroft, *Biochem. Biophys. Res. Commun.*, 1981, **101** (2), 632-638.
19. H. R. Morris and M. Panico, *Biochem. Biophys. Res. Commun.*, 1981, **101** (2), 623-631.
20. M. Barber, R. S. Bordoli, R. D. Sedgwick and A. N. Tyler, *Nature*, 1981, **293** (5830), 270-275.
21. K. Tanaka, Y. Ido, S. Akita, Y. Yoshida and T. Yoshida. *Laser desorption of Proteins up to 34'000 by MALDI*, in *Second Japan-China Symposium on Mass Spectrometry*, 1987, Takarazuka Hotal, Osaka, Japan.

22. M. Karas, D. Bachmann, U. Bahr and F. Hillenkamp, *Int. J. Mass Spectrom. Ion Proc.*, 1987, **78**, 53-68.
23. M. Karas and F. Hillenkamp, *Anal. Chem.*, 1988, **60**, 2299-2301.
24. C. D. Mowry and M. V. Johnston, *Rapid Commun. Mass Spectrom.*, 1993, **7**, 569-575.
25. V. V. Laiko, S. C. Moyer and R. J. Cotter, *Anal. Chem.*, 2000, **72** (21), 5239-5243.
26. V. V. Laiko, M. A. Baldwin and A. L. Burlingame, *Anal. Chem.*, 2000, **72** (4), 652-657.
27. J. L. Wolfender, F. X. Chu, H. Ball, F. Wolfender, M. Fainzilber, M. A. Baldwin and A. L. Burlingame, *J. Mass Spectrom.*, 1999, **34** (4), 447-454.

# CHAPTER 2

# TIME-OF-FLIGHT MASS SPECTROMETRY

Seite Leer /
Blank leaf

Time-of-flight mass spectrometry (TOF-MS) is deceptively simple in concept; a packet of ions with the same kinetic energy drift through an evacuated, field-free tube and arrive at a detector in the order of their mass-to-charge ratios. The detector output current, measured as a function of time, can easily be converted into a mass spectrum. The physics as well as the instrumentation are both remarkably straightforward. In this section, the basic principles and designs for TOF mass spectrometers are introduced. The mass spectrometer used for the experiments is explained in detail and the improvements implemented in the spectrometer are illustrated. The ionization sources used for electrospray ionization measurements are explained including a home made nano electrospray ionization source.

## 2.1 Time-of-flight Mass Spectrometry

### Introduction

The simplest time-of-flight mass spectrometer consists of a short extraction region (usually on the order of a few centimeters), a drift region, and a detector (figure 2.1), all being kept under vacuum. In the source region, the electrical field is usually defined by a voltage placed on the source backing plate and is used to accelerate ions to constant kinetic energy.

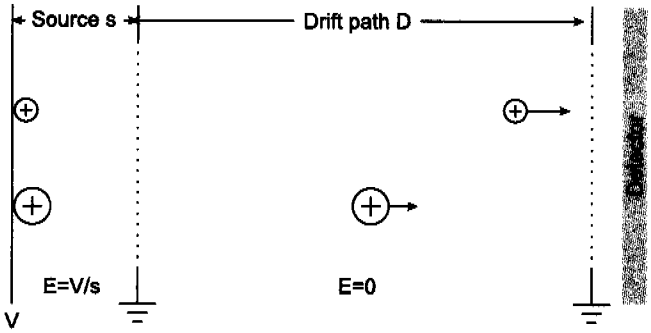


**Figure 2.1: A simple TOF mass spectrometer consisting of a source region s, a drift tube D, and detector.**

Ions may be formed in the gas phase (*e.g.* by electron impact or multiphoton ionization) or directly on the backing plate (*e.g.* by matrix-assisted laser desorption / ionization). If the ions are generated at the backing plate, they are accelerated throughout the entire source-extraction region to the same final kinetic energy and the corresponding velocity (equation 2.1).

$$\frac{m \cdot v^2}{2} = e \cdot V \qquad \text{(Eq 2.1)}$$

| | |
|---|---|
| *m* | *mass of the ion* |
| *v* | *velocity of the ion* |
| *e* | *charge of the electron* |
| *V* | *potential difference the ion is travelling through* |

The resulting flight time of the ions thus depend on the square root of their masses (equation. 2.2).

$$t = \sqrt{\frac{m}{2 \cdot e \cdot V}} \cdot D \qquad \text{(Eq 2.2)}$$

$t$ *flight time*

$D$ *drift length*

Mass resolution in a mass spectrometer is defined as m/Δm. In a TOF mass spectrometer in which ions are accelerated to constant energy its dependence on time resolution can be derived as follows:

$$m = \left(\frac{2 \cdot e \cdot V}{D^2}\right) \cdot t^2 \qquad \text{(Eq 2.3)}$$

$$\Delta m = \frac{dm}{dt} \cdot \Delta t = \left(\frac{2 \cdot e \cdot V}{D^2}\right) \cdot 2 \cdot t \cdot \Delta t \qquad \text{(Eq 2.4)}$$

$$\frac{m}{\Delta m} = \frac{t}{2 \cdot \Delta t} \qquad \text{(Eq 2.5)}$$

$\Delta m$ *full width at half-maximum (FWHM) of the mass signal*

$\Delta t$ *FWHM of the time signal*

Thus, mass resolution depends on time resolution and therefore upon laser pulse width, detector response, recorder bandwidths and digitizing rates.

### Time, Space, and Energy Distributions

From the very beginning, TOF mass spectrometers were known as low resolution instruments. Besides the specifications of the detector and digitizer, the spread in time-of-flight reflects many properties of the ion in addition to its mass, including uncertainties in the time of formation, its initial location in the extraction field, its initial kinetic energy, and metastable fragmentation. All these factors contribute to an overall low mass resolution.

Temporal distributions include actual distribution in the time of ion formation as well as limitations of ion detection and time-recording devices. Distribution in the time of ion formation results in a constant time difference ($\Delta t$) which remains constant as the ions approach the detector. Because the mass resolution is given by $t/2\Delta t$, the resolution can be enhanced by increasing the length of the flight tube. The same holds true

for time distributions arising from laser pulse width, detector response, and recording bandwidth and digitizing rates. An early method to correct for distributions in time of ion formations has been demonstrated by Wiley and McLaren [1]. The ions were formed in a field-free source region and then extracted by a drawout pulse with a rise time of only 40 ns (*time lag focusing*). By using an extraction pulse it is also possible to couple a TOF instrument with a continuous ion source (*i.e.* electrospray ionization, electron impact ionization).

When the ions are produced within the source, they are formed with some initial kinetic energy ($U_0$) leading to an initial kinetic energy distribution. But only the initial kinetic energy along the time-of-flight axis influences the arrival times (equation. 2.6).

$$t = \sqrt{\frac{m}{2 \cdot (e \cdot V + U_0)}} \cdot D \qquad \text{(Eq 2.6)}$$

$U_0$ *initial kinetic energy along the flight path*

Ions with initial velocities in direction of the flight tube will arrive sooner at the detector than those with no initial velocity, resulting in fronting of the mass spectral peak towards the low-mass side. It is also possible that initial velocities for some ions are directed away from the flight tube. These ions turn around in the source and exit the source with the same energy as the ions with the initial velocity in direction of the flight tube but with a constant time difference Δt (turn-around time). Arriving later at

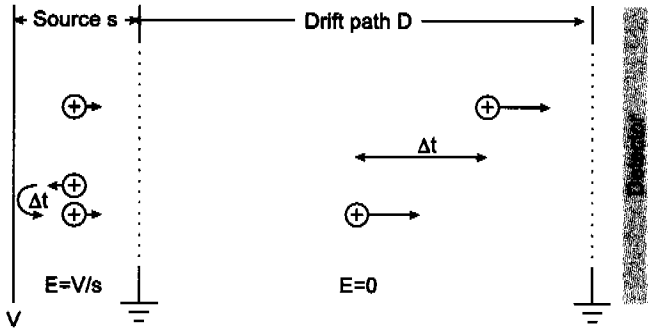


**Figure 2.2: Scheme demonstrating the effect of ions with initial velocities in the opposite direction of the flight tube.**

the detector, they contribute to a tailing of the mass spectral peak towards the high-mass side of the peak. The effect of the turn-around time can be reduced by longer flight distances and thus longer flight times. The effect of initial kinetic energy spreading are in general reduced by higher acceleration voltages, that is by making $eV >> U_0$.

Ions formed at different regions in the source (spatial distribution) will be accelerated through different distances in the extraction fields leading to a distribution of the final kinetic energies. The ions closer to the exit of the source leave the source sooner but have lower kinetic energies and thus arrive later at the detector. This distribution is more pronounced in methods where the ions are formed in the gas phase (*i.e.* photo-ionization) than in methods where the ions are desorbed from a surface (*i.e.* MALDI). The higher energy ions will catch up with the slower ions in the *space-time focal plane.* The space-time focal plane is located in the drift tube at the point at which ions have spent the same amount of time in the extraction and drift regions. The location of the plane is independent of mass but is not exactly a plane but rather has also an expansion in direction of the flight path. The location of the space-time focal plane can be calculated according to equation 2.7 [2].

$$d = 2 \cdot \sqrt{s^2 + s \cdot \Delta s} \cong 2 \cdot s \qquad \text{(Eq 2.7)}$$

*d* distance of the space-time focal plane in the flight tube

*s* distance in the source from the flight tube of the first ion

*Δs* difference of acceleration length for the second ion relative to the first one

**Dual-stage Extraction**

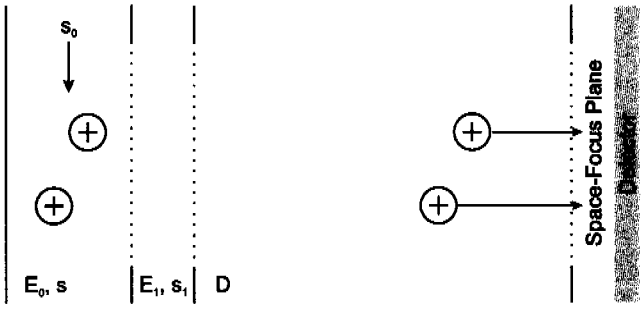


**Figure 2.3: Principle of a dual-stage extraction. The distance d to the space-time focal plane can be varied by choosing the potentials $E_0$ and $E_1$ properly.**

Because the space-time focal plane is independent of mass, ions with different masses are focused at the plane at different time. However, mass dispersion at this short distance from the source is usually not sufficient to allow the location of the detector at this point. By using a *dual-stage extraction* [1], the space-time focus can be moved to a plane much further away from the source. The distance d of the space-time focal plane can be calculated according to equation 2.8.

$$d = 2 \cdot \sigma^{3/2}\left[\frac{1}{s_0^{1/2}} - \frac{2 \cdot s_1}{s_0^{1/2} \cdot (\sigma^{1/2} + s_0^{1/2})^2}\right] \qquad \text{(Eq 2.8)}$$

with $\sigma = s_0 + \frac{E_1}{E_0} \cdot s_1$

$d$ *distance of the space-time focal plane in the flight tube*

$s_0$ *distance of the ions in the first extraction stage*

$s_1$ *length of the second extraction stage*

$E_0$ *first extraction field*

$E_1$ *second extraction field*

In instruments with dual-stage extraction, the second extraction field ($E_1$) is generally much larger than the first ($E_0$), with larger ratios of $E_1/E_0$ moving the space-time focal plane further from the source. For arbitrary combinations of extraction fields, the space-time focal plane will be of first-order, which is sufficient to focus ions with a minimum initial spatial distribution. However, dual-stage extraction configuration can be designed to produce a second order space-time focal plane [3, 4] in order to improve focusing and accommodate broader initial spatial distributions. Thus, the second-order space-time focal plane is more appropriately used as the focal point for a reflectron (where initial spatial distribution has been converted to a kinetic energy distribution), than as a location for a detector.

### Energy Focusing with Reflectrons

An important invention in the field of energy focusing is the reflectron [5, 6]. Its most characteristic feature is an ion mirror consisting of one (*single-stage*) or two (*dual-stage*) electric fields. Consider a space focus of an ion source as a start point for the flight of ions of one distinct mass, with no spatial or temporal distributions, but with different kinetic energies. After the drift length, the ions with higher kinetic energy enter the ion mirror first, followed by those with lower kinetic energy. While the former penetrate deeper into the reflecting field than the latter, they exhibit in a longer residence time within the reflector than the lower energy ions. By choosing the appropriate potentials and geometry, the shorter flight time of high energy ions in the field-free drift region is compensated for by their longer residence time within the reflector.

### Orthogonal Extraction

As a pulsed technique, matrix-assisted laser desorption / ionization is easily compatible with time-of-flight mass spectrometry and has been responsible for renewed interest and active development in the field. In contrast, electrospray ionization is a continuous ionization technique that, like electron impact, chemical ionization, and fast atom bombardment is more compatible with scanning instruments such as quadrupole and sector mass spectrometers. Furthermore, the ions generated by ESI are multiply charged and have a wide energy spread. Therefore the approach of orthogonal extraction, where the initial kinetic energy spread is orthogonal to the flight direction, leads to much better resolution as pulsed extraction techniques [1]. Dawson and Guilhaus [7] showed the advantages of orthogonal extraction, improvement of both duty cycle and resolution, for an electron impact mass spectrometer and Dodonov et al. [8] reported the first orthogonal extraction ESI TOF mass spectrometer.

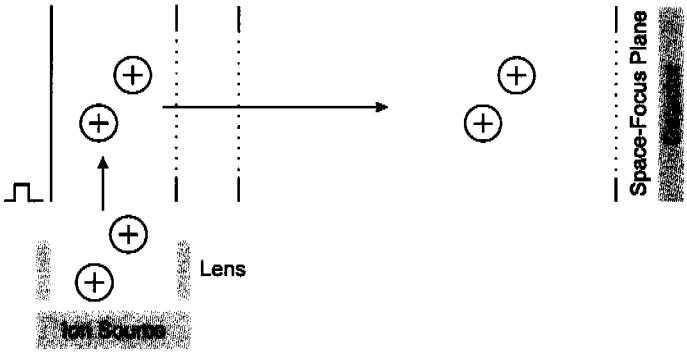


**Figure 2.4: Principle of orthogonal extraction: after ions are generated within the ion source, they are collimated by a lens and orthogonally accelerated into the flight-tube by a pulsed electric field.**

### Detectors

After the ions have travelled along the flight path, they will reach the detector. The detector registers the ion impact on its active surface and converts it into an electric signal. Response and dead time of the detector are key figures which significantly influence the resolution and sensitivity of the mass spectrometer. Most of the available detectors exhibit a mass dependent sensitivity that is reduced with increasing mass-to-charge ratio of the detected ions. An exception is the cryo tunnel junction detectors [9] which shows equal sensitivity throughout the whole mass range and additionally is able to measure the energy of the arriving ions. This opens the possibility to determine the charge state of the arriving ions according to their energy. Thus it

is possible to distinguish between singly and multiply charged ions with the same m/z ratio.

There are two major kinds of detectors employed in mass spectrometry: electron multipliers (EM) end microchannel plate (MCP).

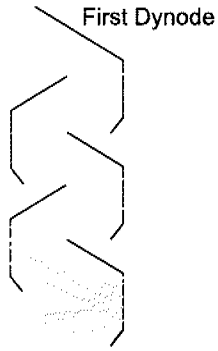


**Figure 2.5: Principle of an electron multiplier. The arriving ion is hitting the first dynode (conversion dynode) and produces secondary electrons. These electrons are accelerated and amplified by the following dynodes leading to a strong output current for a signal.**

In a electron multiplier, the ion is hitting an active surface causing the emission of secondary electrons. These secondary electrons are then amplified in a cascade of electrodes, each producing more than one electron per impact. This results in an avalanche of electrons leading in the output of an electric current signal.

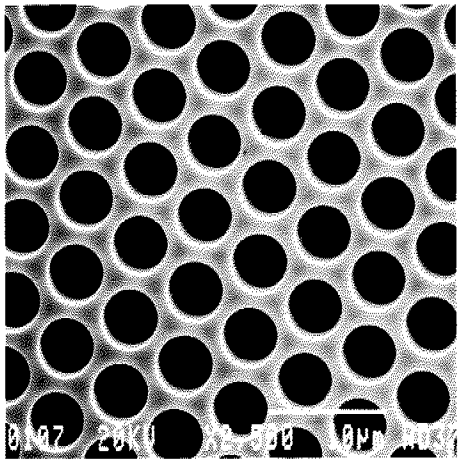

**Figure 2.6: SEM-image of the channels of a MCP detector. The diameter of one channel is approximately 4-5 μm. Reprinted from [10].**

The microchannel plate detector [11] consists of a large array of channels ($5.5 \cdot 10^5$ channels in a 25 mm diameter MCP). Each channel can detect one ion at a time. If an ion hits a channel, some electrons are emitted. These electrons hit again the wall of the channel several times leading to an electron avalanche and to an electric signal at the end of the channel. The MCP consists of many small detectors whereas the EM detec-

tor consists of one large detector. The dead time of one channel is much larger than the dead time of an EM detector. But since the MCP detector consists of many channels this usually does not influence the sensitivity of the detector. Because of the faster rise time of the MCP detectors, there are nowadays more MCP detectors used in time-of-flight mass spectrometry than electron multipliers.

| | EM (ETP 14824) | MCP (Burle) |
|---|---|---|
| Pulse width (FWHM) | 4.5 ns | 350 ps |
| Recovery time | <30 ns | ms for a channel |
| Maximum pulse amplitude | 500 mV into 50 Ω | N/A |
| Maximum output current sustained | 5 μA | N/A |
| Dark count | 3 counts $min^{-1}$ | 5 counts $min^{-1}$ |

**Table 2.1: Specifications for typical EM and MCP detectors.**

## 2.2 Time-of-Flight Mass Spectrometer

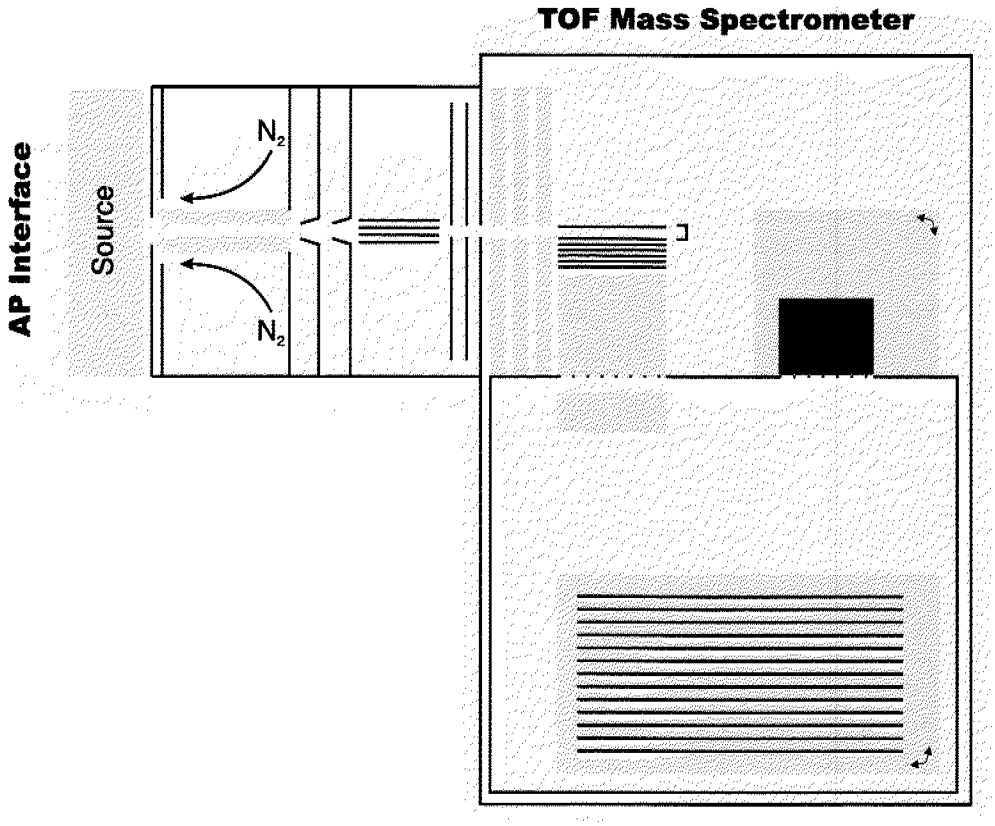


**Figure 2.7: Schematic representation of the time-of-flight mass spectrometer used for ESI and AP-MALDI experiments. It consists of an atmospheric pressure interface, guiding the ions from atmospheric pressure to the high vacuum, and of the TOF main chamber where the ions are separated according to their m/z ratios. For a detailed explanation, see the text.**

The time-of-flight instrument used for electrospray (ESI) and for atmospheric pressure MALDI (AP-MALDI) experiments (figure 2.7) is a α-prototype instrument from Agilent (USA). It can be divided into four major parts: an ionization source, the atmospheric pressure (AP) interface, the time-of-flight mass analyzer, and the signal processing unit. The ionization source is separately discussed later on, the other three parts are described in the following paragraphs.

### Atmospheric Pressure Interface

The main function of the AP interface is the transport of the ions, generated at atmospheric pressure (*e.g.* by ESI, AP-MALDI, API), into the high vacuum in the mass ana-

lyzer. However, in order to achieve good mass resolution and good sensitivity in the mass analyzer, the ions leaving the AP interface must be collimated and need to have a defined kinetic energy.

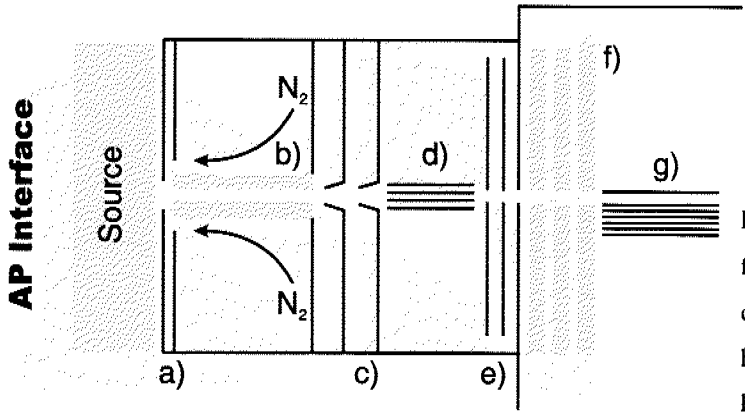


**Figure 2.8: Details of the AP interface: a) inlet, b) heatable transfer capillary, c) skimmers, d) rf-only hexapole, e) einzel lens, f) Einzel lens, g) orthogonal injection.**

The following description of the ion flight path refers to figure 2.8. After the ions are generated by the corresponding ion source, they are guided by electric fields through a countercurrent of nitrogen heated to between 100 - 350 °C and with a flow rate of 0 - 4 slm into the heated transfer capillary (100 - 350 °C) and from there into the first vacuum stage (p = 1 Torr). Flying through the transfer capillary, the ions are decelerated to lower kinetic energies. Thereafter, the ions are accelerated through the second vacuum stage ($p=8 \cdot 10^{-3}$ Torr) into the third one. The vacuum stages one, two and three are separated by two skimmers. The third vacuum stage ($P = 1.3 \cdot 10^{-3}$ Torr) consists of a rf-only hexapole and of three apertures defining an einzel lens.

The mean free path for ions in the hexapole can be calculated according to Maxwell [12]. Assuming a temperature of T = 20 °C = 293.15 K, a pressure of $p = 1 \cdot 10^{-3}$ Torr and the collision cross section of the small peptide LIVTQTMK (933.2 Da, $\sigma = 2.44$ nm$^2$) [15], the mean free path in the hexapole is 8.8 mm. Note that the ions oscillate in the hexapole and therefore the effective travelling distance in the hexapole is much larger than the length of the hexapole. By the resulting collisions in the hexapole the ions loose energy and the ion beam is collimated in the hexapole (*collisional cooling*) improving the resolution of the mass spectra. In our instrument, the hexapole was operated at a frequency of 240 kHz and with an amplitude between 1 and 30 V. The subsequent Einzel lenses focus the ion beam further into the high vacuum chamber

**Einzel Lens**

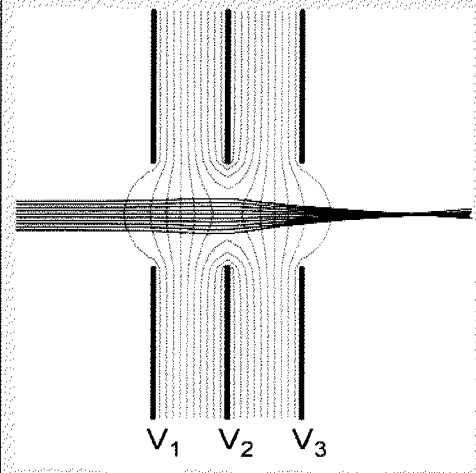


This term refers to a three-element electrostatic lens operated symmetrically, with $V_3$=$V_1$ and with $V_2$ taking any appropriate value. Historically the einzel, or unipotential, lens described a system with $V_2$ held at the potential of the cathode. The major advantage is that the focal properties, depending on voltage ratios, are the same for all values of $V_1$=$V_3$. The disadvantage is that the aberrations of this lens are greater than those of the symmetric lens with $V_2 > V_{1,3}$. The picture shows the equipotential lines (red) for the einzel lens and theoretical ion trajectories (black).

$$L = \frac{0.707}{\pi \cdot d^2 \cdot n} = \frac{0.707 \cdot k \cdot T}{p \cdot \sigma} \qquad \text{(Eq 2.9)}$$

| | |
|---|---|
| $L$ | *mean free path* |
| $d$ | *radius of the ion cross section* |
| $n$ | *ion density* |
| $k$ | *Bolzmann constant (1.38066 10-23 J K$^{-1}$)* |
| $T$ | *temperature* |
| $p$ | *pressure* |
| $\sigma$ | *collision cross section* |

($1 \cdot 10^{-6}$ Torr). Then the ions are focused and accelerated by a cylindric lens assembly into the mass analyzer.

By choosing the potentials at the end of the transfer capillary and of the first skimmer accordingly, it is possible to define the harshness of the desolvation and transfer process. The transmission efficiency for the mass range of interest is optimized, too. Higher potentials lead to harsher desolvation conditions. Thus, it is possible to determine the relative gas-phase stability of noncovalent assemblies by cone voltage driven dissociation [16]. Figure 2.9 shows a ESI mass spectrum of the noncovalent complex

## Collisional Focusing Effects in Radio Frequency Multipoles

In order to reduce the kinetic energy distribution of ions in z-direction (flight direction of the ions) as well as in x/y-direction in an atmospheric pressure interface, a collision damping rf-only multipole can be employed. By reducing the energy spread in z-direction, the mass dependence of the detector of an orthogonal injection TOF-MS can be reduced. Reducing the energy spread in x/y-direction will decrease the initial kinetic energy in direction of the flight-path in the TOF analyzer and therefore improve the resolution. Additionally, by losing kinetic energy in the multipole, the ions are focused onto the multipole axis. The diagram shows a computer simulation of ion motion in a quadrupole ion guide for myoglobin ions obtained by Krutchinsky et al [13]. (A) shows the projection of ion trajectories on the y/z-plane. (B) shows the energy in z-direction ($E_z$) as a function of position along the quadrupole z-axis, where $E_z=½\cdot m\cdot v_z^2$. (C) shows the energy in the x/y-plane ($E_r$) of the ions as a function of position along the quadrupole z-axis, where $E_r=½\cdot m\cdot V_r^2$. Hang et al. published some practical considerations when using radio frequency-only quadrupole ion guide for atmospheric pressure ionization sources with time-of-flight mass spectrometry [14].

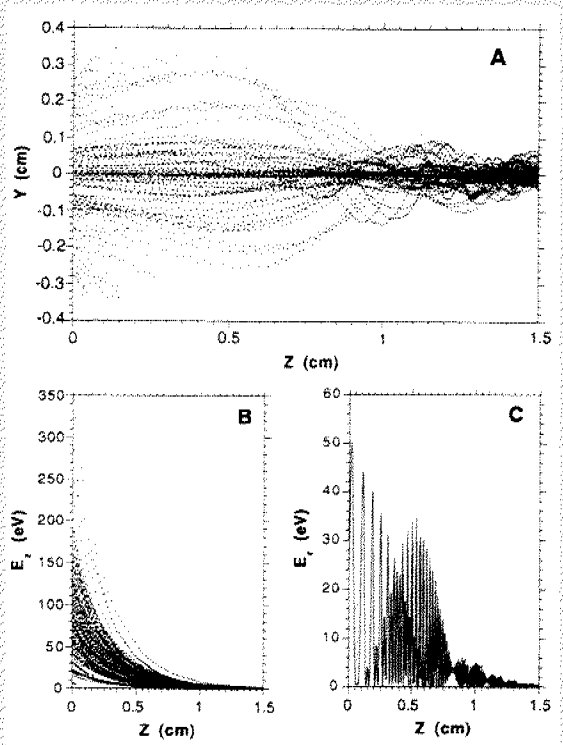


**Reprinted by permission of Elsevier from [13]. Copyright 1998 by the American Society for Mass Spectrometry.**

adenylate kinase with $P^1$,$P^5$-di(adenosine-5')pentaphosphate recorded at (a) soft conditions and (b) harsh conditions. The latter lead to the dissociation of the complex.

The TOF mass analyzer basically is unlimited in mass, however the AP interface is not. The interface must be optimized for a certain mass range, and even then the mass range is limited by the frequency and the precision of the hexapole. The highest m/z ratio measured with the current instrument was 7344 Th, representing the +6 ion of the trimer of chorismate mutase.

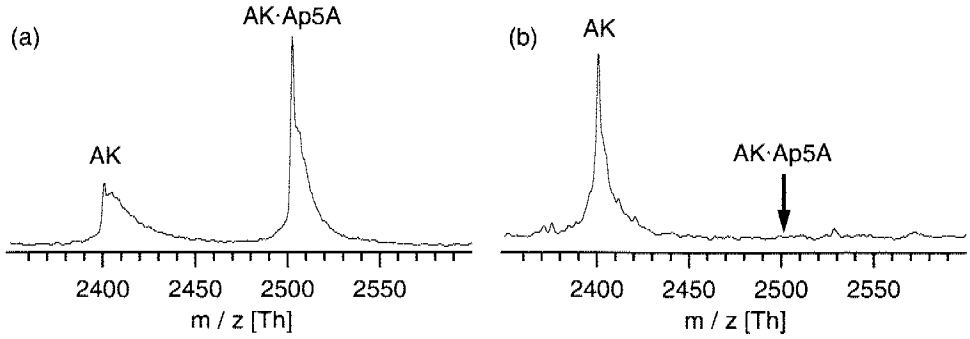


**Figure 2.9: Positive ion mode ESI mass spectra of 10 µM AK and 20 µM Ap5A in 5 mM $NH_4AcO$ when a) soft conditions and b) harsh conditions in the AP interface had been chosen. The strong tailing in the peaks in a) is induced by remaining solvent and buffer adducts resulting from the soft conditions.**

## Ways to Optimize the AP Interface for High Mass Transmittance

### Potential of the exit capillary and the first skimmer

The potential of the exit capillary as well as the potential difference between the exit capillary and the first skimmer must be increased in order to allow the high molecular weight ions to be transmitted to the subsequent stages. The low molecular weight ions will be spread by higher energy collisions in the first stage and their transmittance will be reduced.

### Hexapole (collisional cooling)

The amplitude of the rf frequency of the hexapole must be increased such that the high m/z ions can be cooled effectively. Additionally the pressure in the hexapole should be increased because high mass ions need more collisions in order to be cooled. Going to high amplitudes leads to the suppression of low molecular weight ions.

## Time-of-flight Mass Analyzer

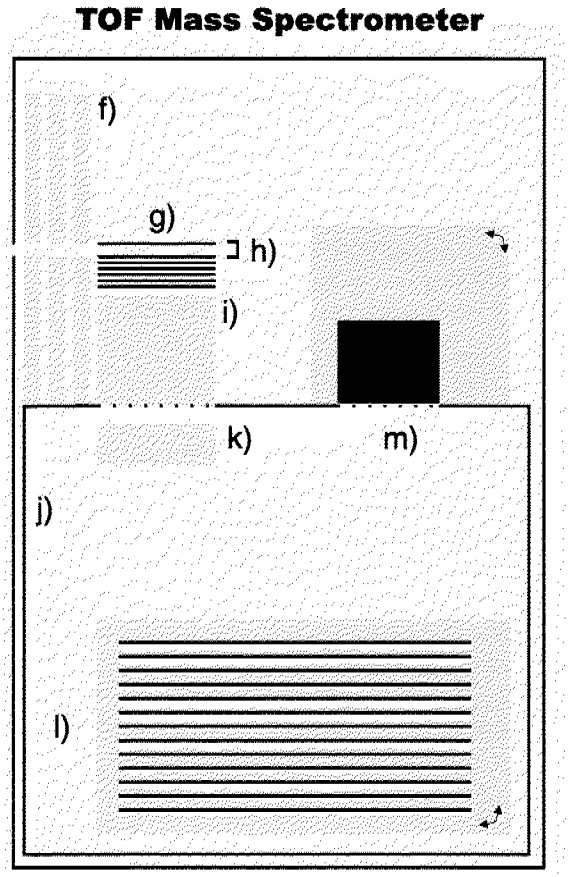


**Figure 2.10: Details of the TOF mass analyzer. f) orthogonal injection, g) pusher, h) Faraday cup, i) acceleration, j) flight chamber, k) vertical deflection, l) reflectron, m) detector.**

The time-of-flight mass analyzer can be operated in two modes: It can be used to measure the total ion current injected into the analyzer. In this mode the potential at the pusher plate remains constant assuring that the ions reach the Faraday cup. To determine the total ion current, the current at the Faraday cup, a simple copper electrode, is measured. Unfortunately, the measured currents are in the range of picoampères and therefore difficult to measure.

In the TOF mode the pusher plate is pulsed with a high potential (1.4 - 2.4 kV, depending on the reflectron type used) with a repetition rate between 4 kHz and 2 kHz depending on the desired mass range of the measurement. To circumvent switching of the pulser between too high potentials, the flight chamber is biased on -6 kV and the ions are accelerated by a Wiley-McLaren electrode arrangement into the flight chamber. After entering the flight chamber the ions can be vertically deflected by deflection plates in order to guide the ion beam onto the detector. Because the

alignment of the instrument is very precise, no vertical deflection was usually necessary. Thereafter, the ions enter a reflectron and are reflected onto the detector.

Two types of reflectrons had been employed. First a dual-stage reflectron was used leading to higher resolution (a resolution of 2400 could be achieved) but to less sensitivity because of two grids defining the two electric fields in the reflectron. In order to enhance the sensitivity and to reduce fragmentation at the grids, the dual stage reflectron was exchanged by a single-stage reflectron leading to a final resolution of 1200. For detecting the ions, an electron multiplier as well as an optically decoupled multichannel plate detector had been employed. The reflectron as well the detector could be tilted within the instrument in order to optimize the ion flight path and the resolution.

**Signal Processing**

For signal acquisition a HP-743 mainframe computer equipped with an analog to digital (A/D) converter board and a TOF board, both prototype boards, were used. The signal from the detector is DC decoupled and preamplified prior to digitalization by the A/D converter. An arbitrary number of transients is summed on the acquisition mainframe and the result is sent to a personal computer for storage and further processing. The mainframe was controlled remotely by a personal computer.

## 2.3 Improvements to the Time-of-Flight Mass Spectrometer

### Ghost Peaks

When the instrument was taken over, its performance was not satisfactory. A number of improvements were made during the course of this thesis, some of which are discussed here in further detail. Ghost peaks series with slightly shorter flight times and less intensity than the mass signal were found for each mass signal (figure 2.11).

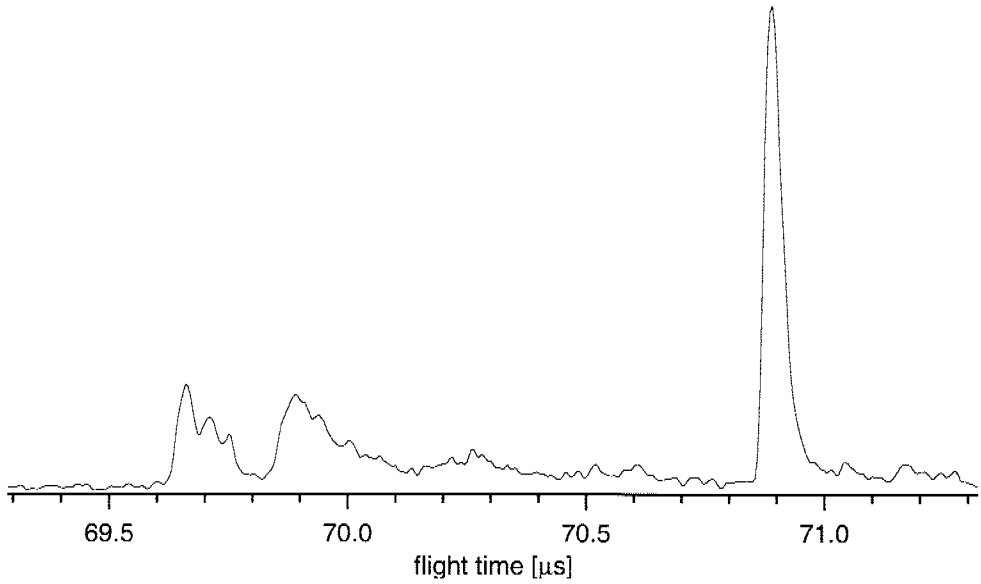


**Figure 2.11: Positive ion mode ESI mass spectrum of HP-Tuning standard showing the typical ghost peaks observed between 69.5 and 70 µs for the main peaks at 70.9 µs.**

These ghost peaks resulted from secondary electrons generated at the exit grid of the flight-chamber towards the detector. In the beginning, the potential of the detector was more positive than the flight-chamber. This resulted in a deceleration of the ions onto the detector surface and to an acceleration of any negatively charged species generated at the exit grids. In this case, the secondary electrons generated by the collisions of the positively charged ions with the exit grid are accelerated to the detector and generate the ghost peaks. In order to prevent the latter phenomenon and to improve the detector signal, *i.e.* acceleration of the ions onto the detector surface, the potential of the detector surface must be more negative than the flight chamber. The electron multiplier used in the instrument allowed a potential difference of -2.4 kV,

whereas the flight chamber was on -6 kV. Using the electric circuit shown in figure 2.12, the entire detector was floated with a more negative potential such that the active detection area could be kept at a potential of -6 kV. As a result, spectra without any ghost peaks could be obtained (figure 2.13). The source of the secondary electrons was identified and deleted.

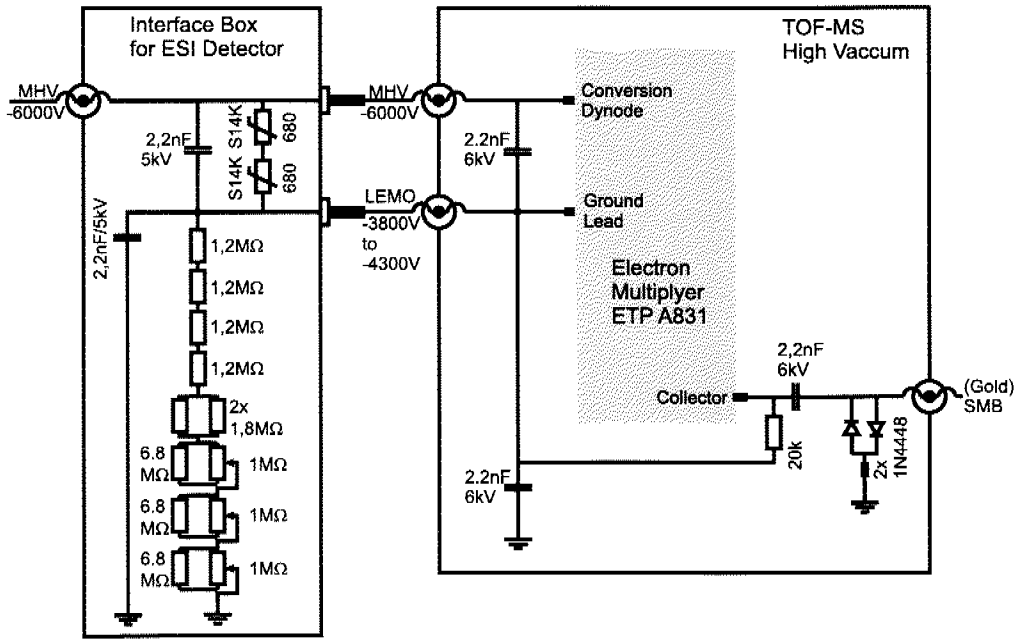


**Figure 2.12: Electric scheme to put the detector on a floating potential between -3800 and -4300 V.**

### Signal-to-noise ratio

Working with weak signal intensities, the signal-to-noise ratio improved far less than with the theoretically expected factor of $\sqrt{n}$. As it can also be seen in figure 2.13, periodical noise was recorded due to oscillation of the high voltage source (HCN 140-12500, Fug, Germany). By adding a resistor to the entrance of the potential source (figure 2.14) the periodical disturbance could be reduced by a factor of ~3. Nevertheless the results were not yet satisfactory. Therefore the detector was changed to an optically decoupled detector (Burle Bipolar TOF Detector, Burle, USA).

The optically decoupled detector consists of an multichannel plate detector, a scintillator, and a photomultiplier (figure 2.15). Ions hitting the MCP are converted to electrons which are amplified. The resulting electron avalanche is hitting the scintillator

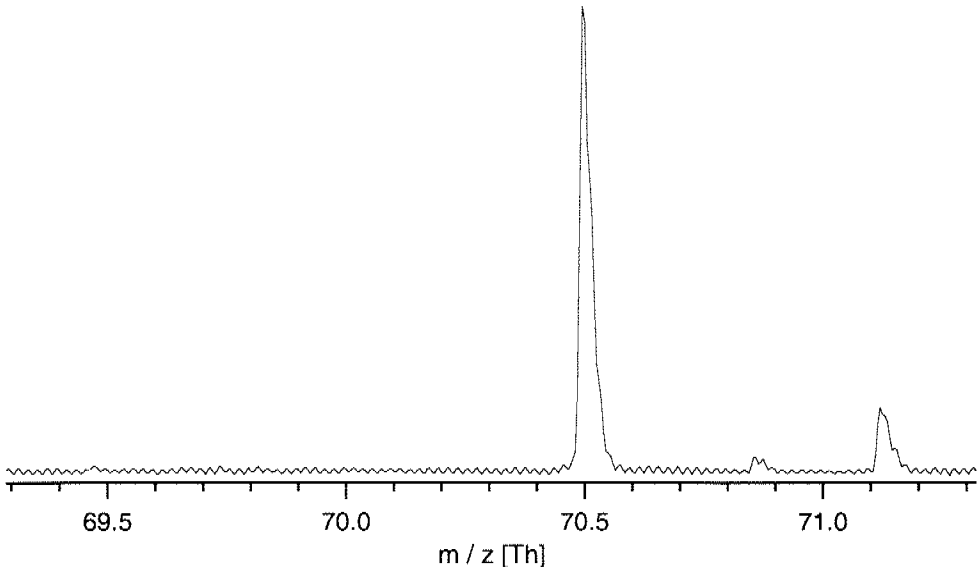


**Figure 2.13: Positive ion mode ESI mass spectrum of HP-Tuning standard recorded with the new detector setup showing no more ghost peaks.**

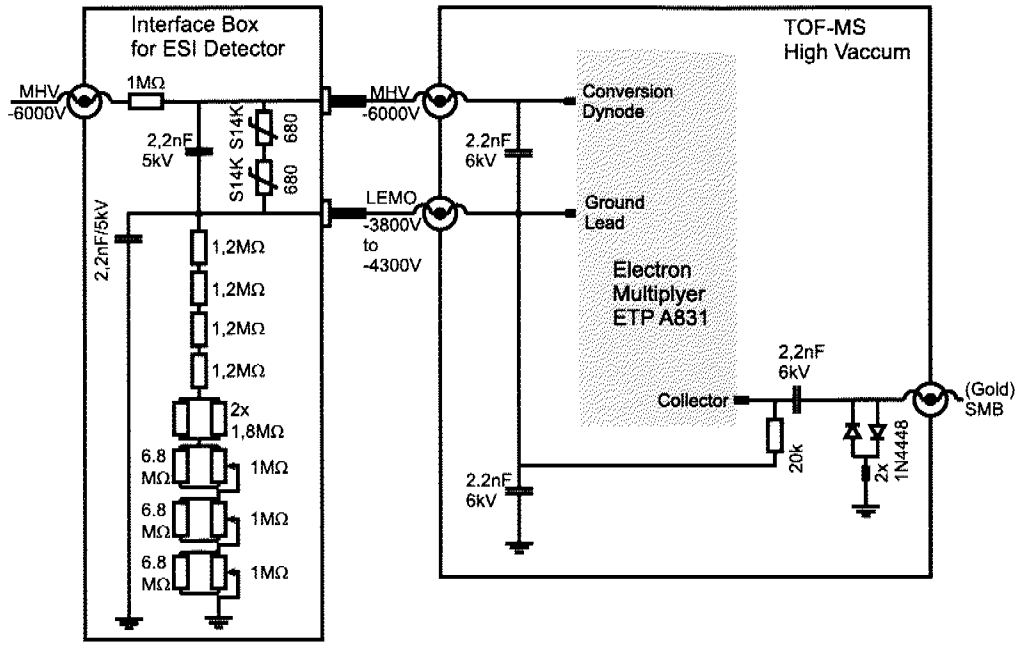


**Figure 2.14: Electric scheme to put the detector on a floating potential between -3800 and -4300 V. In order to reduce disturbing oscillation from the potential source, a 1 MΩ resistor has been added to the entrance.**

surface inducing the scintillator molecules to emit light. The light is detected by the photomultiplier whereas the photomultiplier is electrically decoupled from the other elements. The potentials of the MCP (input and output potential) and the scintillator

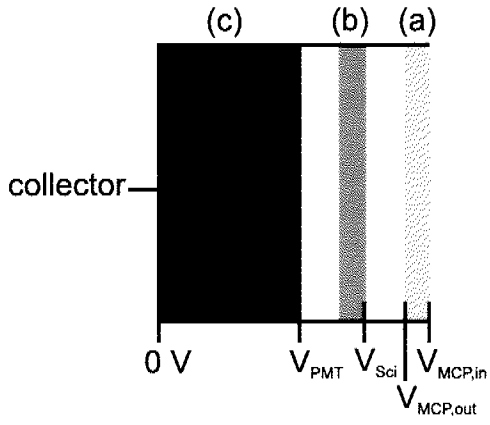


**Figure 2.15: Scheme of the bipolar detector: (a) MCP detector, (b) scintillator, (c) photomultiplier tube. The detector could be controlled by the potentials: $V_{MCP,in}$, $V_{MCP,out}$, $V_{Sci}$, and $V_{PMT}$.**

can be biased with ±10 kV. The analyte signal of the HP Tuning Standard could be further improved by employing the new detector (figure 2.16).

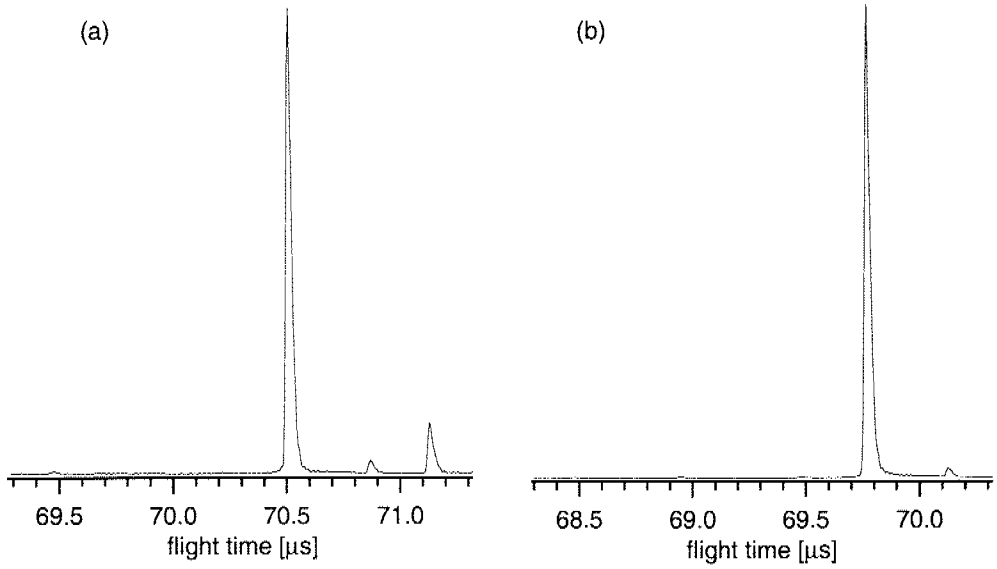


**Figure 2.16: Positive ion mode ESI mass spectrum of HP-Tuning standard detected by (a) the improved electron multiplier setup and (b) the optically decoupled MCP detector. The signal-to-noise ratio could be further improved.**

## Ionization Source

The original ionization source delivered with the mass spectrometer was a pneumatically assisted electrospray or *ionspray* (figure 2.17) with an inner diameter of the spraying capillary of 120 µm. In this setup the electrospray could be assisted by nitrogen gas with a back pressure between 0 and 1 bar. Additionally the dry spraying gas helps the evaporation of the droplet's solvent. This source compared to ESI sources

without pneumatic assistance yields ESI spectra of high quality even with an unstable Taylor cone. This allows the use of higher flow rates, *e.g.* when coupling to a HPLC is employed, and can also simplify the measurement with samples in water at high buffer content.

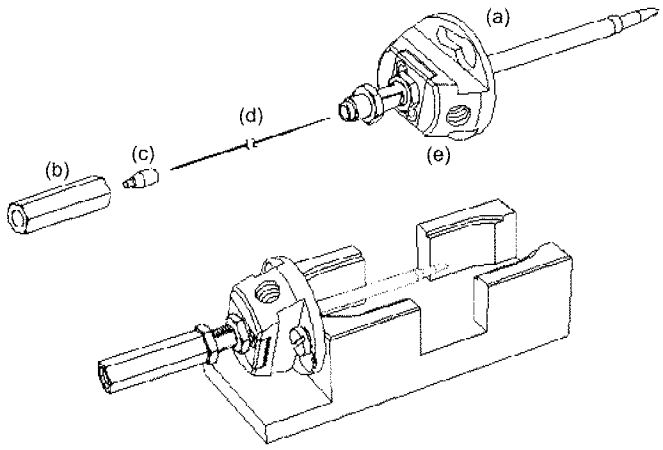


**Figure 2.17: Ionspray spray assembly consisting of (a) spray house, (b) union to connect to liquid delivery source, (c) ferrule, (d) spray capillary, and (e) connection for the spray gas.**

Nevertheless, the tolerance of ionspray and of classical electrospray against remaining salts is limited. Using nanoelectrospray (nanoESI) improves this tolerance and allows higher buffer and salt contents to be used. The nanoESI was introduced by Mann [17, 18] and Caprioli [19, 20] and their co-workers almost at the same time. Caprioli called it *microspray*, referring to the inner diameter of the spray capillary in the range of several micrometers. Mann called it *nanospray* referring to the droplet size emitted by the electrospray. He also showed that the ionization efficiency is improved significantly by using smaller inner diameters of the spray capillaries [17], thus reducing the flow rate from several µl to several hundred nl did not result in decrease in the detected ion signal. Nowadays one distinguishes between on-line nanoESI, using spray capillaries with inner diameters of 10 to 15 µm, and off-line nanoESI using spray capillaries with inner diameters of 1 to 4 µm.

In order to check the suitability of off-line nanoESI for our own experiments, an off-line nanoESI source was developed (figure 2.18). Spray capillaries with inner diameters of 1 µm were purchased from NewObjective Inc. (USA). To provide an electric contact to the spraying solution the tips have a conductive coating on the tip. The electric connection between the needle coating and the electric circuit was established by

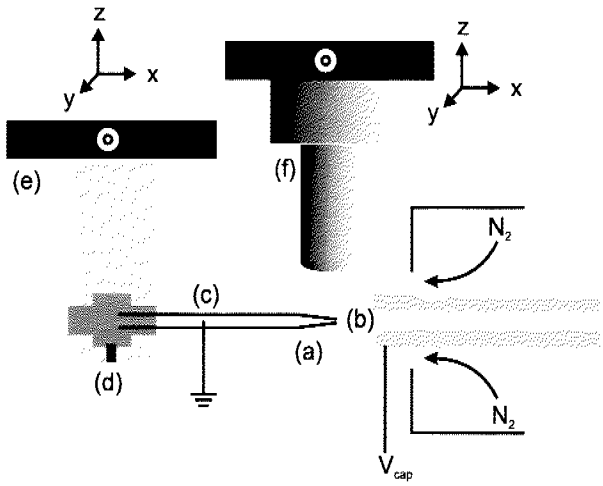


**Figure 2.18: Scheme of the nanoESI source developed consisting of (a) nanospray needle, (b) atmospheric interface of the MS, (c) electric contact to the nanospray needle, (d) holder for the nanospray needle, (e) x/y/z translation stage, (f) CCD camera mounted on a x/y/z translation stage.**

using silver glue and a micro clamp. Figure 2.19 shows a spectrum of native myoglobin recorded with nanoESI in positive ion mode. It is apparent that the peaks show not as many buffer and solvent adducts as for classical electrospray and thus are narrower. This is a direct result of smaller droplets being produced by the spray. However, using off-line nanoESI means that spray needles can be used just once and therefore the reproducibility is poor. What's more, filling of the needle is not easy and needs some training. We found that the needles were best filled with help of a gel loader pipette tip.

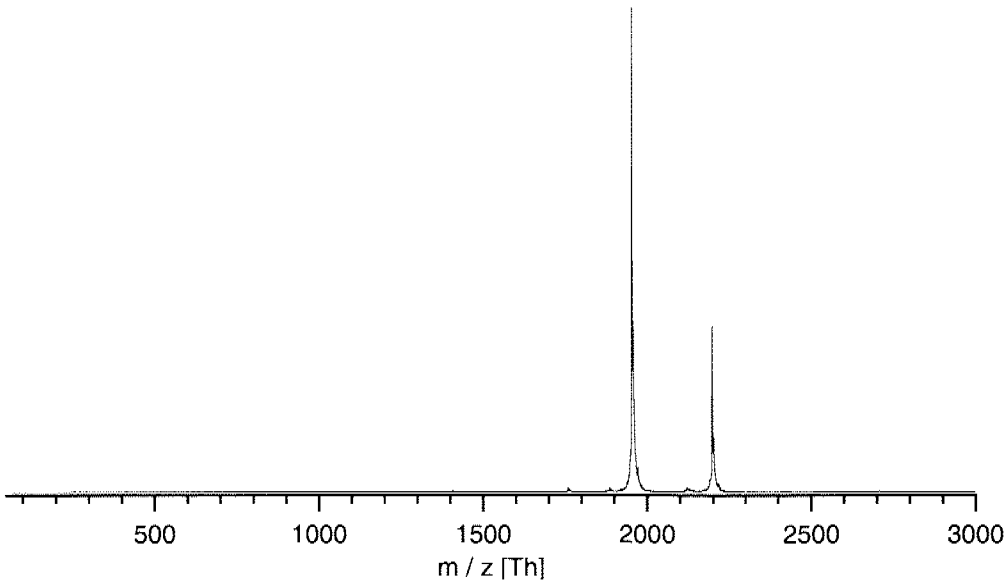


**Figure 2.19: Positive ion mode nanoESI mass spectrum of 10 μM myoglobin and 10 mM NH4AcO in water. The signal shows no tailing indicating that there are no buffer or solvent adducts.**

Because the signals obtained with classical ionspray were sufficient, the nanoESI was not used for the experiments presented in the thesis.

In addition to the ESI sources, different sources for atmospheric pressure matrix assisted laser desorption / ionization have been developed and are explained in this thesis.

## 2.4 Summary

Although TOF-MS is simple in concept, challenges in the implementation may arise. In a set of technical changes, the poor signal intensities could be improved significantly and the ghost peaks could be avoided by introducing a new detector system into the instrument. In order to enhance the flexibility for ionization by ESI, a nanoESI source had been developed in addition to the present ionspray source. We have successfully shown that the nanoESI source is less sensitive against salts in the analyte solution and leads to less buffer and solvent adducts for the ions observed. These improvements led to a state-of-the-art instrument for mass spectrometric investigations of current problems.

## 2.5 References


1. W. C. Wiley and I. H. McLaren, *Rev. Sci. Instr.*, 1955, **26**, 1150-1157.
2. R. J. Cotter, *Time-of-Flight Mass Spectrometry: Instrumentation and Applications in Biological Research*, ACS Professional Reference Books, 1997, Washington, DC, American Chemical Society.
3. R. Weinkauf, K. Walter, C. Weickhardt, U. Boesl and E. W. Schlag, *Z. Naturforsch. Teil A*, 1989, **44**, 1219-1225.
4. U. Boesl, R. Winkauf and E. W. Schlag, *Int. J. Mass Spectrom. Ion Proc.*, 1992, **112**, 121-166.
5. B. A. Mamyrin, V. I. Karataev, D. V. Shmikk and V. A. Zagulin, *Sov. Phys - JETP*, 1973, **37**, 45.
6. B. A. Mamyrin, 1966, Russia, No. 198034.
7. J. H. J. Dawson and M. Guilhaus, *Rapid Commun. Mass Spectrom.*, 1989, **3**, 155.
8. A. F. Dodonov, I. V. Chernushevich and V. V. Laiko. *Orthogonal Extraction ESI-TOF-MS*, in *12th Int. Mass Spectrometry Conference*, 1991, Amsterdam (NL).
9. M. Frank, S. E. Labov, G. Westmacott and W. H. Benner, *Mass Spectrom. Rev.*, 1999, **18**, 155-186.
10. B. Laprade and R. Starcher, *The 2 Mircron Pore Microchannel Plate: Development of the world's fastest detector*, 2001, BURLE Electro-Optics, Inc., Sturbridge, MA.
11. J. L. Wiza, *Nuc. Instr. Methods*, 1979, **162**, 587-601.
12. H. Lindner, *Physik für Ingenieure*, 1993, Leipzip, Fachbuchverlag.
13. A. N. Krutchinsky, I. V. Chernushevich, V. L. Spicer, W. Ens and K. G. Standing, *J. Am. Soc. Mass Spectrom.*, 1998, **9** (6), 569-579.
14. W. Hang, C. Lewis and V. Majidi, *Analyst*, 2003, **128**, 273-280.
15. P. D. Mosier, A. E. Counterman and P. C. Jurs, *Anal. Chem.*, 2002, **74** (6), 1360-1370.
16. J. M. Daniel, S. D. Friess, S. Rajagopalan, S. Wendt and R. Zenobi, *Int. J. Mass Spectrom.*, 2002, **216**, 1-27.
17. M. Wilm and M. Mann, *Anal. Chem.*, 1996, **68** (1), 1-8.

18. M. S. Wilm and M. Mann, *Int. J. Mass Spectrom. Ion Process.*, 1994, **136** (2-3), 167-180.
19. P. E. Andren, M. R. Emmett and R. M. Caprioli, *J. Am. Soc. Mass Spectrom.*, 1994, **5** (9), 867-869.
20. M. R. Emmett and R. M. Caprioli, *J. Am. Soc. Mass Spectrom.*, 1994, **5** (7), 605-613.

# CHAPTER 3

# QUANTITATIVE DETERMINATION OF NONCOVALENT BINDING INTERACTIONS

Seite Leer /
Blank leaf

For a number of years, soft ionization mass spectrometry has been used for studying noncovalently bound complexes. An intriguing question in this context is whether MS experiments can be used to measure the interaction strength. A number of recent studies have addressed this question. The results of these studies, as well as the methods employed are explained in the present chapter. It is distinguished between solution-phase methods where the MS serves as detector for the solution phase and gas-phase methods, where interaction strengths in the gas phase are measured. With a few exceptions, no agreement exists between solution-phase and gas-phase binding energies. The main reason is that electrostatic and dipolar noncovalent interactions are strengthened in the absence of solvent shielding, while other noncovalent interactions, *i.e.* hydrophobic interactions, become less important in the absence of solvent.

**Adapted from:**

J. M. Daniel, S. D. Friess, S. Rajagopalan, S. Wendt, and R. Zenobi, *Int. J. Mass Spectrom.*, 2002, **216**, 1-27.

## 3.1 Introduction

A number of established analytical methods are being used for the quantitative study of noncovalent macromolecular interactions. These all work in the solution phase and include optical spectroscopy (*e.g.* UV absorption, circular dichroism (CD), and fluorescence), nuclear magnetic resonance (NMR), light scattering, differential scanning calorimetry, and isothermal titration calorimetry [2]. Mass spectrometry is a novel tool for studying biomolecular structures and noncovalent interactions; it can provide data on the functional properties of biomacromolecules complementary to that obtained from more traditional techniques. Smith and co-workers have discussed the advantages of mass spectrometry compared to other biophysical methods for investigating noncovalent interactions [3, 4]. For example, mass spectrometry has undisputed advantages over NMR for studying proteins with poor solubility and high molecular weight. NMR is limited to studies of proteins with a molecular weight less than 30'000 Da, while mass spectrometry has been used to study proteins and protein complexes with molecular masses approaching 1'000'000 Da [5-8]. Unlike NMR or CD, techniques that measure average of properties of biomacromolecules, soft ionization mass spectrometry in connection with H-D exchange can provide detailed and quantitative information about the kinetics of protein folding [9].

McLafferty has often referred to the three "S" advantages of mass spectrometry: specificity, sensitivity, and speed [10]. Most importantly, the sensitivity of MS based methods (picomole to femtomole range) allows the investigation of very small quantities of material, which renders MS a very useful method in cases where only a microgram or less of a valuable protein may be available for a study. In addition, accuracy and mass range of modern instruments are very useful. A fourth "S" advantage in the context of noncovalent interactions should include stoichiometry [11]: the number of ligands that form a unique and biologically relevant complex is an important issue in many systems, a quantity that is easily obtained from mass spectrometry. Another great advantage of mass spectrometry as an analytical tool, especially applicable to identification of unknown molecules, is the possibility to carry out tandem mass spectrometry experiments or even $MS^n$, leading to an exponential increase in data and information [12].

## 3.2 Noncovalent Interactions

Atoms and molecules can interact together leading to the formation of either a new molecule (reactive channel) or a molecular cluster (nonreactive channel). The former is clearly a covalent interaction; the latter is termed a noncovalent, since no covalent bond is neither formed nor broken. Noncovalent interactions were first recognized by J. D. van der Waals in the nineteenth century [13], and are of primary importance in our world (see below).

The properties of the original subsystems in a molecular cluster are relatively unperturbed compared to the isolated molecules. Nevertheless, the stronger the noncovalent interaction, the larger the changes in the properties of the subsystem. Most pronounced changes occur in H-bonded systems, and the change of stretch frequencies upon complex formation can be hundreds of wavenumbers ($cm^{-1}$). Noncovalent interactions are considerably weaker (by one or two orders of magnitude) than covalent interactions. The role of noncovalent interactions in nature was fully recognized in the last decades; they play an important role in chemistry and physics, moreover, are of key importance in biology. The structures of liquids, solvation phenomena, molecular crystals, the structures of biomacromolecules such as DNA and proteins, and molecular recognition are only a few phenomena determined by noncovalent interactions.

$$H + G \underset{k_{-1}}{\overset{k_1}{\rightleftharpoons}} H{\cdot}G \qquad \text{(Eq 3.1)}$$

| | |
|---|---|
| *H* | *host molecule* |
| *G* | *guest molecule* |
| *HG* | *host-guest noncovalent complex* |
| $k_1$ | *reaction rate constant for the complexing reaction (bimolecular)* |
| $k_{-1}$ | *reaction rate constant for the dissociation reaction (unimolecular)* |

The noncovalent complex formation shown in equation 3.1 is in any case reversible. Given enough time and constant conditions, these complexing and dissociation reactions will lead to equilibrium concentrations of free host, free guest and complex. The

equilibrium concentrations are defined according to equation 3.2, and are determined by the kinetics of the forward and backward reaction.

$$K_A = K_D^{-1} = \frac{k_1}{k_{-1}} = \frac{[H \cdot G]}{[H][G]} \qquad \text{(Eq 3.2)}$$

$K_A$ *association constant*

$K_D$ *dissociation constant*

$k_1$ *reaction rate constant for the complexing reaction (bimolecular)*

$k_{-1}$ *reaction rate constant for the dissociation reaction (unimolecular)*

$[H \cdot G]$ *concentration of the noncovalent complex*

$[H]$ *concentration of the free host*

$[G]$ *concentration of the free guest*

According to collision theory, the maximum theoretical reaction rate constant for complex formation ($k_1$) is about $10^{10}$ $s^{-1}M^{-1}$. This is the rate constant for diffusion controlled reactions. The $k_1$ values for protein-protein interactions strongly depend on the geometry of the interaction and on electrostatic parameters, and most of these rate constants typically level around $10^3$ - $10^4$ $s^{-1}M^{-1}$. The $k_1$ for protein - ligand (protein and small ligand) complex reactions reach values around $10^6$ - $10^9$ $s^{-1}M^{-1}$. Table 3.1 shows the rate constants for different reactions.

| | |
|---|---|
| **α-Chymotrypsin / α-Chymotrypsin** | $k_1 = 3.7 \times 10^4$ $s^{-1}M^{-1}$ |
| **Lactat dehydrogenase / NADH** | $k_1 \approx 10^9$ $s^{-1}M^{-1}$ |
| **Lysozym / $(NAG)_2$** | $k_1 \approx 10^7$ $s^{-1}M^{-1}$ |

**Table 3.1: Association rate constants of protein - protein and protein - ligand systems. NADH = nicotinamide adenine dinucleotide, NAG = N-acetylglucosamine.**

The dissociation reaction rate constant ($k_{-1}$) is much smaller than the diffusion controlled value because the noncovalent interaction energy has to be overcome. Designing drugs usually means to minimize the dissociation rate constant in order to block the binding site of the target protein as long as possible. The half life time of complexes can be calculated according to equation 3.3. If the association rate constant ($k_1$) and the association constant ($K_A$) is known or can be estimated, the loss of complex

$$t_{1/2} = \frac{ln2}{k_{-1}} \qquad \text{(Eq 3.3)}$$

$t_{1/2}$ *half life time of a noncovalent complex*

$k_{-1}$ *reaction rate constant for the dissociation reaction (unimolecular)*

during the transfer of the ions into the TOF-MS can be estimated. Note that the interaction strength and therefore the rate constants in the gas phase differ from the one in solution. With appropriate methods, the gas-phase stability as well as the solution-phase stability can be explored.

The relation between the Gibbs free energy and the association and dissociation constants is explained in equations 3.4 and 3.5. At equilibrium $\Delta G=0$ and therefore the

$$\Delta G = \Delta H - T \cdot \Delta S = \Delta G^{\circ} + R \cdot T \cdot lnK_A = \Delta G^{\circ} - R \cdot T \cdot lnK_D \qquad \text{(Eq 3.4)}$$

$$\Delta G^{\circ} = -R \cdot T \cdot lnK_A = R \cdot T \cdot lnK_D \qquad \text{(Eq 3.5)}$$

$\Delta G$ *Gibbs free energy of the reaction*

$\Delta H$ *reaction enthalpy*

$T$ *temperature*

$\Delta S$ *reaction entropy*

$\Delta G°$ *Gibbs free energy of the reaction for all activities = 1*

$K_A$ *association constant for the noncovalent complex*

$K_D$ *dissociation constant for the noncovalent complex*

free binding energy of the noncovalent complex determines the equilibrium constants. Note that association and dissociation constants are temperature dependent.

For an association constant $K_A = 10^9$ M, free binding energy of $\Delta G° = -53$ kJ mol$^{-1}$ (at 37 °C) can be calculated. Such binding is very weak compared to the binding enthalpy of a covalent C-C bond of 348 kJ mol$^{-1}$. In order to obtain a change of $K_A$ of one order of magnitude, the free binding energy must be increased by 5.9 kJ mol$^{-1}$ at body temperature and by 5.7 kJ mol$^{-1}$ at room temperature, respectively.

## Types of Noncovalent Interactions

Noncovalent interactions can come in many different flavours. Table 3.2 summarizes the types of noncovalent interactions that occur between particles that are either charged, carry a dipole moment, or are polarizable [14].

| Type of noncovalent interaction | Formula | Name |
|---|---|---|
| Charge - charge | $\frac{Q_1 \cdot Q_2}{4 \cdot \pi \cdot \varepsilon \cdot \varepsilon_0 \cdot r}$ | Coulomb Energy |
| Charge - dipole (fixed dipole) | $-\frac{Q \cdot u \cdot \cos\theta}{4 \cdot \pi \cdot \varepsilon \cdot \varepsilon_0 \cdot r^2}$ | |
| Charge - dipole (freely rotating dipole) | $-\frac{Q^2 \cdot u^2}{6 \cdot (4 \cdot \pi \cdot \varepsilon \cdot \varepsilon_0)^2 \cdot k \cdot T \cdot r^4}$ | |
| Dipole - dipole (fixed dipole) | $-\left(\frac{u_1 \cdot u_2}{4 \cdot \pi \cdot \varepsilon \cdot \varepsilon_0 \cdot r^3} \cdot (2\cos\theta_1 \cos\theta_2 - \sin\theta_1 \cos\phi \sin\theta_2)\right)$ | |
| Dipole - dipole (freely rotating dipole) | $-\frac{u_1^2 \cdot u_2^2}{3 \cdot (4 \cdot \pi \cdot \varepsilon \cdot \varepsilon_0)^2 \cdot k \cdot T \cdot r^6}$ | Keesom energy |
| Charge - nonpolar | $-\frac{Q^2 \cdot \alpha}{2 \cdot (4 \cdot \pi \cdot \varepsilon \cdot \varepsilon_0)^2 \cdot r^4}$ | |
| Dipole - nonpolar (fixed dipole) | $-\frac{u^2 \cdot \alpha \cdot (1 + 3 \cdot \cos^2\theta)}{2 \cdot (4 \cdot \pi \cdot \varepsilon \cdot \varepsilon_0)^2 \cdot r^6}$ | |
| Dipole - nonpolar (freely rotating dipole) | $-\frac{u^2 \cdot \alpha}{(4 \cdot \pi \cdot \varepsilon \cdot \varepsilon_0)^2 \cdot r^6}$ | Debye energy |
| Nonpolar - nonpolar | $-\frac{3}{2} \cdot \frac{\alpha_{01} \cdot \alpha_{02}}{(4 \cdot \pi \cdot \varepsilon \cdot \varepsilon_0)^2 \cdot r^6} \cdot \frac{I_1 \cdot I_2}{I_1 + I_2}$ | London dispersion energy |
| Hydrogen bond | Special, directed interaction | |
| Hydrophilic interaction | Special interaction | |
| Hydrophobic interaction | Special interaction | |

**Table 3.2: Types of noncovalent interactions. $Q$ = charge, $u$ = dipole moment, $r$ = distance, $\alpha$ = polarizability, $\varepsilon$ = dielectric constant, $I$ = first ionization potential, $\theta$ = angle between dipole and vector connecting the interacting particles, $\phi$ = polar angle of second dipole. Adapted from Israelachvili [14].**

The equations given in table 3.2 give the energies of interaction. Coulomb interactions between two charges are long-range and strong, and can be attractive or repulsive, dependent on the polarity of the charges involved. Dipole-dipole interactions can also be attractive or repulsive, dependent on the relative angular orientation of the interacting dipoles. All other interactions are attractive because permanent or induced dipoles can orient in order to accommodate the forces acting on them. Even particles without any charge or dipole moment can attract themselves, by virtue of their polarizability (London dispersion force). A rough classification can be made according to the distance dependence of noncovalent interactions, which varies between a $1/r$ distance dependence for Coulomb energy to the well known $1/r^6$ distance dependence for all van der Waals energies. Another important fact to note is that all interaction energies contain a $1/\varepsilon$ term, *i.e.*, in the presence of a medium with high dielectric constant such as water, the interaction energy drops by an appropriate factor. This is an important consideration when comparing solution-phase with gas-phase interaction energies, where the solvent medium is absent. Interaction energies based on charges, dipoles, and polarizability are thus expected to increase when going from solution into the gas phase (attractive and repulsive). A notable exception is the hydrophobic interaction, which is an unusually strong attraction between two hydrophobic binding partners in water. Conversely, in the absence of solvent, a hydrophobic interaction is substantially weaker. Like hydrophobic interactions, hydrophilic interactions and hydrogen bond interaction are not readily described by a simple formula. Hydrogen bonds are directed interactions of primarily electrostatic nature, worth about 10 - 40 kJ $mol^{-1}$. Both hydrophobic interactions and hydrogen bonds are of great importance for the three-dimensional structure of biomacromolecules, as well as for the formation of noncovalent complexes in nature.

**Protein - Ligand Interaction**

The interaction between proteins (*e.g.* enzymes, receptors) and ligands (*e.g.* agonist, antagonist) must be described on a molecular level in order to understand the parameters for these interactions. In biological systems, the binding of a ligand to a receptor or enzyme can provoke different effects: signaling, transportation, opening/closing of channels, and enzymatic reactions (*e.g.* phosphorylation or glycosylation). Already in 1913, Paul Ehrlich concluded that the surface properties of the receptor and the ligand

must match in order to bind: *Corpora non agunt nisi fixata.* In 1956, Linus Pauling came to the conclusion that for enzymatic reactions, the conformation of the transition state of the reaction binds stronger to the enzyme as the substrate or the product. If the product or the substrate would bind very strong to the enzyme, the enzyme would be inhibited by the bound product or substrate (partial agonist).

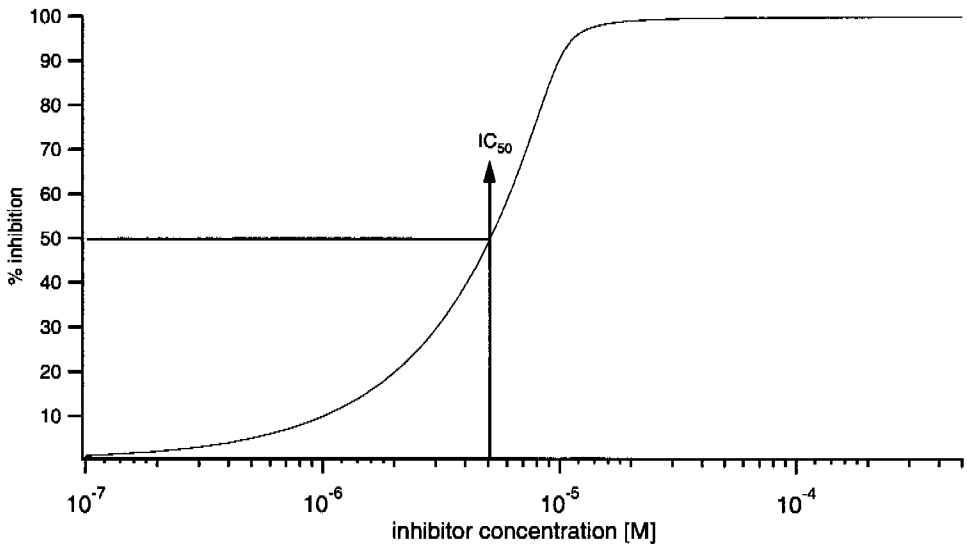


**Figure 3.1: Theoretical curve to calculate the $IC_{50}$ value. The model is based on a enzyme concentration of 10 µM and an association constant of $10^7$ $M^{-1}$.**

In biochemistry, the $IC_{50}$ method is often used to characterize the binding properties of an inhibitor. The $IC_{50}$ method measures the inhibitor concentration at which the enzyme activity drops to 50 % (figure 3.1). In contrast to the $K_A$ and $K_D$, the $IC_{50}$ value depends on the enzyme concentration used for the measurement. Cheng and co-workers calculated the correlation between the dissociation constant and the measured $IC_{50}$ value for different binding mechanisms [15]. When a group of inhibitory compounds have an identical mechanism of action, a direct comparison of the $IC_{50}$ values among them will suffice to determine the relative efficacy, provided the assays are performed under the same conditions. However, in certain cases, when the $K_A$ of each compound is required, it may be impractical to perform the kinetic studies required to determine the $K_A$ for each individual compound. In this situation, it is still possible to calculate the $K_A$ values, provided one knows the $K_A$ of one compound, by using the relationship described in equation 3.6.

$$\frac{IC_{50,1}}{IC_{50,2}} = \frac{K_{D,1}}{K_{D,2}} \qquad \text{(Eq 3.6)}$$

$IC_{50,1}$ *$IC_{50}$ concentration for the first inhibitor*

$IC_{50,2}$ *$IC_{50}$ concentration for the second inhibitor (binding by the same mechanism as inhibitor 1)*

$K_{D,1}$ *dissociation constant for the first inhibitor*

$K_{D,2}$ *dissociation constant for the second inhibitor*

This only holds true with certain assumptions. When comparing the $IC_{50}$ values of compounds that inhibit a specific enzyme derived from the same source, but reported from different laboratories, a few important factors must be considered: The assays must be conducted under the same conditions and the compounds need to have the same reaction mechanism for their inhibitory effect.

## 3.3 Determination of Noncovalent Interaction Energies by MS

Soft ionization mass spectrometry, in particular matrix-assisted laser desorption / ionization (MALDI) and electrospray ionization (ESI), is well known for its ability to bring high molecular weight biomolecules into the gas phase. It has been shown that the ionization is soft enough for preserving noncovalent complexes [16-19]. Review articles by Smith and Zhang [3], Przybylski and Glocker [20], Winston and Fitzgerald [9], Smith et al. [21], Loo [11], Pramanik et al. [22] on ESI-MS and by Hillenkamp [23] on MALDI-MS as applied to noncovalent complexes have been published. It is normally a greater challenge to apply MALDI-MS to noncovalent complexes, because the weak interaction forces have to survive both the sample crystallization as well as the laser desorption / ionization event. MALDI is therefore believed to be somewhat less "soft" than ESI.

A recurring question concerns the applicability of mass spectrometric methods to measure noncovalent interaction strengths. There are several approaches to measure the stability of such complexes in the gas phase. However, the interaction strengths changes by changing the solvation and thus these values are only applicable to the gas phase and not to the solution-phase behavior. Even if only relative binding strength were determined by gas-phase methods, it is not assured that the ranking of binding strengths is the same in solution. There are also different solution-phase approaches where MS is used as a detector for the conditions in the solution. As long as the ionization and measurement by MS does not influence the equilibria, it is possible to estimate the energies involved in the noncovalent interaction.

## 3.4 Specificity of Noncovalent Interactions

A peak at the mass of an alleged complex is not a sufficient criterion to prove its specificity, binding might in fact occur to a unexpected binding site and therefore be a false positive [24]. Key to determining the specificity of noncovalent interactions are suitable controls. Controllable factors need to directly influence the outcome of the mass spectrometric measurement, otherwise the mass spectrum does not reflect the investigated system properly [25]. There are several ways to probe the specificity of noncovalent complexes [21], the two most important being chemical and experimental strategies. For a comprehensive collection of the following and other examples, see ref [26].

Chemical strategies most often involve judicious modification in the sequence of biopolymers that weaken or disable the interaction, *e.g.*, base mismatch in oligonucleotides, covalent modification of amino acid residues in peptides, or the use of mutant proteins. The corresponding signals of the complexes in the mass spectrum must decrease or disappear completely. Selective covalent modification reactions exist for a variety of amino acids: lysine residues can be converted to homo-argine [27], cysteine thiols can be trimethylamino-ethylated to thialamine [28], comparable routines exist for histidine [29] and more general methods such as methylation or acetylation have been applied as well [30]. Disulfide bonds generally survive enzymatic digests, thus disulfide-bonded fragments and their reduced-free forms allow verification of the cysteine locations [31]. Recently, an elegant way for masking the amino terminus has been presented [32].

A simple alternative to covalent modification is the use of commercial mutants to scan various sequences for their specific interaction [33]. Amide protons next to reactive amino acid residues may sometimes participate in complex formation that involves the protein backbone, thus the use of proline at such positions is a useful strategy to disrupt backbone interactions [34]. An interesting example has been presented by Rostom et al. [35]: they characterized peptide binding properties of a periplasmic peptide receptor by using different amino acids, stereochemical features, different side-chain properties, and acetylation of the amino terminus of the peptides. Binding to the

receptor was found to be insensitive to these chemical modifications, showing that the suspected binding site could not be confirmed. The authors concluded that the bound peptides were encapsulated by the receptor in a solvent-filled cavity and supported this interpretation with further evidence from mass spectral peak widths and from the charge state distribution in the ESI mass spectra.

Experimental strategies include different sample preparation techniques [36] or denaturation as a tool to induce conformational changes [37]. Comparative experimental strategies such as change in temperature or different buffer systems have been described early by Smith and Light-Wahl [38]. Using this strategy, the specificity of zinc finger peptide-oligodeoxynucleotide complexes was demonstrated [39], whereas only unspecified binding between cyclodextrins and a variety of compounds that could potentially form inclusion complexes was found in a MALDI mass spectrometry study [40]. Recently, the comparison of MALDI and ESI data of identical systems has been found to be attractive in this respect, too [34, 41-44]. Clearly, if the mass spectral data should reflect solution conditions, the degree of complexation must not depend on the ionization method used.

When reasoning about the specificity of a complex binding interaction in a mass spectrometric experiment, an implicit assumption is that folded biomolecules participating in this interaction retain a near-native conformation in the gas phase. This is, however, difficult to prove directly. Usually, it is based on fairly indirect evidence, although structurally sensitive MS methods are beginning to emerge [33, 34, 37, 45-49]. An interesting, somewhat more direct way to demonstrate the existence of near native structural elements in gas-phase biomolecules was described by Fenselau and co-workers [50, 51]. They measured the kinetic energy release upon dissociation of multiply charged polypeptide ions in a mass-analyzed ion kinetic energy (MIKE) experiment. The relatively large kinetic energy release was thought to be due to Coulombic repulsion between the charges on the fragments. These authors compared experimental values with calculated Coulombic repulsion obtained from molecular dynamics models, and found a very good agreement. This led them to conclude that the α-helical secondary structure of mellitin as well as multistrand β-pleated sheets survive in the gas phase, whereas single β-strands, *e.g.*, in a polyalanine 16-mer or in

bombesin, forms collapsed structures. Another mass spectrometric technique, the ion mobility spectrometer, was used by Cox and co-workers to select specific conformers for mass analysis [52]. In an ion mobility spectrometer (IMS) the ions are not separated by mass, but by their cross section. The measured cross sections are compared with calculated or known cross sections for different conformations of proteins. Clemmer et al. showed ways to calculate the collision cross sections and found a very good agreement between the calculated and the measured cross sections for over hundred of polypeptides [53, 54]. In this way it is possible to determine the different folding states of a protein in the gas-phase. Purves et al. showed at least three different conformations for ubiquitin in the +8 charge state [55]. These were dependent of solution pH and solvent composition indicating that the solution-phase dictated or at least influenced the gas-phase conformation.

## 3.5 Solution-phase Methods with MS Detection

Conceptually, the simplest way of determining stability constants with a mass spectrometer is to use it as a detector for solution-phase chemistry. It is necessary to ensure that solution-phase parameters, and not gas-phase properties, are actually determined in such an experiment. For instance, it must be avoided that a noncovalent complex partially dissociates in the mass spectrometer after being transferred into the gas phase. ESI-MS has been shown to meet these requirements; properly handled, ESI-MS can be used to determine solution-phase parameters [11, 56-62]. As a second very important condition, the ion formation process shall not disturb the solution-phase equilibria. In ESI-MS, for example, it can be imagined that the changes in pH and ion strength in a shrinking microdroplet shift the position of the equilibrium drastically. In an insightful study by Wang and Agnes [63], this question was addressed using the complexation of strontium with EDTA ($Sr^{2+}$ + $EDTA^{4-}$ ⇆ Sr-$EDTA^{2-}$), where the forward reaction rate is much faster (≈$10^9$ $M^{-1}s^{-1}$) and the backward reaction rate is much slower (1 $s^{-1}$) relative to the time scale of the ESI process ($10^{-2}$ s). A shift of the equilibrium to the right was expected, representing the dynamic changes of the equilibrium due to passage through the ion source. However, these authors found that the deviation in the position of the equilibrium compared to solution phase was smaller than expected, and that monitoring of kinetically labile species by ESI is straightforward. This is a very important issue and is currently under further investigation in our research group of Zenobi.

### Melting Curves

A common method to determine noncovalent interaction strength, most often used in the field of oligonucleotide chemistry, is measuring the melting curve of a complex in solution. The fraction of intact complex is determined as a function of temperature. Detection is typically done using UV absorption, fluorescence, or circular dichroism. From the slope of the melting curve, a transition enthalpy can be derived according to equation 3.7 (see ref. [64]). A mass spectrometric analogue of this approach has been described in the literature. In its simplest implementation, the sample solution is at a defined temperature that is slowly raised during the course of the experiment, and $\alpha$

$$\Delta H = (2 + 2 \cdot n) \cdot R \cdot T_m^2 \cdot \left(\frac{\partial \alpha}{\partial T}\right)_{T = T_m} \qquad \text{(Eq 3.7)}$$

| | |
|---|---|
| $\Delta H$ | *transition enthalpy* |
| $n$ | *molecularity of the association reaction (n = 2 for bimolecular)* |
| $R$ | *molar gas constant* |
| $T_m$ | *melting temperature (normally defined for $\alpha$ = 50 %)* |
| $\alpha$ | *fraction of intact complex* |

is measured mass spectrometrically. The same can be achieved by controlling the temperature of the spray capillary in an ESI source, an option that some manufacturers provide for their instruments. This should not be confused with the "heated capillary method" where the transfer capillary is at elevated temperature. The latter is a gas-phase dissociation method that will be discussed below, while the former is only affecting the temperature of the spray solution, thus measuring solution-phase stability.

An early example of measuring oligonucleotide solution stability constants by MS has been presented by Smith and co-workers [65]. They constructed complementary 2′,5′-linked DNA strands and compared their dissociation behavior in solution with the stability of the natural DNA duplexes of identical base composition. Observing heterodimer formation through Watson-Crick base pairing, the authors determined the relative stabilities of the 2′,5′- and the 3′,5′-linked duplexes by ESI-MS and found a qualitative agreement with complementary solution-phase stability measurements. They finally transformed their data into a melting curve, *i.e.* a plot of the spray capillary temperature vs. the mole fraction of single and double strands.

Another remarkable example has been presented by Fändrich et al. [66] who studied the effect of elevated temperature on the structure of the chaperone GimC/prefolding homologue complex. The authors built a nanoflow device that allowed a reliable adjustment of the temperature of the solution containing the hexameric analyte. When increasing the temperature from 60 to 70 °C, the relative intensity of the signal assigned to the intact hexamer decreased, while that of the dissociation products increased. Peaks corresponding to the intact hexamer appeared between 4 and 5 kDa, while those of dissociation products were found below this m/z range.

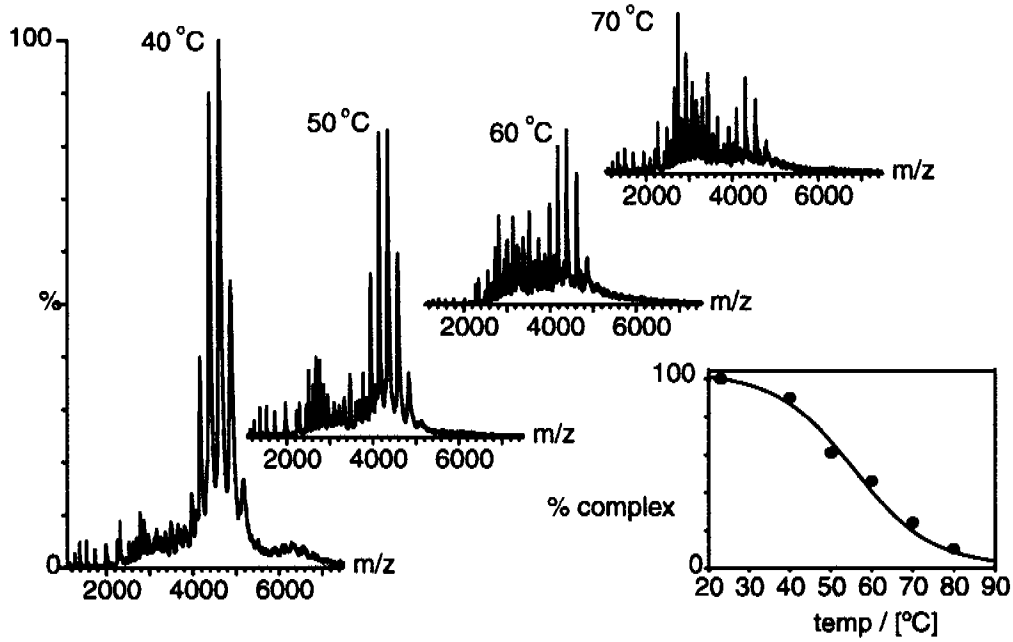


**Figure 3.2: Thermal dissociation of MtGimC monitored by mass spectrometry. Each sample was equilibrated at the desired temperature for 15 min before recording the ESI mass spectrum. Peaks corresponding to intact MtGimC appear between m/z = 4000 and 5000, while dissociation products mostly show up at lower m/z. The fraction of complex was calculated from the sum of the intensity of the ions assigned to the complex signal relative to the total ion counts in each of the spectra (inset). Reprinted with permission from [66]. Copyright 2000 National Academy of Sciences, U.S.A.**

The inset in figure 3.2 presents the results from the ESI-MS spectra in the form of a melting curve: the fraction of complex present was calculated from the sum of the intensity of the ion assigned to the complex and expressed as the percentage of the ion intensity of the hexamer (100%) under ideal physiological conditions. A solution melting (denaturation) temperature of around 60 °C was found for 50% intact complex, in good agreement with data from CD and gel filtration experiments.

**Titration**

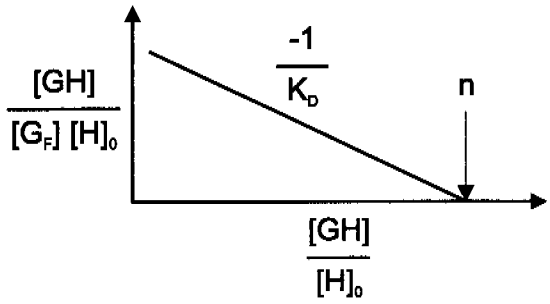


**Figure 3.3: Schematic of a Scatchard plot.**

ESI-MS is typically used to monitor a solution-phase titration for the determination of the equilibrium of a host-guest pair. Generally, the host concentration is kept constant whereas the guest concentration is varied over a range of about two orders of magnitude. The intensity of the complex is then compared to the intensity of the free host for every ligand concentration. This will, however, only work under the assumption that the ionization process does not affect the equilibrium. Often graphical linearization such as Scatchard plots are used for the determination of association or dissociation constants. The ratio of bound (G·H) over free guest ($G_F$) is plotted against the concentration of bound guest, which gives a linear relationship with slope $-1/K_D$ (equation 3.8). If there is more than one binding site, an analysis by a Scatchard plot assumes that these are equivalent and independent.

$$\frac{[G \cdot H]}{[G_F] \cdot [H]_0} = \frac{-1}{K_D} \cdot \frac{[G \cdot H]}{[H]_0} + \frac{n}{K_D} \qquad \text{(Eq 3.8)}$$

| | |
|---|---|
| *[G·H]* | *concentration of bound host-guest complex* |
| *$[G_F]$* | *concentration of free guest* |
| *$[H]_0$* | *total concentration of host* |
| *$K_D$* | *dissociation constant* |
| *n* | *stoichiometry (number of bound guest molecules to one host)* |

One of the first examples using this method was presented by Henion and co-workers [67]. They used negative mode ion spray mass spectrometry to study binding of the antibiotics vancomycin and ristocetin to a peptide ($Ac_2KAA$), representing the carboxyl terminus of a bacterial cell wall protein. The concentration of the antibiotic was kept constant and titration was done by adding $Ac_2KAA$. From a calibration curve

where the $Ac_2KAA$ ion signal intensity is plotted vs. [$Ac_2KAA$] (found to be linear over a range of 0.25 -20 μM) the concentration of the unbound $Ac_2KAA$ could be determined. From these data a Scatchard plot was constructed, which gave binding constants (*e.g.*, $6.25x10^5$ for ristocetin-$Ac_2KAA$ by MS) in good agreement with values from solution-phase methods ($5.0x10^5$ for the same system). The correct stoichiometry of the complexes was also obtained. These authors observed a linear increase in complex signal with increasing concentration of the peptide $Ac_2KAA$ up to equimolar stoichiometry. A problem of this early work was that 50 % acetonitrile was added prior to analysis, representing conditions far from physiological ones. The agreement between the solution-phase binding constant and the value determined by mass spectrometry should thus be regarded with caution, and it should perhaps be clarified whether this is not simply a coincidence.

In solution-phase methods, it is sometimes difficult to recognize binding to two or more different sites, whereas the stoichiometry is easily obtained in MS experiments, because it is the molecular weight that is measured. Using ion spray MS to study the interaction of bovine serum albumin (BSA) with oligonucleotides, Greig et al. [68] identified two different, independent binding sites and determined the dissociation constants using a fit to a second-order polynomial [69] (equation 3.9). They obtained

$$\frac{[H]+[H\cdot G]+[H\cdot G_2]}{[H]} = \frac{[G]^2}{K_{D1}\cdot K_{D2}} + \frac{[G]}{K_{D1}} + 1 \qquad \text{(Eq 3.9)}$$

| | |
|---|---|
| *[H]* | *concentration of free host* |
| *[H·G]* | *concentration of H-G complex* |
| *[H·G$_2$]* | *concentration of G-H-G complex* |
| *[G]* | *concentration of free guest* |
| *$K_{D1}$* | *dissociation constant for the first binding site* |
| *$K_{D2}$* | *dissociation constant for the second binding site* |

$K_D$ values that compared reasonably well to solution-phase data. However, very high charge states of BSA were observed, a possible indication of partial denaturation. A more complex system was investigated by Ayed et al. [70]: citrate synthase (CS) from *Escherichia coli* was titrated with its allosteric inhibitor NADH. In a first step, the association constant $K_A$ of the dimer to hexamer was determined by varying the subunit

concentration of CS. Assuming a simple equilibrium between dimers and hexamers, $K_A$ was determined to be $6.0 \times 10^{10}$ $M^{-2}$. This is the only study where differences in ionization efficiencies were explicitly taken into account.

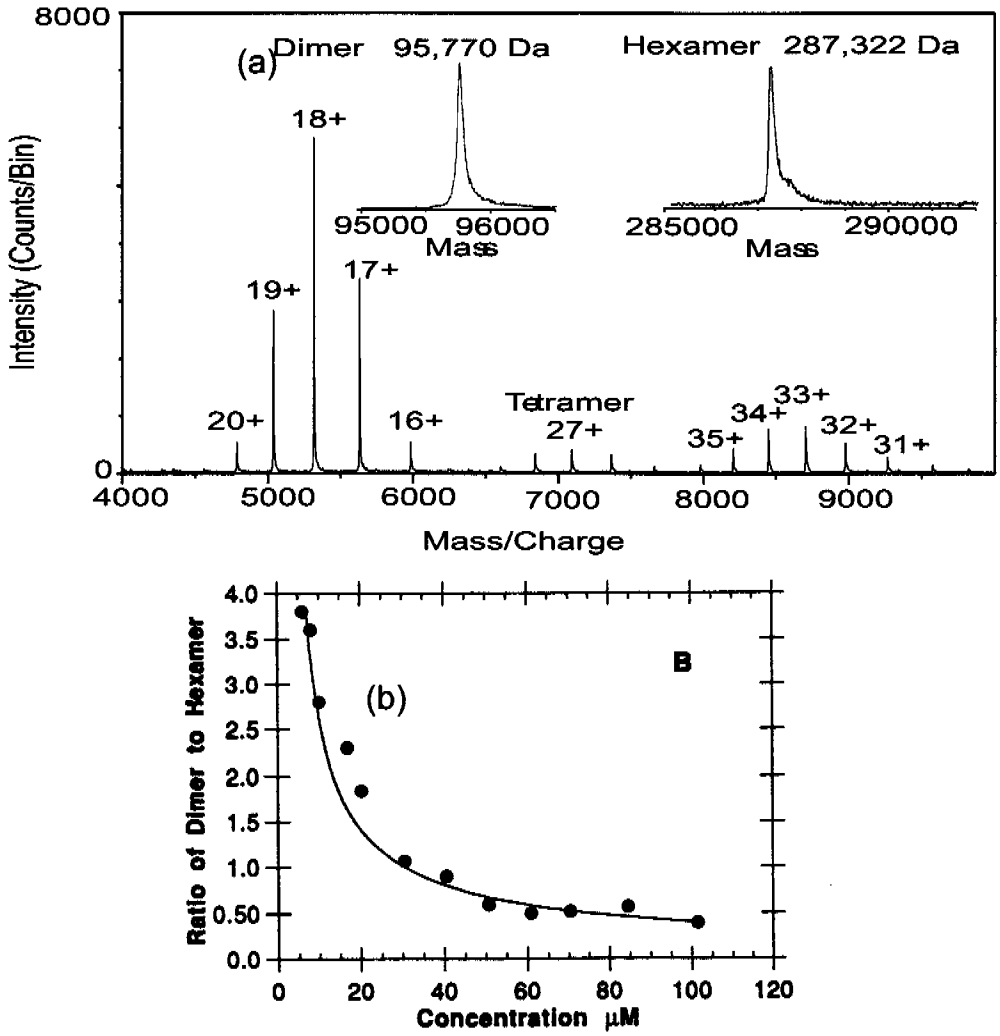


**Figure 3.4: In the upper spectrum an ESI-TOF spectrum of citrate synthase (9 μM subunit concentration) in 5 mM ammonium bicarbonate buffer at pH = 7.5 is shown. Deconvolutions of the regions corresponding to the dimer and the hexamer are shown as insets. A 300 V declustering voltage was used to obtain the spectrum. The lower spectrum shows the dependence of the dimer/hexamer molar concentrations [D]/[H] on the citrate synthase subunit concentration. The integrated peak areas were corrected for different transfer coefficients, as described in [70]. From a fit of the data (solid line) a dimer-hexamer association constant $K_A=[D]/[H]=(6.9\pm0.7)\times10^{10}$ $M^{-2}$ is obtained. Reprinted with permission from [70]. Copyright 1998 John Wiley & Sons Ltd.**

In the same study, the $K_D$ for NADH binding to the dimer or the hexamer was determined by titration a fixed concentration of protein with increasing concentrations of NADH. Different binding sites could be distinguished: a loose binding site per subunit for the dimer ($K_D$ = 28.3 μM), one tight binding site per subunit for the hexamer ($K_D$ = 1.1 μM) and two loose binding sites per subunit for the hexamer with a $K_D$ of about 150 μM. In addition, binding of NADH shifted the equilibrium between dimer and hexamer towards the hexamer, which could be shown for the first time with these mass spectrometric results.

Similar studies have been published by Griffey et al. [71], Sannes-Lowery et al. [69], and Carte et al. [72]. The work by Sannes-Lowery et al. [69] is interesting because different methods were tested for obtaining dissociation constants of RNA-aminoglycoside complexes, *e.g.*, keeping the RNA concentration constant and titrating with the aminoglycoside, or fixing the amino-glycoside and titrating with RNA. This comparison yielded different results, and the authors came to the conclusion that the best method is holding the RNA concentration constant below the expected $K_D$ and titrate with the ligand. This, however, shows that $K_D$ values determined by titration for an unknown system have to be treated with caution.

### Determination of Transfer Coefficients

Mass spectral peak intensities are often taken as a direct measure of solution-phase concentrations. But, does the mass spectrum reflect the solution-phase concentrations of the different species? This is a key question, and it depends on relative vaporization and ionization efficiencies of the different involved molecular species. For a compound X, a transfer coefficient $t_X$ can be defined that accounts for all instrumental and chemical effects that may decrease or enhance the mass spectrometric signal for compound X, $I_X = t_X[X]$. Very few studies address this problem explicitly. Rather, similar transfer coefficients for the free host and the host-guest complex are implicitly assumed, in particular for systems where the guest is much smaller than the host. This assumption is not generally fulfilled.

Johnstone and co-workers [73, 74] employed a correction procedure for taking into account the varying sensitivities toward different noncovalent complexes occurring in fast atom bombardment mass spectrometry (FAB MS). The study of Leize et al. [59] deals with the reasons for different ionization efficiencies. They found the solvation energy of different species to be the key parameter for relative quantification by ESI-MS. For example, an equimolar mixture of LiCl, NaCl, KCl, RbCl, and CsCl yields very different relative intensities in the mass spectrum, with $Cs^+$ being the most intense and $Li^+$ being the least intense peak with only 2% intensity compared to $Cs^+$. The response factor of the metal ion M, $k_M$, was found to depend exponentially on the solvation energy $E_M$ of this ion (equation 3.10), whereas the constant C is depending

$$k_M = C \cdot e^{-(0.015 \cdot E_M)} \qquad \text{(Eq 3.10)}$$

$k_M$ *response factor of the ion*

$C$ *constant taking the ion charge, ion concentration and instrument parameters into account*

$E_M$ *solvation energy*

on the ion charge, the ion concentration and the instrument parameter. In contrast to this, spectra of equimolar mixtures of three or four of these cations in the presence of the same amount of the cryptand 222 showed peak intensities that reflected the proportions calculated from well known solution-phase stability constants. The authors explained these findings with the similar solvation energies of the cryptates, as compared to the different solvation energies of the alkali cations. This seems to argue for the use of uniform transfer coefficients.

Young et al. [75] also addressed the question of different transfer coefficients in titration type experiments using crown ethers. The molar ratio of two salts, *e.g.*, LiCl and KCl was varied from 1:1 to 5:1 and to these solutions, an excess of crown ether was added such that all alkali ions were complexed. Then the ratio of peak intensities of $K^+$ and $Li^+$ was plotted against the ratio of concentrations, yielding a linear relationship with the slope representing the ratio of transfer coefficients. The transfer coefficients of the $Li^+$-crown ether complex was only about half the transfer coefficient of the $K^+$-crown ether complex. This is in contrast to the study of Leize et al. [59], where

the peak intensities of cryptandes complexed with different metal ions were found to reflect the expected solution-phase concentrations. Dubois et al. [76] presented a MALDI study of alkali-crown ether complexes using a special particle/liquid matrix mixture, with glycerol as the liquid matrix. They first determined the transfer coefficients relative to the $Cs^+$-crown ether complex, and were able to determine relative stability constants based on this calibration. Good agreement with results from an earlier electro hydrodynamic mass spectrometry (EHMS) study [77] that had used glycerol as the liquid medium was found. Some of the transfer coefficients reported by Dubois et al. differed by a factor of 5.3, although the same crown ether was used for all complexes. In the work of Ayed et al. [70] the authors take different response factors of citrate synthase dimer and citrate synthase hexamer into account. They calibrate their measurements by measuring a known concentration of pure hexamer and of a specially modified dimer that will not form hexamers. Based on this calibration, peak intensities can be converted to concentrations of dimer or hexamer. This revealed a sensitivity ratio of 1.3, which means that an equimolar mixture of dimers and hexamers would give a peak area ratio of 1.3. These three studies clearly show the importance of taking ionization efficiencies into account. In many cases, they will significantly affect the determination of association constants by mass spectrometric methods.

### Competition Methods

The term "competition methods" indicates that different host-guest complexes are measured simultaneously. One can either use different hosts competing for one guest, or one host and different guests that compete for the same binding site. Information about the absolute binding affinities, relative binding affinities, or selectivities of the different guest or hosts can be obtained.

An interesting technique to determine absolute binding constants of different guests to one host was published by Jørgensen et al. [78]. These authors determined the binding constants of a number of guest molecules with vancomycin and risocetin; all were found to be in good agreement with literature values. Figure 3.5 shows a measurement of the binding constants of vancomycin with three different peptide guests in a single ESI-MS experiment.

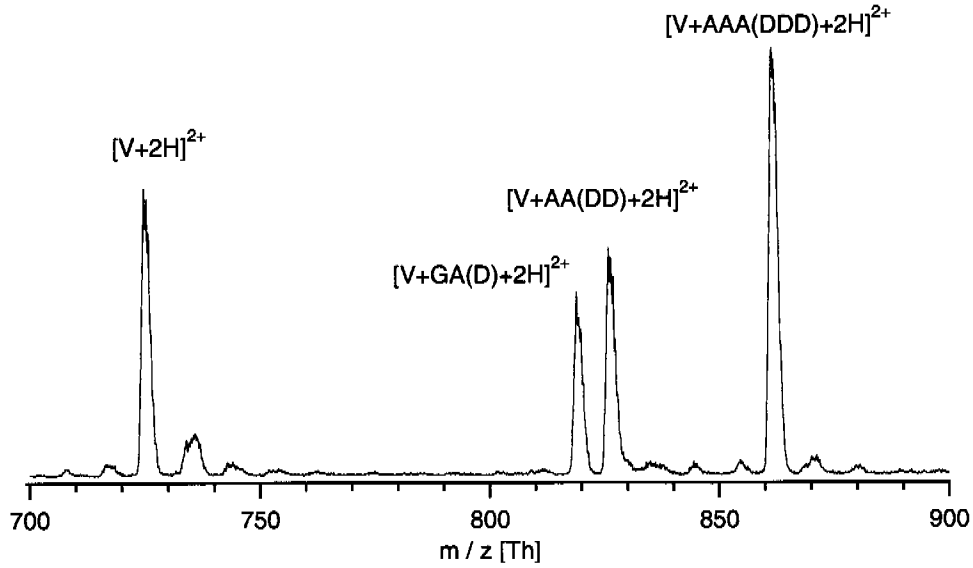


**Figure 3.5: ESI mass spectrum obtained for an equimolar (50 μM) mixture of vancomycin (V), acetyl-D-alanyl-D-alanyl-D-alanine (AAA(DDD)), acetyl-D-alanyl-D-alanine (AA(DD)) and acetyl-glycyl-D-alanine (GA(D)) in 5 mM ammonium acetate buffer at pH 5.1. Reprinted with permission from [78]. Copyright 1998 American Chemical Society.**

The method is based on the measurement of the relative peak intensities of the free host (vancomycin) and the three complexes of the host with three different guests. In solution, the equilibrium concentration of the host and the three complexes is given by equation 3.11. Note that the square brackets denote concentrations, therefore H,

$$[H_i] = \frac{H_i \cdot [H_i]_0}{H + H \cdot G_1 + H \cdot G_2 + H \cdot G_3} \qquad \text{(Eq 3.11)}$$

| | |
|---|---|
| $[H_i]$ | *concentration of any form of the host (H, $HG_1$, $HG_2$ or $HG_3$)* |
| $[H_i]_0$ | *initial concentration of the host* |
| $H_i$ | *peak intensity of any form of the host* |
| $H$ | *peak intensity of the free host* |
| $H{\cdot}G_1$ | *peak intensity of the first host-guest complex* |
| $H{\cdot}G_2$ | *peak intensity of the second host-guest complex* |
| $H{\cdot}G_3$ | *peak intensity of the third host-guest complex* |

$H{\cdot}G_1$, $H{\cdot}G_2$, $H{\cdot}G_3$ refer to the peak intensities. For an equimolar mixture the binding

constant for complex $H{\cdot}G_1$ can be expressed according to equation 3.12. Note that this

$$K_{HG_1} = \frac{[H \cdot G_1]}{[H] \cdot [G_1]} = \frac{[H \cdot G_1]}{[H] \cdot ([H] + [H \cdot G_2] + [H \cdot G_3])} \qquad \text{(Eq 3.12)}$$

$K_{HG1}$ *binding constant for the first host-guest complex*

$[H]$ *concentration of the free host*

$[H{\cdot}G_1]$ *concentration of the first host-guest complex*

$[H{\cdot}G_2]$ *concentration of the second host-guest complex*

$[H{\cdot}G_3]$ *concentration of the third host-guest complex*

equation only holds if equimolar solutions are being used. The major advantage of this method is its speed. Within seconds one can determine the binding constant of several noncovalent complexes at once. A key assumption in this method is that the ionization efficiencies of the host and the complexes are identical. This can only be expected if the host is much heavier than the guest compounds and thus determines the ionization efficiency. A different method for determination of absolute binding constants of mixtures has also been published by Jørgensen et al. [79].

Kempen and Brodbelt recently published a very useful competition method to determine absolute binding constants by ESI-MS [80]. The same method has already been used by Gokel et al. [81] to determine binding constants of $Ca^{2+}$-crown ether complexes using ion selective electrodes and by Goff et al. [82] to determine the binding constants of $Rb^{+}$-crown ethers by NMR. The binding constant of a complex is determined indirectly, by following only the signal of a reference complex with known binding constant. The reference complex must either contain the same guest or the same host as the complex under investigation. The first step is to acquire a calibration curve for the reference complex. The concentration of the reference complex $[H_RG]$ can be calculated for each calibration point. The second step is the actual competition experiment. A spectrum from a solution containing the reference complex and the unknown complex is recorded, but only the concentration of the reference complex in observed and determined with help of the calibration curve. From the concentration of the reference complex in the competition experiment, the binding constant of the unknown complex can be calculated. For the equilibrium in the competition experiment, equations 3.13-3.17 are used. By solving these five equations simultaneously

$$K_R = \frac{[H_R \cdot G]}{[H_R]_F \cdot [G]_F} \quad \text{(Eq 3.13)}$$

$$K_N = \frac{[H_N \cdot G]}{[H_N]_F [G]_F} \quad \text{(Eq 3.14)}$$

$$[G]_F = [G]_T - [H_R \cdot G] - [H_N \cdot G] \quad \text{(Eq 3.15)}$$

$$[H_R]_F = [H_R]_T - [H_R \cdot G] \quad \text{(Eq 3.16)}$$

$$[H_N]_F = [H_N]_T - [H_N \cdot G] \quad \text{(Eq 3.17)}$$

$K_R$ *association constant for the reference complex*

$K_N$ *association constant for the unknown complex*

$[H_R]_T$ *total concentration of the reference host*

$[H_R]_F$ *concentration of the free reference host*

$[H_N]_T$ *total concentration of the reference host*

$[H_N]_F$ *concentration of the free reference host*

$[G]_T$ *total concentration of the guest*

$[G]_F$ *concentration of the free guest*

$[H_R \cdot G]$ *concentration of the reference complex*

$[H_N \cdot G]$ *concentration of the unknown complex*

one can obtain the binding constant of the unknown complex. Stable spray conditions must be found for obtaining a useful calibration curve for the reference complex, and the stability of the spray must persist during the competition experiment. For proteins this is sometimes difficult. Furthermore, the method assumes that the ionization efficiency of the reference complex is constant during the whole measurement, *i.e.*, that the presence of the unknown substance (host or guest) does not influence the ionization efficiency of the reference complex. This may not always be true. The greatest advantage of this method is that the ionization efficiency of the unknown complex does not matter and thus no transfer coefficient needs to be estimated. For example, even if one of the species cannot be ionized (*i.e.* ionization efficiency = 0), it is still possible to determine the binding constants. Once the calibration curve has been established, the method is very fast, which is advantageous for screening a library of guest for the same host. For reference and unknown complexes where the $K_A$ differs by up

to two orders of magnitude, a 1:1:1 concentration ratio can be used in the competition studies. If $K_A$ differs by more than that, the concentration ratio has to be adjusted. Kempen has validated this method using different crown ether host with potassium as the guest, and very good agreement with solution-phase association constants was found.

Relative binding affinities or selectivities can also be determined with competition methods. Experiments and validation studies with different crown ethers, their analogs, and cryptands [83-94], with self-assembling hosts [95], with single and double stranded oligonucleotides [60, 96-102], and with several proteins [61, 62, 103-105] have been reported in the literature.

Cheng et al. used ESI-FT-ICR-MS to determine the relative binding affinities of 16 inhibitors derived from para-substituted benzenesulfonamides to bovine carbonic anhydrase II (BCA II, 29 kDa) in a single competition experiment [106]. They found that the relative abundances of the complex ions were consistent with the binding constants of the inhibitors in solution. For control experiments they prepared a four component mixture of inhibitors with their concentrations inversely proportional to their $K_A$ values. The inhibitors formed 1:1 complexes with BCA II, with approximately identical ion abundances, as expected. Cheng and co-workers also carried out two control experiments to assure that the noncovalent complexes were specific. For the determination of complexes with nearly identical mass they carried out tandem mass spectrometric experiments. The relative intensities of the inhibitors were similar to those obtained from spectra of the intact complexes and correlated with the relative binding affinities in solution. For structural identification of the inhibitors they performed $MS^3$ experiments leading to distinctive fragmentation patterns indicative for the structure of the compounds. In their experiments, they showed very carefully that the ESI-MS method is suited for the determination of the selectivity.

Goolsby et al. [107] published an interesting article about the determination of alkali ion binding selectivities of calixarenes by MALDI and ESI quadrupole MS. Because MALDI is rarely used for this kind of work and since the authors compare the results obtained by MALDI and by ESI, this article deserves some special attention. The

results show some moderate differences in the specific ratio of $K^+$ complexes to $Na^+$ complexes in the MALDI vs. the ESI spectra for each calixarene, but preferences towards $K^+$ or $Na^+$ for the various calixarene are consistent. The evaporation of solvent to dryness may exert some influence on the selectivity derived by MALDI-MS. A problem was the alkali ion contamination of the MALDI matrices, and the large shot-to-shot fluctuations.

## 3.6 Gas-phase Methods

Most ESI-MS studies show that important structural features of large biomolecular assemblies are retained in the gas-phase; even for MALDI this has been found under certain conditions. On the other hand, biomolecules are desolvated upon transfer into the vacuum of the mass spectrometer. This implies that electrostatic interactions and hydrogen bonds, interactions that surely survive the spray process, are largely responsible for maintaining structural features of the vaporized biomolecular ions. Hydrophobic interactions are believed to be partly or completely lost in the gas-phase [61, 108]. In general, therefore, no correlation between the gas-phase stability and the solution-phase stability of noncovalent complexes can be expected. Results from most of the methods discussed below support this conclusion. However, there are some exceptions: in these latter cases it has to be assumed that the dominant interactions are very similar in the gas phase and in solution, and that solvent mediation or screening plays a minor role.

### Cone Voltage Driven Dissociation

Dissociation induced by increasing the *cone* voltage (VC) of the ions in the source-analyzer interface region of an ESI mass spectrometer is a rapid and fairly straightforward method for evaluating relative gas-phase stabilities. This voltage determines the kinetic energy acquired by the noncovalent assembly, and thus the excitation when it collides with other gaseous molecules. Increasing VC allows to start an energetically controlled dissociation. The dissociation of the chaperone GimC/prefolding homologue complex has been studied with this method [66]. The experiments revealed a quaternary arrangement of two central and four peripheral subunits. Increasing VC from 50 to 150 V led to disruption of the hexamer and the observation of a pentameric species. This loss of a single (monomeric) unit as an initial dissociation step suggested that these subunits were located at peripheral positions of the larger assembly, thereby facilitating their selective release as the collision energy was increased.

The VC value needed to dissociate 50% of a noncovalent complex initially present ($VC_{50}$) is taken as a gas-phase stability parameter, *e.g.* of an enzyme-inhibitor complex [109]. This method has been utilized by Van Dorsselaer in a very nice study: their

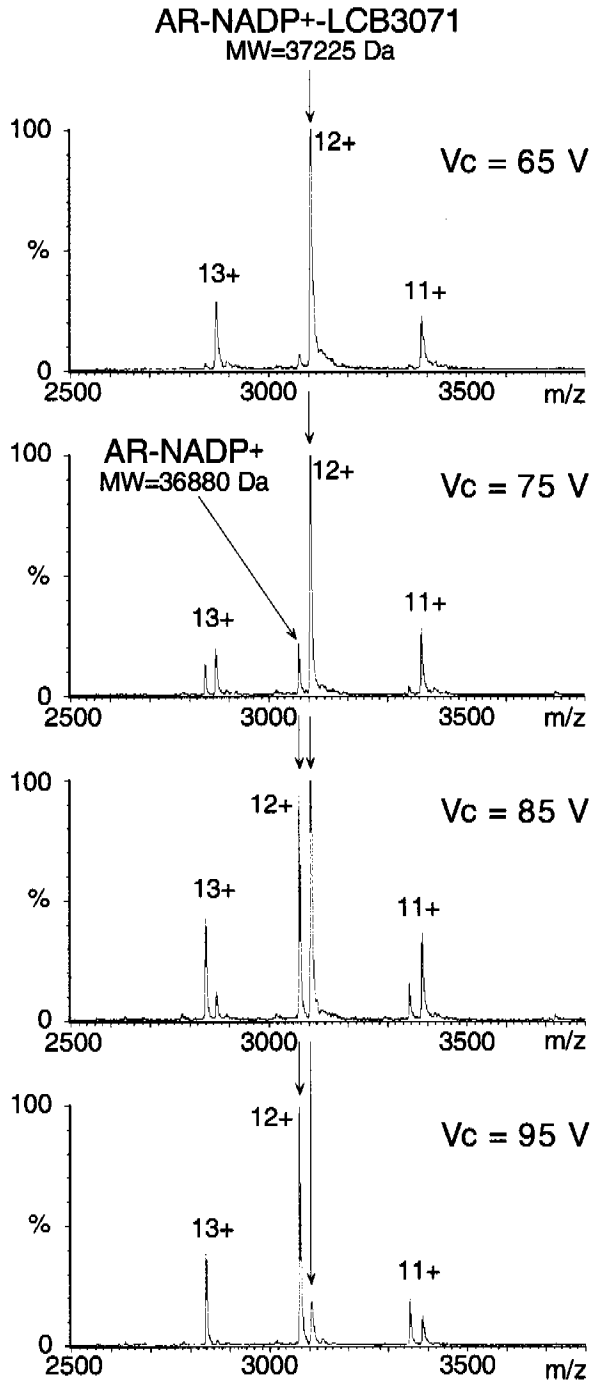


**Figure 3.6: Gas-phase stability study of the enzyme - coenzyme - inhibitor complex aldose reductase-NADP(H)-LCB3071. The ternary complex gradually dissociates in the gas phase when the cone voltage $VC_{50}$ is increased. Spectra were recorded for four different $VC_{50}$ values, 65, 75, 85, and 95 V. The pressure in the source-analyzer interface was kept constant at 2 mbar. Spectra were not corrected for different ionization efficiencies of different compounds, but different responses in ESI analysis have been shown to be irrelevant for the aldose reductase example. Reprinted by permission of Elsevier from [109]. Copyright 1999 by the American Society for Mass Spectrometry.**

methodology allows to rapidly supply information about how inhibitors interact with their target enzyme. Figure 3.6 exemplifies how the $VC_{50}$ value correlates with the energy of the electrostatic and hydrogen bond interactions of the aldose reductase inhibitor noncovalent complex. The ESI mass spectra of an equimolar mixture of aldose reductase, coenzyme ($NADP^+$) and its inhibitor LCB3071 were recorded at various cone voltages. Measuring the $VC_{50}$ values for different inhibitors, the relative

order of gas-phase stabilities was compared to relative interaction energies obtained from X-ray crystallography data. Van Dorsselaer reports a clear correlation between the calculated binding energies and the gas-phase stabilities evaluated by the $VC_{50}$ method. However, no quantitative correlation was found, as the investigated protein may be partially denatured during the MS experiment. The authors point out the striking fact that solution phase parameters ($IC_{50}$ values), giving key information about the inhibition level of a drug, do not follow the order of $VC_{50}$ (= gas phase) values of aldose reductase - inhibitor complexes. This has been postulated in other studies, for example for the dissociation of heme from myoglobin and cytochrome b5 [110] or for the dissociation of oligodeoxynucleotide duplexes [111]. As a general case, a direct quantitative correlation between the gas-phase stabilities and the binding affinities in solution should not be expected.

**Collision Induced Dissociation (CID)**

CID is used to induce unimolecular decay of mass selected ions with sufficient internal energy upon activation by collision with a neutral gas [112] in a collision cell. The energy transfer is influenced by the collision gas pressure in the collision cell, the molecular weight of the collision gas, the cross section of the ions, the injection energy of the ions, and the loss of kinetic energy as they pass through the collision cell. Due to Coulombic repulsion, higher charge state ions have higher collision cross sections; they also experience greater acceleration than ions with lower charges states. Hence, ions bearing more charges collide with more energy, leading to a faster increase in internal energy.

Using ESI-MS/MS, Li et al. [62] compared the relative binding energies of rapamycin and four of its analogs to the cytoplasmic receptor FKBP. They concluded that the gas-phase binding reflects the aqueous solution behavior in these complexes. Wan et al. [113] have used CID in an ion trap mass spectrometer to study the various factors influencing the stability of nucleotide duplex-drug complexes. Analogous to a $VC_{50}$ value, a collision energy $E_{50}$ for 50 % dissociation of the complex was used as a measure of complex stability. The effect of number of charges, number of base pairs, location of the high proton affinity base pair and the number of hydrogen bonds on the

stability of duplex was studied. When the charge states are identical, the stability is proportional to the number of hydrogen bonds in the duplex, correlating well with solution-phase measurements. The stability of noncovalent complexes between duplex oligonucleotides and drug molecules was also studied. By comparing the $E_{50}$ values, the relative stability of the complexes and the mode of binding of the drug molecules were compared. The dissociation of the duplex bound to the drug results in two single strands, one with the drug and one without the drug. Using $E_{50}$ values, it was even possible to differentiate between drugs that were binding in the minor grooves and others that intercalate.

### Blackbody Infrared Radiative Dissociation (BIRD)

BIRD is an interesting method that has been introduced by Dunbar and McMahon [114]. It was more recently extended for the study of large molecules [115, 116], including noncovalent complexes [117-120]. In this method, the blackbody radiation of the heated vacuum chamber walls is employed to dissociate trapped ions. Strictly speaking, only unimolecular dissociation is probed by BIRD. However, the rate of energy exchange between the trapped ions and the chamber walls can greatly exceed the dissociation rate such that the trapped ions have a Boltzmann distribution of internal energy characterized by a temperature. From the temperature dependence of the dissociation rate, activation energies and pre-exponential factors can be determined from an Arrhenius plot. Direct information on the relative thermal stability is thus available, and in the absence of a reverse barrier, the activation energy reflects a threshold dissociation energy. Using the BIRD method, Gross et al. [117] determined the gas-phase dissociation rate of heme from holo-myoglobin to be considerably lower than from holo-hemoglobin α-chain, and somewhat dependent on solution pH and on the ion charge state.

### Heated Capillary Dissociation (Thermal Dissociation in the Gas Phase)

A heated transfer capillary consisting of two independently heated segments can be used to dissociate noncovalent complexes. The complex is first desolvated in the first segment and then dissociated in the second segment. Under these conditions thermal dissociation of the complex takes place in the gas phase. A stable temperature range

of the first segment of the capillary, where desolvation is completed but no dissociation occurs, is first established. Dissociation of the complex is then performed by systematically raising the temperature of the second segment. Lebrilla and co-workers [121, 122] studied heated capillary dissociation (HCD) of cyclodextrin inclusion complexes using this approach in an FT-ICR-MS. HCD graphs were obtained by plotting the normalized intensity of the complex vs. temperature in the second segment.

### Other Gas-phase Methods

Numerous methods have been described in the literature for measuring binding enthalpies and free energies of gas-phase complexes, for example, guided ion beam tandem mass spectrometry [123-126], equilibrium methods for determining metal ion affinities to various ligands [127], photodissociation methods [128-132], and Cooks' kinetic method [133-135].

## 3.7 Summary

Soft ionization mass spectrometry is increasingly used to determine binding constants and binding energies of noncovalent complexes. As shown, one must distinguish between MS methods that measure the dissociation energies of the gas-phase complex ions, and MS-based methods used for monitoring solution equilibria. For the latter, results generally agree well with known solution-phase thermodynamic values. On the other hand, gas-phase MS methods yield interactions energies that typically do not agree with solution-phase values. This is not surprising, because ionic or ion-dipole interactions will become stronger in the absence of solvent screening ($1/\varepsilon$ dependence), while other interactions such as hydrophobic interactions are destabilized in the absence of solvent. A direct comparison should therefore not be attempted, except in cases where one expects to learn something about the nature of the noncovalent interaction itself. The determination of gas-phase binding energies is expected to be very useful for rapid screening of therapeutic agents, since their mode of interaction is designed to be mostly ionic or ion-dipole. In addition, experimental values for gas-phase binding energies can be directly compared to quantum mechanical computations that are typically obtained without incorporating sophisticated solvent shells. Frequently, qualitative trends in binding strength are reported rather than numbers for dissociation / association constants, binding enthalpies, or free energies. The reason is that this field is in the early stages of development, or in a kind of validation phase. One obvious problem is that ionization efficiencies / transfer coefficients are not generally taken into account. However, it has been shown for many systems that they significantly affect the determination of association constants by MS methods. Another shortcoming is that some presumably representative peaks in the mass spectrum are used to determine such trends, whereas taking all relevant peaks (higher order adducts, fragments, other charge states in ESI, etc.) belonging to a certain species would be accurate to quantitatively account for it.

By changing experimental parameters such as the cone voltage in a ESI experiment, a mass spectrometric analog to a melting curve can be constructed. From the slope of this melting curve at the point of 50% dissociation, it should be possible to derive a $\Delta H$ value in complete analogy to equation 3.7 [64]. For this purpose, a number of pos-

sibilities exist: thermal dissociation by HCD is one that has been already discussed. Furthermore, it is known that the plume temperature in MALDI is very close to the sublimation temperature of the matrix used [136]. Thus, different MALDI matrices could also lead to different degrees of complex dissociation by virtue of their sublimation temperature. The result will always be a kind of (gas-phase) melting curve.

Advice for planning future experiments and for appropriate data evaluation includes the following points: (i) assumptions must always be stated explicitly; this is often not the case in published studies. In order to obtain reliable results and for statistical reasons, measurements should be repeated several times. (ii) MALDI should be developed more vigorously for studying noncovalent interactions of biomacromolecules. MALDI is more tolerant to salts and buffers, often necessary ingredients for stabilizing complexes, and has thus some advantages over ESI in special situations. There is even more potential since the development of atmospheric pressure MALDI [137, 138], which is believed to be softer than conventional (vacuum) MALDI. (iii) Last but not least, the time is ripe for combining high accuracy methods such as the kinetic method or guided ion beam mass spectrometry with MALDI or ESI ion sources to study higher molecular weight complexes of biochemical interest.

## 3.8 References


1. J. M. Daniel, S. D. Friess, S. Rajagopalan, S. Wendt and R. Zenobi, *Int. J. Mass Spectrom.*, 2002, **216** (1), 1-27.
2. P. Hensley, *Structure*, 1996, **4**, 367-373.
3. D. L. Smith, Y. Deng and Z. Zhang, *J. Mass Spectrom.*, 1997, **32**, 135-146.
4. R. D. Smith and Z. Zhang, *Mass Spectrom. Rev.*, 1994, **13**, 411-429.
5. Y. Liu and D. L. Smith, *J. Am. Soc. Mass Spectrom.*, 1994, **5**, 19-28.
6. A. A. Rostom, P. Fucini, D. R. Benjamin, R. Juenemann, K. H. Nierhaus, F. U. Hartl, C. M. Dobson and C. V. Robinson, *Proc. Natl. Acad. Sci. U.S.A.*, 2000, **97** (19), 5185.
7. M. A. Tito, K. Tars, K. Valegard, J. Hajdu and C. V. Robinson, *J. Am. Chem. Soc.*, 2000, **122** (14), 3550.
8. W. J. H. Van Berkel, R. H. H. Van Den Heuvel, C. Versluis and A. J. R. Heck, *Protein Science*, 2000, **9** (3), 435-439.
9. R. L. Winston and M. C. Fitzgerald, *Mass Spectrom. Rev.*, 1997, **16** (4), 165-179.
10. F. W. McLafferty, *Science*, 1981, **214**, 280-287.
11. J. A. Loo, *Mass Spectrom. Rev.*, 1997, **16** (1), 1-23.
12. F. W. McLafferty, *J. Am. Soc. Mass Spectrom.*, 1997, **8**, 1-7.
13. K. Muller-Dethlefs and P. Hobza, *Chem. Rev.*, 2000, **100** (1), 143-167.
14. J. N. Israelachvili, *Intermolecular and Surface Forces*, 2nd ed, 1991, London, Academic Press.
15. Y. Cheng and W. H. Prusoff, *Biochem. Pharmacol.*, 1973, **22** (23), 3099-3108.
16. G. Siuzdak, *Proc. Natl. Acad. Sci. U.S.A.*, 1994, **91**, 11290-11297.
17. A. S. Woods, J. C. Buchsbaum, T. A. Worall, J. M. Berg and R. J. Cotter, *Anal. Chem.*, 1995, **67**, 4462-4465.
18. K. Strupat, D. Sagi, J. Peter-Katalinic, H. Bonisch and G. Schafer, *Analyst*, 2000, **125** (4), 563-567.
19. T. B. Farmer and R. M. Caprioli, *J. Mass Spectrom,*, 1998, **33** (8), 697-704.
20. M. Przybylski and M. O. Glocker, *Angew. Chem., Int. Ed.*, 1996, **35** (8), 806-826.
21. R. D. Smith, J. E. Bruce, Q. Wu and Q. P. Lei, *Chem. Soc. Rev.*, 1997, **26** (3),

191-202.

22. B. N. Pramanik, P. L. Bartner, U. A. Mirza, Y.-H. Liu and A. K. Ganguly, *J. Mass Spectrom.*, 1998, **33** (10), 911-920.
23. F. Hillenkamp, *Matrix-Assisted Laser Desorption/Ionization of Non-Covalent Complexes*, in *New Methods for the Study of Biomolecular Complexes*, W. Ens, K. G. Standing and I. V. Chernushevich, Editors, 1998, Kluwer Academic Publishers, Dordrecht, The Netherlands, p. 181-191.
24. J. B. Cunniff and P. Vouros, *J. Am. Soc. Mass Spectrom.*, 1995, **6**, 437-447.
25. W. D. Lehmann, *Massenspektrometrie in der Biochemie*, Spektrum Analytik, 1996, Heidelberg, Spektrum Analytik, Akad. Verl., 342-359.
26. S. D. Friess, J. M. Daniel and R. Zenobi, *Phys. Chem. Chem. Phys.*, 2004, **6** (10), 2664-2675.
27. J. R. Kimmel, *Methods Enzymol.*, 1967, **11**, 584-589.
28. H. A. Itano and R. A. Robinson, *J. Biol. Chem.*, 1972, **247**, 4819-4824.
29. M. Kalkum, M. Przybylski and M. O. Glocker, *Bioconjugate Chem.*, 1998, **9**, 226-235.
30. M. Galvani, M. Hamdan and P. G. Righetti, *Rapid Commun. Mass Spectrom.*, 2000, **14**, 1925-1931.
31. H. Belva, C. Valois and C. Lange, *Rapid Commun. Mass Spectrom.*, 2000, **14**, 224-229.
32. M. Münchbach, M. Quadroni, G. Miotto and P. James, *Anal. Chem.*, 2000, **72**, 4047-4057.
33. S. D. Friess and R. Zenobi, *J. Am. Soc. Mass Spectrom.*, 2001, **12**, 810-818.
34. S. D. Friess, J. M. Daniel, R. Hartmann and R. Zenobi, *Int. J. Mass Spectrom.*, 2001, **219** (1), 269-281.
35. A. A. Rostom, J. R. H. Tame, J. E. Ladbury and C. V. Robinson, *J. Mol. Biol.*, 2000, **296** (1), 269-279.
36. K. O. Börnsen, *Influence of Salts, Buffers, Detergents, Solvents, and Matrices on MALDI-MS Protein Analysis in Complex Mixtures*, in *Methods in Molecular Biology*, J. R. Chapman, Editor, 2000, Humana Press Inc., Totowa, NJ.
37. B. Salih and R. Zenobi, *Anal. Chem.*, 1998, **70** (8), 1536-1543.
38. R. D. Smith and K. J. Light-Wahl, *Biol. Mass Spectrom.*, 1993, **22** (9), 493-501.
39. E. Lehmann, R. Zenobi and S. Vetter, *J. Am. Soc. Mass Spectrom.*, 1999, **10**,

27-34.

40. E. Lehmann, B. Salih, M. Gomez-Lopez, F. Diederich and R. Zenobi, *Analyst*, 2000, **125** (5)), 849-854.
41. K. Strupat, H. Rogniaux, A. Van Dorsselaer, J. Roth and T. Vogl, *J. Am. Soc. Mass Spectrom.*, 2000, **11**, 780-788.
42. T. Vogt, J. Roth, C. Sorg, F. Hillenkamp and K. Strupat, *J. Am. Soc. Mass Spectrom.*, 1999, **10**, 1124-1130.
43. J. Gross, A. Leisner, F. Hillenkamp, S. Hahner, M. Karas, J. Schäfer, F. Lützenkirchen and E. Nordhoff, *J. Am. Soc. Mass Spectrom.*, 1998, **9**, 866-878.
44. N. Potier, P. Barth, D. Tritsch, J.-F. Biellmann and A. Van Dorsselaer, *Adv. Exp. Med. Biol.*, 1997, **414** (Enzymology and Molecular Biology of Carbonyl Metabolism 6), 453-454.
45. S. D. Friess, *Surface Topology Probing of Biomolecules by Noncovalent Receptors*, in *Department of Chemistry and Applied Bioscience*, 2003, Swiss Federal Institute of Technology, Zürich.
46. M. Przybylski, V. Schnaible, J. Kast, S. Bohler, J. Michels, A. Wattenberg, T. A. Fligge, D. Forst, K. Diederichs, U. Nestel, K. Zeth, M. O. Glocker and W. Welte, *NATO ASI Ser. C*, 1998, **510** (New Methods for the Study of Biomolecular Complexes), 17-43.
47. M. Przybylski, *Adv. Mass Spectrom.*, 1995, **13**, 257-283.
48. A. G. Marshall, M. R. Emmett, M. A. Freitas, C. L. Hendrickson and Z. Zhang, *Isotopic amplification, H/D exchange, and other mass spectrometric strategies for characterization of biomacromolecular topology and binding sites*, in *Mass Spectrometry in Biology and Medicine*, A. L. Burlingame, S. A. Carr and M. A. Baldwin, Editors, 2000, Humana Press, Totowa, p. 31-50.
49. S. Akashi and K. Takio, *Protein Sci.*, 2000, **9** (12), 2497.
50. A. Li, C. Fenselau and I. A. Kaltashov, *Proteins: Struct., Funct., Genet.*, 1998, **Suppl. 2**, 22-27.
51. I. A. Kaltashov and C. Fenselau, *Proteins: Struct., Funct., Genet.*, 1998, **27**, 165-170.
52. K. A. Cox, R. K. Julian, R. G. Cooks and R. E. Kaiser, *J. Am. Soc. Mass Spectrom.*, 1994, **5** (3), 127-136.
53. P. D. Mosier, A. E. Counterman, P. C. Jurs and D. E. Clemmer, *Anal. Chem.*,

2002, **74** (6), 1360-1370.

54. A. A. Shvartsburg, K. W. M. Siu and D. E. Clemmer, *J. Am. Soc. Mass Spectrom.*, 2001, **12** (8), 885-888.
55. R. W. Purves, D. A. Barnett, B. Ells and R. Guevremont, *J. Am. Soc. Mass Spectrom.*, 2000, **11** (8), 738-745.
56. R. B. Cole, *Electrospray Ionization Mass Spectrometry: Fundamentals, Instrumentation and Applications*, ed. R. B. Cole, 1997, New York, Wiley.
57. J. S. Brodbelt, *Int. J. Mass Spectrom.*, 2000, **200** (1/3), 57-69.
58. R. Guevremont, K. W. M. Siu, J. C. Y. Le Blanc and S. S. Berman, *J. Am. Soc. Mass Spectrom.*, 1992, **3**, 216-224.
59. E. Leize, A. Jaffrezic and A. Van Dorsselaer, *J. Mass Spectrom.*, 1996, **31**, 537-544.
60. K. A. Sannes-Lowery, P. Hu, D. P. Mack, H.-Y. Mei and J. A. Loo, *Anal. Chem.*, 1997, **69** (24), 5130-5135.
61. C. V. Robinson, E. W. Chung, B. B. Kragelund, J. Knudsen, R. T. Aplin, F. M. Poulsen and C. M. Dobson, *J. Am. Chem. Soc.*, 1996, **118** (36), 8646-8653.
62. Y.-T. Li, Y.-L. Hsieh, J. D. Henion, T. D. Ocain, G. A. Schiehser and B. Ganem, *J. Am. Chem. Soc.*, 1994, **116** (17), 7487-7493.
63. H. Wang and G. R. Agnes, *Anal. Chem.*, 1999, **71**, 3785-3792.
64. L. A. Marky and K. J. Breslauer, *Biopolymers*, 1987, **26** (9), 1601.
65. X. Cheng, Q. Gao, R. D. Smith, K.-E. Jung and C. Switzer, *Chem. Commun.*, 1996, (6), 747-748.
66. M. Fändrich, M. A. Tito, M. R. Leroux, A. A. Rostom, F. U. Hartl, C. M. Dobson and C. V. Robinson, *Proc. Natl. Acad. Sci. U.S.A.*, 2000, **97** (26), 14151-14155.
67. H.-K. Lim, Y. L. Hsieh, B. Ganem and J. Henion, *J. Mass Spectrom.*, 1995, **30** (5), 708-714.
68. M. J. Greig, H.-J. Gaus, L. L. Cummins, H. Sasmor and R. H. Griffey, *J. Am. Chem. Soc.*, 1995, **117**, 10765-10766.
69. K. A. Sannes-Lowery, R. H. Griffey and S. A. Hofstadler, *Anal. Biochem.*, 2000, **280**, 264-271.
70. A. Ayed, A. N. Krutchinsky, W. Ens, K. G. Standing and H. W. Duckworth, *Rapid Commun. Mass Spectrom.*, 1998, **12** (7), 339-344.

71. R. H. Griffey, S. A. Hofstadler, K. A. Sannes-Lowery, D. J. Ecker and S. T. Crooke, *Proc. Natl. Acad. Sci. U.S.A.*, 1999, **96** (18), 10129.
72. N. Carte, F. Legendre, E. Leize, N. Potier, F. Reeder, J.-C. Chottard and A. Van Dorsselaer, *Anal. Biochem.*, 2000, **284**, 77-86.
73. R. A. W. Johnstone, I. A. S. Lewis and M. E. Rose, *Tetrahedron*, 1983, **39** (9), 1597-1603.
74. R. A. W. Johnstone and I. A. S. Lewis, *Int. J. Mass Spectrom. Ion Phys.*, 1983, **46**, 451-454.
75. D.-S. Young, H.-Y. Hung and L. K. Liu, *J. Mass Spectrom.*, 1997, **32**, 432-437.
76. F. Dubois, R. Knochenmuss and R. Zenobi, *Eur. Mass Spectrom.*, 1999, **5**, 267-272.
77. V. F. Man, J. D. Lin and K. D. Cook, *J. Am. Chem. Soc.*, 1985, **107**, 4635-4640.
78. T. J. D. Jørgensen, P. Roepstorff and A. J. R. Heck, *Anal. Chem.*, 1998, **70** (20), 4427-4432.
79. T. J. D. Jørgensen, T. Staroske, P. Roepstorff, D. H. Williams and A. J. R. Heck, *J. Chem. Soc.*, 1999, **Perkin Trans. 2**, 1859-1863.
80. E. C. Kempen and J. S. Brodbelt, *Anal. Chem.*, 2000, **72**, 5411-5416.
81. G. W. Gokel, D. M. Goli, C. Mingati and L. Echegoyen, *J. Am. Chem. Soc.*, 1983, **105**, 6786-6790.
82. C. M. Goff, M. A. Matchetter, N. Shabestary and S. Khazaeli, *Polyhedron*, 1996, **15**, 3897-3903.
83. X. H. Zou, B. H. Ye, H. Li, Q. L. Zhang, H. Chao, J. G. Liu, L. N. Ji and X. Y. Li, *J. Biol. Inorg.Chem.*, 2001, **6** (2), 143.
84. K. Wang and G. W. Gokel, *J. Org. Chem*, 1996, **61**, 4693-4697.
85. S. F. Ralph, P. Iannitti, R. Kanitz and M. M. Sheil, *Eur. Mass Spectrom.*, 1996, **2**, 173-179.
86. E. C. Kempen, J. S. Brodbelt, R. A. Bartsch, M. T. Blanda and D. B. Farmer, *Anal. Chem.*, 2001, **73**, 384-390.
87. S. M. Blair, J. S. Brodbelt, A. P. Marchand, H.-S. Chong and S. Alihodzic, *J. Am. Soc. Mass Spectrom.*, 2000, **11**, 884-891.
88. E. Kempen, J. S. Brodbelt, R. A. Bartsch, Y. Jang and J. S. Kim, *Anal. Chem.*, 1999, **71**, 5493-5500.
89. S. M. Blair, J. S. Brodbelt, A. P. Marchand, K. A. Kumar and H.-S. Chong,

*Anal. Chem.*, 2000, **72**, 2433-2445.

90. A. Reichert, R. Fröhlich, R. Ferguson and A. Kraft, *J. Chem. Soc. Perkin Trans. 1*, 2001, 1321-1328.
91. L. Peters, R. Froehlich, A. S. F. Boyd and A. Kraft, *J. Org. Chem.*, 2001, **66** (10), 3291-3298.
92. M. T. Blanda, D. B. Farmer, J. S. Brodbelt and B. J. Goolsby, *J. Am. Chem. Soc.*, 2000, **122**, 1486-1491.
93. S. M. Blair, J. S. Brodbelt, G. M. Reddy and A. P. Marchand, *J. Mass Spectrom.*, 1998, **33**, 721-728.
94. J. S. Brodbelt, E. Kempen and M. Reyzer, *Struct. Chem.*, 1999, **10**, 213-220.
95. C. A. Schalley, T. Martín, U. Obst and J. Rebek Jr., *J. Am. Chem. Soc.*, 1999, **121**, 2133-2138.
96. A. Triolo, F. M. Arcamone, A. Raffaelli and P. Alvadori, *J. Mass Spectrom.*, 1997, **32** (11), 1186-1194.
97. K. A. Sannes-Lowery, H.-Y. Mei and J. A. Loo, *Int. J. Mass Spectrom.*, 1999, **193** (2/3), 115-122.
98. V. Gabelica, E. De Pauw and F. Rosu, *J. Mass Spectrom.*, 1999, **34**, 1328-1337.
99. O. Baudoin, F. Gonnet, M.-P. Teulade-Fichou, J.-P. Vigneron, J.-C. Tabet and J.-M. Lehn, *Chem. Eur. J.*, 1999, **5** (9), 2762-2771.
100. A. Kapur, J. L. Beck and M. M. Sheil, *Rapid Commun. Mass Spectrom.*, 1999, **13** (24), 2489.
101. K. X. Wan, T. Shibue and M. L. Gross, *J. Am. Chem. Soc.*, 2000, **122** (2), 300-307.
102. Y. L. Hsieh, Y. T. Li, J. D. Henion and B. Ganem, *Biol. Mass Spectrom.*, 1994, **23** (5), 272-276.
103. B. Ganem, Y. T. Li and J. D. Henion, *J. Am. Chem. Soc.*, 1991, **113** (16), 6294-6296.
104. J. A. Loo, P. Hu, P. McConnell and W. T. Mueller, *J. Am. Soc. Mass Spectrom.*, 1997, **8** (3), 234-243.
105. J. Gao, X. Cheng, C. R., G. Sigal, J. E. Bruce, B. L. Schwartz, S. A. Hofstadler, G. A. Anderson, R. D. Smith and G. M. Whitesides, *J. Med. Chem.*, 1996, **39**, 1949-1955.
106. X. Cheng, R. Chen, J. E. Bruce, B. L. Schwartz, G. A. Anderson, S. A. Hofsta-

dler, D. C. Gale and R. D. Smith, *J. Am. Chem. Soc.*, 1995, **117**, 8859-8860.

107. B. J. Goolsby, J. S. Brodbelt, E. Adou and M. Blanda, *Int. J. Mass Spectrom.*, 1999, **193**, 197-204.
108. Q. Wu, J. Gao, D. Joseph-McCarthy, G. B. Sigal, J. E. Bruce, G. M. Whitesides and R. D. Smith, *J. Am. Chem. Soc.*, 1997, **119**, 1157-1158.
109. H. Rogniaux, A. Van Dorsselaer, P. Barth, J. F. Biellmann, J. Barbanton, M. van Zandt, B. Chevrier, E. Howard, A. Mitschler, N. Potier, L. Urzhumtseva, D. Moras and A. Podjarny, *J. Am. Soc. Mass Spectrom.*, 1999, **10**, 635-647.
110. C. L. Hunter, A. G. Mauk and D. J. Douglas, *Biochemistry*, 1997, **36** (5), 1018-1025.
111. V. Gabelica and E. De Pauw, *J. Mass Spectrom.*, 2001, **36**, 397-402.
112. A. K. Shukla and J. H. Futrell, *J. Mass Spectrom.*, 2000, **35** (9), 1069.
113. K. X. Wan, M. L. Gross and T. Shibue, *J. Am. Soc. Mass Spectrom.*, 2000, **11** (5), 450-457.
114. R. C. Dunbar and T. B. McMahon, *Science*, 1998, **279** (Jan. 9), 194-197.
115. S. E. Rodriguez-Cruz, J. S. Klassen and E. R. Williams, *J. Am. Soc. Mass Spectrom.*, 1997, **8**, 565-568.
116. Y. Ge, D. M. Horn and F. W. McLafferty, *Int. J. Mass Spectrom.*, 2001, **210/211** (203-214),
117. D. S. Gross, Y. Zhao and E. E. Williams, *J. Am. Soc. Mass Spectrom.*, 1997, **8**, 519-524.
118. P. D. Schnier, J. S. Klassen, E. F. Strittmatter and E. R. Williams, *J. Am. Chem. Soc.*, 1998, **120**, 9605-9613.
119. J. S. Klassen, P. D. Schnier and E. R. Williams, *J. Am. Soc. Mass Spectrom.*, 1998, **9**, 1117-1124.
120. E. F. Strittmatter, P. D. Schnier, J. S. Klassen and E. R. Williams, *J. Am. Soc. Mass Spectrom.*, 1999, **10**, 1095-1104.
121. F. He, J. Ramirez, B. A. Garcia and C. B. Lebrilla, *Int. J. Mass Spectrom*, 1999, **182** (183), 261-273.
122. B. Garcia, J. Ramirey, S. Wong and C. B. Lebrilla, *Int. J. Mass Spectrom.*, 2001, **210/211**, 215-222.
123. K. M. Ervin and P. B. Armentrout, *J. Chem. Phys.*, 1985, **83**, 166-189.

124. R. H. Schultz, K. C. Crellin and P. B. Armentrout, *J. Am. Chem. Soc.*, 1991, **113**, 8590-8601.

125. P. B. Armentrout, *Thermochemical measurements by guided ion beam mass spectrometry*, in *Advances in gas phase ion chemistry*, N. G. Adams and L. M. Babock, Editors, 1992, JAI, Greennwich, p. 83-119.

126. M. T. Rodgers, K. M. Ervin and P. B. Armentrout, *J. Chem. Phys.*, 1997, **106**, 4499-4508.

127. R. L. Woodin and J. L. Beauchamp, *J. Am. Chem. Soc.*, 1978, **100**, 501-508.

128. L. Sallans, K. R. Lane and B. S. Freiser, *J. Am. Chem. Soc.*, 1989, **111**, 865-873.

129. W. J. van der Hart, *Mass Spectrom. Rev.*, 1989, **8**, 237 -.

130. K. F. Willey, P. Y. Cheng, M. B. Bishop and M. A. Duncan, *J. Am. Chem. Soc.*, 1991, **113**, 4721 -.

131. J. D. Faulk and R. C. Dunbar, *J. Am. Chem. Soc.*, 1992, **114**, 8596-8600.

132. S. Afzaal and B. S. Freiser, *Chem. Phys. Lett.*, 1994, **218**, 254 -.

133. R. G. Cooks, J. S. Patrick, T. Kotiaho and S. A. Mcluckey, *Mass Spectrom. Rev.*, 1994, **13** (4), 287-339.

134. R. G. Cooks and P. S. H. Wong, *Acc. Chem. Res.*, 1998, **31**, 379-386.

135. R. G. Cooks, J. T. Koskinen and P. D. Thomas, *J. Mass Spectrom.*, 1999, **34**, 85-92.

136. C. D. Mowry and M. V. Johnston, *J. Phys. Chem.*, 1994, **98** (7), 1904-1909.

137. V. V. Laiko, M. A. Baldwin and A. L. Burlingame, *Anal. Chem.*, 2000, **72** (4), 652-657.

138. V. V. Laiko, N. I. Taranenko, V. D. Berkout, B. D. Musselman and V. M. Doroshenko, *Rapid Commun. Mass Spectrom.*, 2002, **16** (18), 1737-1742.

# CHAPTER 4

# ADENYLATE KINASE

Seite Leer /
Blank leaf

Noncovalent complexes between chicken muscle adenylate kinase and two inhibitors were investigated with electrospray ionization mass spectrometry under non-denaturing conditions. The two inhibitors used were $P^1,P^4$-di(adenosine-5')tetraphosphate (Ap4A) and $P^1,P^5$-di(adenosine-5') pentaphosphate (Ap5A). The noncovalent nature and the specificity of the complexes are demonstrated with a number of control experiments. Titration experiments allowed the association constants for inhibitor binding to be determined. Since ion yields related to the concentration of the investigated system, a new data evaluation method is presented that is insensitive to the overall ionization efficiency. The $K_A$ values found were 9.0 $10^4$ $M^{-1}$ (Ap4A) and 4.0 $10^7$ $M^{-1}$ (Ap5A), respectively, in very good agreement with the literature.

**Adapted from:**

J. M. Daniel, G. McCombie, S. Wendt, and R. Zenobi, *J. Am. Soc. Mass Spectrom.*, 2003, **14**, 442-448.

## 4.1 Introduction

Soft ionization mass spectrometry is currently involving into a more accepted and robust method for studying noncovalent interactions quantitatively. A method to quantitatively ascertain the noncovalent interaction strength is presented where only the relative signal integrals of a protein and a noncovalent protein-inhibitor complex are determined. In other words, a varying overall ionization efficiency does not affect the results. Furthermore, we present a set of control experiments to verify the specificity of the complex and to rule out any unspecific adducts, *i.e.* in the gas phase. The system studied in this work was adenylate kinase (AK) from chicken muscle and its two noncovalent inhibitors $P^1$,$P^4$-di(adenosine-5')tetraphosphate (Ap4A) and $P^1$,$P^5$-di(adenosine-5')pentaphosphate (Ap5A) (figure 4.1).

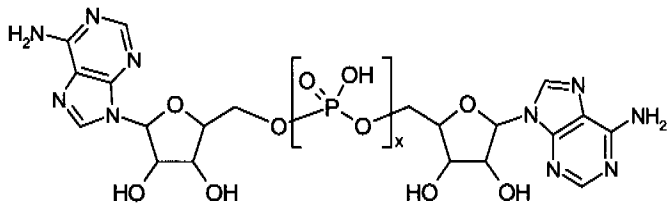

**Figure 4.1: Chemical structure of Ap4A for x=4 and for Ap5A for x=5.**

AK is a phosphotransferase that catalyzes the transfer of the γ-phosphate group of magnesium-adenosine-triphosphate (Mg·ATP) to adenosine-monophosphate (AMP) and therefore plays an important role in the energy metabolism of cells [2]. There are five major types of AK: AK1 (from cytosols of mammalian or vertebrate muscles, with c, h, p and r designating chicken, human, porcine, and rabbit, respectively), AKe (from *Escherichia coli*), AKy (from yeast), AK2 (from mammalian mitochondrial intermembrane space), and AK3 (from mammalian mitochondrial matrix, specific to GTP instead of ATP). AK1 differs from AKe and AKy in lacking a 30-residue loop near position 132 [3]. In all other aspects of structure and function, AK1, and AKe are largely homologous [4]. AK has a molecular weight of 21.6 kDa and its inhibitors are well studied. Therefore this protein-inhibitor system has been chosen for the present study.

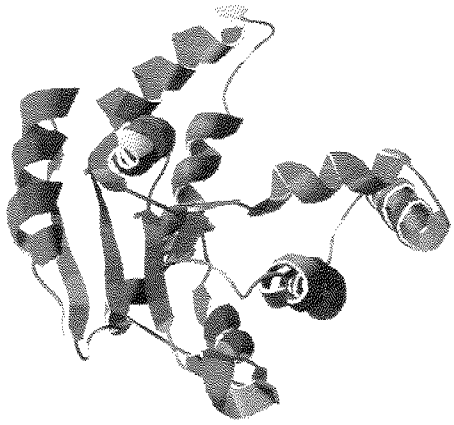

**Figure 4.2: 3D representation of AK (sus scrofa) at 2.1 Å resolution (PDB ID: 102L).**

## 4.2 Experimental Section

### Instrumentation

All experiments were conducted on the α-prototype electrospray orthogonal injection time-of-flight mass spectrometer from Agilent (Palo Alto, California, USA) described in chapter 2. Infusion rates of 3 to 5 μl $min^{-1}$ with a pneumatically assisted ESI source were used ("ion spray"), spray potentials were between 2700 and 3000 V. The source conditions of the instrument were optimized for the transfer of high molecular weight ions and for gentle desolvation conditions by adjusting the different source and transfer potentials. For low energy dissociation experiments the voltage between sampling cone and skimmer was increased from 32 V to 140 V which is sufficient to dissociate noncovalent complexes. Spectra were recorded at a repetition rate of 4 kHz and several 100'000 spectra were summed and transferred to a PC for further processing.

### Materials and Methods

Adenylate kinase (M=21'689 Da) from chicken muscle and myoglobin from horse heart were obtained from Sigma (St. Louis, USA) and used for the titration experiments without prior purification. Since a batch dependent amount of magnesium was found, the samples were treated by adding EDTA, primarily to allow comparison of our results with the literature. All samples were dissolved in water. Ammonium acetate ($H_4NOAc$) and triethylammonium hydrogencarbonate ($(HNEt_3)HCO_3$) were used to buffer the protein-inhibitor solutions; these are well known for conserving noncovalent interactions in ESI [5].

The titration samples contained 10 μM AK, 0 - 8 μM $P^1$,$P^5$-di(adenosine-5')pentaphosphate or 0 - 12 μM $P^1$,$P^4$-di(adenosine-5')tetraphosphate, 50mM $(HNEt_3)HCO_3$, and 500 μM EDTA. Inhibitors were from Fluka (Buchs, Switzerland) and from Sigma (USA), respectively. 8-azido-adenosinetriphosphate (8-$N_3$-ATP) was obtained from Biolog Life Science Institute (Bremen, Germany).

AK was denatured in four different ways: a solution containing 10 μM AK in 10 mM $NH_4AcO$ buffer was incubated with 50% MeOH (HPLC grade) or 5% AcOH (reagent grade), prior as well as after adding the 10 μM Ap5A.

For low energy dissociation experiments, several different solutions were used, including 10 μM AK / 10 μM Ap5A in 50mM $(HNEt_3)HCO_3$ buffer and 10 μM AK / 20 μM Ap5A in 5mM $NH_4AcO$ buffer.

AK was covalently modified in its binding pocket according to a slightly adapted method originally published by Olcott [6] and David [7]. 0.3 μl 5 mM 8-$N_3$-ATP in 10 mM $NH_4AcO$, 0.5 μl 20 mM $MgCl_2$, 12 μl 250 μM AK in 10 mM $NH_4AcO$, and 87 μl 50 mM Tris/HCl (pH=7.2) were mixed on ice and incubated for 30 seconds. The solution was exposed to UV radiation at a wavelength of 254 nm (Westinghouse Electric Corp. Fluorescent & Vapor Lamp Division, Broomfield, NJ., USA) for 75 seconds. Another 0.3 μl 5 mM 8-$N_3$-ATP in 10 mM $NH_4AcO$ was added and again exposed to UV radiation for 75 seconds. The Tris/HCl buffer was exchanged with a NAP-5 gel permeation column (Pharmacia Biotech AB, Sweden) to 10 mM $NH_4AcO$. The remaining activity of the treated AK sample was probed by an assay of Wallimann et al. [8] and was found to be reduced by (25 ± 5) %. The mass of the modified AK was 22'259 Da.

## 4.3 Protein Conformation and Charge State Distribution

Electrospray ionization produces intact and multiply charged, usually protonated, gas-phase ions from proteins in solution. During positive ion mode ESI, unfolded proteins in solution form higher charge states than those in tightly folded conformations. The width of the charge state distribution (CSD) is often about half the CSD of the highest charge state [9]. Figure 4.3 shows an ESI mass spectrum of unfolded myoglobin with a maximum charge state of z = 19 and a width of the CSD of 15 charges. A striking feature of ESI-MS of unfolded proteins is that the average charge state increases in an approximately linear fashion with the molecular mass of the protein. Thus, it is observed that denatured multiply charged proteins show up between 800 and 2000 Da.

Based on the empirical finding that the observed charge states for folded proteins are lower, ESI-MS has become a standard method to probe protein conformational changes in solution. It is often claimed that the ESI CSD is determined by the *accessibility* of basic sites (Arg, Lys, His, amino-terminus) for protonation during electrospray [10]. However, the correlation of the protein conformation and ESI charge state distribution is still a matter of ongoing debate. Relevant factors include the steric protection of basic sites in tightly folded conformations, their intramolecular spacing, and the accessible surface area of the protein. Grandori has recently put forward the interesting hypothesis [11]: the lower charge states observed for folded proteins in positive mode ESI may be related to negatively charged side chains (Asp, Glu) that are buried within the protein interior core. There is evidence that gas-phase protein ions can retain at least some of their solution structure [12-15]; *i.e.* unfolded proteins in solution are generally expected to produce more extended conformations in the gas phase. Consequently, extended protein conformations have a greater capacity to stabilize protons that become attached to basic sites on the protein surface. Most likely, this charge stabilization occurs through intramolecular solvation and through the greater spatial separation of individual charges, both of which serve to reduce electrostatic repulsion. In this sense, the ESI charge state distribution may be considered to be a probe of the overall *compactness* of a protein in solution. Konermann and Douglas observed that CSD changes of cytochrome c selectively reflected alterations of the

protein's tertiary structure, but remained insensitive to secondary structural changes. Comparative results were obtained for a number of other proteins. A general relationship between structural properties of a protein in solution and its ESI CSD, however, cannot be established with certainty at this time.

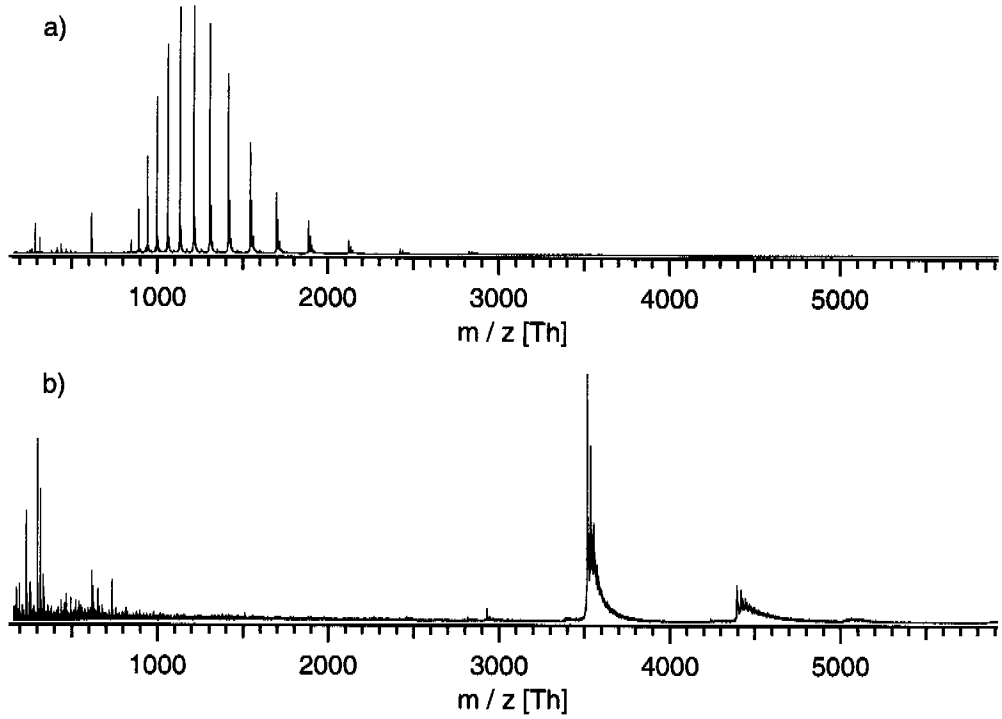


**Figure 4.3: (a) Positive ion mode ESI of 11 μM myoglobin in 48% MeOH and 2% acetic acid. A broad CSD is observed with highest abundance of charge state +12. (b) Positive ion mode ESI mass spectrum of 11 μM myoglobin in $H_2O$ buffered with 50 mM $HNEt_3$ $HCO_3$. A very narrow CSD is observed with highest abundance of charge state of +5. The peak width is broad due to incomplete evaporation of buffer and water molecules.**

Nevertheless, the CSD of an ESI mass spectrum allows a quick control whether the protein has unfolded during the preparation or is still in a folded state. The latter does not mean that it is in its active state! Whether a protein remains in its active form or not is determined by the pH, temperature, ionic strength, and the presence of counterions. Luckily most of the proteins remain folded for a long time at room temperature and even at slightly elevated temperature. But it is necessary to use experimental conditions that preserve the native state of the proteins during transfer from solution into the gas phase. For this purpose, the pH is usually maintained at near-neutral value by using a buffer solution. The volatility of buffer salts is of primary importance for lim-

| Buffer | Structure | pH |
|---|---|---|
| Ammonium acetate | 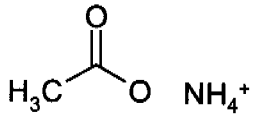 | 6.5-7.5 |
| Trieethylammonium acetate | 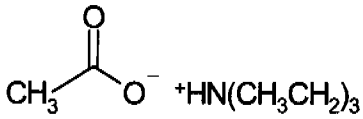 | 7.0 |
| Triethylammonium hydrogencarbonate | 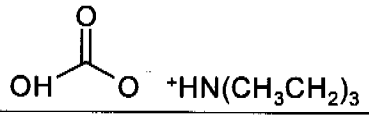 | 8.4-8.6 |

**Table 4.1: The three commonly used buffers in ESI-MS.**

iting the addition of metal ions or solvent molecules. Commonly used buffers are ammonium acetate, triethylammonium acetate, or triethylammonium bicarbonate buffers (table 4.1) [16]. The differences in pH as well as in volatility of the buffer's components influence the CSD of the resulting spectra. In all cases the width of the CSD for the native proteins is narrow but the average number of charges per ion can differ significantly (figure 4.4).

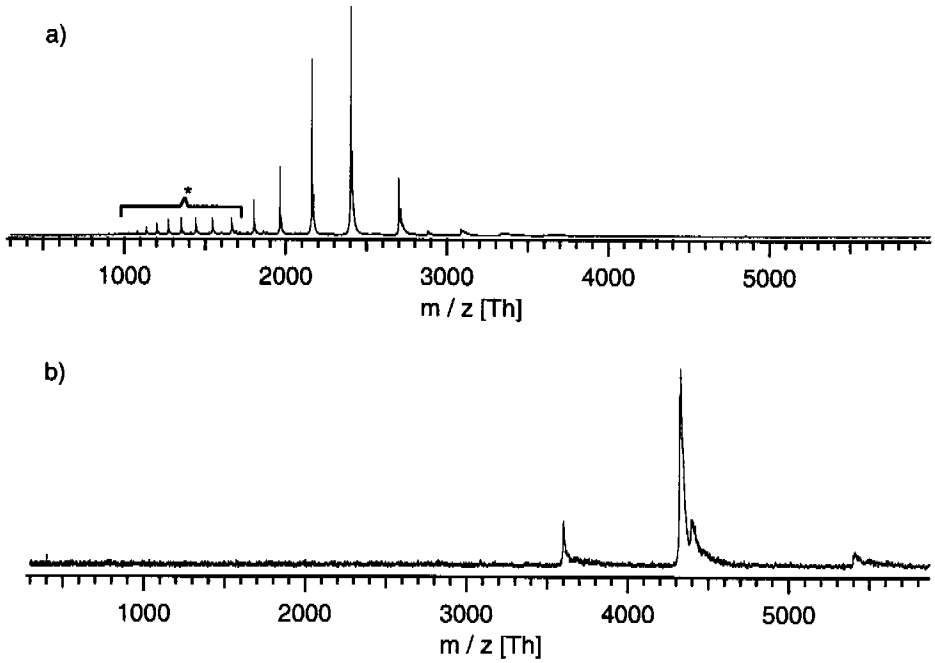


**Figure 4.4: Positive ion mode ESI mass spectra of 10 μM AK in a) 5 mM $NH_4$ AcO, and b) 50 mM $HN(CH_3CH_2)_3$ $HCO_3$, respectively. In the more acidic buffer ($NH_4$ AcO) the multiply charged ion with the highest abundance has charge +10 whereas in the more basic buffer it has charge +5. In a) the CSD at lower intensity (*) indicates a small degree of denaturation of the protein.**

## 4.4 Chemical Control Experiments

For the analysis of large noncovalent complexes, suitable instrumental conditions must be found where desolvation is sufficiently complete to allow mass resolution of all different species, without disruption of the noncovalent complex. This compromise leads to a fairly low signal-to-noise ratio (S/N) which was found to drop even further with increasing inhibitor concentration. Figure 4.5 shows mass spectra of 8.8 μM AK with 8 μM Ap4A (a) and Ap5A (b), respectively. Since the inhibitors carry many phosphate groups, the S/N ratio decreases with higher inhibitor concentration. It is a known behavior in ESI-MS, and it has been described that phosphorylated species reduce the ionization efficiency of the investigated systems.

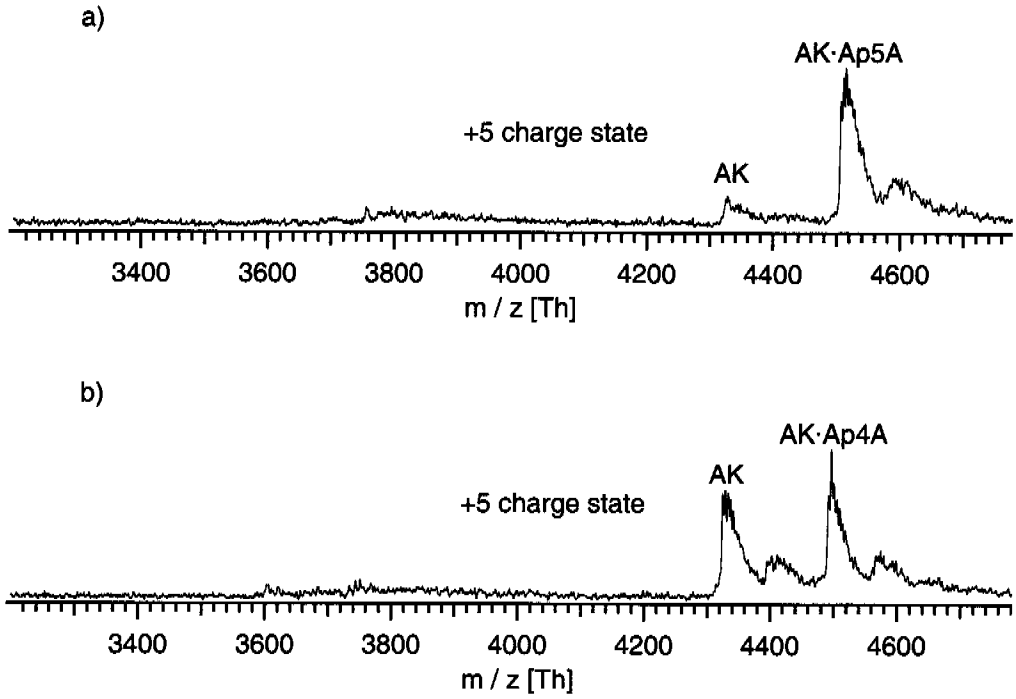


**Figure 4.5: Positive ion mode mass spectrum of 8 μM AK with a) 8 μM Ap4A and b) 8 μM Ap5A, respectively, in 50 mM $(HNEt_3)HCO_3$. Ionization and desolvation are very soft, leading to broad peaks. Many salt and buffer adducts are observed.**

The observed peaks are all quite broad, probably due to an incomplete desolvation leading to remaining water and buffer adducts. However, the signals of free AK and of the complexes are clearly resolved. Dependent on the sample batch, a second, less

abundant peak for AK and for AK·ApXA was detected in some of the spectra. Lack of the possibility to perform MS/MS experiments, the peak could not unambiguously identified, but it is assumed to be due to a contamination from a sequence variant of AK. Since these peaks originate from an AK variant of comparable activity, they are included in the evaluation of the titration experiment as well.

When a signal at the mass of a complex is detected by mass spectrometry, it does not automatically imply that the complex is indeed noncovalent and specific. Therefore a number of control experiments were performed to prove the specificity and the non-covalent nature of the suggested interaction. Figure 4.6 shows spectra of AK with the inhibitor Ap5A at physiological pH. Trace (c) was recorded with soft ionization and desolvation conditions preserving the noncovalent complex, whereas trace (d) represents harsher conditions (increased cone - skimmer voltage) leading to low energy dissociation of the complex. It is obvious that the total ionization efficiency and especially the transfer efficiency is decreased for harsher conditions. This is explained by more ions scattered into the vacuum due to higher energy collisions in the source. The present data shows the +5 charge state and was recorded using 10 μM AK and 10 μM Ap5A in 50 mM triethylammonium bicarbonate. Identical behavior was found for other solution conditions, *e.g.*, 10 μM AK, 20 μM Ap5A in 5 mM ammonium acetate. The complex was always dissociated under harsher interface conditions, while the protein itself remained intact. We can thus safely assume that this complex is of non-covalent nature.

Further control experiments included methanol or acetic acid induced denaturation of AK both prior to and after adding Ap5A to the solution. An intact tertiary structure of the protein is needed to form and maintain the noncovalent complex. Upon denaturation, no complexes could be observed, giving additional strong evidence for its specificity (see figure 4.6).

The last control experiment should confirm the binding of the inhibitor in the active site of the protein. Therefore, AK was covalently modified as outlined in the experimental section. In brief, the active site is blocked by a covalently bound ATP mimic with proven binding within the active site. Because the modification reaction was not

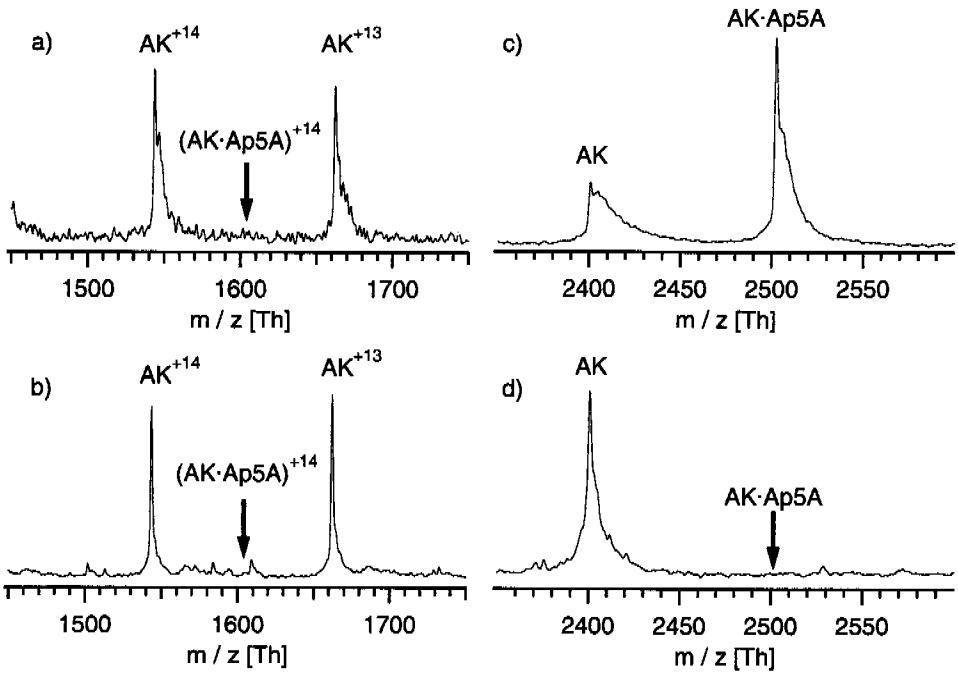


**Figure 4.6: Positive ion mode mass spectra of 10 μM AK, 16 μM Ap5A whereas the protein has been denatured with 64% MeOH prior a) and after b) adding the inhibitor. The lack of complex signal indicates that the structure of the protein is essential to the binding of the inhibitor. Positive ion mode mass spectrum of 10 μM AK and 20 μM Ap5A in 5 mM NH4AcO whereas the collision energy in the source is kept low c) and is set to higher values for d). The lack of complex signal in d) indicates that the binding is indeed of noncovalent nature.**

complete, the resulting sample contained both modified and unmodified AK which were easily identified by their different masses. Figure 4.7 shows the mass spectrum of this modified AK sample in the presence of Ap5A at physiological pH. Almost no inhibitor binding of the modified AK is observed, suggesting that the inhibitor Ap5A binds exclusively in the active site of the unmodified protein. The results of all control experiments are fully consistent with specific noncovalent inhibitor binding in the active site of the protein. The second inhibitor, Ap4A, is much less well studied than Ap5A. For example, no crystal structure data exist for AK-Ap4A complexes. It is assumed that Ap4A also forms a similar complex with AK, as suggested by other studies [17, 18].

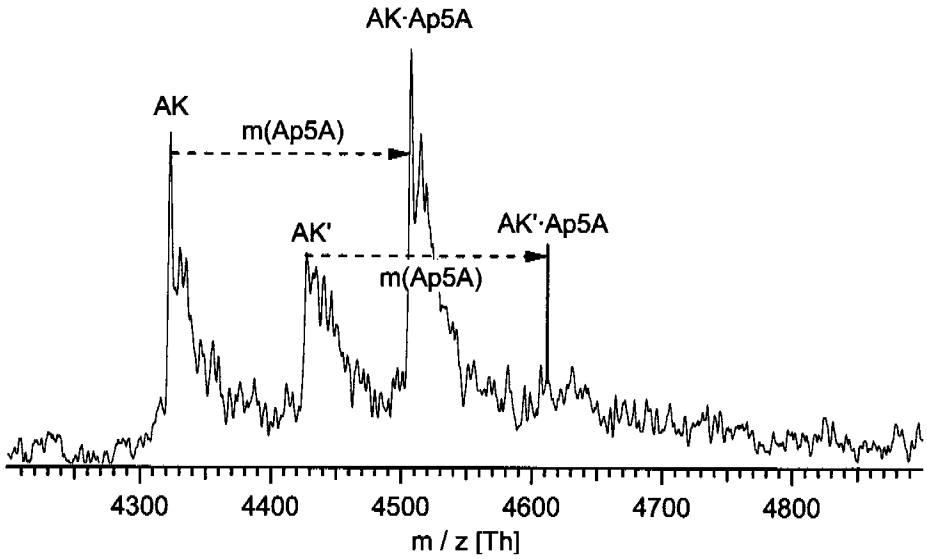


**Figure 4.7: Positive ion mode mass spectrum of a reaction mixture (10 μM total protein) of AK and covalently modified AK (AK′) with 10 μM Ap5A (with respect to the total concentration of AK and AK′) in 50 mM $(HNEt_3)HCO_3$. Almost no binding to AK′ is observed.**

## 4.5 Titration Experiments

In the following section, the equations of complex formation of AK with its inhibitor ApXA are described. Square brackets denote concentrations of the different species.

$$K_A = \frac{[AK \cdot ApXA]}{[AK] \cdot [ApXA]} \quad \text{(Eq 4.1)}$$

$$[AK]_0 = [AK] + [AK \cdot ApXA] \quad \text{(Eq 4.2)}$$

$$[ApXA]_0 = [ApXA] + [AK \cdot ApXA] \quad \text{(Eq 4.3)}$$

*KA* *association constant*
*$[AK]_0$* *total concentration AK*
*[AK]* *concentration of free AK*
*$[ApXA]_0$* *total concentration ApXA*
*[ApXA]* *concentration of free ApXA*
*[AK·ApXA]concentration of noncovalent complex*

Experimentally, the ratio $R_{AK}$ of complex and bare protein is determined (equation 4.4), assuming that the measured intensities reflect concentrations in solution. These

$$R_{AK} = \frac{[AK \cdot ApXA]}{[AK]} \quad \text{(Eq 4.4)}$$

$R_{AK}$ *ratio of complex to free AK*

equations can be solved for $K_A$ for known values of $[AK]_0$ and $[ApXA]_0$ (equations 4.5-4.6).

$$K_A = \frac{R_{AK}^2 + R_{AK}}{[ApXA]_0 \cdot (1 + R_{AK}) - ([AK]_0 \cdot R)} \quad \text{(Eq 4.5)}$$

A more robust global data evaluation takes into account all data points, and can be achieved by a least square fit of experimental values $R_{AK}$ vs. known $[ApXA]_0$ values to an expression which is obtained by solving the above equations for $R_{AK}$. This yields equation 4.6, where $K_A$ is the only adjustable parameter.

$$R_{AK} = \frac{1}{2}(-1-(K_A \cdot [AK]_0) + K_A \cdot [ApXA]_0 + \sqrt{4 \cdot K_A \cdot [ApXA]_0 + (K_A \cdot [ApXA]_0 - (K_A \cdot [AK]_0) - 1)^2}) \quad \text{(Eq 4.6)}$$

The fit described in equation 4.6 is preferable to a Scatchard plot (see, for example [19]) or other form of data linearization that are used for graphical evaluation of protein inhibition, especially for statistical error analysis. A similar approach was chosen by Greig et al. [20] who used a fit to a second order polynomial in order to determine two dissociation constants of a BSA-oligonucleotide complex. In the present approach, the ratio $R_{AK}$ of peak areas for the [AK] and [AK·ApXA] signals is used to determine the association constant. A good baseline correction is important to obtain reliable results, particularly when one of the peaks is hardly visible. Several different baseline correction methods were therefore tested. In the simplest approach, a constant value was subtracted from the data. In a more refined method, a line was fitted to the baseline allowing the correction of a sloping baseline. In the third method, a linear baseline was calculated for each peak, allowing correction for different slopes in the baseline. In the most sophisticated method, an arbitrary mathematical form of the baseline was allowed. The differences between these methods were found to be negligible. Therefore the simplest baseline correction method was used throughout.

For the determination of solution-phase binding constants by means of mass spectrometry, it is necessary that the experiment fulfills two conditions. First, the ionization efficiency of the protein and the complex should be identical. Second, the noncovalent complex must survive the ionization process, the transfer into the vacuum, and the acceleration in the TOF instrument. The first condition is probably fulfilled in the present case: identical charge distributions were found for the bare protein and the protein-inhibitor complexes. Also, the tertiary structure and the mass of the bare protein and the complex are similar. During the titration experiments, the total ionization efficiency decreased with increasing concentration of the inhibitor. Since we only determine the ratio of the complex and the bare protein, this has no effect on the titration results as long as the assumption of equal ionization efficiencies for both species holds. The second condition should be fulfilled, too. For this particular case, electrostatic and dipolar interactions are involved in the stabilization of the

complex [21, 22]; these are forces that are expected to increase upon removal of the solvent.

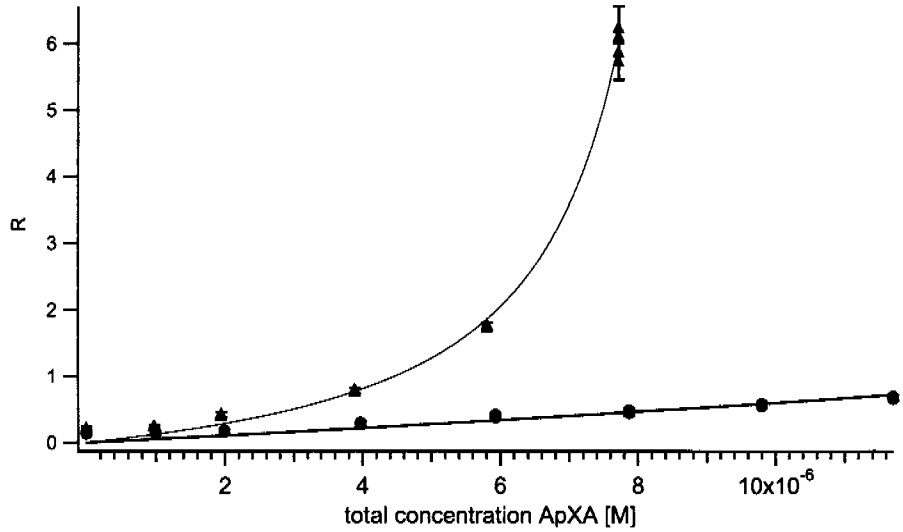


**Figure 4.8: Result of the titration experiments of AK with Ap5A (filled triangle, $K_A$ = $4.0 \cdot 10^7$ $M^{-1}$) and AK with Ap4A (filled circle, $K_A$ = $9.0 \cdot 10^4$ $M^{-1}$). The lines are fitted data with eq. 4.6.**

The association constants for the AK·ApXA system were determined as described above. The experimentally obtained R-values are plotted against the total inhibitor concentrations used for the titration. In Figure 4.8, this plot is shown for both noncovalent inhibitors. The lines represent a fit for the association constant obtained by solving equation 4.6. The association constant for AK and Ap5A is $K_A = 4.0 \times 10^7$ $M^{-1}$, for AK and Ap4A $K_A = 9.0 \times 10^4$ $M^{-1}$. Because the $K_A$ value for this particular system depends on the magnesium concentration of the solution, any remaining magnesium was masked by adding an excess of EDTA (see experimental section). The relative standard deviations for the specific inhibitor concentrations were between 1.6 and 5.0 %. The confidence interval for $K_A$ is difficult to estimate, but it will most probably be less than an order of magnitude. In Table 4.2, the experimentally obtained values are compared to previously published data. Values determined by mass spectrometry for AK from chicken muscle lie in the same range as literature values for different species and are therefore in very good agreement. These results also validate the conditions for the titration. It shows that the postulated conditions and assumptions are justifiable.

| Complex | Species | $K_A$ [$M^{-1}$] | Reference |
|---|---|---|---|
| AK1-Ap4A | Chicken muscle | $9.0 \times 10^4$ | This work, [1] |
| AKe-MgAp4A | *Escherichia coli* | $2.3 \times 10^4$ | [2] |
| AKe-Ap4A | *Escherichia coli* | $7.7 \times 10^4$ | [2] |
| AK1-MgAp4A | Pig muscle | $9.1 \times 10^4$ | [18] |
| AK1-Ap5A | Chicken muscle | $4.0 \times 10^7$ | This work, [1] |
| AKe-MgAp5A | *Escherichia coli* | $6.7 \times 10^7$ | [2] |
| AKe-Ap5A | *Escherichia coli* | $1.0 \times 10^7$ | [2] |
| AK1-MgAp5A | Rabbit muscle | $2.8\text{-}5.0 \times 10^8$ | [23] |
| AK1-MgAp5A | Pig muscle | $3.4 \times 10^7$ | [18] |

**Table 4.2: Comparison of the association constants measured and published in the literature**

## 4.6 Summary

The successful determination of solution-phase association constants of noncovalent protein-inhibitor complexes by ESI mass spectrometry has been demonstrated. Mass spectrometry has great potential for becoming a widely used method in this area due to its sensitivity and speed. This method allows screening of drug libraries with respect to their association constants towards a target protein. In this case, control experiments to confirm the noncovalent nature and the specificity of the complexes are only necessary to prevent overestimations of association constant due to unspecific aggregation or covalent binding. For "misses", *i.e.* inhibitors with low $K_A$, such control will usually not be necessary. Furthermore, the present analysis assumes that all complexes formed in solution survive in the mass spectrometer during the measurement, and that the ionization efficiency of the uncomplexed protein and of the protein-inhibitor complex are identical. These assumptions are true for the present system, but must be validated when investigating unknown systems.

## 4.7 References


1. J. M. Daniel, G. McCombie, S. Wendt and R. Zenobi, *J. Am. Soc. Mass Spectrom.*, 2003, **14** (5), 442-448.
2. J. Reinstein, I. R. Vetter, I. Schlichting, R. Rösch, A. Wittinghofer and R. S. Goody, *Biochem.*, 1990, **29**, 7440-7450.
3. G. H. W. Haase, M. Brune, J. Reinstein, E. F. Pai, A. Pingoud and A. Wittinghofer, *J. Mol. Biol.*, 1989, **207**, 151-162.
4. T. Dahnke and M.-D. Tsai, *J. Biol. Chem.*, 1994, **269**, 8075-8081.
5. D. Lemaire, G. Marie, L. Serani and O. Laprévote, *Anal. Chem.*, 2001, **73**, 1699-1706.
6. M. C. Olcott, M. L. Bradley and B. E. Haley, *Biochem.*, 1994, **33**, 11935-11941.
7. S. S. David and B. E. Haley, *Biochem.*, 1999, **38**, 8492-8500.
8. T. Wallimann, D. C. Turner and H. M. Eppenberger, *J. Cell Biol.*, 1977, **75**, 297-317.
9. R. D. Smith, J. A. Loo, C. G. Edmonds, C. J. Barinaga and H. R. Udseth, *Anal. Chem.*, 1990, **62** (9), 882-899.
10. J. A. Loo, *Bioconjugate Chem.*, 1995, **6** (6), 644-665.
11. R. Grandori, *J. Mass Spectrom.*, 2003, **38** (1), 11-15.
12. M. F. Jarrold, *Acc. Chem. Res.*, 1999, **32** (4), 360-367.
13. Q. Y. Wu, J. M. Gao, D. JosephMcCarthy, G. B. Sigal, J. E. Bruce, G. M. Whitesides and R. D. Smith, *J. Am. Chem. Soc.*, 1997, **119** (5), 1157-1158.
14. C. L. Hunter, A. G. Mauk and D. J. Douglas, *Biochem.*, 1997, **36** (5), 1018-1025.
15. P. A. Sullivan, J. Axelsson, S. Altmann, A. P. Quist, B. U. R. Sunqvist and C. T. Reimann, *J. Am. Soc. Mass Spectrom.*, 1996, **7** (4), 329-341.
16. D. Lemaire, G. Marie, L. Serani and O. Laprevote, *Anal. Chem.*, 2001, **73** (8), 1699-1706.
17. D. L. Purich and H. J. Fromm, *Biochim. Biophys. Acta*, 1972, **276**, 563-567.
18. P. Feldhaus, T. Fröhlich, R. S. Goody, M. Isakov and R. H. Schirmer, *Eur. J. Biochem.*, 1975, **57** (1), 197-204.
19. J. A. Loo, P. Hu, P. McConnell and W. T. Mueller, *J. Am. Soc. Mass Spectrom.*, 1997, **8**, 234-243.

20. M. J. Greig, H.-J. Gaus, L. L. Cummins, H. Sasmor and R. H. Griffey, *J. Am. Chem. Soc.*, 1995, **117**, 10765-10766.
21. Z. Shi, I. L. Byeon, R. Jiang and M.-D. Tsai, *Biochem.*, 1993, **32**, 6450-6458.
22. C. W. Müller and G. E. Schulz, *J. Mol. Biol.*, 1992, **224**, 159-177.
23. G. E. Lienhard and I. I. Secemski, *J. Biol. Chem.*, 1973, **248**, 1121-1123.

Seite Leer /
Blank leaf

# CHAPTER 5

# CHORISMATE MUTASE

Seite Leer /
Blank leaf

Another case study of the present thesis is the chorismate mutase system. The dissociation constant of chorismate mutase and a transition state analogue (TSA) inhibitor were quantitatively determined by electrospray ionization mass spectrometry. The enzyme forms a homotrimer in its native state with three identical and independent substrate binding sites; therefore the system presents a complex stoichiometry. By choosing appropriate conditions in the ESI source, the chorismate mutase trimer as well as the noncovalent chorismate mutase - inhibitor complexes were detected. However, the spectra exhibited broad peaks, which originated from the chosen soft ionization and desolvation conditions, the high protein mass (43.5 kDa), and the low charge states. This is a typical challenge in analyzing noncovalent protein complexes. Due to the low molecular weight of the transition state analogue (226 Da), the homotrimer and the protein - inhibitor complexes with one, two, or three inhibitors bound cannot be resolved. To obtain relative peak areas of the different species, appropriate peak shapes were fitted to the deconvoluted signals corresponding to the free enzyme and its complexes with the inhibitor. Hence, the dissociation constants could be calculated from the relative peak areas and were in good agreement with known solution-phase data. In order to verify the specificity of the interaction, titration experiments with different enzyme variants as well as different inhibitors were performed. A plot of the number of bound inhibitors versus added inhibitor concentration revealed a saturation behavior at a 3:1 (inhibitor: functional trimer) stoichiometry for the TSA. This method may be generally useful for the interpretation of mass spectra for noncovalent complexes that exhibit broad peaks in the high m/z range.

**Adapted from:**

S. Wendt, G. McCombie, J. Daniel, A. Kienhöfer, D. Hilvert and R. Zenobi, *J. Am. Soc. Mass Spectrom.*, 2003, **14** (12), 1470-1476.

## 5.1 Introduction

With the rapid progress in genomic sequencing and proteomics, noncovalent interactions of proteins with their binding partners are becoming a major focus of attention. A straightforward method for the determination of relative binding strengths with low sample consumptions is desirable, especially in drug development, where large libraries of potential ligands (*e.g.* inhibitors) are often screened.

Soft ionization mass spectrometry, such as electrospray ionization, is able to provide useful information about noncovalent assemblies involving biological macromolecules, including their complexes with small ligands and inhibitors. Numerous studies have been published on this topic, and a number of good reviews have appeared [2-4]. Increasingly, the quantitative determination of dissociation constants of noncovalent complexes by mass spectrometry is being addressed, too (see chapter 3 and ref. [5]). In order to employ a mass spectrometer successfully as a detector for solution-phase chemistry, the complexes must survive the ionization and desolvation process. Only a small number of studies have appeared in the literature reporting the quantitative investigation of protein inhibition by mass spectrometry [6-10]. Among these, the studies by Greig et al. [9] and Ayed et al. [11] discussed interactions with larger proteins and enzymes.

The most obvious advantages of mass spectrometry include the possibility of obtaining the mass and stoichiometry of a complex in a straightforward way, the short measurement times, and the small amount of analyte required. It could represent a useful method for determining binding constants of mutant proteins, where classical activity measurements cannot distinguish between residual activity of the mutant and activity due to wild type enzyme still present as an impurity. A difficulty of mass spectrometry using very soft ionization is that adducts from solvent and buffer can survive the ionization process: this is not in favor, since these will broaden the signals such that it becomes difficult or impossible to fully resolve the protein and its complexes in the spectrum. In the present thesis, this challenge is addressed by a new data evaluation procedure.

In the current study, we have used chorismate mutase (E.C. 5.4.99.5) from *Bacillus subtilis* (BsCM), a model for protein assembly as well as ligand binding. BsCM catalyzes the rearrangement of chorismate to prephenate, the first step in the biosynthesis of the aromatic amino acids phenylalanine and tyrosine. Since chorismate mutases are found in bacteria, fungi, and higher plants, the design of novel inhibitors for this enzyme might be of importance for the development of new herbicides and antibacterial therapeutics. The structure and function of BsCM are well characterized [12, 13]: the crystal structure shows a homotrimeric pseudo-β-barrel surrounded by α-helices with three solvent accessible binding sites at the subunit interfaces. In solution the three binding sites are all identically shaped and independent. A BsCM monomer has a molecular weight of 14'489 Da, leading to a molecular weight of 43'467 Da for the functional trimer (the abbreviation BsCM represents the functional trimeric enzyme). Several inhibitors have been reported for chorismate mutases, including the endo-oxabicyclic transition state analogue (TSA) designed by Bartlett and co-workers [14] that is used in this study (figure 5.1). This system allows the investigation of the stability of the noncovalent trimer as well as the stability of BsCM-inhibitor complexes with mass spectrometry.

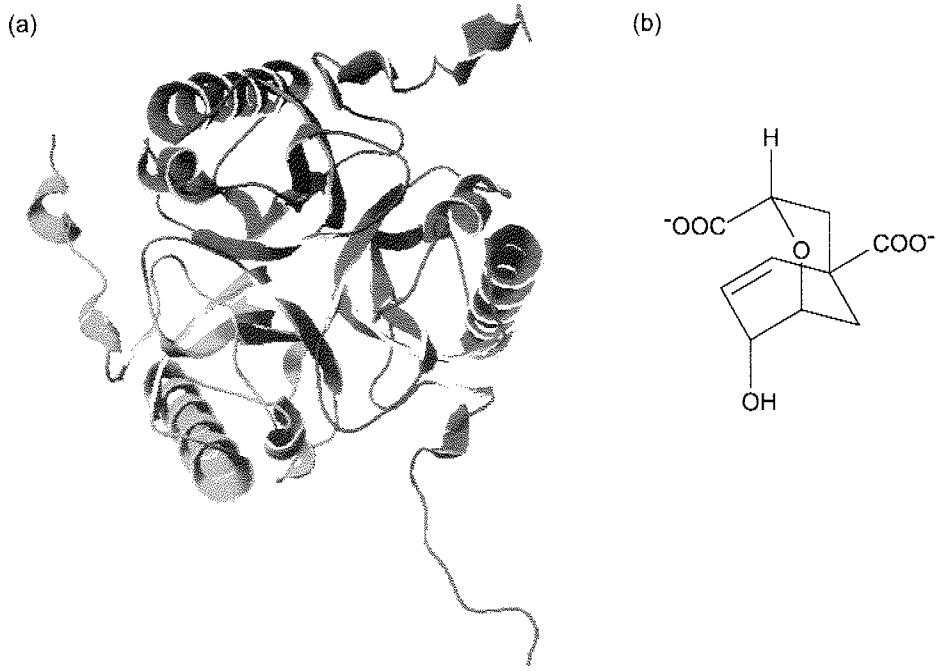


**Figure 5.1: (a) 3D representation of BsCM trimer in a view looking down the barrel / pseudothreefold axis (PDB ID: 1DBF). (b) The endo-oxabicyclic transition state analogue (TSA).**

## 5.2 Experimental Section

### Instrumentation

All experiments were conducted on the α-prototype electrospray orthogonal injection time-of-flight mass spectrometer from Agilent (Palo Alto, California, USA). The mass resolution of the instrument is around 1100 in the mass range employed here. Infusion rates of 1 to 5 μl $min^{-1}$ with a pneumatically assisted ESI source were used. The spray potentials were between 2700 and 3000 V. The source conditions of the instrument were optimized for transfer of high molecular weight ions and for gentle desolvation conditions by adjusting the different source and transfer potentials. 1'000'000 transients per spectrum were summed and transferred to a PC for further processing. The potential applied to the exit of the transfer capillary is variable and is referred to $V_{ex}$ below; the potential at the first skimmer is denominated $V_{sk1}$.

### Chorismate Mutase

Wild-type BsCM was produced in *E. coli* and purified as described by Hilvert and coworkers [15]. The truncated mutant $BsCM^{1-120}$ was generated by PCR amplification of the gene segment encoding residues 1-120 of BsCM using plasmid pKET3-W [16] as template and T7PRO2 (TAATACGACTCACTATAGGG) and SVSF-7-L121* (AACTCCTCGAG**TTA**GCTTAAATCGGGCCTCAATA) as the forward and reverse primer, respectively. The nucleotides for the stop codon replacing the triplet encoding $Leu^{121}$ are shown in bold. The gene fragment was purified, digested with BsrGI and XhoI, and ligated into the acceptor fragment obtained by digesting pKET3-W with the same enzymes. The insert in the resulting plasmid, pAK-L121*, was verified by sequencing using primer 04-T7TR (CAGCAGCCAACTCAGCTTCCTTTC) [17]. The chorismate mutase deficient *E. coli* strain KA13 [18] transformed with pAK-L121* afforded 40 mg of purified $BsCM^{1-120}$ per 1 liter of culture. The molecular weight of the mutant protein was confirmed by ESI-MS (experimental result 13'691 ± 2 Da; calculated 13'689 Da). By polyacrylamide gel electrophoresis no impurities were observed. ESI-MS showed that the N-terminal methionine is partially removed, as it is often observed in bacterial proteins, but this has no effect on the enzymatic activity. However, it leads to

a low-mass shoulder that can be seen in some of the ESI mass spectra presented below.

Prior to ESI-MS measurements, the proteins were desalted three times by gel filtration (NAP-5 column, Amersham Pharmacia Biotech, Uppsala, Sweden). ESI measurements were made with a concentration of 10 μM protein monomer, corresponding to 3.3 μM BsCM in the active trimeric form, dissolved in 10 to 20 mM triethyl ammonium bicarbonate buffer (pH ≈ 8). Protein concentrations were determined by UV spectroscopy prior to desalting. Recovery factors of the desalting columns were ≥ 97%, thus uncorrected values of protein concentration were used.

### Inhibitors

The transition state analogue (TSA) was synthesized according to literature procedures [14]. In addition, adamantyl-1-phosphonate (AP), synthesized according to a previously published procedure [19], was used as a very weak BsCM inhibitor. Both inhibitors were generous gifts of the group of Prof. Hilvert.

### Inhibition Assays

The enzymes were assayed as previously described [15] at pH = 7.5 in 50 mM potassium phosphate buffer or in triethylammonium bicarbonate (TEAB) buffer, respectively. The estimation of the $K_D$ values for the different inhibitors is based on the classical Michaelis Menten equation for competitive binding (eq. 5.1). The Dixon method [20, 21], used for estimation of $K_D$ values, arises from linearization of eq 5.1

$$v = \frac{v_{max} \cdot [S]}{K_m \cdot \left(1 + \frac{[I]_0}{K_D}\right) + [S]} \qquad \text{(Eq 5.1)}$$

$v$ *reaction rate of the enzyme catalyzed reaction*

$v_{max}$ *maximum reaction rate* ($v_{max}=k_{cat}\cdot[E]_{total}$)

$[S]$ *substrate concentration*

$K_m$ *Michaelis constant*

$[I]_0$ *inhibitor concentration*

$K_D$ *dissociation constant of the enzyme - inhibitor complex*

$$\frac{1}{v} = \frac{1}{v_{max}} \cdot \left[1 + \frac{K_m}{[S]}\right] + \frac{K_m \cdot [I]_0}{v_{max} \cdot [S] \cdot K_D} \qquad \text{(Eq 5.2)}$$

$$K_D = -[I]_0 \qquad \text{(Eq 5.3)}$$

(eq 5.2). A plot of 1/v versus $[I]_0$ yields a straight line. When $1/v = 1/v_{max}$, eq 5.2 reduces to eq 5.3, allowing an estimation of $K_D$ based on the absolute value of the inhibitor concentration at this point. The Dixon method requires an assumption of enzyme stability and of a strictly reversible binding mechanism, as it is expected for transition state analogues [22]. The enzyme was used at a concentration of 10 nM and the substrate between 25 and 400 μM for BsCM and between 20 and 2000 μM for $BsCM^{1-120}$. The inhibitor concentration was varied between 0.5 and 50 μM depending on the experimentally determined $K_D$ value. $K_D$ values obtained by this method are reported per binding pocket, whereas in our analysis of the mass spectrometric data, $K_D$ values refer to the concentration of the total trimer concentrations. Thus, the $K_D$ values obtained by mass spectrometry were divided by a factor of 3 for suitable comparison with literature and measured solution-phase data.

### Modeling of the Deconvoluted Peak of the Bare Chorismate Mutase Trimer

To model the shape of the deconvoluted peak of the bare chorismate mutase trimer a function is needed which closely follows the data but rejects the noise. A smoothing spline function as described in reference [23] was used to achieve the smoothest curve that lies within the given tolerance of the measured data. Empirically, it was found that a tolerance corresponding to 1% of the total amplitude gave satisfactory results for the data sets.

### Calculating the Ratio of Peaks

As long as binding sites are identical and independent, as is the case for BsCM [13], a probability P of a binding site being occupied by an inhibitor can be defined ($0 < P < 100\%$). The concentration of the various enzyme-inhibitor complexes can then be expressed as described in equations 5.4 to 5.7, where the factor 3 accounts for the statistical permutations of the complex. Since the total enzyme concentration $[BsCM]_0$ is

known, the entire complex distribution is defined by P. In other words, only a single fitting parameter describes the relative peak areas.

$$[BsCM] = (1-P)^3 \cdot [BsCM]_0 \quad \text{(Eq 5.4)}$$

$$[BsCM \cdot I] = 3 \cdot (1-P)^2 \cdot P \cdot [BsCM]_0 \quad \text{(Eq 5.5)}$$

$$[BsCM \cdot I_2] = 3 \cdot (1-P) \cdot P^2 \cdot [BsCM]_0 \quad \text{(Eq 5.6)}$$

$$[BsCM \cdot I_3] = P^3 \cdot [BsCM]_0 \quad \text{(Eq 5.7)}$$

*$[BsCM]_0$ total enzyme concentration*

*$[BsCM]$ concentration of free enzyme*

*$[BsCM \cdot I_n]$ concentration of BsCM with n inhibitors bound (n=1,2,3)*

*$P$ probability of a binding site to be occupied*

### Calculating Dissociation Constants

The dissociation constants were calculated based on the general theory of multiple equilibria using only peak ratios. For the three equilibria, three dissociation constants $K_i$ can be defined and expressed with the $K_D$ for binding to an individual site of the enzyme as described in equations 5.8 to 5.10 [24].

$$K_1 = \frac{[I] \cdot [BsCM]}{[BsCM \cdot I]} = \frac{1}{3} \cdot K_D \quad \text{(Eq 5.8)}$$

$$K_2 = \frac{[I] \cdot [BsCM \cdot I]}{[BsCM \cdot I_2]} = K_D \quad \text{(Eq 5.9)}$$

$$K_3 = \frac{[I] \cdot [BsCM \cdot I_2]}{[BsCM \cdot I_3]} = 3 \cdot K_D \quad \text{(Eq 5.10)}$$

*$[I]$ free inhibitor concentration*

*$K_D$ dissociation constant*

*$K_i$ dissociation constant for binding to an individual binding sites i of the protein where already i-1 inhibitors are bound (i=1,2,3)*

The peak ratios can be calculated according to equations 5.11 to 5.13, where P is obtained from the fit to the data.

$$\frac{[BsCM]}{[BsCM \cdot I]} = \frac{1-P}{3 \cdot P} \qquad \text{(Eq 5.11)}$$

$$\frac{[BsCM \cdot I]}{[BsCM \cdot I_2]} = \frac{1-P}{P} \qquad \text{(Eq 5.12)}$$

$$\frac{[BsCM \cdot I_2]}{[BsCM \cdot I_3]} = \frac{3 \cdot (1-P)}{P} \qquad \text{(Eq 5.13)}$$

The total concentration of the enzyme $[BsCM]_0$ and the total concentration of the inhibitor $[I]_0$ are given by equation 5.14 and 5.15. Inserting equations 5.11, 5.12, and

$$[BsCM]_0 = [BsCM] + [BsCM \cdot I] + [BsCM \cdot I_2] + [BsCM \cdot I_3] \qquad \text{(Eq 5.14)}$$

$$[I]_0 = [I] + [BsCM \cdot I] + 2 \cdot [BsCM \cdot I_2] + 3 \cdot [BsCM \cdot I_3] \qquad \text{(Eq 5.15)}$$

5.13 into equation 5.14 and solving for [BsCM], and inserting equations 5.11, 5.12, 5.13, and 5.16 into equation 5.15 and solving for [I], the calculated concentrations for the enzyme and inhibitor are found:

$$[BsCM] = (1-P)^3 \cdot [BsCM]_0 \qquad \text{(Eq 5.16)}$$

$$[I] = [I]_0 - 3 \cdot P \cdot [BsCM]_0 \qquad \text{(Eq 5.17)}$$

By inserting equation 5.12 and 5.17 into equation 5.9, $K_D$ can be calculated from one single measurement (equation 5.18). $K_D$ was determined for seven titration points in

$$K_D = \frac{(I_0 - 3 \cdot P \cdot [BsCM]_0) \cdot (1-P)}{P} \qquad \text{(Eq 5.18)}$$

the range from 0 to 50 µM TSA where satisfactory fits were obtained. From these seven $K_D$ values the mean and the standard deviation were calculated.

## 5.3 Observation of Chorismate Mutase Trimers

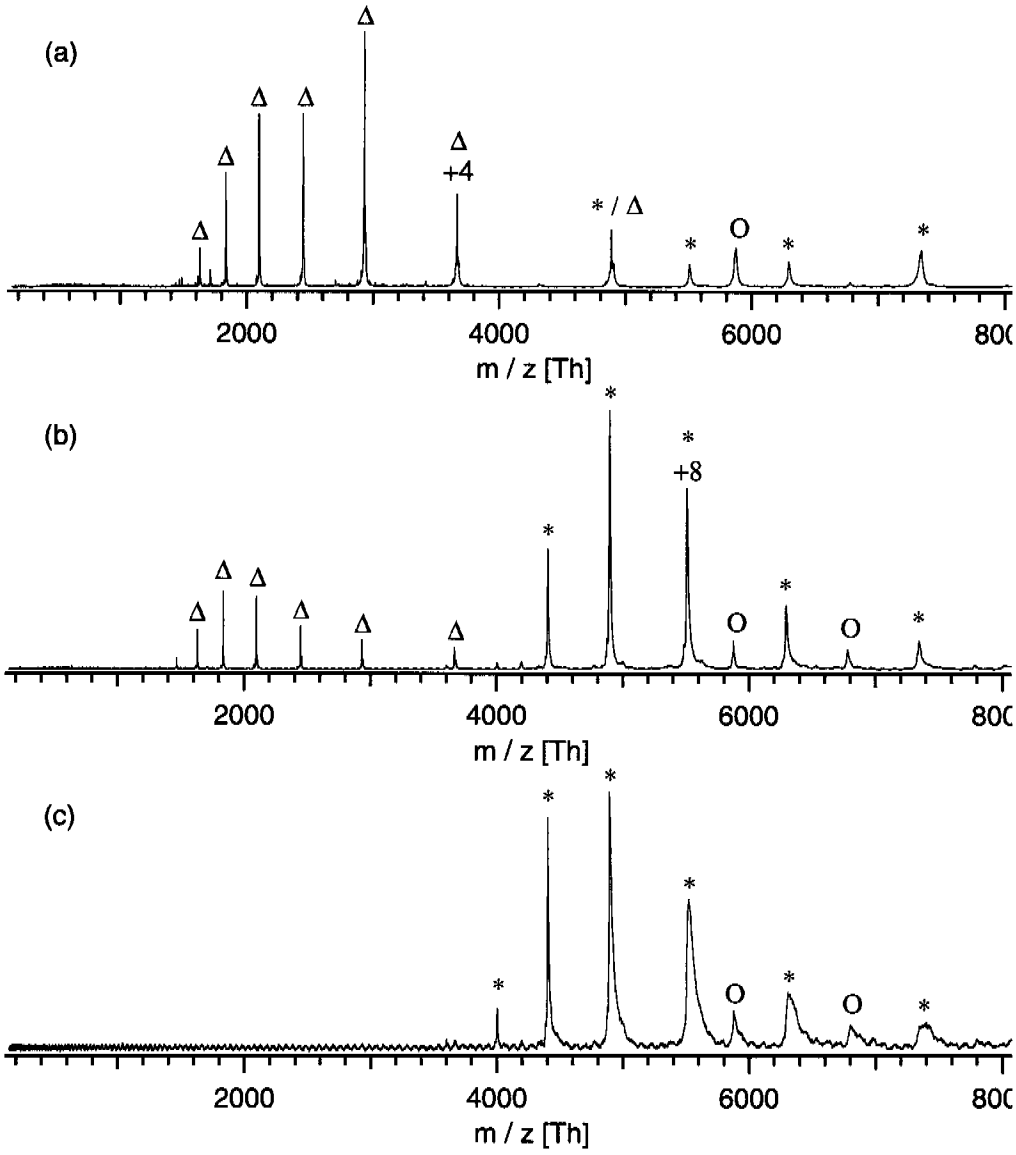


**Figure 5.2: Positive ion mode ESI mass spectra of a solution of 3.3 μM BsCM. By decreasing $V_{sk1}$ (a→c) and hence going to softer conditions, peaks corresponding to the trimer (*) become the abundant species detected, peaks corresponding to the monomer (Δ) disappear. In all spectra, we observed a small fraction of dimer (O).**

In order to detect specific noncovalent interaction between proteins and bound inhibitors, the preservation of a near-native structure of the protein during transfer from solution into the gas phase is essential. As the active form of BsCM is a homotrimer, it is necessary to observe the trimer in the mass spectrum. Lemaire et al. showed that multiply charged ions generated in triethylammonium bicarbonate (TEAB) buffered

solutions were significantly more stable than those formed in other buffers such as ammonium bicarbonate or ammonium acetate [25]. Our own experiments confirmed this observation and generally TEAB was used at concentrations between 10 and 20 mM. Furthermore, spectrophotometric assays confirmed that BsCM retains its full activity in this buffer. Using soft desolvation conditions, *i.e.* low $V_{sk1}$, the homotrimer was detected whereas using harsher conditions (at increased $V_{sk1}$), the trimer partly dissociated into monomers that were not previously observed in solution under physiological conditions (figure 5.2). Negligible amounts of dimers could be observed. However, no signals for tetramers or pentamers could be observed under any of the employed conditions. The low signal intensities of the dimers and the absence of higher multimers than trimers led us to the conclusion that only specific native-like protein-protein interactions account for the observation of trimeric species at low $V_{sk1}$. The latter conclusion is further supported by the binding constants determined by mass spectrometric methods described later in this chapter and the comparable results to solution-phase data.

## 5.4 Detection of Trimer - Inhibitor Complexes

To be able to detect noncovalent complexes, very soft conditions in the ESI source must be chosen in order to prevent the complex from dissociation. However, reasonable desolvation of the complexes is required in order to obtain a reasonable signal-to-noise ratio and to avoid extensive adduct formation. Therefore a compromise between softness and completeness of desolvation must be found for the operating conditions of the electrospray source. Figure 5.3 presents the $[BsCM + 8{\cdot}H^+]^{8+}$ peak of the BsCM trimer from spectra of a solution (3.3. μM BsCM and 10 μM TSA in 10 mM TEAB) recorded at different $V_{ex}$ and $V_{sk1}$ values. Using harsh desolvation conditions (high voltages), the peak of BsCM is very intense and the detected mass is only slightly larger than the calculated one of uncomplexed BsCM trimer (5.3a). The small mass differences arise from incomplete desolvation of the native trimer and buffer molecule adducts, as described by Kebarle and co-workers [26]. Going to softer condi-

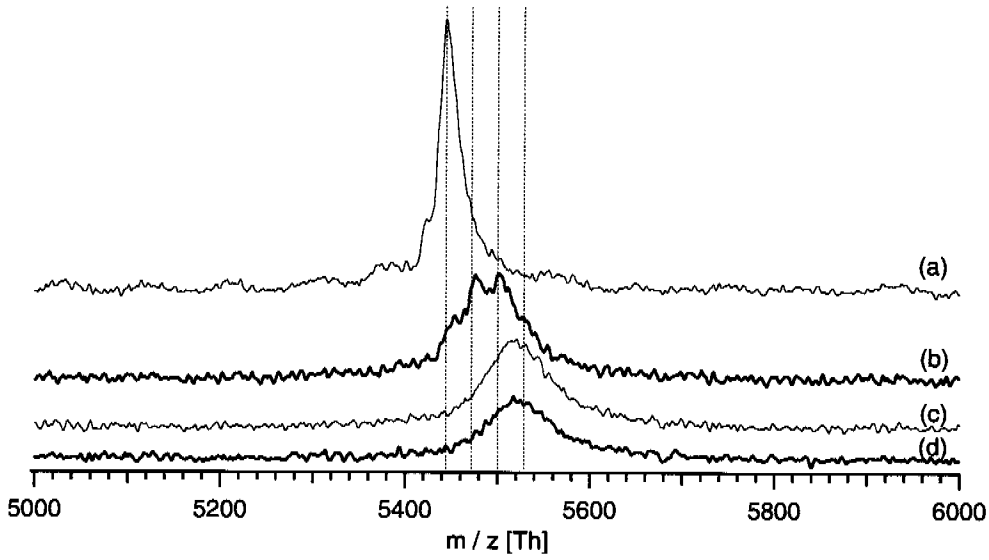


**Figure 5.3: Positive ion mode ESI mass spectra ($[BsCM+8{\cdot}H]^{8+}$ charge state) of a solution of 3.3 μM BsCM and 10 μM TSA inhibitor at different desolvation conditions. From top to bottom conditions become increasingly softer: (a) $V_{ex}$ = 250 V, $V_{sk1}$ = 138; (b) $V_{ex}$ = 150 V, $V_{sk1}$ = 83; (c) $V_{ex}$ = 100 V, $V_{sk1}$ = 55; (d) $V_{ex}$ = 50 V, $V_{sk1}$ = 28. The vertical lines represent the mass of bare BsCM trimer and the calculated peak positions of BsCM with one, two and three inhibitors bound. Note the mass shift towards the $BsCM{\cdot}I_3$ complex as the conditions become softer. The low-mass shoulder is due to partial removal of N-terminal methionine, as often observed in bacterial proteins.**

tions by decreasing $V_{ex}$ and $V_{sk1}$, a clear shift to higher masses is observed. The peak also becomes broader but nevertheless shows partial resolution of the different BsCM-inhibitor complexes (figure 5.3b). With even softer conditions the peak shifts further into the direction of higher mass (figure 5.3c) with the maximum close to the theoretical mass of the BsCM·$I_3$ complex, while the resolution of the different complex peaks, however, is lost. A further decrease in $V_{ex}$ and $V_{sk1}$ does not result in a further shift towards higher mass but only to a loss in signal intensity (figure 5.3d). The latter observation indicates that the complexes are preserved during the desolvation. The titration experiments are carried out under the conditions used for spectrum 5.3c since under these conditions the complex does not appear to dissociate in the gas phase, while signal intensity is still reasonable. It should be noted that the monomeric enzyme subunit is not evident in any of the spectra shown in figure 5.3.

## 5.5 Titration Experiments with Different Inhibitors and Chorismate Mutase Mutants

In mass spectrometry not only specific noncovalent complexes are observed but unspecific adducts may be detected as well. Therefore prior to estimate any binding constants from mass spectrometric data, the specificity of the observed complex must be verified. Since the mass is the main observable in the mass spectrum, it cannot be decided from one single experiment whether the inhibitor is located in the binding pocket or simply bound non-specifically onto the surface of the protein. In the present case BsCM mutant in addition to wild type BsCM, as well as the much weaker AP inhibitor ($K_D$ > 4 mM) were used to address this question. The mutant species ($BsCM^{1-120}$) was shorter by the last seven C-terminal amino acids in the sequence and exhibited reduced enzyme activity and ligand affinity, as reported previously for other randomly truncated BsCM mutants [27].

A series of experiments was performed by varying the concentration of the TSA or AP inhibitors in the presence of 3.3 μM BsCM or $BsCM^{1-120}$. Since the peaks corresponding to the free enzyme and its complexes with one, two or three inhibitor molecules could not be clearly resolved, the statistical number of bound inhibitor molecules was determined. The recorded spectra were deconvoluted to represent +0 charge state only; then the spectra were smoothed, and the average mass at every inhibitor concentration was obtained. The mass difference Δm between this average mass and the mass of the free protein was finally divided by the mass of the inhibitor to yield the number of bound inhibitor molecules. In figure 5.4 the results for BsCM·TSA, $BsCM^{1-120}$·TSA, and BsCM·AP are plotted against the added inhibitor concentration. In the case of wild type BsCM binding TSA, a saturation curve is found, while a upper limit at a 20 fold molar excess of inhibitor, which slightly exceeds the theoretical maximum of three bound inhibitors. At this excess and under the conditions of low salt concentration and soft ionization, some nonspecific binding can apparently occur. However, the clear saturation behavior at a value of three inhibitors per trimer is taken as evidence for a specific binding to the binding pocket. The results for $BsCM^{1-120}$·TSA and for BsCM·AP show a lower increase in binding of inhibitor, which can be attributed to weaker binding.

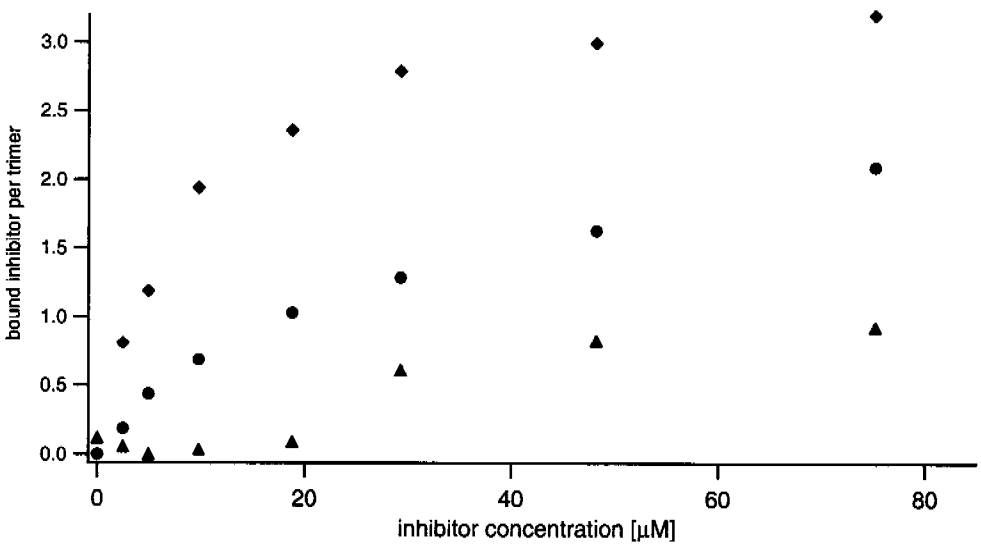


**Figure 5.4: The number of bound inhibitors vs. inhibitor concentration for BsCM·TSA (black) and $BsCM^{1-120}$· TSA (blue), and BsCM·AP (red). Protein concentration was 3.3 μM in all cases. The number of bound inhibitors was determined from the deconvoluted spectra, see text.**

## 5.6 Calculation of $K_D$

The binding of the inhibitor to BsCM showed an apparent dependence on the charge state, *i.e.* peak intensity ratios of complex relative to bare enzyme appeared to be different for every charge state. A reasonable explanation for this observation is that the change in charge state distribution in the ESI mass spectrum is caused by a conformational change induced upon binding of the inhibitor into the active site. Additionally, the amino acids within the binding site are not accessible upon binding and therefore cannot be protonated. Consider, for example, a most abundant charge state of $[BsCM+10\cdot H]^{10+}$ for the naked protein and a maximum charge state of $[BsCM\cdot I+9\cdot H]^{9+}$ after binding the inhibitor. An overlay of the two ESI mass spectra will then result in different intensity ratios at every peak, showing an apparent charge state dependent inhibitor binding. Therefore all charge states have to be taken into account for the evaluation of the dissociation constants and thus all spectra were deconvoluted prior to the analysis (representing the charge state z=0; without any protons attached).

The resulting deconvoluted peaks of some selected spectra are shown in figure 5.5. For the evaluation of the data the relative contributions of the free enzyme and the individual complexes, *i.e.* the ratio of BsCM/BsCM·I, BsCM·I/BsCM·$I_2$ and BsCM·$I_2$/ BsCM·$I_3$, need to be determined. Due to large overlapping peaks, these ratios cannot be read out directly from the spectra. Therefore the data were fitted as follows: The deconvoluted peak of a spectrum of free BsCM was modeled by a smoothing spline function. The assumption that the peaks of the protein-inhibitor complexes differ only in their position on the mass scale and their amplitude but not in their shape allows the contribution of all four BsCM/BsCM-inhibitor species to be determined from the shape of the previously determined BsCM signal. For fitting the spectra, two additional parameters were needed, one to account for the baseline level and a scaling factor that accounts for the absolute intensity of each spectrum. Since all binding sites are identical and independent and therefore do not show any allosteric or cooperative effect [13], only a single fitting parameter, a probability P that describes the occupation of a binding site by an inhibitor, fully determines the ratio of all four peaks.

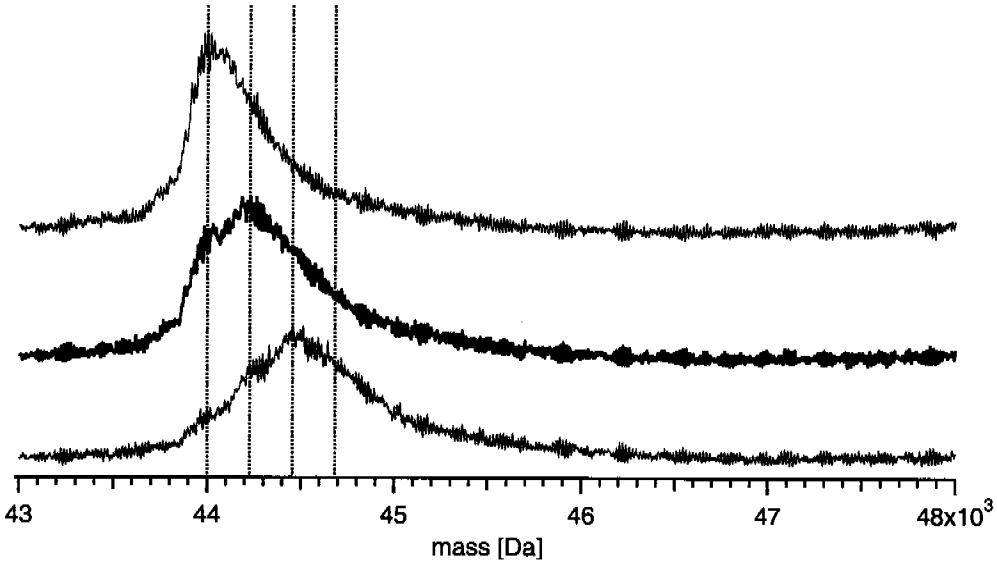


**Figure 5.5: Deconvoluted ESI mass spectra of BsCM (black), BsCM plus 2.5 μM TSA (blue) and BsCM plus 10 μM TSA (red). BsCM concentration was 3.3 μM. The vertical lines represent the peak position of bare BsCM determined by ESI-MS and the calculated peak positions of BsCM with one, two, and three inhibitors bound.**

Figure 5.6 depicts an example of such a fit. As it is readily observed the raw data are matched very well. At higher inhibitor concentrations, starting from 50 μM which corresponds to a 15-fold excess, the fits were less good, probably due to the onset of unspecific binding of inhibitor to the enzyme. Therefore only data for inhibitor concentrations below 50 μM were used to calculate the $K_D$ value. The fitting parameter affords the relative peak areas for BsCM, BsCM·I, BsCM·$I_2$, BsCM·$I_3$, allowing a dissociation constant to be calculated for each titration point as explained in the experimental section.

For the wild type enzyme BsCM and the TSA inhibitor a $K_D$ of 1.7±1 μM was determined, which compares well with the value of 1.0±0.2 μM determined in the solution-phase assay. In the literature values, between 1.7 μM [28] and 3 μM [13], have been reported. For the truncated enzyme $BsCM^{1-120}$ and TSA, a $K_D$ of 37±6 μM has been determined by mass spectrometry whereas a standard solution assay gave 25±1.7 μM. Again, the $K_D$ values determined by mass spectrometry and the solution-phase assay are in good agreement. Systematic errors can be introduced if the actual initial enzyme concentration used for the measurements is lower than quoted, due to losses

during the desalting process or precipitation while freezing and thawing the protein solutions.

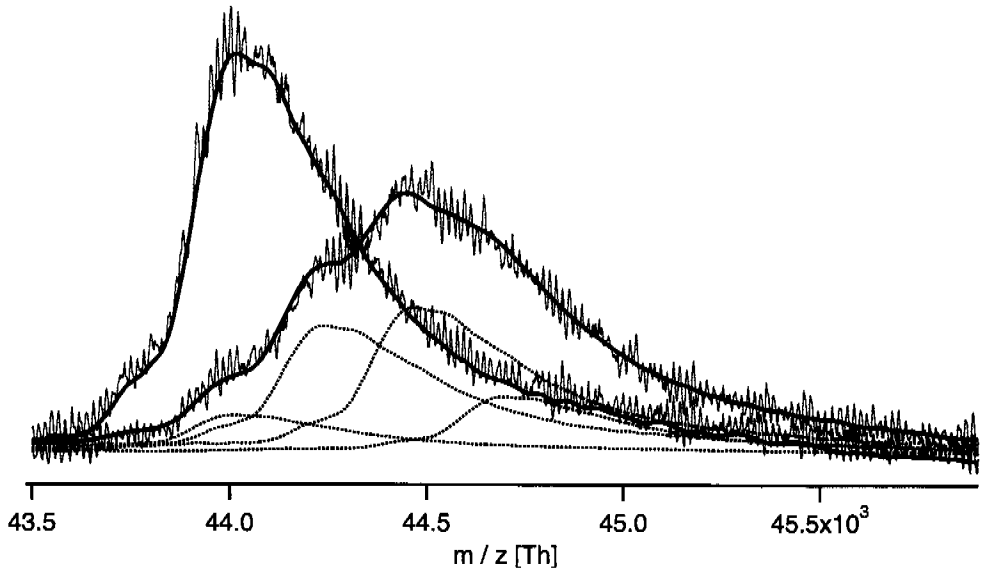


**Figure 5.6: Representative figure of the fitted mass spectra. The blue line represents the function fitted to the deconvoluted mass spectrum of bare BsCM. The dotted lines are this function scaled and shifted by the inhibitor mass zero, one, two, or three times. The solid line is the sum of these four functions fitted to the deconvoluted spectra of BsCM plus 10 μM TSA. BsCM concentration was 3.3 μM.**

| Complex | $K_D$ [μM] | Source |
|---|---|---|
| BsCM - TSA | 1.7 ± 1 | mass spectrometry |
| | 1.0 ± 0.2 | solution phase assay |
| | 1.7 | Cload et al. [28] |
| | 3 | Gray et al. [13] |
| $BsCM^{1-120}$ - TSA | 37 ± 6 | mass spectrometry |
| | 25 ± 1.7 | solution phase assay |

**Table 5.1: Dissociation constants measured in the present work, and compared to literature values.**

## 5.7 Summary

Broad peaks impose a true challenge when measuring noncovalent protein complexes by ESI-MS. Since it is necessary to maintain the native structure of the protein for substrate or inhibitor binding, the number of charges on the protein is usually low, leading to high m/z ratios, representing a region where the instrumental resolution drops. In addition, the preservation of weak noncovalent interaction obligates the use of very soft desolvation conditions in the ESI source which leads to a further increase in peak width due to solvent and buffer adducts. It has been shown that such obstacles can be overcome by modeling the signal of noncovalent protein-inhibitor complexes as the sum of four signal peaks derived from the signal of the *bare* (trimeric) enzyme. Dissociation constants for BsCM and TSA as well as for $BsCM^{1-120}$ and TSA could be obtained. The absolute $K_D$ values determined by MS are in good agreement with solution-phase and literature data.

## 5.8 References


1. S. Wendt, G. McCombie, J. Daniel, A. Kienhofer, D. Hilvert and R. Zenobi, *J. Am. Soc. Mass Spectrom.*, 2003, **14** (12), 1470-1476.
2. J. L. Beck, M. L. Colgrave, S. F. Ralph and M. M. Sheil, *Mass Spectrom. Rev.*, 2001, **20** (2), 61.
3. J. A. Loo, *Mass Spectrom. Rev.*, 1997, **16** (1), 1-23.
4. J. A. Loo, *Int. J. Mass Spectrom.*, 2000, **200** (1-3), 175-186.
5. J. M. Daniel, S. D. Friess, S. Rajagopalan, S. Wendt and R. Zenobi, *Int. J. Mass Spectrom.*, 2002, **216** (1), 1-27.
6. J. A. Loo, P. Hu, P. McConnell and W. T. Mueller, *J. Am. Soc. Mass Spectrom.*, 1997, **8** (3), 234-243.
7. C. V. Robinson, E. W. Chung, B. B. Kragelund, J. Knudsen, R. T. Aplin, F. M. Poulsen and C. M. Dobson, *J. Am. Chem. Soc.*, 1996, **118** (36), 8646-8653.
8. H.-K. Lim, Y. L. Hsieh, B. Ganem and J. Henion, *J. Mass Spectrom.*, 1995, **30** (5), 708-714.
9. M. J. Greig, H.-J. Gaus, L. L. Cummins, H. Sasmor and R. H. Griffey, *J. Am. Chem. Soc.*, 1995, **117**, 10765-10766.
10. J. M. Daniel, G. McCombie, S. Wendt and R. Zenobi, *J. Am. Soc. Mass Spectrom.*, 2003, **14** (5), 442-448.
11. A. Ayed, A. N. Krutchinsky, W. Ens, K. G. Standing and H. W. Duckworth, *Rapid Commun. Mass Spectrom.*, 1998, **12** (7), 339-344.
12. Y. M. Chook, H. Ke and W. N. Lipscomb, *Proc. Natl. Acad. Sci. U.S.A.*, 1993, **90** (18), 8600-8603.
13. J. V. Gray, D. Eren and J. R. Knowles, *Biochemistry*, 1990, **29** (37), 8872-8878.
14. P. A. Bartlett, Y. Nakagawa, C. R. Johnson, S. H. Reich and A. Luis, *J. Org. Chem.*, 1988, **53** (14), 3195-3210.
15. P. Kast, C. Grisostomi, I. A. Chen, S. Li, U. Krengel, Y. Xue and D. Hilvert, *J. Biol. Chem.*, 2000, **275** (47), 36832-36838.
16. P. Mattei, P. Kast and D. Hilvert, *Eur. J. Biochem.*, 1999, **261** (1), 25-32.
17. F. Sanger, S. Nicklen and A. R. Coulson, *Proc. Natl. Acad. Sci. U. S. A.*, 1977, **74** (12), 5463-5467.
18. G. MacBeath, P. Kast and D. Hilvert, *Biochemistry*, 1998, **37** (28), 10062-

10073.

19. H. S. Chao and G. A. Berchtold, *Biochemistry*, 1982, **21** (11), 2778-2781.
20. M. Dixon, *Biochem. J.*, 1952, **55**, 170-171.
21. R. Kitz and I. B. Wilson, *J. Biol. Chem.*, 1962, **237** (10), 3245-3249.
22. T. S. Maurer and H. Fung, *AAPS Pharmasci.*, 2000, **2** (1), 1-10.
23. C. Reinsch, *Numer. Math.*, 1967, **10**, 177-183.
24. C. Tanford, *Physical Chemistry of Macromolecules*, 1961, New York, Wiley, p. 526.
25. D. Lemaire, G. Marie, L. Serani and O. Laprevote, *Anal. Chem.*, 2001, **73** (8), 1699-1706.
26. N. Felitsyn, M. Peschke and P. Kebarle, *Int. J. Mass Spectrom.*, 2002, **219** (1), 39-62.
27. M. Gamper, D. Hilvert and P. Kast, *Biochemistry*, 2000, **39** (46), 14087-14094.
28. S. T. Cload, D. R. Liu, R. M. Pastor and P. G. Schultz, *J. Am. Chem. Soc.*, 1996, **118** (7), 1787-1788.

# CHAPTER 6

# FLOW-INJECTION ATMOSPHERIC PRESSURE MATRIX ASSISTED LASER DESORPTION / IONIZATION

Seite Leer /
Blank leaf

A new technique is presented for the coupling of atmospheric pressure matrix assisted laser desorption / ionization (AP-MALDI) mass spectrometry with liquid delivery systems. Mass measurements of a wide variety of analytes, including polymers, peptides, phosphopeptides, glycopeptides, and oligosaccharides, are demonstrated using a co-dissolved matrix, *i.e.* α-cyano-4-hydroxycinnamic acid (HCCA). Improvements in terms of sensitivity are achieved by optimizing the position and the shape of the exit capillary and by using a Nd:YAG laser (355 nm) at 1 kHz repetition rate. Two calibration experiments promise a good applicability of the presented coupling method for quantitative measurements. The limit of detection achieved by optimizing the setup is 50 nM for peptides in a methanol solution containing 25 mM HCCA.

**Adapted from:**

J. M. Daniel, S. Ehala, S. D. Friess and R. Zenobi, *Analyst*, 2004, **129**, 574-578.

## 6.1 Introduction

Matrix assisted laser desorption / ionization coupled with time-of-flight mass spectrometry is, besides electrospray ionization, one of the most important analytical tools in the investigation of proteins, peptides, nucleic acids, organometallic compounds, and synthetic polymers. Since the development of the technique by Hillenkamp and Karas [2-4] as well as initial efforts by Tanaka [5], significant improvements of the method have been achieved. A wide variety of different matrices have been developed: solid matrices [6-12], including unconventional approaches with sulfur [13] or fullerene derivatives [14], ionic liquids [15, 16], covalently modified sol-gel films [17], solid-liquid two-phase matrices [18-23], liquid matrices [24-29], including water, and co-dissolved matrices in different solvents [30, 31]. Sze and co-workers [30] prepared different matrix solutions by mixing a solid matrix (*e.g.* HCCA) with glycerol and adding a compound to enhance the solubility of the matrix in glycerol. They observed analyte signals with excellent shot-to-shot and sample-to-sample reproducibility. The high-mass limit achieved was serum bovine albumin at 67'000 Da. Matrix-free techniques, such as desorption / ionization on silicon (DIOS) [32, 33] are gaining popularity. Despite the many possible matrices, organic matrices that are co-crystallized with the analyte, still remain the standard for mass spectrometric measurements. Conventional MALDI sources are operated under high vacuum to achieve a large mean free path of ions in the spectrometer. Thus all materials employed have to be vacuum stable in order to allow the high vacuum to be maintained, limiting the matrices and solvents used for the experiments.

Laiko et al. [35, 36] recently discovered that a MALDI source may be effectively operated at atmospheric pressure (AP-MALDI). AP-MALDI produces results that are largely comparable to those of conventional vacuum MALDI. However, there are additional advantages, such as the simplified sample handling and the possibility to use a wide variety of liquid matrices. There is also some evidence that AP-MALDI produces molecular ions with lower internal energies than those generated by vacuum MALDI, which is beneficial for the analysis of noncovalent complexes or fragile analytes. For example, Burlingame and co-workers obtained mass spectra of several phosphorylated peptides (conotoxins) from the venom of the marine gastropod *con-*

**Desorption / Ionization on Silicon (DIOS)**

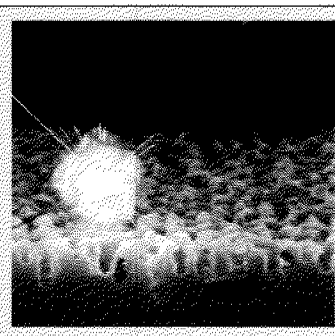

A very interesting approach is the matrix-free desorption and ionization on porous silicon introduced by Siuzdak and co-workers [32]. Direct laser desorption / ionization has been extensively studied, yet is not widely used due to the severe molecular degradation usually observed upon direct exposure to laser radiation. However, the utility of direct laser desorption / ionization for biomolecular analysis could be highly beneficial due to the drastically simplified sample preparation, the elimination of matrix background ions, and the potential for rapid analyses. Since the matrix serves to trap analyte molecules as well as to absorb laser radiation, nanoporous materials were investigated and porous silicon was found to be an effective medium for desorbing compounds and generating intact ions in the gas phase. DIOS has demonstrated characteristics similar to MALDI in that intact molecules are observed at the femtomole and attomole level with little or no fragmentation. Most importantly, the complete absence of matrix material allows the technique to be applied to small molecules. Optimum performance is typically obtained for molecules with molecular weights less than 3000 Da. Most existing MALDI mass spectrometers can be used to perform DIOS by simply changing the sample plate; no spectrometer modification is necessary. DIOS has been shown to work with different laser wavelengths; the energy deposited in the target rather than the wavelength of the irradiation is crucial [34].

*nus pennaceus* [37]. They observed that the mass spectra obtained by vacuum MALDI in positive ion mode generally produced dephosphorylated ions, whereas those from atmospheric pressure MALDI produced molecular ions of intact phosphorylated species. AP-MALDI has experienced significant improvements [38-43] and is now commercially available for most mass spectrometers with atmospheric pressure interfaces, *e.g.* ESI instruments. However, it should not be neglected that the sensitivity in AP-MALDI is still far from satisfactory. The transport of the ions generated at atmospheric pressure into the high vacuum automatically includes ion losses in the different stages of the atmospheric pressure interface and therefore the sensitivity is drastically lowered.

The different approaches coupling to liquid chromatography (LC) and capillary electrophoresis (CE) to MALDI MS have been comprehensively summarized in recent review articles [44-47]. They can be divided into two categories: off-line and on-line coupling methods. Off-line coupling is already well established and widely used. It offers the possibility to collect fractions for analysis and to store them over long periods of time for archiving. There are several reports on off-line coupling of CE or LC separation techniques with MALDI MS: the effluents were either collected in fractions in an array of cups [48], on a coaxial fraction collector [49], on a moving belt like system [50] with the matrix solution being subsequently added to the sample, or they were applied continuously onto a MALDI target previously coated with matrix [51-53].

**LC / MALDI Coupling by Spotting**

The most widely used method today is the spotting. There are basically two possibilities how to prepare the MALDI target: either the effluent of the chromatographic system is mixed with matrix solution prior to be spotted onto a MALDI sample plate or, alternatively, the effluent of the chromatographic system is directly spotted onto a sample plate previously coated with matrix. With use of piezoactuated cells it is nowadays possible to spot sample volumes in the range of nanoliters. Instead of spotting matrix / analyte solutions, there is also the possibility to draw a continuous trace onto a MALDI sample plate. These approaches are all off-line and analysis of the MALDI data is performed after recording the chromatographic trace.

On-line coupling provides immediate results and therefore reduces the time of analysis. The on-line delivery of liquid samples to MALDI MS is continuously improved and several approaches have emerged [28, 46, 54-57], including the use of special frits [57, 58], aerosol liquid introduction [59], operation at elevated pressure [60] and a rotating ball inlet (ROBIN) [61].

Using the key benefit of AP-MALDI, *i.e.* no high vacuum has to be maintained, a new and simple, yet powerful on-line coupling procedure is introduced in the following section. The dissolved analytes, *e.g.* delivered by a liquid chromatographic system, are mixed with co-dissolved matrix. The analyte / matrix mixture is directly desorbed

and ionized at the exit of a capillary at atmospheric pressure and the ions are introduced into a time-of-flight mass spectrometer by orthogonal extraction [62]. The great benefit of this method is that the parameters of the separation, such as solvents and flow rates, do not have to be altered because there is no need for vacuum compatibility. The matrix is added after the separation, and the overall flow rate can be regulated by using splitting valves prior to the desorption.

## 6.2 Experimental Section

### Instrumentation and Development of an Optimized Set-up

All experiments were conducted on the α-prototype electrospray orthogonal injection time-of-flight mass spectrometer from Agilent (Palo Alto, California, USA) described in chapter 2. The source conditions of the instrument were optimized for the transfer of the singly charged ions and for gentle desolvation by adjusting the different source and transfer potentials. Spectra were recorded with a repetition rate of 4 kHz and a couple of 100'000 spectra were summed and transferred to a PC for further processing. The mass spectrometric interface exhibits a cut-off for masses below 120 Da and therefore data in this mass range is not shown in the following figures.

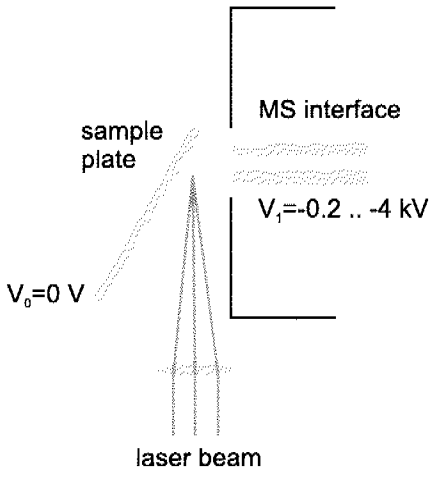


**Figure 6.1: Schematic of our home-built AP-MALDI source used for co-crystallized samples. The analyte / matrix mixture is co-crystallized onto the sample plate. The analyte is desorbed and ionized by focusing a pulsed laser onto the sample plate. The ions are guided by electric fields to the interface of the mass spectrometer.**

Three home-built AP-MALDI sources were used in the experiments. Figure 6.1 shows the AP-MALDI source used for co-crystallized samples. The matrix / analyte mixture is deposited and co-crystallized onto the stainless steel sample plate. The sample plate is kept at 0 V whereas the inlet of the mass spectrometer is between -200 and -4000 V. A pulsed laser is focused onto the target surface and used for desorption.

The first generation AP-MALDI source used for the desorption of liquid matrix / analyte / solvent mixture is shown in figure 6.2. The analyte / matrix mixture is connected to the exit capillary by a HPLC coupling. The mixture is delivered through the exit capillary with a syringe pump (Harvard Apparatus, USA) or a micro flow pump (ISCO, Germany) at flow rates between 1 μl $min^{-1}$ and 10 μl $min^{-1}$. A small droplet is

formed at the end of the capillary. A pulsed laser beam is focused from below onto the surface of the droplet, desorbing and ionizing matrix and analyte. The ions produced are guided by electric fields to the inlet of the mass spectrometer interface. Two different exit capillaries were employed: A static fused silica capillary (50 µm i.d., 360 µm o.d., Upchurch Scientific, USA), and a piezo driven micro pump (Gesim mbH, Germany) with which droplets can be ejected up to a frequency of 1 kHz.

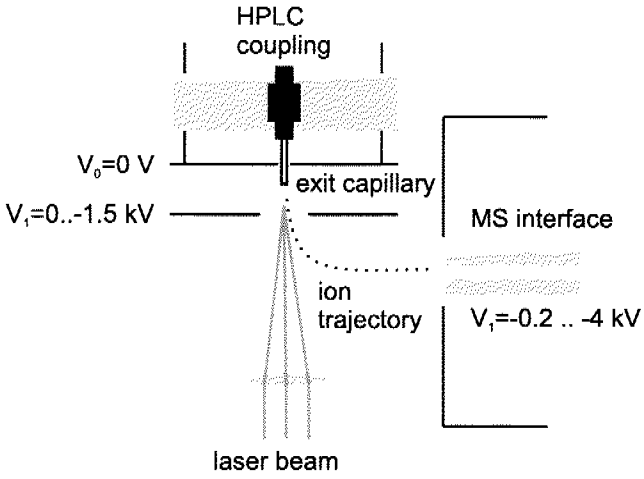


**Figure 6.2: Schematic of the first generation flow-injection setup. The liquid is connected by a HPLC coupling to the ionization source, the laser is focused to the end of the exit capillary and the liquid analyte / matrix mixture is desorbed and ionized. The ions are guided by electric fields to the interface of the mass spectrometer.**

The second generation liquid AP-MALDI source (figure 6.3) is slightly modified: the desorption and ionization is performed closer to the mass spectrometer's interface and the inlet to the mass spectrometer is changed in order to enhance the ion collection efficiency by using a counter current of heated nitrogen (2 slm). The ions generated close to the source are attracted by the electric potential but also by the nitrogen stream. Only static fused silica capillaries were employed as exit capillaries in this setup.

A nitrogen laser (337 nm, 20 Hz, 200 µJ pulse$^{-1}$, Laser Science Inc., USA) and, alternatively, a "Power Chip" Laser (Nd:YAG, 355 nm, 1 kHz, 15 µJ pulse$^{-1}$, JDS Uniphase, USA) were employed to generate the ions. To obtain the analyte / matrix mixture, either the analyte solution was premixed with matrix solution and infused, or the analyte and matrix were mixed online by a mixing T.

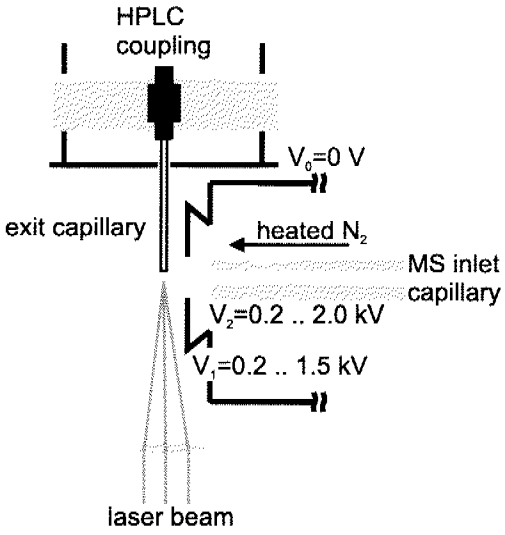


**Figure 6.3: Schematic of the second generation flow-injection setup. The liquid is connected by a HPLC coupling to the ionization source, the laser is focused to the end of the exit capillary and the liquid analyte / matrix mixture is desorbed and ionized. The ions are guided by electric fields and by the stream of nitrogen to the interface of the mass spectrometer.**

## Materials

The MALDI matrices α-cyano-4-hydroxycinnamic acid (HCCA, M = 189.2 Da), 2,5-dihydroxybenzoic acid (DHB, M = 154.1 Da), protoporphyrin IX (M = 562.7 Da), 6-aza-2-thiothymine (ATT, M = 143.2 Da), 4-nitroaniline (PNA, M = 138.1), 3,5-dimethoxy-4-hydroxycinnamic acid (sinapic acid, M = 224.2 Da), and 3,4-dihydroxy-cinnamic acid (caffeic acid, M=180.2 Da) were purchased from Fluka (Buchs, Switzerland). Harmane (M = 182.2 Da) was obtained from Acros (Geel, Belgium). The liquid matrix N-(4-methoxybenzylidene)-4-butylaniline (MBBA, M = 267.4 Da) was purchased from Aldrich (ST. Louis, USA). The peptide analytes angiotensin II (M = 1046 Da), [$Ile^7$]-angiotensin III (M= 897 Da), α-casein(90-96), bradykinin(1-7), $P_{14}R$, as well as the proteins insulin, ubiquitin, and cytochrome c were purchased from Sigma (St. Louis, USA). The phosphorylated and non-phosphorylated form of the peptide pp60 c-src(521-533) were obtained from Bachem (Bubendorf, Switzerland), the glycopeptide actinomycin D and the polyethylene glycol (PEG1000, M = 800-1200 Da) were from Fluka. The oligosaccharides α-, β-, and γ-cyclodextrin were purchased from Sigma. All solvents, matrices and analytes were obtained at the highest purity available and used as received.

## 6.3 Results and Discussion

In order to get familiar with atmospheric pressure MALDI and to optimize the atmospheric interface of the mass spectrometer, experiments with co-crystallized matrix / analyte mixtures were performed. Figure 6.4 shows a spectrum of bradykinin fragment 1-7, angiotensin II and $P_{14}R$ with PNA as matrix.

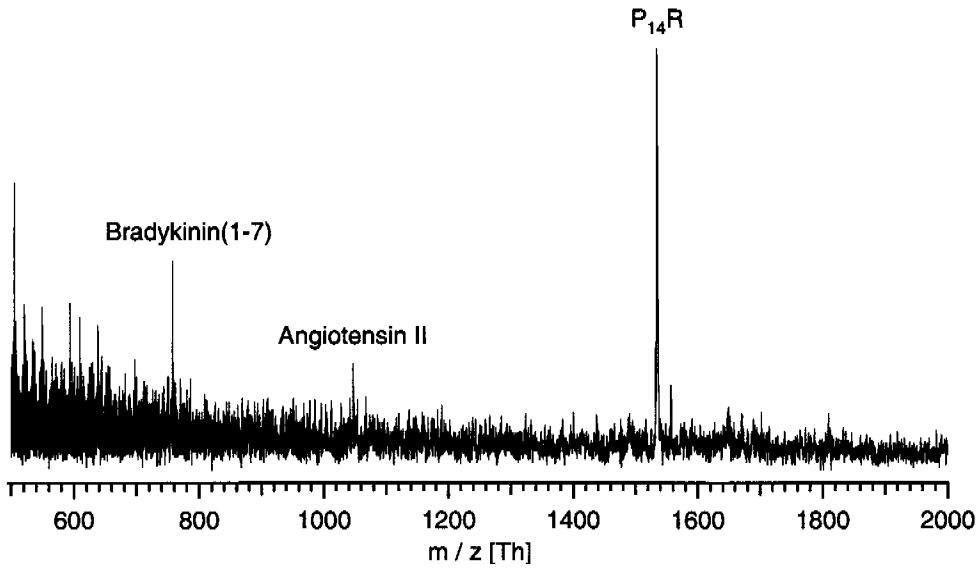


**Figure 6.4: Positive ion mode AP-MALDI mass spectrum of 100 µM bradykinin(1-7), 100 µM angiotensin II, and 100 µM P14R in $H_2O$ co-crystallized with 0.1 M PNA in $H_2O$/ ACN (1:1/v:v).**

To explore the applicability of flow-injection atmospheric pressure MALDI, liquid as well as solid matrices dissolved in different solvents were investigated. Starting with the known system of polyethylene glycol in MBBA, it could be shown that the basic principle of flow injection AP-MALDI is feasible with our setup, using a static fused silica capillary and a nitrogen laser. Fig 6.5a shows a positive ion mode flow-injection AP-MALDI of 1 mM PEG1000 in MBBA:MeOH (1:1/v:v). The flow rate was 5 µl $min^{-1}$; no additional sodium was added to the sample. For PEG1000 the intact $Na^+$ cationized oligomer distribution is observed. It is not a prerequisite that the matrix is a liquid, since dissolved solid matrices can also be successfully employed [30]. Fig 6.5b shows a spectrum of 20 µM α-casein(90-96) and 15 µM angiotensin II in 25 mM methanolic HCCA. In Fig 6.5c, a mass spectrum of 50 µM angiotensin II and 80 µM

harmane in water is presented. Figure 6.6 shows three injections of 500 nl 4 µM angiotensin II in 25 mM methanolic HCCA. 25 mM methanolic HCCA was used as eluent for this measurement. The result clearly shows the applicability of the proposed method for coupling liquid chromatography to AP-MALDI.

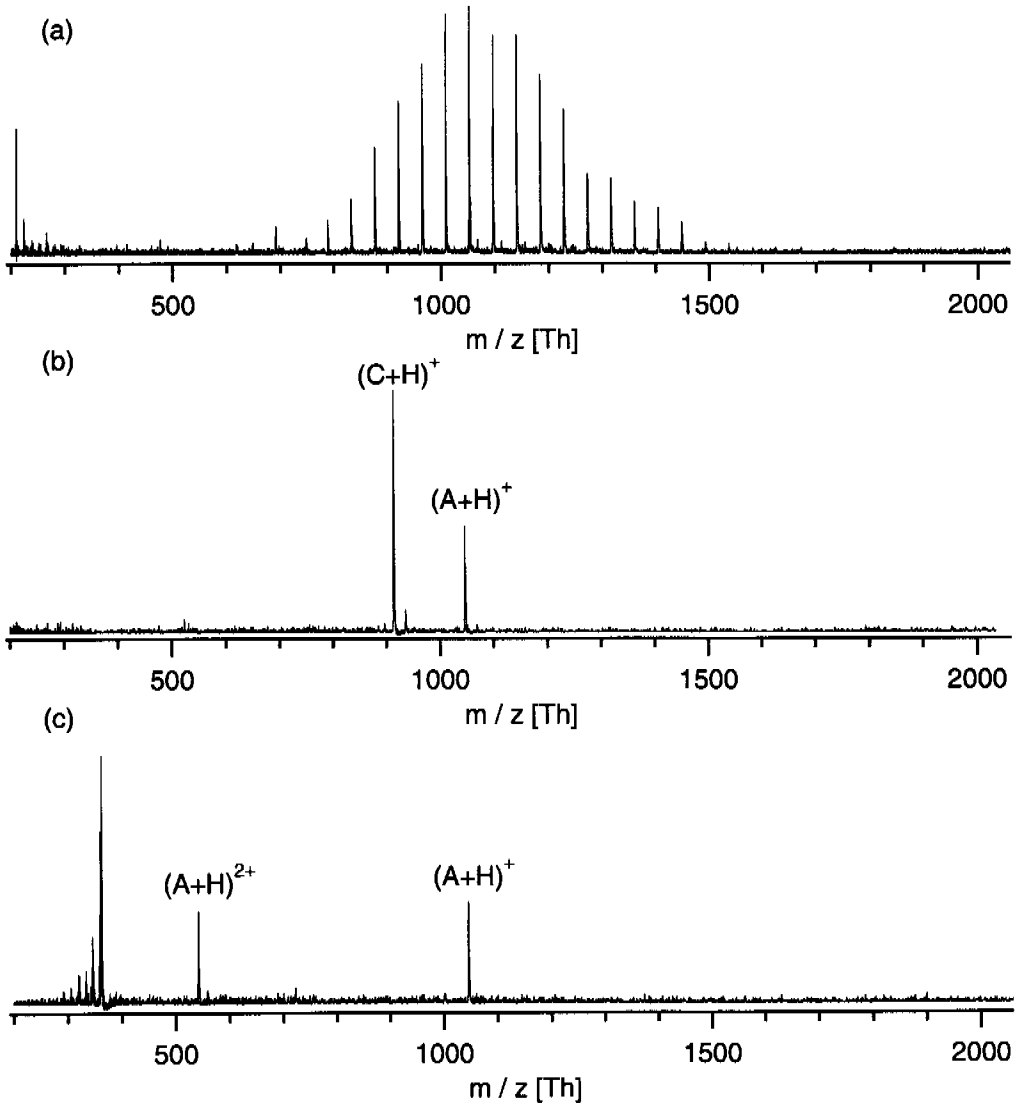


**Figure 6.5: Positive ion mode flow-injection AP-MALDI mass spectra of different analytes, matrices, and solvents. (a) 1 mM PEG 1000 in MBBA:MeOH 1:1 with a flow rate of 5 µl $min^{-1}$. (b) 20 µM α-casein(90-96) (C), 15 µM angiotensin II (A) and 25 mM HCCA in MeOH with a flow rate of 1 µl $min^{1}$. (c) 50 µM angiotensin II (A) and 80 µM harmane in $H_2O$ with a flow rate of 10 µl $min^{-1}$.**

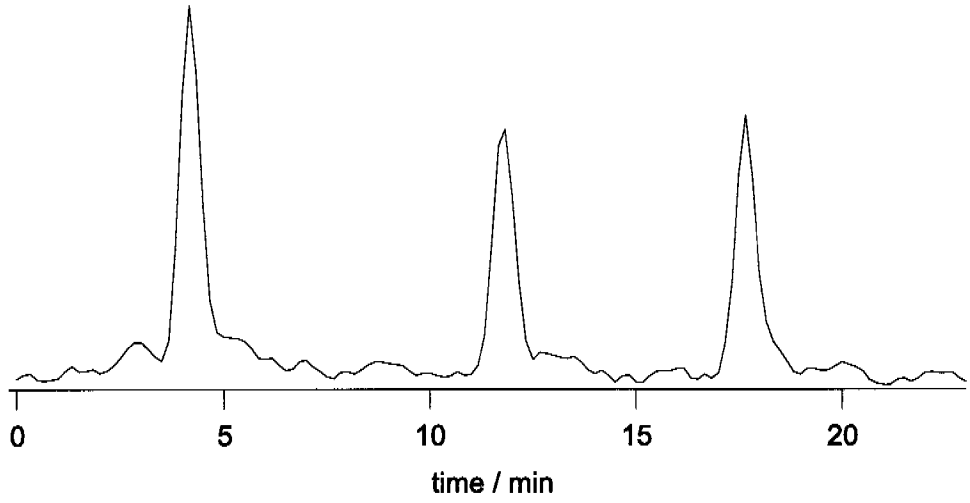


**Figure 6.6: Three flow injections of 500 nl 4 μM angiotensin II in 25 mM methanolic HCCA; the mobile phase consisted of 25 mM methanolic HCCA and the flow rate was 1 μl $min^{-1}$. A loss in sensitivity is observed during the measurement.**

The suitability of different matrices in methanol and water was investigated and the results are summarized in table 6.1. One of the major drawbacks encountered using UV-MALDI matrices is their solubility. While many of them show a fairly good solubility in methanol, the solubility in water is often poor, leading to low matrix concentrations in the final analyte / matrix mixtures. Nevertheless, it was possible to measure angiotensin II with all matrices in water and methanol, except with protoporphyrin IX in methanol (table 6.1). Although angiotensin II could not be detected in the latter experiment, a strong matrix ion signal was detected, indicating that desorption / ionization occurs but that the analyte signal may be suppressed by the matrix. The overall signal-to-noise ratio for water samples is worse than the ones achieved in methanol, but both solvents can be successfully employed for measurements. To enhance the matrix concentration in water samples and to further improve the signal-to-noise ratio, it will be necessary to find new matrices with better solubility in water in order to achieve a better desorption / ionization.

The above experiments were carried out with a nitrogen laser (337 nm) at a repetition rate of only 20 Hz and with a static fused silica exit capillary. To make better use of the fast data acquisition of the time-of-flight mass spectrometer (4000 transients per second in our instrument), a Nd:YAG laser (355 nm) with a repetition rate of 1 kHz was employed. The signal-to-noise ratio of 50 μM angiotensin II and 25 mM HCCA in

| Matrix | MeOH | $H_2O$ |
|---|---|---|
| HCCA | ++ | + |
| DHB | + | ++ |
| Protoporphyrin IX | – | + |
| ATT | ++ | + |
| Harmane | + | ++ |
| PNA | ++ | ++ |
| Sinapic acid | ++ | + |
| Caffeic acid | ++ | + |

**Table 6.1: MALDI mass signal response of angiotensin II with different matrices in methanol and water: ++ good signal response, + detectable signal, - no analyte ion detected.**

methanol improved by a factor of > 2 (figure 6.7a and 6.7b). Although the pulse energy of the high repetition rate laser is lower (15 μJ $pulse^{-1}$), the better beam profile allowed to achieve a comparable laser fluence, which is the relevant parameter for successful MALDI experiments [63-65].

Using a static fused silica capillary, the droplets formed at its end have dimensions of millimeters. Because the laser must be focused exactly onto the surface of the droplet, either the focus needs to be adapted according to the droplet size, or optics with long working distance must be employed, respectively. It is, however, more convenient if each laser shot is focused onto a droplet of defined and constant size. Therefore the fused silica exit capillary was changed to a piezo pump usually employed for pipetting picoliter volumes. The piezo pump allowed to eject the droplets after each laser shot and to provide for each laser shot a fresh droplet of defined size. The improvement achieved is encouraging: the signal-to-noise ratio improved by a factor of three in comparison with the fused silica capillary (figure 6.7b and 6.7c).

In liquid MALDI, no co-crystallization of analyte and matrix is necessary, the analyte and matrix are equally distributed within the droplets, at least if neither of them is a surfactant. This is in contrast to conventional MALDI samples, where segregation effects of matrix and analyte often occur, leading to the formation of "sweet spots".

The liquid AP-MALDI also allowed us to perform quantitative measurements, as shown in figure 6.8. Angiotensin II was used as an internal standard to account for

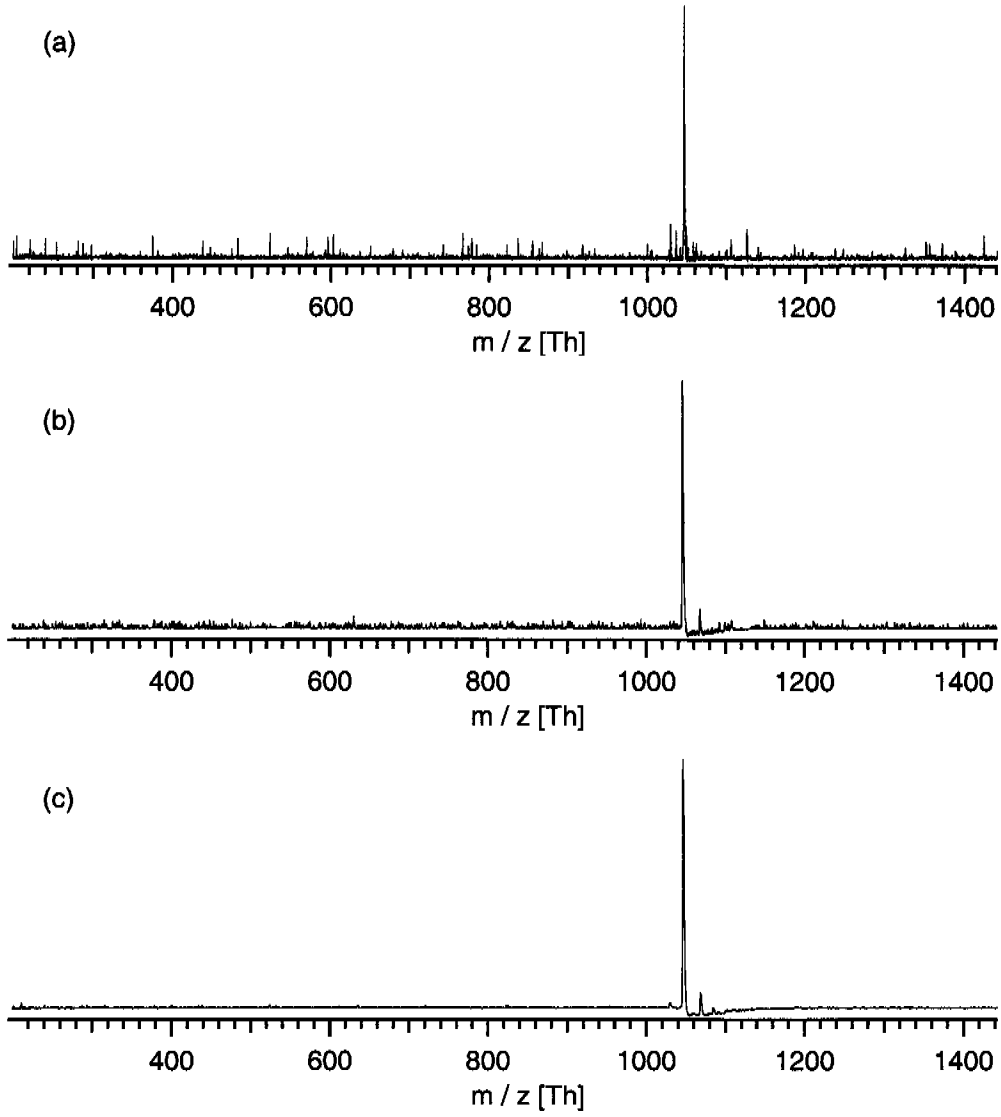


**Figure 6.7: Positive ion mode flow-injection AP-MALDI mass spectra with different lasers and exit capillaries. (a) 50 µM angiotensin II and 25 mM HCCA in MeOH, flow rate 10 µl $min^{-1}$, nitrogen laser (20 Hz, 337 nm). (b) 50 µM angiotensin II and 25 mM HCCA in MeOH, flow rate 5 µl $min^{-1}$, Power Chip Laser (1 kHz, 355 nm). (c) 50 µM angiotensin II and 25 mM HCCA in MeOH, flow rate 5 µl $min^{-1}$, Power Chip Laser (1 kHz, 355 nm), droplet ejection at 1 kHz. Note the increasing signal-to-noise ratio from experiments (a) to (c).**

fluctuations in the total ion current. To estimate the standard deviations and confidence intervals, each concentration was measured ten times. The remarkably small deviations indicate that the error of preparing the calibration solutions is larger than the error of the measurements. For α-casein(90-96) the measured concentrations are as

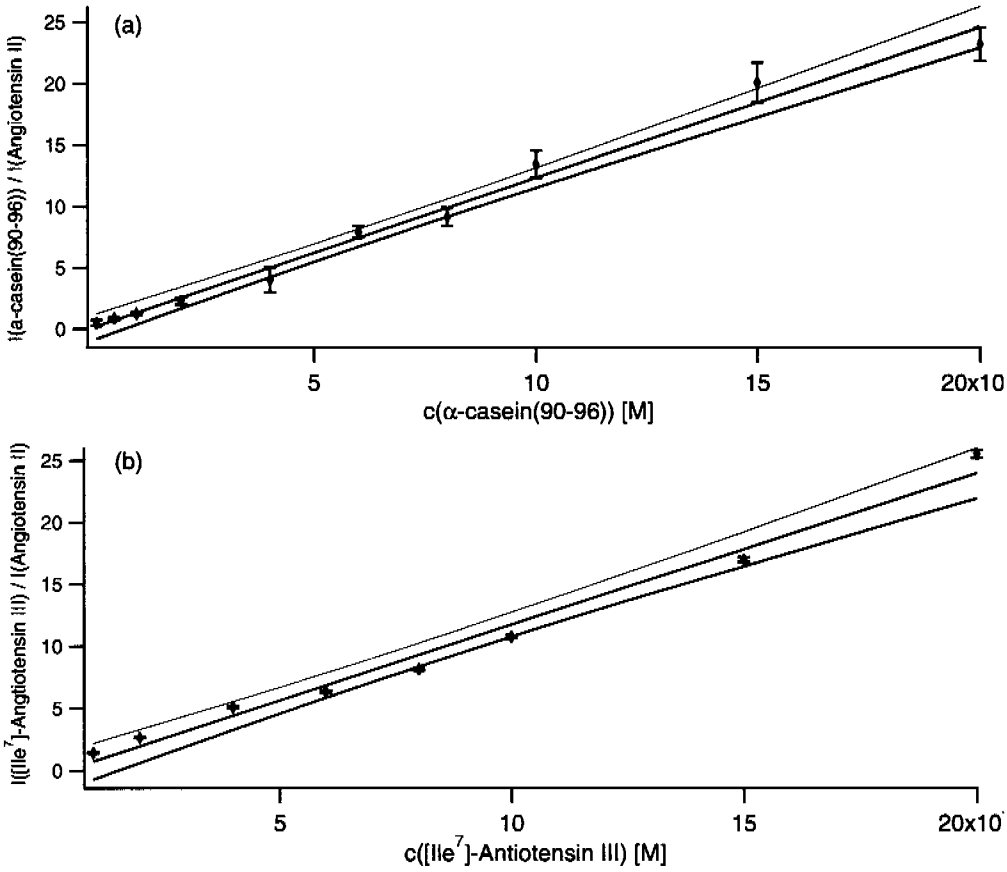


**Figure 6.8: Quantitative measurement with flow injection AP-MALDI. (a) 0.1 µM to 20 µM α-casein(90-96) with each 15 µM angiotensin II and 25 mM HCCA in MeOH. (b) 1 µM to 20 µM [Ile$^7$]-angiotensin III with each 15 µM angiotensin II and 25 mM HCCA in MeOH. The middle lines indicate the linear fit, the upper and lower lines the 95 % confidential intervals, respectively.**

low as 500 nM or 83 fmol consumed, for a clearly detectable analyte ion signal. Thus with the current setup, concentrations down to 500 nM or 83 fmol are accessible.

In order to achieve comparable sensitivity to conventional AP-MALDI and ESI mass spectrometry, the limit of detection must be further improved. The lower detection limit of AP-MALDI for compounds in the mass range of 800 to 1700 Da was estimated by Moyer et al. [41] to be 10 to 50 fmol. By improving the setup for ion collection, resulting in the second generation AP-MALDI interface (figure 6.3), the limit of detection (LoD) could be lowered by one order of magnitude to a final LoD of 50 nM or 8.3 fmol analyte (figure 6.9). The ions generated by the impact of the laser are dragged

into the mass spectrometric interface not only by electric forces but also by the aerodynamic flow of the dried nitrogen enhancing the ion transmission significantly.

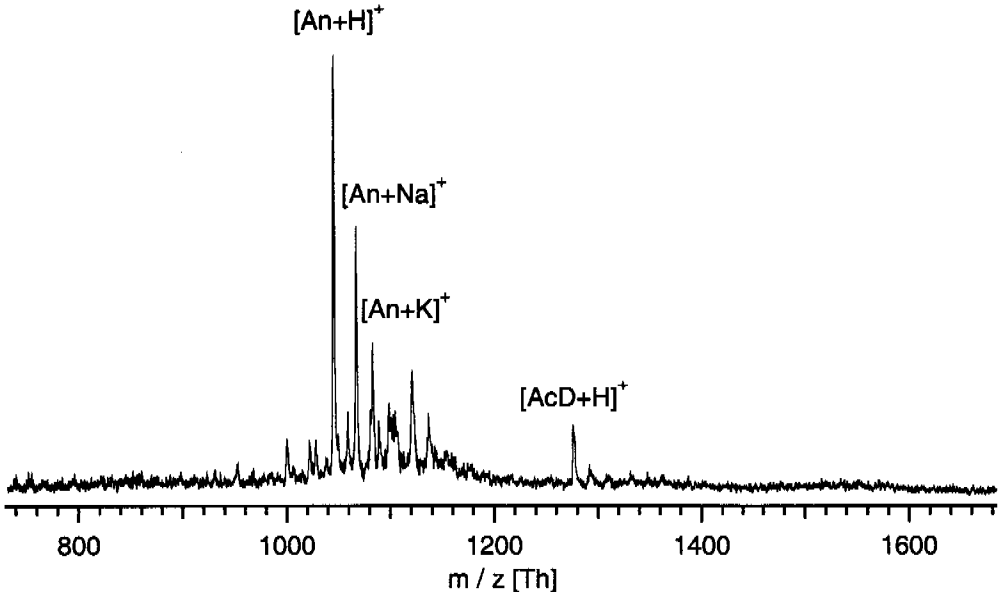


**Figure 6.9: Positive ion mode flow-injection AP-MALDI mass spectrum of 0.05 µM actinomycin D (AcD), 10 µM angiotensin II (An), 25 mM HCCA in methanol. 8.3 fmol AcD was consumed during the acquisition.**

To show the wide applicability of flow-injection AP-MALDI, different classes of compounds were measured with HCCA co-dissolved in methanol. Figure 6.10 shows a spectrum of a mixture containing the oligosaccharides α-, β-, and γ-cyclodextrin. As expected from the structure of the compounds, no protonated species can be observed. Sodiated as well as potassiated molecular ion peaks can be detected for all three species. The sodiated matrix adducts were also detected for β- and γ-cyclodextrin.

In recent years, a major interest arose in the posttranslational modification of proteins and peptides. Two of the major posttranslational modifications are glycosylation and phosphorylation. To determine the site of the modification, the proteins are often digested and the fragments are analyzed. Figure 6.11a shows the spectrum of the glycopeptide actinomycin D (13 µM in methanol with 25 mM HCCA). Due to the lack of any favorable protonation sites, the sodiated and potassiated molecular ion peaks were again detected with a very good signal-to-noise ratio. Very low fragmentation is

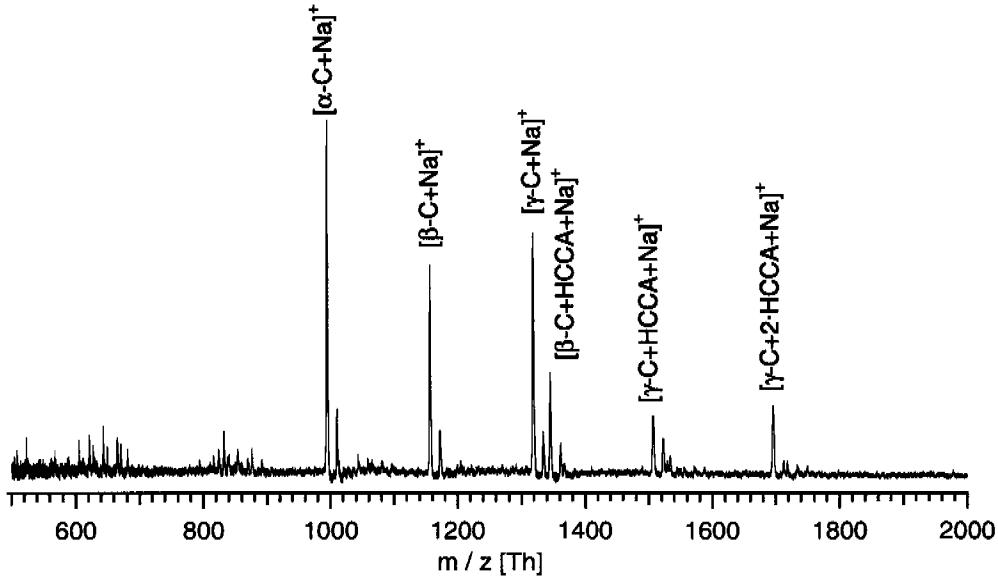


**Figure 6.10: Positive ion mode flow-injection AP-MALDI mass spectrum of 10 µM α-, β-, and γ-cyclodextrin, 25 mM HCCA in methanol delivered with a flow rate of 1 µl $min^{-1}$. The sodiated molecular ion peaks can be observed for all species. Also he sodiated matrix adducts are observed for β- and γ-cyclodextrins.**

observed. Figure 6.11b shows a spectrum of a mixture of pp60 c-src(521-533) non-phosphorylated (H3256), and phosphorylated (H3258), 5 µM each with 25 mM HCCA in methanol. For both species the protonated as well as the sodiated molecular ion peaks were observed. Although the signal of the non-phosphorylated peptide is about 4 times higher, the phosphorylated peptide shows a good signal as well. This proves that the method is suitable for proteomic applications.

In the previous paragraphs, we have shown that our flow-injection AP-MALDI setup is suitable for many different classes of analytes. However, the upper mass limit of the ionization method is equally important. Figure 6.12 shows spectra of ubiquitin (8565 Da) and cytochrome c (~13000 Da). For both proteins only the doubly and triply charged molecular ion peaks could be observed. This is due to the upper mass limit of the atmospheric transfer interface for the TOF instrument, which is around 7500 Th. The low ion yield of the doubly and especially triply charged ions prevented the measurement of higher mass analytes. Sze et al. [30] showed spectra of bovine serum albumin (67000 Da) recorded from a solution of glycerol, HCCA, and 2-aminoquiniline with conventional vacuum MALDI. This supports our expectation that the upper mass limit is not yet reached. Unfortunately most atmospheric pressure mass

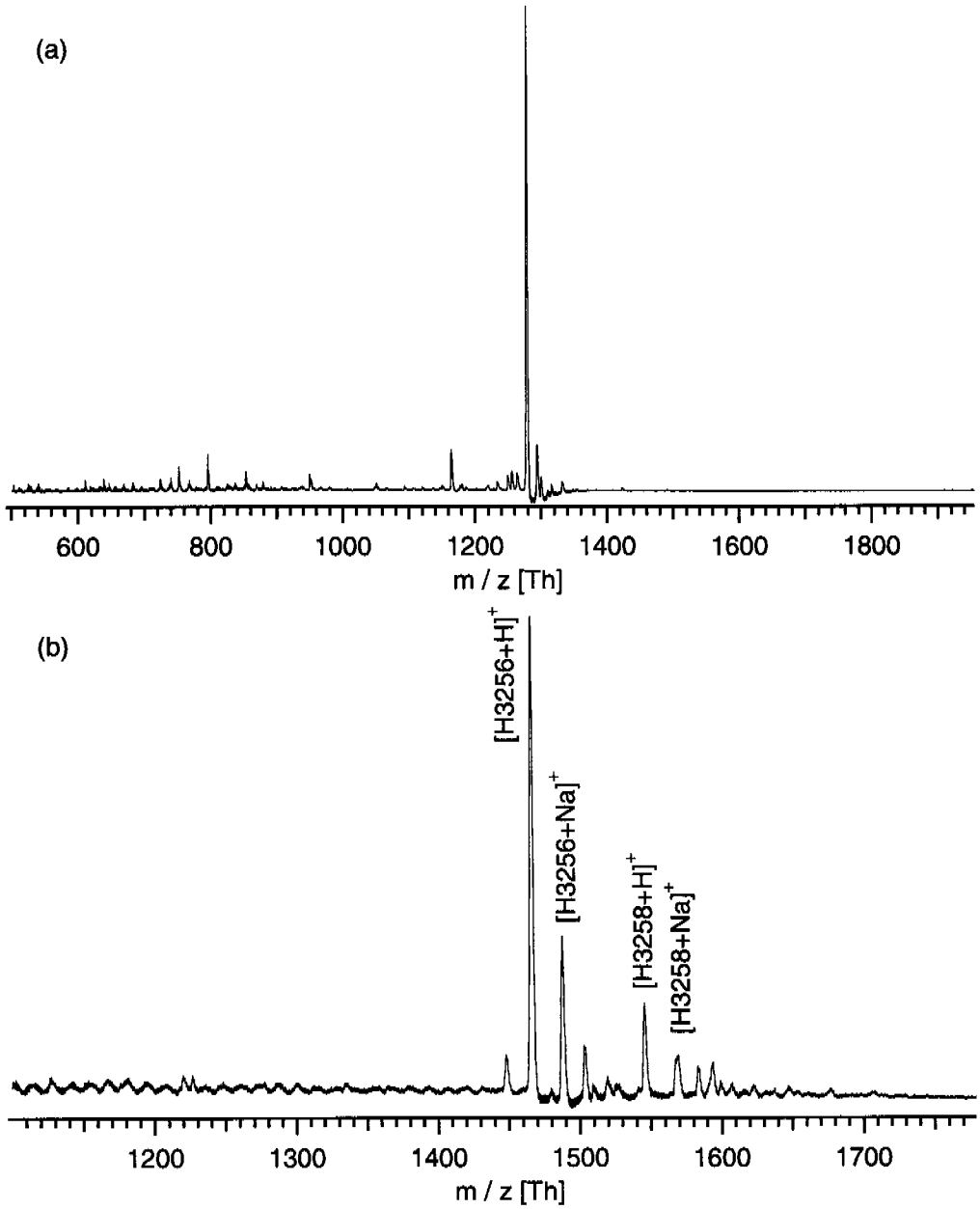


**Figure 6.11: (a) Positive ion mode flow-injection AP-MALDI mass spectrum of 13 µM actinomycin D, 25 mM HCCA in methanol delivered with a flow rate of 0.5 µl $min^{-1}$. A very good signal-to-noise ratio could be achieved. (b) Positive ion mode flow-injection AP-MALDI mass spectrum of 5 µM pp60 c-src(521-533) phosphorylated (H3258), 5 µM pp60 c-src(521-533) non-phosphorylated (H3256), 25 mM HCCA in methanol delivered with a flow rate of 1 µl $min^{-1}$. The protonated as well as the sodiated molecular ion peaks could be observed.**

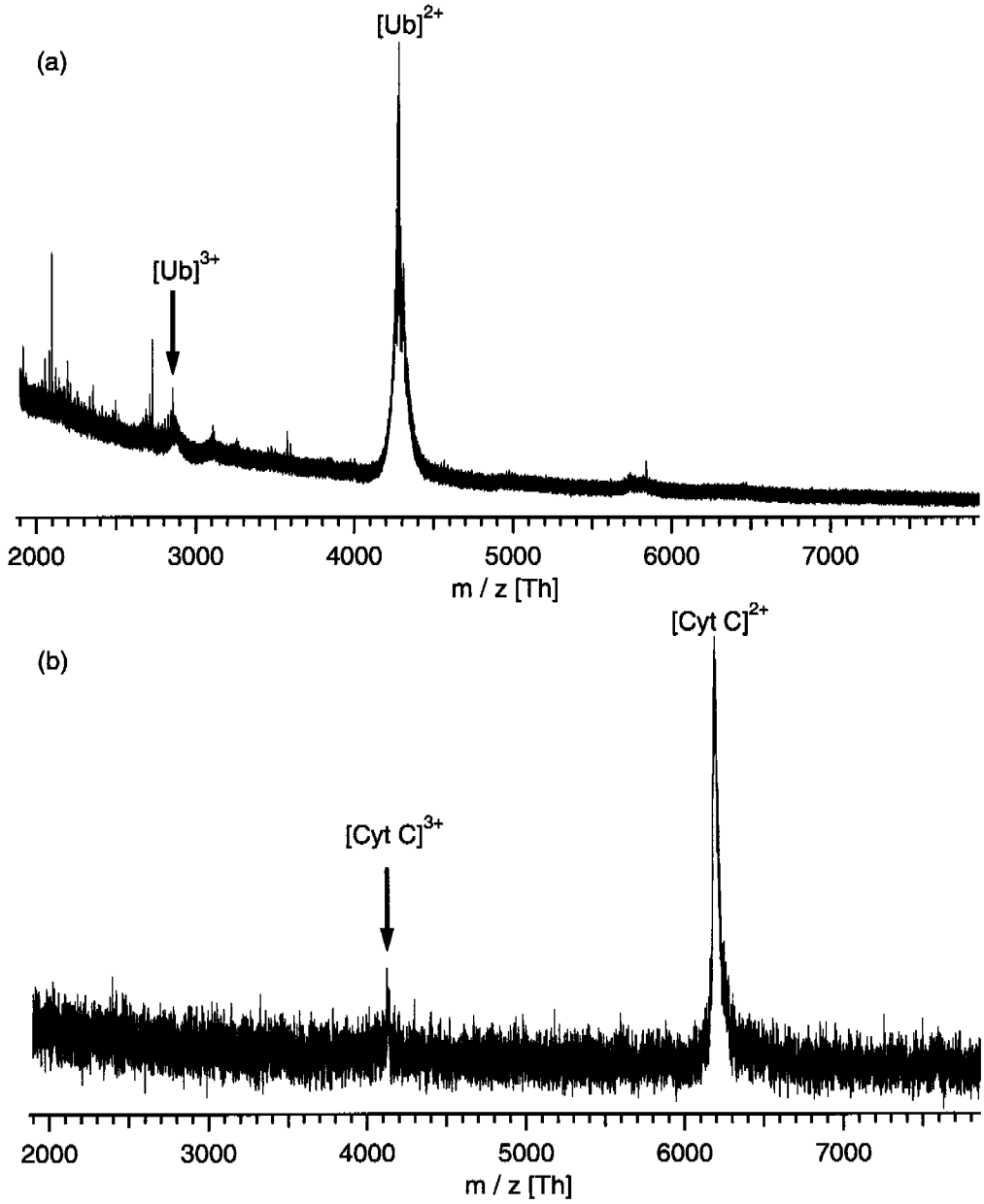


**Figure 6.12: Positive ion mode flow-injection AP-MALDI mass spectrum of a) 15 µM ubiquitin, 50 mM HCCA in methanol delivered with a flow rate of 1 µl $min^{-1}$ and b) 10 µM cytochrome c, 25 mM HCCA in 60% methanol, 32% acetonitrile, and 8% water delivered with a flow rate of 1 µl $min^{-1}$. Because of the mass limit of the AP interface, only the doubly and triply charged molecular ion peaks could be detected.**

spectrometric interfaces, especially the electrospray interfaces are optimized for a m/z ratio between 1 and 6000 Th and do not transmit high mass ions efficiently, making it difficult or impossible to detect high mass compounds by AP-MALDI.

## 6.4 Summary

The technique of flow injection atmospheric pressure MALDI as a novel way for on-line coupling of liquid sample delivery to AP MALDI mass spectrometry is presented and successfully applied to a variety of matrices and different solvents, polymers as well as peptides. The current limit of detection achieved is about 50 nM. Due to the homogeneous distribution of matrix and analytes within the droplets, quantification becomes feasible. These are important prerequisites for a detector for liquid chromatography (LC). Besides the fact that the concentration of known effluents can be calibrated and quantified and the information about the effluents is monitored on-line, it should be possible to collect spare sample droplets on a target and to use them for further mass spectrometric analyses or to archive samples. Furthermore, it is well known that water can be employed as matrix in IR-MALDI experiments (see chapter 7). If water can indeed be directly used as matrix, no additional matrix has to be added to the sample solution. This is especially interesting for measuring biological samples under non-denaturing conditions. Taking advantage of the benefit of liquid MALDI, *i.e.* of the homogeneous distribution of matrix and analyte within the sample droplets, liquid MALDI may be employed to further investigate the first shot phenomenon observed when measuring non-covalent complexes with conventional MALDI. In contrast to conventional MALDI measurements with liquid matrices in vacuum, the solvents, matrices and analytes do not need to be vacuum stable and therefore a new field of applicable systems arises.

## 6.5 References


1. J. M. Daniel, S. Ehala, S. D. Friess and R. Zenobi, *Analyst*, 2004, **129**, 574-578.
2. M. Karas, D. Bachmann and F. Hillenkamp, *Anal. Chem.*, 1985, **57** (14), 2935-2939.
3. M. Karas, D. Bachmann, U. Bahr and F. Hillenkamp, *Int. J. Mass Spectrom. Ion Process.*, 1987, **78**, 53-68.
4. M. Karas and F. Hillenkamp, *Anal. Chem.*, 1988, **60** (20), 2299-2301.
5. K. Tanaka, H. Waki, Y. Ido, S. Akita, Y. Y. and T. Yoshida, *Rapid Commun. Mass Spectrom.*, 1988, **2** (8), 151-153.
6. F. H. Song, *Rapid Commun. Mass Spectrom.*, 2003, **17** (15), 1802-1807.
7. A. Marie, S. Alves, F. Fournier and J. C. Tabet, *Anal. Chem.*, 2003, **75** (6), 1294-1299.
8. B. J. Bauer, C. M. Guttman, D. W. Liu and W. R. Blair, *Rapid Commun. Mass Spectrom.*, 2002, **16** (12), 1192-1198.
9. S. Timpin, A. Rouhanipour, R. Az, H. J. Rader and K. Mullen, *Rapid Commun. Mass Spectrom.*, 2001, **15** (15), 1364-1373.
10. L. Ulmer, J. Mattay, H. G. Torres-Garcia and H. Luftmann, *Eur. J. Mass Spectrom.*, 2000, **6** (1), 49-52.
11. L. Przybilla, J. D. Brand, K. Yoshimura, H. J. Rader and K. Mullen, *Anal. Chem.*, 2000, **72** (19), 4591-4597.
12. S. F. Macha, P. A. Limbach and P. J. Savickas, *J. Am. Soc. Mass Spectrom.*, 2000, **11** (8), 731-737.
13. A. V. Streletskiy, I. V. Kouvitchko, S. E. Esipov and O. V. Boltalina, *Rapid Commun. Mass Spectrom.*, 2002, **16** (2), 99-102.
14. J. T. Shiea, J. P. Huang, C. F. Teng, J. Y. Jeng, L. Y. Wang and L. Y. Chiang, *Anal. Chem.*, 2003, **75** (14), 3587-3595.
15. S. Carda-Broch, A. Berthod and D. W. Armstrong, *Rapid Commun. Mass Spectrom.*, 2003, **17** (6), 553-560.
16. D. W. Armstrong, L. K. Zhang, L. F. He and M. L. Gross, *Anal. Chem.*, 2001, **73** (15), 3679-3686.
17. Y. S. Lin and Y. C. Chen, *Anal. Chem.*, 2002, **74** (22), 5793-5798.
18. T. Yalcin, W. E. Wallace, C. M. Guttman and L. Li, *Anal. Chem.*, 2002, **74**

(18), 4750-4756.

19. P. Dietemann, M. Kalin, S. Zumbuhl, R. Knochenmuss, S. Wulfert and R. Zenobi, *Anal. Chem.*, 2001, **73** (9), 2087-2096.
20. M. Schurenberg, K. Dreisewerd and F. Hillenkamp, *Anal. Chem.*, 1999, **71** (1), 221-229.
21. M. J. Dale, R. Knochenmuss and R. Zenobi, *Anal. Chem.*, 1996, **68** (19), 3321-3329.
22. J. Sunner, E. Dratz and Y. C. Chen, *Anal. Chem.*, 1995, **67** (23), 4335-4342.
23. K. Breuker, R. Knochenmuss and R. Zenobi, *Int. J. Mass Spectrom.*, 1998, **176** (1-2), 149-159.
24. S. Berkenkamp, F. Kirpekar and F. Hillenkamp, *Science*, 1998, **281** (5374), 260-262.
25. T. W. D. Chan, A. W. Colburn and P. J. Derrick, *Org. Mass Spectrom.*, 1992, **27** (1), 53-56.
26. T. Fujita, Y. Itagaki, M. Hisaka, H. Naoki, T. Nakajima and M. Andriantsiferana, *Rapid Commun. Mass Spectrom.*, 1997, **11** (10), 1115-1119.
27. J. B. Williams, A. I. Gusev and D. M. Hercules, *Macromolecules*, 1996, **29**, 8144-8150.
28. R. M. Whittal, L. M. Russon and L. Li, *J. Chromatogr. A*, 1998, **794** (1-2), 367-375.
29. C. E. Von Seggern, S. C. Moyer and R. J. Cotter, *Anal. Chem.*, 2003, **75** (13), 3212-3218.
30. E. T. P. Sze, T. W. D. Chan and G. Wang, *J. Am. Soc. Mass Spectrom.*, 1998, **9** (2), 166-174.
31. S. J. Lawson and K. K. Murray, *Rapid Commun. Mass Spectrom.*, 2002, **16** (12), 1248-1250.
32. J. Wei, J. M. Buriak and G. Siuzdak, *Nature*, 1999, **399** (6733), 243-246.
33. E. P. Go, J. E. Prenni, J. Wei, A. Jones, S. C. Hall, H. E. Witkowska, Z. X. Shen and G. Siuzdak, *Anal. Chem.*, 2003, **75** (10), 2504-2506.
34. R. A. Kruse, X. L. Li, P. W. Bohn and J. V. Sweedler, *Anal. Chem.*, 2001, **73** (15), 3639-3645.
35. V. V. Laiko, S. C. Moyer and R. J. Cotter, *Anal. Chem.*, 2000, **72** (21), 5239-5243.

36. V. V. Laiko, M. A. Baldwin and A. L. Burlingame, *Anal. Chem.*, 2000, **72** (4), 652-657.
37. J. L. Wolfender, F. X. Chu, H. Ball, F. Wolfender, M. Fainzilber, M. A. Baldwin and A. L. Burlingame, *J. Mass Spectrom.*, 1999, **34** (4), 447-454.
38. V. V. Laiko, N. I. Taranenko, V. D. Berkout, B. D. Musselman and V. M. Doroshenko, *Rapid Commun. Mass Spectrom.*, 2002, **16** (18), 1737-1742.
39. C. S. Creaser, J. C. Reynolds and D. J. Harvey, *Rapid Commun. Mass Spectrom.*, 2002, **16**, 176-184.
40. J. A. McLean, W. K. Russell and D. H. Russell, *Anal. Chem.*, 2003, **75** (3), 648-654.
41. S. G. Moyer and R. J. Cotter, *Anal. Chem.*, 2002, **74** (17), 468A-476A.
42. M. C. Galicia, A. Vertes and J. H. Callahan, *Anal. Chem.*, 2002, **74**, 1891-1895.
43. V. M. Doroshenko, V. V. Laiko, N. I. Taranenko, V. D. Berkout and H. S. Lee, *Int. J. Mass Spectrom.*, 2002, **221** (1), 39-58.
44. K. K. Murray, *Mass Spectrom. Rev.*, 1997, **16** (5), 283-299.
45. A. I. Gusev, *Fresenius J. Anal. Chem.*, 2000, **366** (6-7), 691-700.
46. H. Orsnes and R. Zenobi, *Chem. Soc. Rev.*, 2001, **30** (2), 104-112.
47. E. Gelpi, *J. Mass Spectrom.*, 2002, **37** (3), 241-253.
48. W. Weinmann, C. E. Parker, L. J. Deterding, D. I. Papac, J. Hoyes, M. Przybylski and K. B. Tomer, *J. Chromatogr. A*, 1994, **680** (2), 353-361.
49. K. L. Walker, R. W. Chiu, C. A. Monnig and C. L. Wilkins, *Anal. Chem.*, 1995, **67** (22), 4197-4204.
50. P. A. Vanveelen, U. R. Tjaden, J. Vandergreef, A. Ingendoh and F. Hillenkamp, *J. Chromatogr.*, 1993, **647** (2), 367-374.
51. H. Y. Zhang and R. M. Caprioli, *J. Mass Spectrom.*, 1996, **31** (9), 1039-1046.
52. G. S. McLeod, J. Axelsson, R. Self and P. J. Derrick, *Rapid Commun. Mass Spectrom.*, 1997, **11** (2), 214-218.
53. S. Hsieh, K. Dreisewerd, R. C. van der Schors, C. R. Jimenez, J. R. Stahl-Zeng, F. Hillenkamp, J. W. Jorgenson, W. P. M. Geraerts and K. W. Li, *Anal. Chem.*, 1998, **70** (9), 1847-1852.
54. L. Li, A. P. L. Wang and L. D. Coulson, *Anal. Chem.*, 1993, **65** (4), 493-495.
55. G. Grigorean, J. Wronka, C. Martin, F. Laukien and I. J. Amster. in *43rd ASMS Conference on Mass Spectrometry and Allied Topics*, 1995, Atlanta, GA.

56. S. Y. Chang and E. S. Yeung, *Anal. Chem.*, 1997, **69** (13), 2251-2257.
57. E. F. Lehmann, *Do MALDI Mass Spectra Reflect Condensed-Phase Chemistry? and Development of a Continous-Flow Interface for MALDI Mass Spectrometry*, 1999, Swiss Federal Institute of Technology (ETH Diss. Nr. 13311), Zürich.
58. Q. Zhan, A. Gusev and D. M. Hercules, *Rapid Commun. Mass Spectrom.*, 1999, **13** (22), 2278-2283.
59. K. K. Murray and D. H. Russell, *Anal. Chem.*, 1993, **65** (18), 2534-2537.
60. L. He, L. Liang and D. M. Lubman, *Anal. Chem.*, 1995, **67**, 4127-4132.
61. H. Orsnes, T. Graf, H. Degn and K. K. Murray, *Anal. Chem.*, 2000, **72** (1), 251-254.
62. H. Orsnes, R. Zenobi and J. M. Daniel, *Atmospheric-pressure Ionization Device and Method for Analysis of a Sample*, 2002, Europ. Patent, No. EP1193730.
63. P. Demirev, A. Westmann, C. T. Reimann, P. Håkansson, D. Barofsky, B. U. R. Sundqvist, Y. D. Cheng, W. Seibt and K. Siegbahn, *Rapid Commun. Mass Spectrom.*, 1992, **6**, 187-191.
64. G. Westmacott, W. Ens, F. Hillenkamp, K. Dreisewerd and M. Schürenberg, *Int. J. Mass Spectrom.*, 2002, **221**, 67-81.
65. R. Zenobi and R. Knochenmuss, *Mass Spectrom. Rev.*, 1998, **17**, 337-366.

Seite Leer /
Blank leaf

# CHAPTER 7

# ATMOSPHERIC PRESSURE INFRARED DESORPTION FROM SOLUTION

Seite Leer /
Blank leaf

Pure water as well as water containing glycerol and 3-nitrobenzyl alcohol (NBA) were investigated with respect to their function as matrices in atmospheric pressure infrared ionization from solution (AP-IRIS). Water containing 20 % glycerol was found to be the best composition for a matrix to measure the small peptides angiotensin II and bradykinin from a deposited droplet. Results obtained from single droplet AP-IRIS are presented for these peptides. It could be shown, that the desorption and ionization of single droplets with a infrared laser is feasible. In contradiction to the results for deposited droplets, the addition of glycerol did not improve the signal for single droplet AP-IRIS: pure water was found to be the best matrix.

## 7.1 Introduction

Interestingly, the first method to desorb and ionize non-volatile, thermally labile biomolecules was neither electrospray ionization (ESI) nor matrix assisted laser desorption / ionization (MALDI) but laser desorption ionization (LDI), a precursor of MALDI, where a pulsed $CO_2$ laser was employed [1]. Posthumus and co-workers showed spectra of peptides showing very low fragmentation without using any matrix. Further development of LDI by Tanaka [2] and Hillenkamp [3-5] led to the discovery of MALDI, essentially associated with the use of pulsed UV lasers. After a short time of method and instrumentation development, UV-MALDI MS has become an established technique for the analysis of a wide range of biomolecules and polymers.

Hillenkamp and co-workers presented the first results for MALDI with a pulsed infrared (IR) laser in 1990: they showed the applicability of an Er:YAG laser with an emission wavelength of 2.94 μm (pulse width 200 ns) for desorption of large biomolecules [6], including results for a monoclonal antibody (M ≈ 150'000 Da). They employed a wide variety of matrices in their study, *e.g.* caffeic acid, succinic acid, glycerol, and urea. Shortly after this first study, they compared the former results with results obtained by using a $CO_2$ laser with an emission wavelength of 10.6 μm (pulse width 70 ns) [7]. Both methods provided similar results. A tendency of IR-MALDI to generate higher charge states compared to UV-MALDI could be observed. In the meantime, IR-MALDI has been employed in a wide variety of applications including the detection of proteins [8-10], oligonucleotides [11-16], double stranded DNA [17], sialylated carbohydrates [18], the probing of phospho- and glycopeptides [19], and the investigation of noncovalent sugar complexes [20]. An interesting application is the investigation of proteins electroblotted after polyacrylamide gel electrophoresis by IR-MALDI [21, 22].

In order to achieve desorption and ionization by IR irradiation, different vibrations can be excited: the stretching vibrations O-H, N-H, and C-H in the range of 2.7 - 4.0 μm, the stretching vibration of the carbonyl group C=O in the range of 5.5 - 6.5 μm, or the bending vibration O-H or the stretching vibration C-O around 10 μm. Different

lasers were used to excite at these wavelengths: Er:YAG (2.94 μm) [18, 23, 24], optical parametric oscillators (OPO) [25-27], free electron lasers (FEL) [28-30], and $CO_2$ (10 μm) lasers [7, 31, 32]. The many possible excitation wavelengths opened up possibilities to employ a wide variety of matrices, *e.g.* succinic acid, fumaric acid, nicotinic acid, glycerol, and water. With respect to the measurement of biomolecules, especially to the investigation of noncovalent complexes, physiological conditions are desirable. Therefore the investigation of liquid matrices, in particular water, is of great interest. Several publications appeared using glycerol / water mixtures [26, 33-35] and frozen water [8, 22, 32, 36-38] as matrix for IR-MALDI experiments. The introduction of AP-MALDI by Laiko et al. [39, 40] allowed the use of non-vacuum stable liquid matrices, *e.g.* liquid water, as matrices for IR-MALDI. Doroshenko and co-workers presented results for IR-AP-MALDI using a pulsed OPO infrared laser where glycerol and water were used as matrices [26]. Cotter and co-workers utilized this approach to investigate intact, fully sialylated molecular species [18].

The comparison of UV- and IR-MALDI reveals that IR-MALDI can be essentially used for all fields for which UV-MALDI has proven to work, whereas the current UV-MALDI performance is, however, generally not reached [41]. Nevertheless, IR-MALDI has been demonstrated to be advantageous whenever particularly large and / or labile compounds are analyzed; samples which are often not amenable to UV-MALDI mass analysis. IR-MALDI is generally regarded as the softer desorption method and leads to lower degree of metastable ion fragmentation. Hillenkamp and co-workers demonstrated the generation of intact protein ions with molecular weights exceeding 500 kDa by IR-MALDI [42].

The possibility to employ liquid matrices, however, offers inherent advantages: liquid matrices provide homogeneous sample morphology and a high shot-to-shot signal stability should result [42]. With solid state matrices in IR-MALDI, higher laser fluences are needed due to the smaller absorption coefficients for IR and the resulting higher penetration depth of the laser irradiation. The sample consumption is much higher than in the case of UV-MALDI, which frequently allows only a very limited number of laser exposures per sample spot. However, the spectra recorded by UV- and IR-MALDI have a high degree of similarity, although electronic (UV-MALDI)

and vibrational excitation (IR-MALDI) occurs. Therefore a similar mechanism was originally proposed [10]. However, Dreisewerd et al. recently presented results indicating that the desorption / ionization mechanism for solid and liquid state matrices in IR-MALDI may be different [41, 43]. Doroshenko and co-workers introduced the new term *atmospheric pressure infrared ionization from solution (AP-IRIS)* in order to distinguish between the different mechanisms [44]. They found that the sensitivity of AP-IRIS is even better than the sensitivity of AP-UV-MALDI. These findings strongly increase the interest in IR-MALDI and IRIS. There is one major drawback to use these methods: IR lasers are very expensive and exhibit a considerably lower long-term stability and therefore still require more efforts for maintenance (*e.g.* adjustment of the laser resonator).

Several coupling techniques to connect chromatographic systems, *e.g.* high performance liquid chromatography (HPLC) or capillary electrophoresis (CE), to IRIS MS have been presented. Murray and co-workers presented the coupling of CE with IR-MALDI [45]. In this work, ethanol mixed with low concentrations of glycerol were used as effluents for CE, delivered on-line to a stainless steel frit forming the MALDI target in the vacuum of the mass analyzer, and finally desorbed / ionized directly from this frit. Twerenbold et al. described a micro-machined silicon injector device with which small droplets were transferred into the high vacuum of the mass spectrometer [46]. By desorbing these droplets by a $CO_2$ laser, they showed spectra of insulin and lysozyme. Very recently Niemeyer and co-workers reported a method where a water filament with a diameter of 10 μm is generated in vacuum and irradiated by a pulsed IR laser [47]. They showed spectra of polymers and proteins.

Our present experiments focus on a flow-injection AP-IRIS source to couple any liquid chromatographic system to MS. In order to eliminate the need for mixing the analyte solution with matrix, we focus on using AP-IRIS with water as the main matrix component. For that purpose the suitability of water containing small amounts of additives are elucidated. We present a possible coupling method based on single droplet desorption / ionization which provides an identical target for each laser shot.

## 7.2 Experimental Section

### Instrumentation

All experiments were conducted on a LCQ Classic QIT (Thermo Finnigan, USA) mass spectrometer. For "deposited droplets" measurements a substantially modified Mass Tech (USA) Model 110 AP MALDI source was used [48]. For single droplet measurements the AP-IRIS source described in figure 7.1 was used. Droplets are generated by a piezoactuated flow through cell (Picology AB, Sweden) and directed towards the mass spectrometer interface. The laser, synchronized to the droplet ejection, is focused onto the flying droplets shortly before the interface. For ionization, a powerful Yb:YAG pumped optical parametric oscillator infrared laser was used (SESI, USA). The laser provided 30 ns pulses with an energy of 0.5 - 0.8 mJ per pulse with a repetition rate of 5 Hz. The wavelength of the laser was tunable in the region of 2.8 - 3.1 μm, but the laser was utilized at 2.94 μm in this work. In previous IR-AP-MALDI studies [18, 26, 49], an electric potential between the sample target plate and the intake capillary of the mass spectrometer was applied. According to previous finding [44] this is not necessary for AP-IRIS and therefore no potential differences between sample target plate and intake capillary were applied.

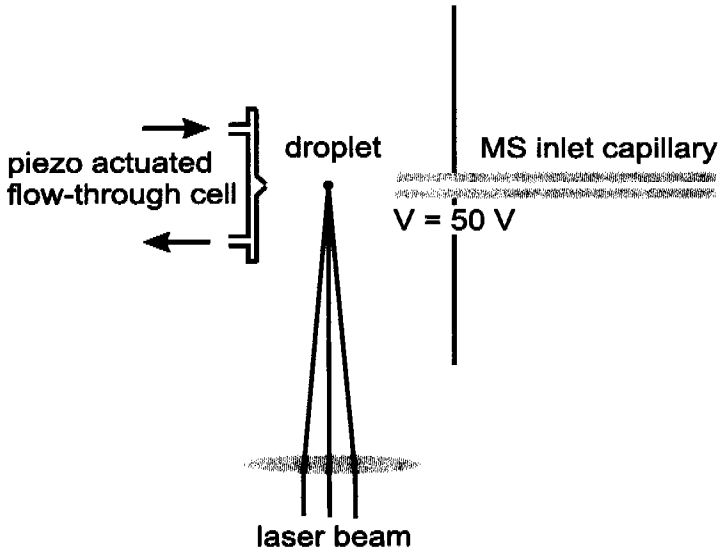


**Figure 7.1: Schematic of the source used for single droplet AP-IRIS experiments. Droplets are generated by a piezoactuated flow-through cell and directed towards the mass spectrometer interface. The laser, synchronized to the droplet ejection, is focused onto the flying droplets shortly in front of the interface.**

## Materials

Glycerol and 3-nitrobenzyl alcohol (NBA) were purchased from Fluka (Buchs, Switzerland). The peptides angiotensin II and bradykinin were obtained from Fluka. Molecular biology grade water was purchased from Cambrex (Rockland, USA). All solvents, matrices, and analytes were obtained at highest purity available and used as received.

## 7.3 Results and Discussion

We have previously shown that AP-MALDI, using co-dissolved matrices, *e.g.* HCCA, is feasible (see chapter 6 and ref [50]). Such a strategy, however, is not well suited to couple LC instrumentation to AP-MALDI on-line; no co-dissolved matrix should be needed. Rather, the effluent itself should be used directly as the matrix. Especially if low flow rates are employed (*e.g.* μ-HPLC), homogeneously mixing two liquid streams at flow rates smaller than 1 μl $min^{-1}$ is quite challenging.

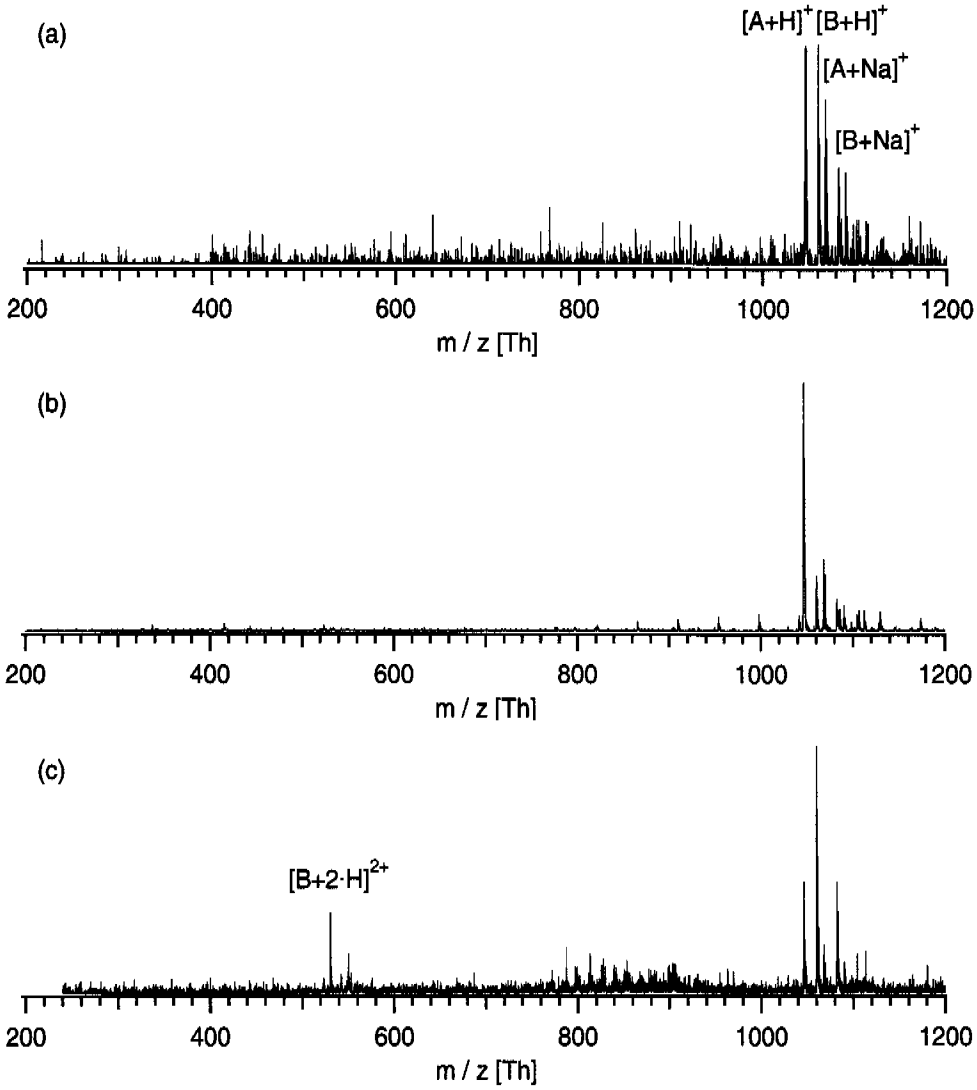


**Figure 7.2: Positive ion mode AP-IRIS spectrum of 5 μM bradykinin (B), 5 μM angiotensin II (A) and a) 0 % glycerol, b) 20 % glycerol, and c) 1% NBA. The signal-to-noise ratio of angiotensin increased by a factor of 8 by adding 20 % glycerol and by a factor of 3 by adding 1 % NBA compared to the results obtained with pure water.**

In the field of proteomics and noncovalent complexes, water as the main component and therefore as matrix has to be considered. As previously reported the addition of small amounts of glycerol can enhance the signal intensity of the measured analytes enormously. Figure 7.2 shows spectra of an aqueous peptide mixture consisting of 5 μM angiotensin II and 5 μM bradykinin with different amounts of either glycerol or NBA. In all spectra, the protonated as well as the sodiated molecular ion peaks are observed. The addition of 20 % glycerol improves the signal-to-noise ratio of angiotensin II by a factor of 8, and already a content of only 1 % NBA gives a improvement by a factor of 3. The relative abundance of angiotensin II and bradykinin are different when using glycerol or NBA as additives. Actually, even a high intensity of the doubly charged molecular ion signal of bradykinin can be observed when adding 1 % NBA. This could be interesting regarding CID-MS/MS experiments, because the confidence level of protein identification is raised if doubly charged ions are used as par-

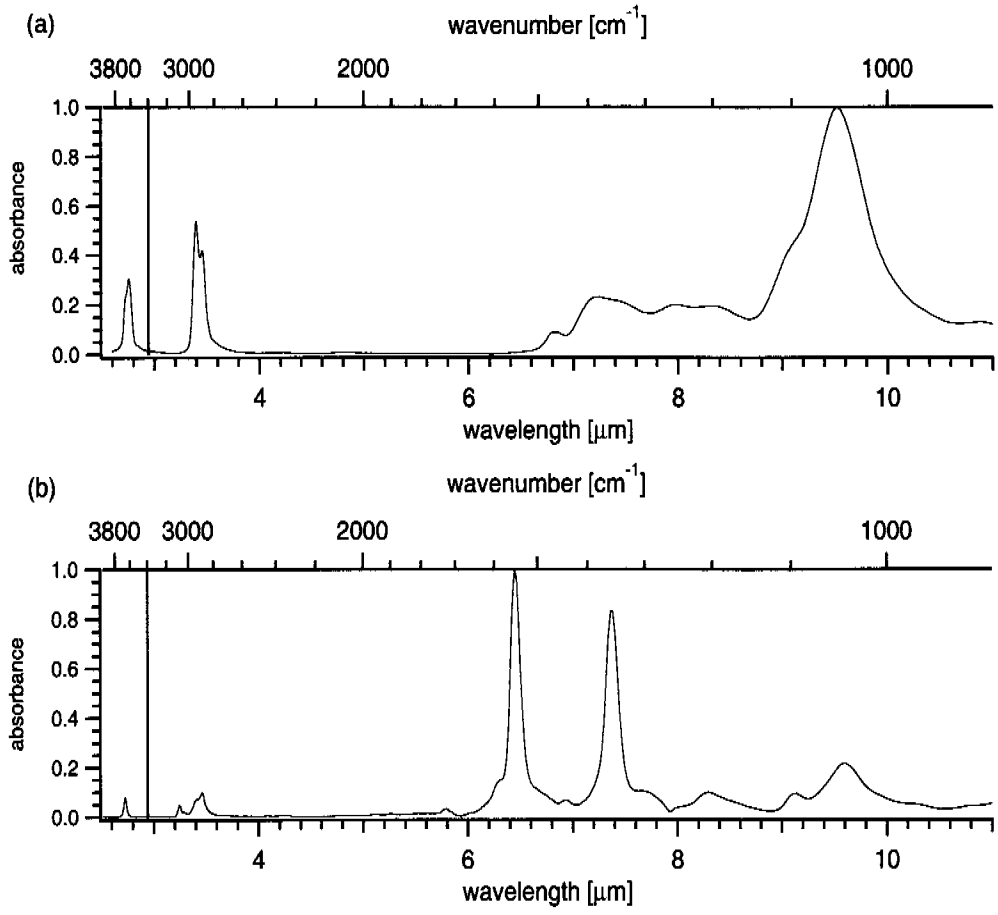


**Figure 7.3: Infrared absorbance spectra of a) glycerol and b) NBA. Whereas few absorbance is observed for glycerol at 2.94 μm (red lines), there is no absorbance observed for NBA at this wavelength.**

ent ions [51]. According to the infrared absorbance spectra (figure 7.3), there is observed a slight absorbance for glycerol at 2.94 μm but not for NBA. NBA improves the obtained signal for IRIS with water but does not absorb any laser radiation at the wavelength used. This indicates that not only the absorbance of the matrix but also the inherent properties of the sample solution, *e.g.* surface tension and viscosity, play an important role for successful desorption and ionization. In order to find the best conditions, the glycerol content was increased systematically and the integral of the signal of angiotensin II and bradykinin were used to observe the signal response (figure 7.4). The best conditions could be found for 20 % glycerol content. Unfortunately,

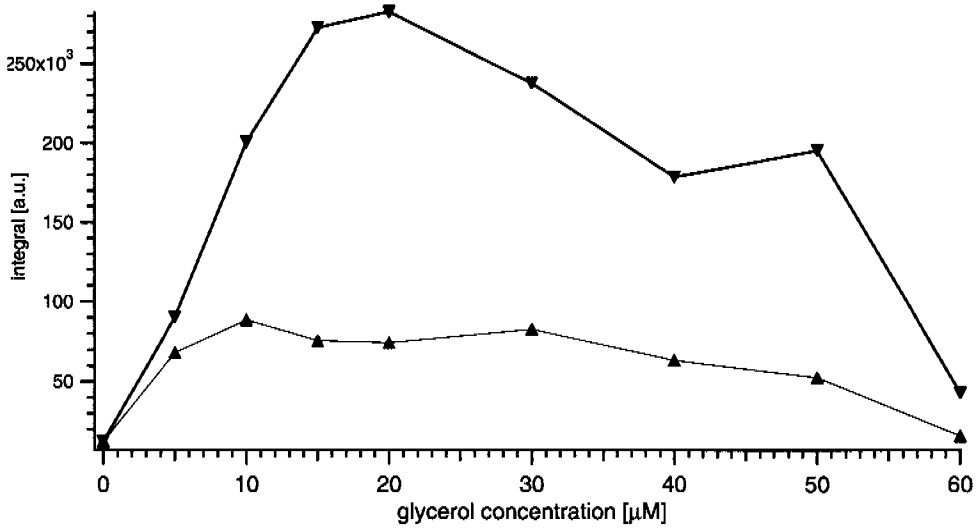


**Figure 7.4: Signal integral for angiotensin II (black) and bradykinin (red) observed for AP-IRIS measurements of 5 μM angiotensin II, 5 μM bradykinin in water with different contents of glycerol. The best conditions are observed for 20 % glycerol in water.**

the same experiments could not be performed using NBA as an additive because the solubility of NBA is only about 1 % in water. These findings are not very encouraging since it is even more difficult to mix water with glycerol than with methanolic solutions of HCCA due to the high viscosity of glycerol.

A problem arising in on-line coupling is the contamination and the resulting memory effects in the detection system: the performance of the detector, *i.e.* AP-IRIS interface, needs to stay constant. The best way to guarantee high reproducibility is to provide identical conditions for each desorption / ionization event. This is achieved by using a piezoactuated droplet generation: A constant flow of analyte solution is connected

to the piezoactuated flow-through cell. By applying a potential pulse to the piezo element of the cell, a droplet is ejected with a velocity around 1 m $s^{-1}$ orthogonal to the sample flow in the direction of the mass spectrometric interface (figure 7.1). By synchronizing the droplet ejection and the laser pulse, it was possible to focus the laser onto the flying droplets. Figure 7.5a shows a spectrum of 15 µM angiotensin II, 15 µM bradykinin in water and figure 7.5b shows a spectrum of 15 µM angiotensin II, 15 µM bradykinin, 10 % glycerol in water. In 7.5a, a weak signal of the molecular ions could be observed and astonishingly little chemical noise is recorded. Surprisingly, the addition of glycerol did not improve the signal-to-noise ratio whereas much more chemical noise was detected (figure 7.5b). This is in contradiction with the results

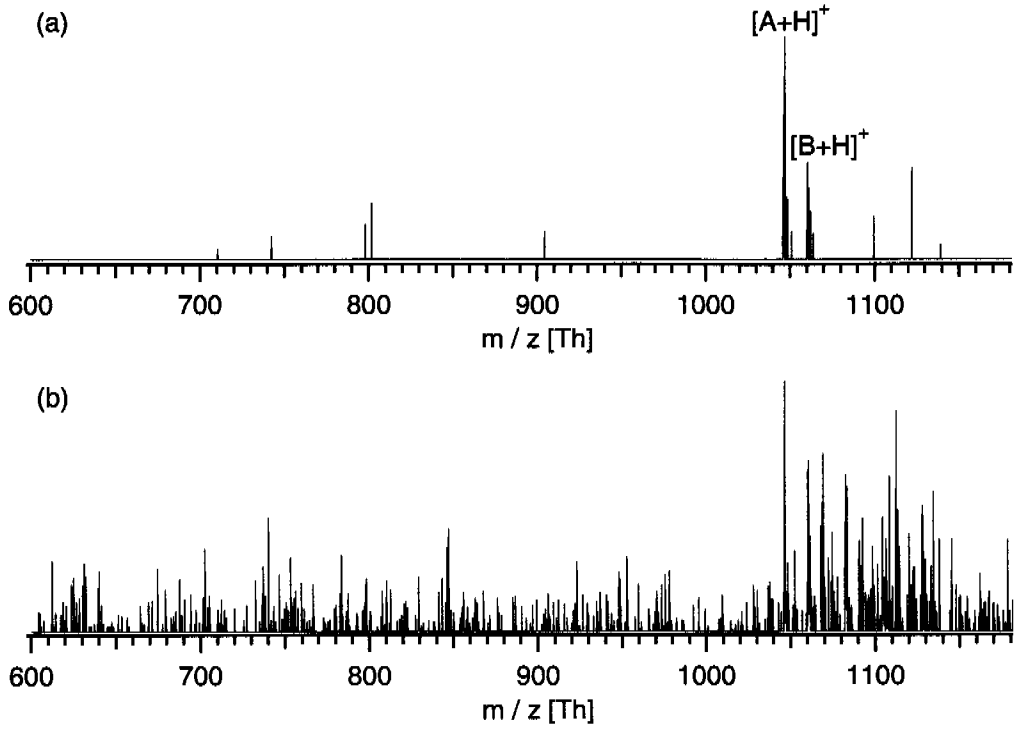


**Figure 7.5: Positive ion mode single droplet AP-IRIS of 15 µM angiotensin II, 15 µM bradykinin in a) pure water and b) water with 10 % glycerol. The addition of glycerol did not improve the signal as expected; a higher abundance of chemical noise was induced.**

found for deposited droplets. There are two major differences for deposited droplet and flying droplet desorption experiments which may be accountable for the different behavior: a) The shape of the irradiated surface. While the surface of the deposited droplet is approximately flat, the flying droplet's surface is spherical. b) The depos-

ited droplet interacts with the sample target plate whereas the flying droplet does not have any interaction with a solid support. There is more need for knowledge about the exact mechanism and more experiments necessary to fully explain this behavior.

According to the manufacturer's specifications of the piezoactuated flow-through cell, the diameter of the emitted droplets is 50 μm [52]. Using a concentration of 15 μM peptide, the resulting amount of analyte is as low as 980 amol per droplet. Therefore, only a very weak signal is expected. We are confident that the signal-to-noise ratio could be improved by enhancing the repetition rate of the IR laser. Once the sensitivity is improved, this setup could be used for standard measurements and for coupling liquid chromatography to AP-IRIS.

## 7.4 Summary

The performance of pure water and water containing different amounts of glycerol and NBA as a matrix for AP-IRIS was investigated. It was found that for a deposited droplet, water with 20 % of glycerol gives the best results. The addition of 1 % NBA to water evenly improves the signal significantly. However, the limited solubility of NBA in water prevents the addition of higher amounts. A single droplet AP-IRIS experiment revealed that for single droplet desorption / ionization, the addition of glycerol is not beneficial. The overall sensitivity using an IR laser with a repetition rate of 5 Hz is too low. We believe that the use of higher repetition rate IR lasers could improve the signal-to-noise ratio remarkably, whereas high repetition rate IR lasers are unfortunately not commercially available. However, a high repetition rate IR laser could be possibly built by using a Raman shifter or an OPO pumped with a high repetition rate UV laser. Another interesting approach would be to use a continuous working IR laser instead of a pulsed one. By ejecting droplets with a velocity of 1 $m \cdot s^{-1}$, they would cross the laser focus within around 100 µs. It would be interesting if similar results could be obtained as with a pulsed IR laser. Obtaining higher sensitivity, this coupling approach would offer a stable detector showing high reproducibility for liquid chromatography without any memory effects.

## 7.5 References


1. M. A. Posthumus, P. G. Kistemaker and H. L. C. Meuzelaar, *Anal. Chem.*, 1978, **50** (7), 985-991.
2. K. Tanaka, H. Waki, Y. Ido, S. Akita, Y. Y. and T. Yoshida, *Rapid Commun. Mass Spectrom.*, 1988, **2** (8), 151-153.
3. M. Karas, D. Bachmann and F. Hillenkamp, *Anal. Chem.*, 1985, **57** (14), 2935-2939.
4. M. Karas, D. Bachmann, U. Bahr and F. Hillenkamp, *Int. J. Mass Spectrom. Ion Process.*, 1987, **78**, 53-68.
5. M. Karas and F. Hillenkamp, *Anal. Chem.*, 1988, **60** (20), 2299-2301.
6. A. Overberg, M. Karas, U. Bahr, R. Kaufmann and F. Hillenkamp, *Rapid Commun. Mass Spectrom.*, 1990, **4** (8), 293-296.
7. A. Overberg, M. Karas and F. Hillenkamp, *Rapid Commun. Mass Spectrom.*, 1991, **5** (3), 128-131.
8. P. Kraft, S. Alimpiev, E. Dratz and J. Sunner, *J. Am. Soc. Mass Spectrom.*, 1998, **9** (9), 912-924.
9. J. D. Sheffer and K. K. Murray, *J. Mass Spectrom.*, 2000, **35** (1), 95-97.
10. S. F. Niu, W. Z. Zhang and B. T. Chait, *J. Am. Soc. Mass Spectrom.*, 1998, **9** (1), 1-7.
11. E. Nordhoff, A. Ingendoh, R. Cramer, A. Overberg, B. Stahl, M. Karas, F. Hillenkamp and P. F. Crain, *Rapid Commun. Mass Spectrom.*, 1992, **6** (12), 771-776.
12. S. Berkenkamp, F. Kirpekar and F. Hillenkamp, *Science*, 1998, **281** (5374), 260-262.
13. E. Nordhoff, R. Cramer, M. Karas, F. Hillenkamp, F. Kirpekar, K. Kristiansen and P. Roepstorff, *Nucleic Acids Res.*, 1993, **21** (15), 3347-3357.
14. C. E. Costello, E. Nordhoff and F. Hillenkamp, *Int. J. Mass Spectrom. Ion Process.*, 1994, **132** (3), 239-249.
15. S. J. Lawson and K. K. Murray, *Rapid Commun. Mass Spectrom.*, 2002, **16** (12), 1248-1250.
16. E. Nordhoff, F. Kirpekar, M. Karas, R. Cramer, S. Hahner, F. Hillenkamp, K. Kristiansen, P. Roepstorff and A. Lezius, *Nucleic Acids Res.*, 1994, **22** (13),

2460-2465.

17. F. Kirpekar, S. Berkenkamp and F. Hillenkamp, *Anal. Chem.*, 1999, **71** (13), 2334-2339.
18. C. E. Von Seggern, S. C. Moyer and R. J. Cotter, *Anal. Chem.*, 2003, **75** (13), 3212-3218.
19. R. Cramer, W. J. Richter, E. Stimson and A. L. Burlingame, *Anal. Chem.*, 1998, **70** (23), 4939-4944.
20. C. E. Von Seggern and R. J. Cotter, *J. Am. Soc. Mass Spectrom.*, 2003, **14** (10), 1158-1165.
21. K. Strupat, M. Karas, F. Hillenkamp, C. Eckerskorn and F. Lottspeich, *Anal. Chem.*, 1994, **66** (4), 464-470.
22. Y. C. Xu, M. W. Little, D. J. Rousell, J. L. Laboy and K. K. Murray, *Anal. Chem.*, 2004, **76** (4), 1078-1082.
23. D. Feldhaus, C. Menzel, S. Berkenkamp, F. Hillenkamp and K. Dreisewerd, *J. Mass Spectrom.*, 2000, **35** (11), 1320-1328.
24. B. A. Budnik, K. B. Jensen, T. J. D. Jorgensen, A. Haase and R. A. Zubarev, *Rapid Commun. Mass Spectrom.*, 2000, **14** (7), 578-584.
25. C. Menzel, K. Dreisewerd, S. Berkenkamp and F. Hillenkamp, *J. Am. Soc. Mass Spectrom.*, 2002, **13** (8), 975-984.
26. V. V. Laiko, N. I. Taranenko, V. D. Berkout, M. A. Yakshin, C. R. Prasad, H. S. Lee and V. M. Doroshenko, *J. Am. Soc. Mass Spectrom.*, 2002, **13** (4), 354-361.
27. J. D. Sheffer and K. K. Murray, *Rapid Commun. Mass Spectrom.*, 1998, **12** (22), 1685-1690.
28. Y. Naito, S. Yoshihashi-Suzuki, K. Ishii and K. Awazu, *Nucl. Instrum. Methods Phys. Res. Sect. A-Accel. Spectrom. Dect. Assoc. Equip.*, 2004, **528** (1-2), 609-613.
29. W. P. Hess, H. K. Park, O. Yavas and R. F. Haglund, *Appl. Surf. Sci.*, 1998, **129**, 235-241.
30. R. Cramer, R. F. Haglund and F. Hillenkamp, *Int. J. Mass Spectrom.*, 1997, **169**, 51-67.
31. W. Z. Zhang, S. F. Niu and B. T. Chait, *J. Am. Soc. Mass Spectrom.*, 1998, **9** (9), 879-884.

32. M. E. Belov, S. S. Alimpiev, V. V. Mlynsky, S. M. Nikiforov and P. J. Derrick, *Rapid Commun. Mass Spectrom.*, 1995, **9** (14), 1431-1436.
33. C. Menzel, K. Dreisewerd, S. Berkenkamp and F. Hillenkamp, *Int. J. Mass Spectrom.*, 2001, **207** (1-2), 73-96.
34. V. L. Talrose, M. D. Person, R. M. Whittal, F. C. Walls, A. L. Burlingame and M. A. Baldwin, *Rapid Commun. Mass Spectrom.*, 1999, **13** (21), 2191-2198.
35. K. L. Caldwell and K. K. Murray, *Appl. Surf. Sci.*, 1998, **129**, 242-247.
36. C. E. Von Seggern, B. D. Gardner and R. J. Cotter, *Anal. Chem.*, 2004, **76** (19), 5887-5893.
37. M. L. Baltz-Knorr, K. E. Schriver and R. F. Haglund, *Appl. Surf. Sci.*, 2002, **197**, 11-16.
38. S. Berkenkamp, M. Karas and F. Hillenkamp, *Proc. Natl. Acad. Sci. U. S. A.*, 1996, **93** (14), 7003-7007.
39. V. V. Laiko, M. A. Baldwin and A. L. Burlingame, *Anal. Chem.*, 2000, **72** (4), 652-657.
40. V. V. Laiko, S. C. Moyer and R. J. Cotter, *Anal. Chem.*, 2000, **72** (21), 5239-5243.
41. K. Dreisewerd, S. Berkenkamp, A. Leisner, A. Rohlfing and C. Menzel, *Int. J. Mass Spectrom.*, 2003, **226** (1), 189-209.
42. S. Berkenkamp, C. Menzel, M. Karas and F. Hillenkamp, *Rapid Commun. Mass Spectrom.*, 1997, **11** (13), 1399-1406.
43. K. Dreisewerd, *Chem. Rev.*, 2003, **103** (2), 395-425.
44. V. V. Laiko, P. V. Tan, N. I. Taranenko, M. A. Yakshin, C. R. Prasad and V. M. Doroshenko. *Atmospheric pressure infrared ionization from solution (AP IRIS)*, in *Proceedings of the 51st ASMS Conference on Mass Spectrometry and Allied Topics*, 2003, Montreal.
45. S. J. Lawson and K. K. Murray, *Rapid Commun. Mass Spectrom.*, 2000, **14** (3), 129-134.
46. D. Twerenbold, A. Netuschill, N. de Rooij, P. Luginbuhl, D. Gerber, D. Gritti, Y. Gonin, F. Rossel and J. L. Vuilleumier, *Proteomics*, 2002, **2** (4), 436-440.
47. B. Abel, A. Charvat, F. Gessler and J. Niemeyer. *Liquid Injection Mass Spectrometry for the Quantitative Analysis of Natural and Synthetic Polymers, Ana-*

*kon*, 2005, Regensburg, Germany.

48. P. V. Tan, N. I. Taranenko, V. V. Laiko, M. A. Yakshin, C. R. Prasad and V. M. Doroshenko, *J. Mass Spectrom.*, 2004, **39** (8), 913-921.
49. C. E. Von Seggern, P. E. Zarek and R. J. Cotter, *Anal. Chem.*, 2003, **75** (23), 6523-6530.
50. J. M. Daniel, S. Ehala, S. D. Friess and R. Zenobi, *Analyst*, 2004, **129**, 574-578.
51. R. Cramer and S. Corless, *Rapid Commun. Mass Spectrom.*, 2001, **22** (15), 2058-2066.
52. T. Laurell, L. Wallman and J. Nilsson, *J. Micromech. Microeng.*, 1999, **9**, 369-376.

# CHAPTER 8

# SUMMERY AND OUTLOOK

Seite Leer /
Blank leaf

After improving the electrospray ionization (ESI) mass spectrometer, ESI mass spectrometry was successfully applied to investigate noncovalent interactions and to determine the association constant of complexes. Additionally, two methods to couple liquid chromatography to atmospheric pressure matrix assisted laser desorption/ ionization (AP-MALDI) were presented. The first is based on UV-AP-MALDI and co-dissolved matrices; it shows a wide applicability including the possibility for quantification. The second method is based on atmospheric pressure infrared ionization from solution and on single droplet desorption; a aqueous peptide solution was measured successfully with a limit of detection in the fmole range.

## 8.1 ESI-MS of Noncovalent Complexes

Two examples demonstrated that ESI-MS can successfully be applied to determine the interaction strength of proteins with noncovalent inhibitors. The specificity of these interactions was proven by carefully selected control experiments. The association constants are in good agreement with literature values.

Although these results are very encouraging, there are several factors that need further investigation. Following the electrospray process, the initial droplet shrinks due to solvent evaporation and the concentration of all species is increasing. Therefore, the equilibrium concentrations for a bimolecular complex reaction may change, too. Agnes and Wang found that the observed association constant measured by ESI-MS for the reaction of EDTA and Sr reflected the solution conditions, little or no shift of the equilibrium due to the droplet shrinking process could be observed [1]. This initial finding is perhaps not be valid for other reactions, and must be investigated further.

Moreover, the droplets produced in the electrospray process have been hypothesized to consist of two phases: the charged surface layer and the inner, electroneutral bulk solution. It is believed that the measured signal intensities reflect the concentration of the analyte in the surface layer rather than in the bulk solution of the droplets. Therefore hydrophobic compounds show higher abundance than hydrophilic compounds. Assuming identical ionization efficiencies for a host and the host-guest complex means that their partitioning between surface layer and bulk solution be identical. If not, this can influence the measured association constants significantly. Brodbelt and coworkers address this problem in a recent publication [2] but further investigations are needed.

In our work, it is assumed that the noncovalent complex is not dissociated in the gas phase. Due to the lower permeability in the vacuum, electrostatic and dipolar interactions get stronger. Because the investigated interactions are mainly of this kind, the above assumption is justified. In contrast, hydrophobic interactions can be lost in vacuum due to the absence of solvent. The question arises if it is possible to observe hydrophobic complexes at all and if yes, wheter the observed signal intensities reflect the concentrations in solution.

## 8.2 Liquid Chromatography Coupled to AP-MALDI

For UV-AP-MALDI we have shown good sensitivity as well as a wide applicability of the method, including quantification. Nevertheless, the mixing of effluent with co-dissolved matrix is not satisfying. In recent years, it has been shown that ionic liquids can be employed as MALDI matrices [3-5]. Further more, He et al. showed that ionic liquids can be added to the eluents in liquid chormatography to enhance the chromatographic resolution [6]. The interesting question arises whether ionic liquids could be used to enhance the chromatographic resolution and at the same time be used as matrix for the desorption/ionization. This should be studied.

The single droplet desorption/ionization approach with an infrared laser is very promising. The method still lacks in sensitivity, but there are three suggestions how to improve it. First, instead of droplets with a diameter of 50 μm, bigger droplets could be employed to generate more ions per desorption event. Secondly, instead of using single droplet desorption, desorption out of an open channel could be implemented. We obtained some preliminary results by using the piezoactuated flow through cell. The piezo element was turned off and the laser was directed into the nozzle directly onto the liquid flow. The results were encouraging but unfortunately the nozzle disintegrated within several minutes, probably due to the stress waves generated by irradiating the water sample. Finally, by employing an infrared laser with a high repetition rate (*e.g.* 1 kHz) and the same repetition rate for the droplet generation, a higher fraction of the effluent could be used for detection. Unfortunately, high repetition rate IR lasers are not commercially available in the 3 μm range. But they could be built by using an optical parametric oscillator (OPO) or a Raman shifter pumped with a high repetition rate laser. Instead of using a high repetition rate infrared laser, one can imagine to use a continuous wave infrared laser. By directing droplets through the laser beam, a laser pulse would be generated.

## 8.3 References


1. H. Wang and G. R. Agnes, *Anal. Chem.*, 1999, **71**, 3785 - 3792.
2. C. L. Sherman and J. S. Brodbelt, *Analytical Chemistry*, 2005, **77** (8), 2512-2523.
3. D. W. Armstrong, L. K. Zhang, L. F. He and M. L. Gross, *Analytical Chemistry*, 2001, **73** (15), 3679-3686.
4. S. Carda-Broch, A. Berthod and D. W. Armstrong, *Rapid Commun. Mass Spectrom.*, 2003, **17** (6), 553-560.
5. L. S. Santos, R. Haddad, N. F. Hoehr, R. A. Pilli and M. N. Eberlin, *Analytical Chemistry*, 2004, **76** (7), 2144-2147.
6. L. J. He, W. Z. Zhang, L. Zhao, X. Liu and S. X. Jiang, *J. Chromatogr. A*, 2003, **1007** (1-2), 39-45.

# APPENDIX A

# AGILENT α-PROTOTYPE ESI-TOF

Seite Leer /
Blank leaf

## A.1 Instrumental Layout

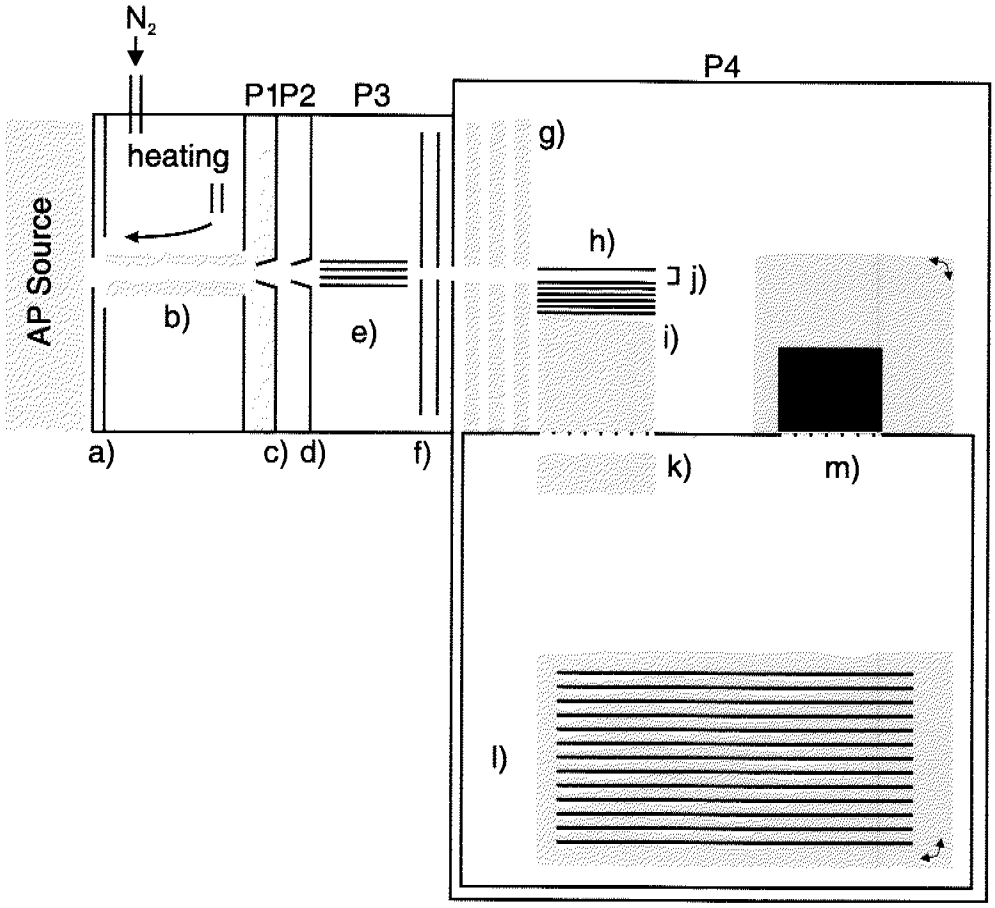


**Figure A.1: Layout of the a-Prototype TOF. For a detailed description see text.**

The atmospheric pressure interface of the mass spectrometer consists of a) the sampling aperture, having a counter current of heated nitrogen, b) the heatable transfer capillary leading to the first pumping stage P1, c) the first skimmer dividing the first and second pumping stage P2, d) the second skimmer dividing the second and the third pumping stage P3, e) the rf-only hexapole, and f) three ring electrodes defining an Enisle lens. The flow rate of the nitrogen is set between 2 slm for AP-MALDI and nannies experiments to 4 slm for conventional ESI experiments. The temperature of the nitrogen can be varied between room temperature and 350 °C.

The main chamber of the TOF instrument consists of g) an Einzel lens, h) the pusher plate to accelerate the ions into the TOF, i) the acceleration electrodes to accelerate the ions, j) the Faraday cup to measure the total ion current, k) the vertical deflection

plates, l) the single stage reflectron, and m) the bipolar MCP detector (Burle Industries Inc., USA). The field-free flight path of the ions is within a flight chamber at elevated potential.

The instrument consists of four pumping stages. Pumping stage one is pumped by a rotary vacuum pump with 30 $m^3\ h^{-1}$ (Duo 030A, Pfeiffer Vacuum Technology AG, Germany). The second pumping stage is pumped by connecting it to a turbomolecular pump (Ext250HIISO100, BOC Edwards, UK), pumping stage three, at 3/4 height of the rotors. The turbomolecular pump is connected to a rotary vacuum pump (Trivac D168, Leybold Vacuum GmbH, Germany) providing a pumping speed of 16 $m^3\ h^{-1}$. The forth pumping stage P4 is the main chamber of the TOF instrument and is pumped by two turbomolecular pumps (Ext250HIISO100, BOC Edwards) connected to rotary vacuum pumps with 10 $m^3\ h^{-1}$ (Trivac D10E, Leybold Vacuum GmbH) and 12 $m^3\ h^{-1}$ (Duo 012A, Pfeiffer Vacuum Technology AG), respectively. Table A.1 summarizes the typical pressures achieved using a capillary temperature of 300 °C. The pressure in P1 can be enhanced by limiting the pumping speed of the pump with a needle valve. The pressure in P3 can be enhanced by introducing nitrogen with a leaking valve.

| P1 | P2 | P3 | P4 |
|---|---|---|---|
| $1.3 \cdot 10^{0}$ mbar | $1.1 \cdot 10^{-2}$ mbar | $1.7 \cdot 10^{-3}$ mbar | $1.3 \cdot 10^{-6}$ mbar |

**Table A.1: Typical pressures achieved in the different pumping stages using a transfer capillary temperature of 300 °C.**

The reflectron as well as the detector are mounted on tilting devices: they can be tilted by micrometer screws from outside the main chamber in order to optimize the peak shape and sensitivity.

## A.2 Potentials

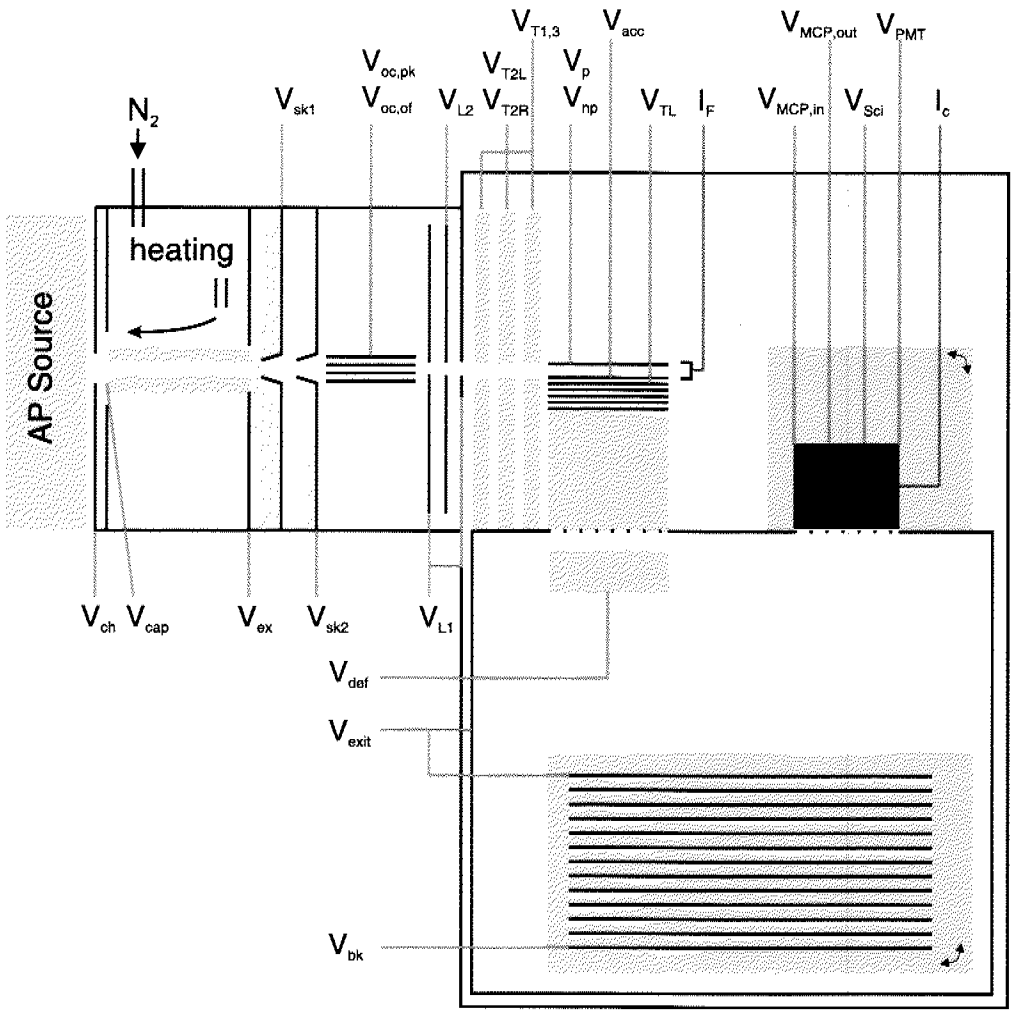


**Figure A.2: Definition of the different potentials. For a detailed description see text.**

The explanations and the typical settings for the various potentials are shown in table A.2. Not all of the mentioned potentials are applied directly to the electrodes as shown in the scheme. In fact, most of them are controlled by different controllers and computer boards explained in the following paragraphs.

Many of the potentials are controlled by a computer board managed by a personal computer and the software TOF -VOLTS, which is a beta release software. The output for the different channels of the computer board is between 0 and 15 V. If potentials higher than 15 V are required, the output is connected to a high voltage element (Ultravolt Inc., USA) delivering potentials in the desired range. Unfortunately, the

| Potential | Explanation | Typical Setting |
|---|---|---|
| $V_{ch}$ | inlet potential; used in ESI as spray potential | 0 .. -5 kV |
| $V_{cap}$ | transfer capillary inlet potential | 0 .. -5 kV |
| $V_{ex}$ | transfer capillary exit potential | 200 V |
| $V_{sk1}$ | potential of skimmer 1 | 110 V |
| $V_{sk2}$ | potential of skimmer 2 | 0 V |
| $V_{oc,of}$ | offset potential of the hexapole | 0 V |
| $V_{oc,pk}$ | amplitude potential of the hexapole | 1 .. 30 V |
| $V_{L1}$ | potential of the first and third electrodes of the first einzel lens | -50 V |
| $V_{L2}$ | potential of the second electrode of the first einzel lens | -56 V |
| $V_{T1,3}$ | potential of the first and third electrodes of the second einzel lens | -87 V |
| $V_{T2L}$ $V_{T2R}$ | potential of the second electrode of the second einzel lens; the second einzel lens consists of two electrode providing the possibility to deflect the ions | 346 V |
| $V_p$ | potential of the draw out pulse | 1.4 kV |
| $V_{np}$ | potential when no draw out pulse is applied | -54 V |
| $V_{acc}$ | potential of the extraction electrode | -54 V |
| $V_{TL}$ | potential of the second acceleration electrode | -980 V |
| $I_F$ | current output when measuring the total ion current | in the range of pA |
| $V_{def}$ | potential difference of the vertical deflection plates | 0 V |
| $V_{exit}$ | potential of the flight box | -5760 V |
| $V_{bk}$ | potential of the back plate of the single stage reflectron | 1408 V |
| $V_{MCP,in}$ | potential of the active surface of the MCP detector | -6 kV |
| $V_{MCP,out}$ | potential of the backside of the MCP detector | -5.1 kV |
| $V_{Sci}$ | potential of the scintillator | -3 kV |
| $V_{PMT}$ | potential of the photo multiplier tube | 700 V |
| $I_c$ | collector current of the photo multiplier tube | 100 .. 3000 mV into 50 Ω |

**Table A.2: Definition of the various potentials used in the atmospheric pressure interface and the TOF mass analyzer.**

units selected in TOF-VOLTS on the computer are arbitrary: the number of steps between 0 and 15 V can be defined by the programmer. Table A.3 summarized all potentials controlled by the computer, their units in TOF-VOLTS, their high voltage element (if any), and their effective output potential.

| Potential | Units TOF-VOLTS | HV-Element | Potential [V] |
|---|---|---|---|
| $V_{ch}$ | 750 .. 0 | -6500 V | 0 .. -6500 |
| $V_{cap}$ | 750 .. 0 | -6500 V | 0 .. -6500 |
| $V_{ex}$ | 0 .. 750 | 500 V | 0 .. 500 |
| $V_{sk1}$ | 0 .. 750 | 275 V | 0 .. 275 |
| $V_{sk2}$ | 0 .. 1500 | direct output | 0 .. 15 |
| $V_{oc,of}$ | 0 .. 1500 | direct output | 0 .. 15 |
| $V_{L1}$ | 0 .. 1500 | direct output | 0 .. 15 |
| $V_{T1,3}$ | 750 .. 0 | -270 V | 0 .. -270 |
| $V_{T2L}$ | 750 .. 0 | -530 V | 0 .. -530 |
| $V_{T2R}$ | | | |
| $V_{exit}$ | 750 .. 0 | -6400 V | 0 .. -6400 |
| $V_{bk}$ | 0 .. 750 | 6400 V | 0 .. 6400 |

**Table A.3: Conversion of TOF-VOLTS units to the effective potentials.**

The hexapole is controlled by a home-built rf-generator where the offset and amplitude potentials, *i.e.* $V_{oc,of}$ and $V_{oc,pk}$, can be externally controlled. The frequency of the hexapole is fixed at 240 kHz. Whereas $V_{oc,of}$ is controlled by the computer, $V_{oc,pk}$ is controlled by an external power supply (EA 3002R, Elektro Automatik, Germany), because of the higher current consumption of the rf-generation.

The potential $V_{L2}$ of the second electrode of the first einzel lens is controlled by an external power supply (HCN14-150, Fug Elektronik GmbH, Germany).

The potential at the pusher plate is controlled by a high voltage switch (figure A.3). The working scheme is shown in figure figure A.4. When the TTL input on the high voltage switch is low, the potential applied on the electrode is $V_{np}$, and when the TTL input is high, the potential $V_p$ is applied. The TTL signal is generated by a pulse delay generator (DG535, Standford Research Systems Inc., USA) triggered by the acquisition board (prototype, Agilent, USA) of the acquisition computer. In all experiments a drawout pulse of 4.5 µs was applied. To measure the total ion $I_F$ current arriving in the TOF instrument by the Faraday cup, the high voltage switch must be turned off and the potential $V_{np}$ must be maintained at the pusher plate. Because of the higher current consumption during pulsing, the potentials $V_{np}$ and $V_p$ are controlled by external power supplies (HCN14-650 and HCN140-3500, Fug Elektronik GmbH).

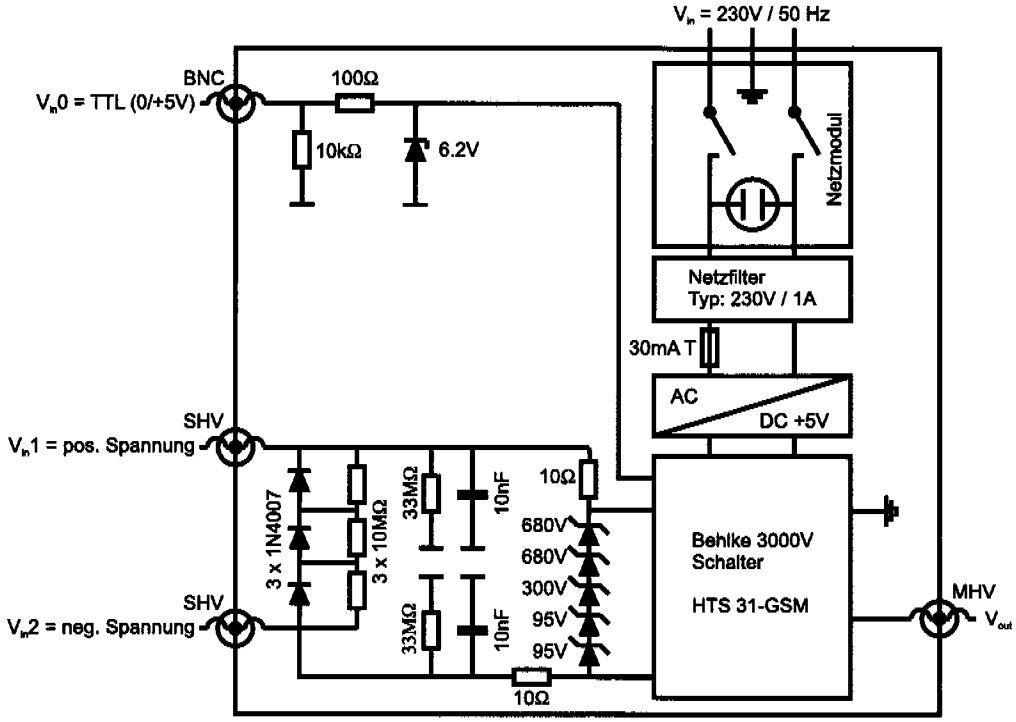


**Figure A.3: Electric scheme of the high voltage switch.**

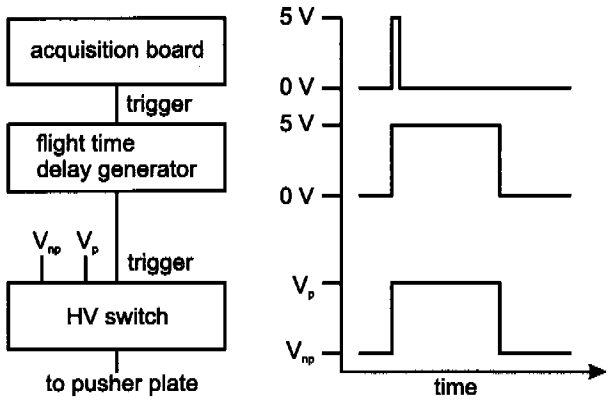


**Figure A.4: Working scheme of the high voltage pulser to provide the potentials at the pusher plate.**

In order to guarantee that the ions can be injected into the extraction source without any deflections, the potential $V_{acc}$ is not set by a power supply. It is generated by a potential adder which adds to the potential of $V_{np}$ ±15 V. It has been shown that the geometry of the instrument is precise and no potential difference between $V_{np}$ and $V_{acc}$ must be applied.

Because the flight chamber is on a high potential $V_{exit}$, the potential difference $V_{def}$, set to the vertical deflection plates, must be added to the potential $V_{exit}$ prior to be applied to the electrodes. This is achieved by using a home-built high voltage adder

where the potential difference $V_{def}$ between the deflection plates can be selected. It has been shown that the geometry of the instruments is precise and no potential difference between the deflection plates is needed.

In order to prevent any sparking in the detector assembly, the potentials for the detector are controlled by a specialized power supply (PF1055, Burle Industries Inc.). The potential difference between the MCP ($V_{MCP}$) and between the MCP output and the scintillator ($V_{Sci}$) are specified. To these potentials a bias potential ($V_{bias}$) between -10 to 10 kV is added prior to be applied to the detector. Because the detector is optically decoupled, the potential of the photomultiplier tube ($V_{PMT}$) and therefore the gain of the PMT can be selected independently.

## A.3 Signal Processing

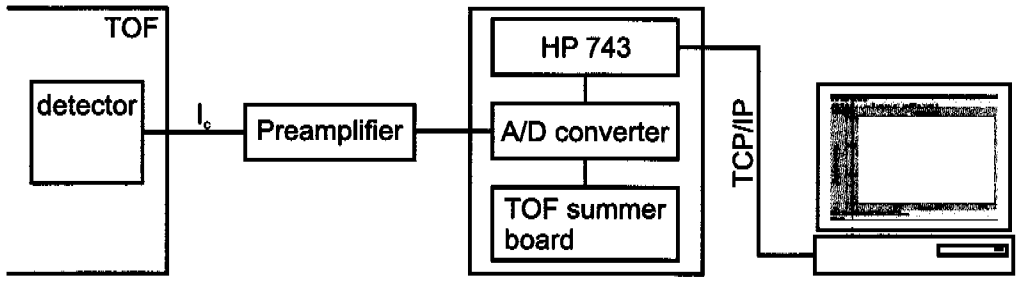


**Figure A.5: Scheme of the signal processing: the detector signal is preamplified and digitized by a A/D converter. An arbitrary number of transients is summed on the HP 743 mainframe computer and the transferred to a personal computer for storage and further processing.**

The signal of the detector is preamplified prior to analog/digital conversion by the A/D converter (250 MHz) of the HP mainframe computer. An arbitrary number of transients are summed prior to be transferred to the personal computer for further processing. The length of the transients can be specified and therefore the duty-cycle as well as the upper mass limit can be selected.

The mainframe computer, HP 743, is a unix based computer consisting of a processor board, an A/D converter board, a TOFsummer board (prototype board), and an external hard drive. The mainframe computer is usually controlled over a TCP/IP connection by the personal computer. If no network connection can be established, a connection can be initiated by a RS232 interface. Unfortunately this interface can just be used for troubleshooting since the TOF software, TOFAcquire, only supports TCP/IP connection. The trigger to initiate a measurement cycle is provided by the TOFsummer board.

On the personal computer, the beta-release software TOFAcquire is used to remote control the mainframe and to acquire mass spectra.

# APPENDIX B

# SOFTWARE

Seite Leer /
Blank leaf

## B.1 Batch Processing of Spectra

In order to simplify and accelerate the analysis of the spectra obtained by titration experiments, a software for batch processing of any count of spectra has been implemented. With this application it is possible to apply the same operations (*e.g.* integration, background correction) on a set of specified files. The software is written in Java™ and therefore compatible to most operating systems including Windows, Macintosh, Linux and Unix. Figure B.1 shows the use case diagram for the application.

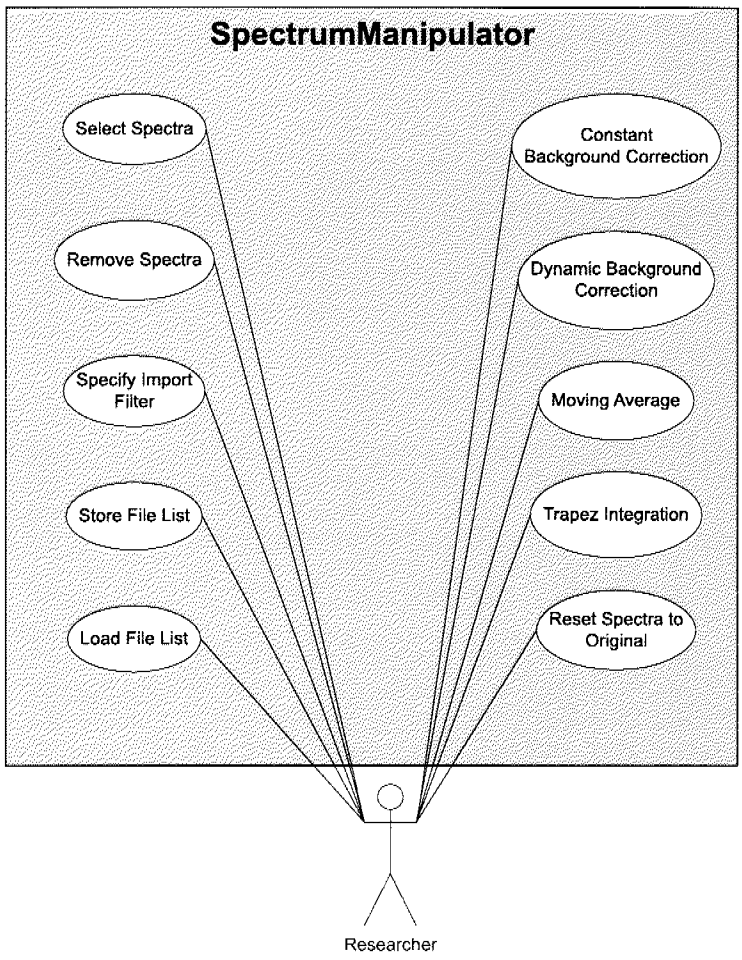


**Figure B.1: Use case diagram of the application. The user can select a set of spectra and perform a series of operations.**

### Starting the Application

In order to start the application, Java must be installed. It is recommended to use Java 2 Runtime Environment, Standard Edition version 1.4.2. A free download is offered at *http://java.sun.com/downloads/index.html.*

If the application is not yet precompiled, *i.e.* there are no *.class files, it is necessary to precompile the application prior to start it. Open a command shell and use the following steps to compile the program.

```
Eingabeaufforderung
Microsoft Windows XP [Version 5.1.2600]
(C) Copyright 1985-2001 Microsoft Corp.

C:\Dokumente und Einstellungen\daniel>cd c:\SpectrumManipulator

C:\SpectrumManipulator>javac SpectrumManipulator.java
Note: .\RunningBatchRunner.java uses or overrides a deprecated API.
Note: Recompile with -deprecation for details.

C:\SpectrumManipulator>
```

Open a command shell and use the following steps to run the application.

```
Eingabeaufforderung - java SpectrumManipulator
Microsoft Windows XP [Version 5.1.2600]
(C) Copyright 1985-2001 Microsoft Corp.

C:\Dokumente und Einstellungen\daniel>cd c:\SpectrumManipulator

C:\SpectrumManipulator>java SpectrumManipulator
```

After the startup the application window shown in figure B.2 will appear.

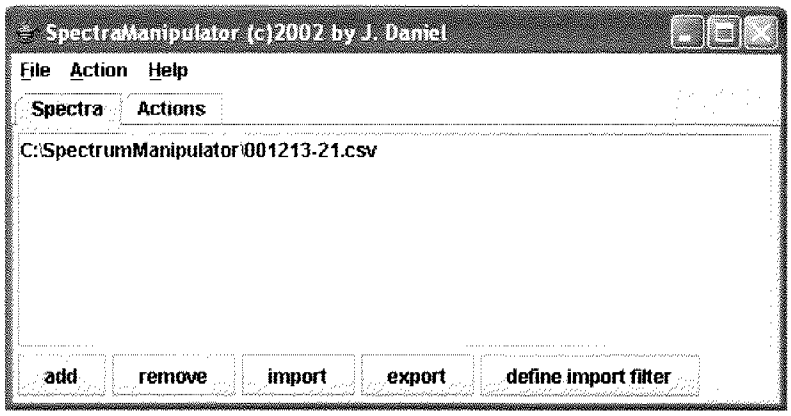


**Figure B.2: Startup window of the application.**

### Define a Set of Files

To define a set of files containing spectra the tab *spectra* has to be selected. The spectra need to be in a delimited ascii format. There are five different commands that can be performed by pressing the according buttons at the bottom of the window (figure B.2).

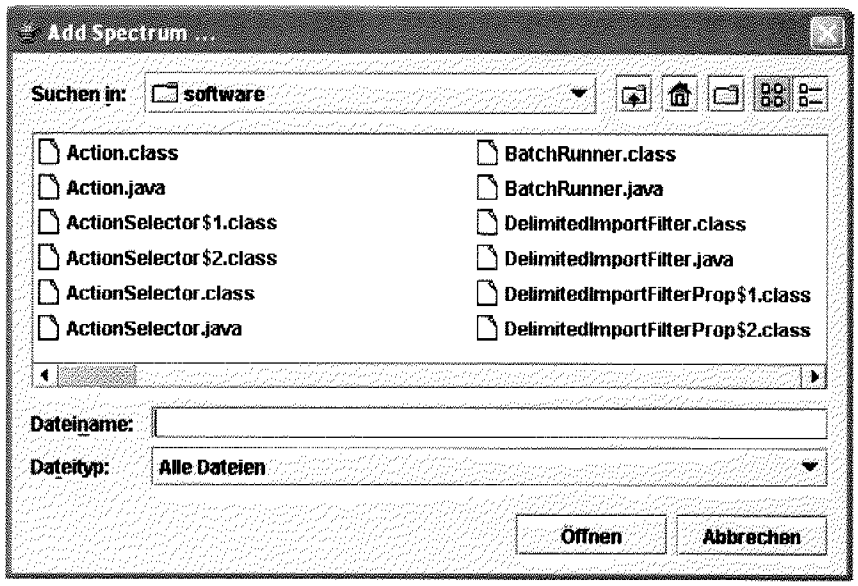


**Figure B.3: File selection dialog with multiple selection capability.**

By pressing the *add* button, a file selection dialog with multiple selection capabilities (figure B.3) is opened. Spectra files that shall be included into the analysis can be selected and by approving the dialog, the files are included into the file list. By selecting different files in the file list and pressing the *remove* button, the previously added spectra files are removed from the file list. File lists can be stored and loaded by pressing the buttons *export* or *import*, respectively.

To define the import filter to read the spectra files, press the button *define import filter.* Please be aware that for all files in the file set the same import filter is employed. In the import filter dialog (figure B.4), the delimiting character as well as the number of lines, that are skipped prior to read the mass spectral data, are specified.

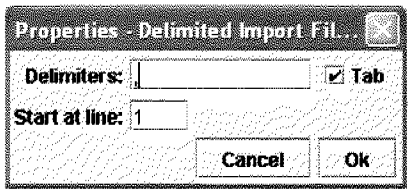


**Figure B.4: Definition of the import filter for the spectra. The delimiter as well as the number of lines to skip can be specified.**

### Define the Operations

To define the operations to be performed on the specified spectra, the tab *Actions* has to be selected. By pressing the *add* button, a new action is added and by selecting an action and pressing *remove*, the action is removed. By selecting an action and pressing

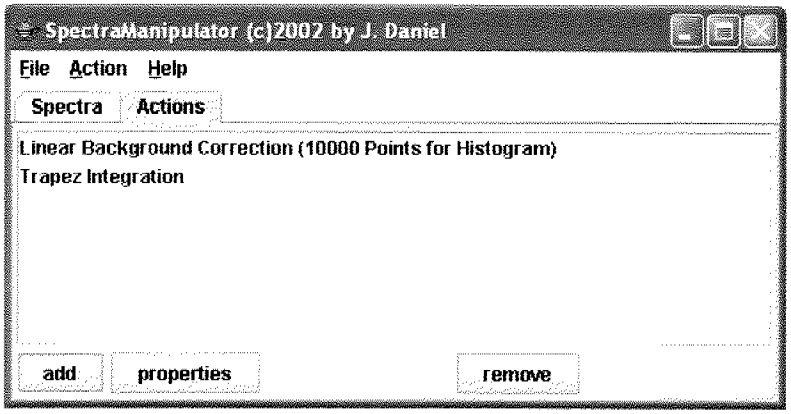


**Figure B.5: Window to specify the actions to be performed.**

*properties*, the settings for the action are specified. Different actions are implemented: *Constant Background Correction, Dynamic Background Correction, Moving Average, Trapez Integration, Reset Spectrum to Original*. Please be aware that the sequence of operations can be essential to the outcome of the results. All manipulations on the spectra are stored and the following action will employ the modified spectrum to perform its action.

### Constant Background Correction

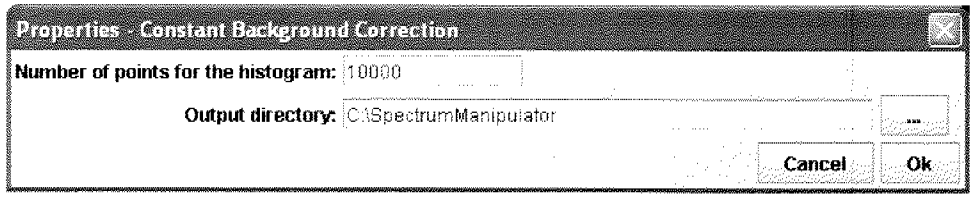


**Figure B.6: Properties for the constant background correction.**

The constant background correction calculates a histogram of intensities occurring in a spectrum whereas the *number of histogram points* (x-axis) can be defined (figure B.6). Assuming that there is more noise in a spectrum than peaks, the constant background is chosen at the maximum of the histogram and is subtracted from the spectrum. The constant background corrected spectra are saved at the location *output directory*. Figure B.7a shows a spectrum of 11 µM myoglobin whereas the red line denotes the determined constant background level. In figure B.7b the histogram used for determination is presented.

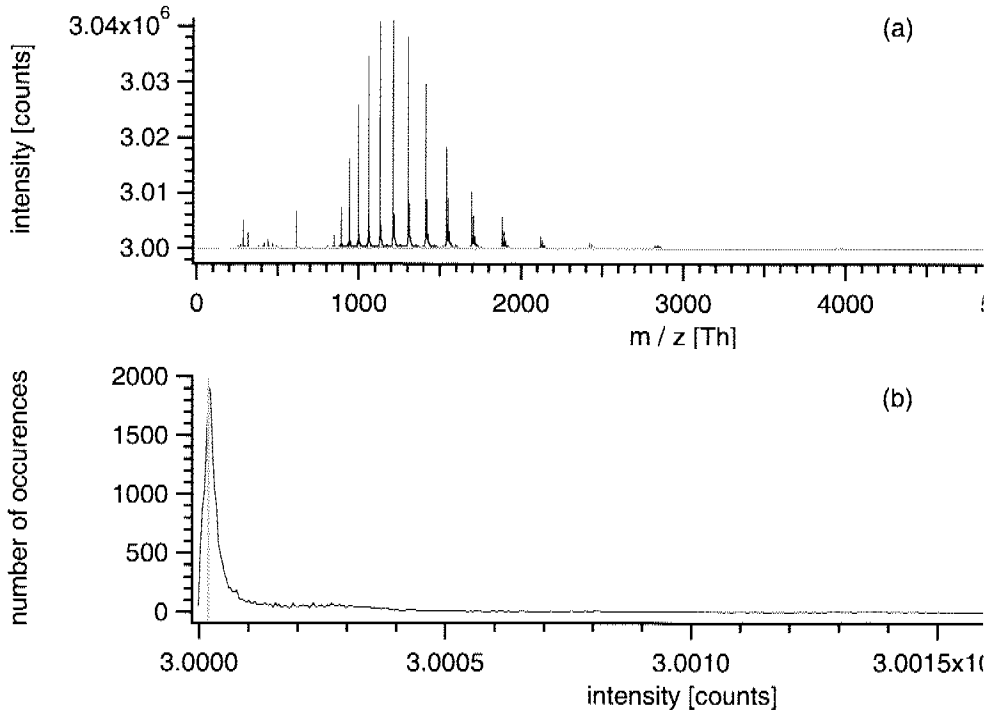


**Figure B.7: (a) Positive ion mode ESI of 11 μM myoglobin in 50 % water, 48% MeOH, and 2% acetic acid. The red line denotes for the determined constant background level. (b) Histogram of the spectrum shown in (a). The x-value of the maximum (red line) is taken as constant background level.**

## Dynamic Background Correction

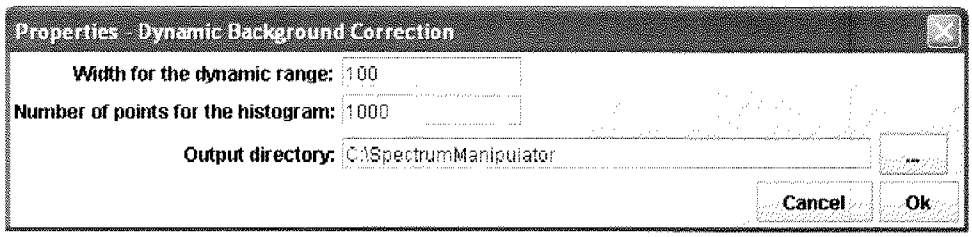


**Figure B.8: Properties for the dynamic background correction.**

The dynamic background correction calculates for each data point individually a background correction taking a number of neighboring points into account (*width of the dynamic range*) (figure B.8). For the data point and its neighboring points a histogram of its intensities is calculated and the intensity at the maximum of the histogram is subtracted from the data point, similar to the constant background correction. Please note that this correction only works if the assumption remains true that in the mass range is more noise than signal peaks. Therefore the width of the dynamic range has to be significantly larger than the peak width. Figure B.9a shows an enlarged

spectrum of 11 µM myoglobin in 50 % water, 48 % MeOH, and 2 % acetic acid, whereas the red line denotes for the calculated background. In figure B.9b the final result is shown. Using this method also chemical background, as it is observed for myoglobin, can be corrected.

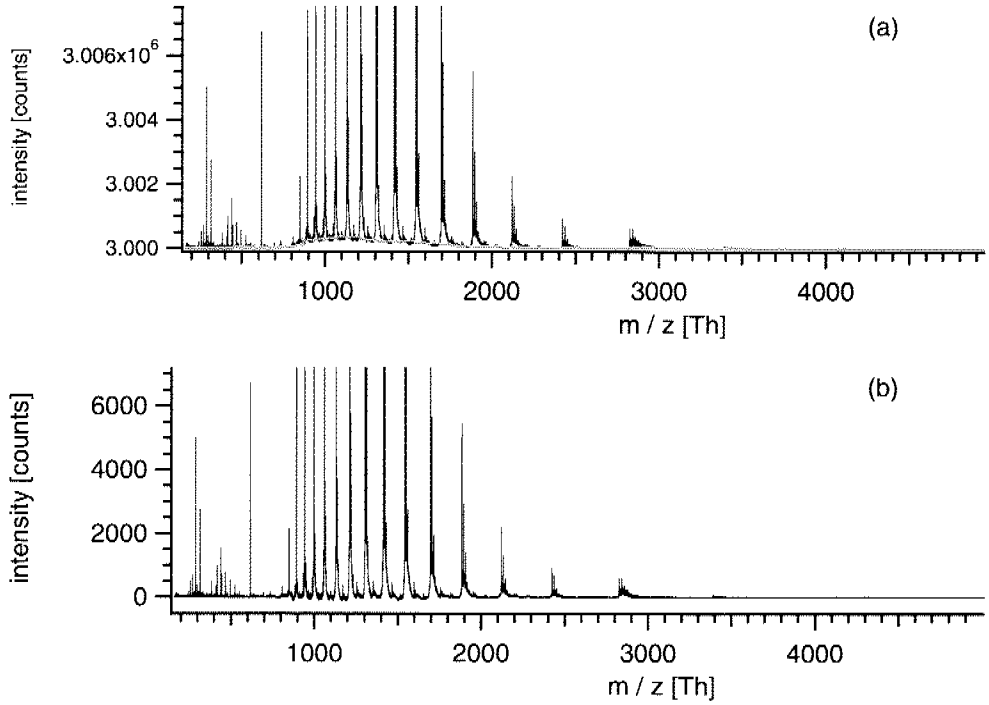


**Figure B.9: (a) Positive ion mode ESI of 11 µM myoglobin in 50 % water, 48% MeOH, and 2% acetic acid. The red line denotes for the determined background. (b) Resulting background corrected spectrum of (a).**

## Moving Average

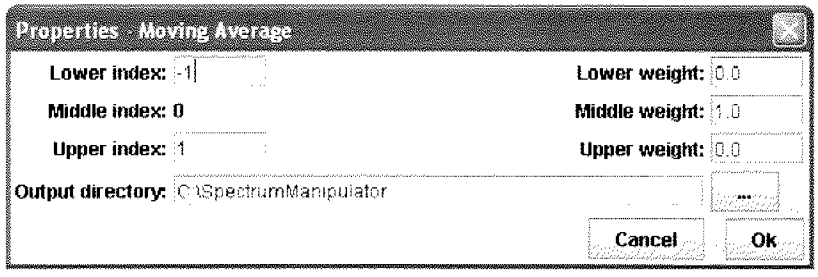


**Figure B.10: Properties for the moving average.**

The moving average allows to smooth the spectra. A trapezoidal moving average function can be defined by selecting the number of points used with smaller (lower index) and higher (upper index) mass (figure B.10). For the three points (lower index,

upper index, data point) a weight can be specified. For a standard moving average the lower and upper weight will be 0 and the middle weight will be 1. The averaged spectra are stored at the location *output directory*.

### Trapez integration

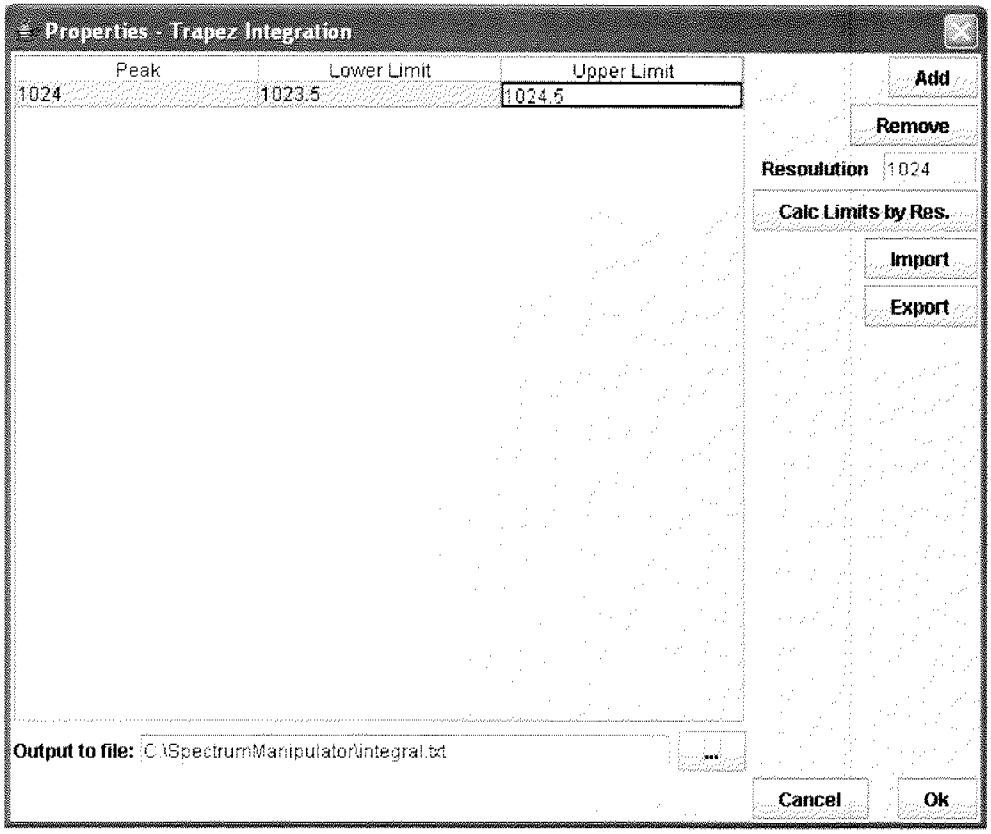


**Figure B.11: Properties for the trapez integration.**

In the trapez integration a whole set of peaks, including upper and lower integration limits, can be chosen for integration (figure B.11). The output of the integration for all spectra are summarized in the file specified in *Output to file*. Integration ranges are be added and removed by pressing the *add* or *remove* button, respectively. The list of integration ranges can be stored for later use by selecting the entries to store and press *export*. By pressing *import* previously stored integration ranges are loaded. By specifying the resolution of the mass spectrum and pressing *Calc limits by Res.* the integration ranges for peaks are automatically calculated according to the resolution.

### Reset Spectrum to Original

This action does not have any properties. This action resets the spectrum to its initial state, thus all modifications are discarded.

Below there is the source code of the classes used for the manipulation and interpretation of the spectra. All code dealing with thread control, data storage, and the graphical user interface (GUI) are omitted.

### DynamicBackgroundCorrection.java

```
import java.util.*;
import java.io.*;
import java.awt.*;

public class DynamicBackgroundCorrection implements Action {
  protected int nPointsHistogramm=1000;
  protected int nPointWidth=100;
  protected File baseDir=Settings.getLastFile();

  public DynamicBackgroundCorrection() {}
  public String getName() { return "Dynamic Background Correction"; }
  public int getNPointsHistogramm() { return  nPointsHistogramm;}
  public void setNPointsHistogramm(int n) { nPointsHistogramm = n;}
  public int getNPointWidth() { return nPointWidth;}
  public void setNPointWidth(int n) { nPointWidth = n;}
  public File getBaseDir() { return baseDir; }
  public void setBaseDir(File baseDir) { this.baseDir = baseDir; }
  public void startSequence() {}
  public void stopSequence() {}
  public void runCalculation(Spectrum spec) {
    double y[] = new double[spec.getArrayY().length];
    double yOrg[] = spec.getArrayY();
    for(int i=0; i<y.length; i++) {
      y[i] = yOrg[i] - getNoiseLevel(spec, i-(int)(nPointWidth/
                                          2), i+(int)(nPointWidth/2));
    }
    spec.setArrayY(y);
    spec.calculateMinMax();
```

```
    saveResults(spec.getArrayX(), spec.getArrayY(), new
        File(baseDir.getPath()+ File.separator +
        spec.getSourceFile().getName()));
  }
  protected double[] subarray(double x[], int startIndex, int stopIndex) {
    if (startIndex < 0) {startIndex=0;}
    if (stopIndex > (x.length-1)) {stopIndex=x.length-1;};
    double y[] = new double[stopIndex-startIndex+1];
    for (int i=startIndex; i<= stopIndex; i++) {
      y[i-startIndex] = x[i];
    }
    return y;
  }
  protected void saveResults(double[] x, double[] y, File file)
  {
    try {
      Logger.getLogger().info("Store output to: " + file.getPath());
      PrintWriter pw = new PrintWriter(new FileWriter(file));
      for (int i=0; i<x.length; i++) {
        pw.println("" + x[i] + "\t" + y[i]);
      }
      pw.close();
    } catch (IOException e) {
      Logger.getLogger().error("IO during store of
                              LinearBackgroundCorrection result: " + e);
    }
  }
  protected double getMin(double x[]) {
    double min = Double.MAX_VALUE;
    for (int i=0; i<x.length; i++) {
      if (x[i] < min) {min = x[i];}
    }
    return min;
  }
  protected double getMax(double x[]) {
    double max = Double.MIN_VALUE;
    for (int i=0; i<x.length; i++) {
      if (x[i] > max) {max = x[i];}
    }
```

```
    return max;
  }
  protected double getNoiseLevel(Spectrum spec, int lowerIndex,
                                                    int upperIndex) {
    int y[] = new int[nPointsHistogramm];
    double x[] = new double[nPointsHistogramm];
    double minX = spec.getMinY(), maxX = spec.getMaxY();
    // set boundaries
    if (lowerIndex < 0) { lowerIndex = 0; }
    if (upperIndex >= spec.getArrayY().length) { upperIndex =
                                    spec.getArrayY().length-1; }
    // generate Histogramm
    double specY[] = spec.getArrayY();
    for (int i=lowerIndex; i<=upperIndex; i++) {
      y[(int)Math.round((specY[i]-minX)*(nPointsHistogramm-1)/
                                                    (maxX-minX))] += 1;
    }
    double maxY=Double.MIN_VALUE;
    int indexMaxY = -1;
    for (int i=0; i<y.length; i++){
      if (maxY < y[i]) { maxY = y[i]; indexMaxY = i;}
    }
    return minX + (maxX-minX)/(nPointsHistogramm-1)*indexMaxY;
  }
  public boolean showProperties(Frame parent) {
    DynamicBackgroundCorrectionProp prop = new
                          DynamicBackgroundCorrectionProp(parent, this);
    return prop.showDialog();
  }
  public String toString() {
    return "Dynamic Background Correction (Width: " +
        nPointWidth + "; Points Histogramm: " + nPointsHistogramm + ")";
  }
}
```

## ConstantBackgroundCorrection

```
import java.util.*;
import java.io.*;
import java.awt.*;
```

```
public class ConstantBackgroundCorrection implements Action {
  protected int nPointsHistogramm=10000;
  protected File baseDir=Settings.getLastFile();
  public ConstantBackgroundCorrection() {}
  public String getName() { return "Constant Background Correction";}
  public int getNPointsHistogramm() { return nPointsHistogramm;}
  public void setNPointsHistogramm(int n) { nPointsHistogramm = n;}
  public File getBaseDir() { return baseDir; }
  public void setBaseDir(File baseDir) { this.baseDir = baseDir; }
  public void startSequence() {  }
  public void stopSequence() {}
  public void runCalculation(Spectrum spec) {
    double noiseLevel = getNoiseLevel(spec);
    double y[] = spec.getArrayY();
     for(int i=0; i<y.length; i++) {
      y[i] -= noiseLevel;
    }
    spec.calculateMinMax();
    saveResults(spec.getArrayX(), spec.getArrayY(), new
                                File(baseDir.getPath() + File.separator +
                               spec.getSourceFile().getName()));
  }
  protected void saveResults(double[] x, double[] y, File file) {
    try {
      Logger.getLogger().info("Store output to: " + file.getPath());
      PrintWriter pw = new PrintWriter(new FileWriter(file));
      for (int i=0; i<x.length; i++) {
        pw.println("" + x[i] + "\t" + y[i]);
      }
      pw.close();
    } catch (IOException e) {
      Logger.getLogger().error("IO during store of
                              ConstantBackgroundCorrection result: " + e);
    }
  }
  protected double getNoiseLevel(Spectrum spec) {
    int y[] = new int[nPointsHistogramm];
    double x[] = new double[nPointsHistogramm];
```

```
    double minX = spec.getMinY(), maxX = spec.getMaxY();
    double specY[] = spec.getArrayY();
    // generate x-axis
    for (int i=0; i<x.length; i++) {
      x[i] = minX + (maxX-minX)/(nPointsHistogramm-1)*i;
    }
    // generate Histogramm
    for (int i=0; i<specY.length; i++) {
      y[(int)Math.round((specY[i]-minX)*(nPointsHistogramm-1)/
                                                    (maxX-minX))] += 1;
    }
    double maxY=Double.MIN_VALUE;
    int indexMaxY = -1;
    for (int i=0; i<y.length; i++){
      if (maxY < y[i]) { maxY = y[i]; indexMaxY = i;}
    }
    return x[indexMaxY];
  }
  public boolean showProperties(Frame parent) {
    ConstantBackgroundCorrectionProp prop = new
                        ConstantBackgroundCorrectionProp(parent, this);
    return prop.showDialog();
  }
  public String toString() {
    return "Linear Background Correction (" + nPointsHistogramm + "
                                              Points for Histogram)";
  }
}
```

## MovingAverage.java

```
import java.util.*;
import java.io.*;
import java.awt.*;

public class MovingAverage implements Action {
  protected int lowerIndex=-1, upperIndex=1, middleIndex=0;
  protected double lowerWeight=0.0, middleWeight=1.0,
                   upperWeight=0.0;
  protected File baseDir=Settings.getLastFile();
```

```
public MovingAverage() {}
public String getName() { return "Moving Average"; }
public File getBaseDir() { return baseDir; }
public void setBaseDir(File baseDir) { this.baseDir = baseDir; }
public void setLowerIndex(int index) {
  if (lowerIndex > -1) lowerIndex=-1;
  lowerIndex = index;
}
public int getLowerIndex() { return lowerIndex; }
public void setUpperIndex(int index) {
  if (upperIndex <= 0) upperIndex=1;
  upperIndex = index;
}
public int getUpperIndex() { return upperIndex; }
public void setLowerWeight(double w) { lowerWeight = w; }
public double getLowerWeight() { return lowerWeight; }
public void setUpperWeight(double w) { upperWeight = w; }
public double getUpperWeight() { return upperWeight; }
public void setMiddleWeight(double w) { middleWeight = w; }
public double getMiddleWeight() { return middleWeight; }
public void startSequence() { }
public void stopSequence() {}
public void runCalculation(Spectrum spec) {
  double y[] = spec.getArrayY();
  double y2[] = new double[y.length], f;
  double count = 0;
  for (int i=0; i<y.length; i++){
    y2[i] = 0;
    count =0;
    for(int n=-1; n>=lowerIndex;  n--) {
      if ((i+n) >= 0) {
        count += f = -n*(middleWeight-lowerWeight)/lowerIndex+
                                                    middleWeight;
        y2[i] += f*y[i+n];
       } else {break;}
     }
     y2[i] += y[i]*middleWeight;
     count += middleWeight;
     for (int n=1; n<=upperIndex; n++) {
```

```
        if ((n+i)<y.length) {
          count += f=n*(upperWeight-middleWeight)/
                                                upperIndex+middleWeight;
          y2[i] += f*y[i+n];
        } else { break;}
      }
      y2[i] /= count;
    }
    spec.setArrayY(y2);
    spec.calculateMinMax();
    saveResults(spec.getArrayX(), spec.getArrayY(), new
      File(baseDir.getPath() + File.separator +
      spec.getSourceFile().getName()));
  }
  protected void saveResults(double[] x, double[] y, File file) {
    try {
      Logger.getLogger().info("Store output to: " + file.getPath());
      PrintWriter pw = new PrintWriter(new FileWriter(file));
      for (int i=0; i<x.length; i++) {
        pw.println("" + x[i] + "\t" + y[i]);
      }
      pw.close();
    } catch (IOException e) {
      Logger.getLogger().error("IO during store of
                          MovingAverage result: " + e);
    }
  }
  public boolean showProperties(Frame parent) {
    MovingAverageProp prop = new MovingAverageProp(parent,this);
    return prop.showDialog();
  }
   public String toString() {
    return "Moving Average (lowerIndex=" + lowerIndex + ";
      lowerWeight=" + lowerWeight + "; middleIndex=0;
      middleWeight=" + middleWeight + "; upperIndex=" +
      upperIndex + "; upperWeight=" + upperWeight + ")";
  }
}
```

### ResetSpectrum.java

```
import java.util.*;
import java.io.*;
import java.awt.*;

public class ResetSpectrum implements Action {
  public ResetSpectrum() {}
  public String getName() { return "Reset Spectrum"; }
  public void startSequence() {}
  public void stopSequence() {}
  public void runCalculation(Spectrum spec) {
     spec.releaseSpectrum();
  }
  public boolean showProperties(Frame parent) {
    return true;
  }
  public String toString() {
    return "Reset Spectrum to original";
  }
}
```

### TrapezIntegration.java

```
import java.awt.*;
import java.io.*;
import java.util.*;

public class TrapezIntegration implements Action {
  protected  Vector peaks=new Vector();
  protected  File outputFile=new File(Settings.getLastFile(),
                                                    "untitled.txt");
  protected  Vector temporaryOutput;
  public TrapezIntegration() { }
  public String getName() { return "Trapez Integration"; }
  public File getOutputFile() { return outputFile; }
  public void setOutputFile(File outputFile) {
    this.outputFile = outputFile;
  }
  public Vector getPeaks() { return peaks; }
```

```
public void setPeaks(Vector peaks) { this.peaks = peaks; }
public void startSequence() {
  Peak peak;
  String temp;
  // Temp output
  temporaryOutput = new Vector();
  // header
  temporaryOutput.add("Automatic Integration (Trapezoid)
                                                (c)2002 by J. Daniel\n");
  // write integration informations
  temporaryOutput.add("Peak Informations\n\nPeak\tlower
                                                  limit\tupper limit");
  temp = "Spectrum\ttotal integral\tIntegral(all peaks)";
  for (int i=0; i<peaks.size(); i++) {
    peak = (Peak)peaks.elementAt(i);
    temporaryOutput.add(""+peak.peak+"\t"+peak.lowerLimit+
                                                "\t"+peak.upperLimit);
    temp += "\t" + peak.peak;
  }
  temporaryOutput.add("\nResult of the Integration\n");
  temporaryOutput.add(temp);
}
public void stopSequence() {
  // write results to file
  Logger.getLogger().info("save integration results to " +
                                                outputFile.getPath());
  try {
    PrintWriter pw = new PrintWriter(new FileWriter(outputFile));
    for (int i=0; i<temporaryOutput.size(); i++) {
      pw.println((String)temporaryOutput.elementAt(i));
    }
    pw.close();
  } catch (IOException e) {
    Logger.getLogger().error("Integraton results could not be
                                                saved: " + e);
  }
}
public void runCalculation(Spectrum spec) {
  double x[] = spec.getArrayX();
```

```
    double y[] = spec.getArrayY();
    // calculate total integral
    double totalIntegral = integrate(x, y, 0, x.length-1);
    double peakIntegrals = 0;
    double integral[] = new double[peaks.size()];
    Peak peak;

    for (int i=0; i<peaks.size(); i++) {
      peak = (Peak)peaks.elementAt(i);
      peakIntegrals += integral[i] =
          integrate(x,y,spec.getIndexForX(peak.lowerLimit),
          spec.getIndexForX(peak.upperLimit));
    }
    // generate output
    String temp = spec.getSourceFile().getName()+ "\t" +
                          totalIntegral + "\t" + peakIntegrals;
    for (int i=0; i<peaks.size(); i++) {
      temp += "\t" + integral[i];
    }
    temporaryOutput.add(temp);
  }
  public static double integrate(double x[], double y[],
                                 int lowerIndex, int upperIndex) {
    double integral = 0;
    if (lowerIndex == upperIndex) { return 0; }
    for (int i=lowerIndex; i<upperIndex; i++) {
      integral += (y[i]+y[i+1])/2*(x[i+1]-x[i]);
    }
    return integral;
  }
  public boolean showProperties(Frame parent) {
    TrapezIntegrationProp dlg = new TrapezIntegrationProp(parent, this);
    return dlg.showDialog();
  }
  public String toString() {
    return "Trapez Integration";
  }
}
class Peak {
```

```
  public double peak;
  public double lowerLimit;
  public double upperLimit;

  public Peak(double peak, double lowerLimit, double upperLimit) {
    this.peak = peak;
    this.lowerLimit = lowerLimit;
    this.upperLimit = upperLimit;
  }
  public static double getLowerLimit(double peak, double resolution) {
    return peak-(peak/resolution);
  }
  public static double getUpperLimit(double peak, double resolution) {
    return peak+(peak/resolution);
  }
}
```

## Curriculum Vitae

| | |
|---|---|
| **28.09.1975** | born in Rheinfelden, Switzerland, as the second child of Adolf Daniel and Rose-Marie Daniel now Hablützel. |
| **1982-1990** | Primary and Secondary School. |
| **1990-1995** | Highschool "Kantonsschule Im Lee", Winterthur; Matura Type C (Mathematics / Science). |
| **1995-1999** | Chemistry studies at ETH Zurich. |
| **2000** | Diploma in chemistry, ETH Zurich. |
| **2000-2005** | Ph.D. thesis in chemistry, ETH Zurich. |
| | |
| **8.2004** | Marriage with Daniela Daniel-Ebneter. |
| | |
| **1995-1999** | Programmer for Adoculos GmbH. |
| **1998** | 3 months at Paul Scherrer Institute (PSI), Villigen, Switzerland. |
| **2000-2003** | Assistant in lab courses in Analytical Chemistry. |
| **2002-2003** | Research advisor for an exchange student. |
| **2000-2004** | Assistant coach in floorball. |
| **2004** | 1 month at Mass Tech Inc., Columbia, USA. |
| **since 2002** | Associate of OOTech GmbH, Switzerland. |